Lock Head Sustainability

A parametric study into the design of lock heads with mitre gates and single leaf gates

F.G. de Wit

TUDelft

VolkerWessels

Lock Head Sustainability

A parametric study into the design of lock heads
with mitre gates and single leaf gates

by

F.G. de Wit   4329767

in partial fulfillment of the requirements for the degree of

Master of Science
in Civil Engineering

Supervisors:	Dr. ir. drs. C. R. Braam,	Delft University of Technology
	ir. W. F. Molenaar,	Delft University of Technology
	ir. J.C. Galjaard,	Volkerwessels Infra Competence Centre
	ir. D.K. Kosterink,	Volkerwessels Infra Competence Centre

Preface

This thesis is part of my journey in obtaining a Masters Degree in Civil Engineering at the Technical University of Delft. The master track I have followed is Structural Engineering with a specialisation in Hydraulic Structures at the faculty of Civil Engineering and Geosciences.

This report is written in collaboration with TU Delft and Volkerwessels Infra Competence Centre. Through the following thesis I hope to contribute to a more sustainable future in the construction industry.
My research is intended for the preliminary design stage of the lock head design with a single leaf gate or a mitre gate.

First of all I would like to thank my family & friends who supported me during the duration of my master thesis. It was not the easiest time of my life with a car accident, a master project on a dead end, my mother battling for her life in the hospital and the out brake of the COVID-19 virus. I am glad and very thankful that it all ended well.
I would also like to thank my supervisors at the TU Delft who gave me some useful advice when my project was on a dead end. I want to thank Wilfred Molenaar in particular for helping me to structure the report.
Furthermore I would like to thank my supervisors and their colleagues at Volkerwessels Infra Competence Centre for their help and support. I would like to thank Martinus van de Ruitenbeek in particular for helping me with the parametric model and inviting me for different code labs.

Edward de Wit

Delft, 2020

Summary

Sustainability and the emission of CO_2 is a present and recurrent topic in our everyday life. The same holds for construction companies. One of the main materials contractors use is concrete. The concrete production process contributes for up to 9.5% to the CO_2 emission worldwide (Olivier et al., 2014). The goal of the Dutch government is to lower this number. For this reason, the Dutch government has signed the Betonakkoord together with producers of concrete and contractors. The goal of the Betonakkoord is to improve the collaboration within the concrete chain to increase the sustainability, to use sustainable concrete, to reduce the CO_2 emission with 30% relative to 1990, to make the life-cycle of concrete more circular by means of a circular design, to increase the lifetime and re-use of materials and lastly to promote innovations (Betonakkoord, 2018).

In this research an effort is made to contribute to the goals of the Betonakkoord. This is done by optimising the design of big and bulky structures consisting out of a lot of concrete, namely lock heads. Lock heads are part of the navigation lock. Lock heads support the opening and closing gate, retain the water as well as the groundwater, retain the soil and transfer the loads via the walls and the floor to the foundation.

The main research question answered in this thesis is phrased as follows: *How can the design of lock heads be optimised to increase the sustainability?*

The study starts with a study into sustainability and how it can be assessed. For this purpose, the Milieu Kosten Indicator (MKI) has been used. The MKI indicates the costs to society to undo the negative consequences of a functional unit (i.e. a lock head). Alongside the CO_2 emission, the MKI takes various environmental categories into account as well.

The next step of this research provides an overview of lock heads and their functional requirements based on literature study. Furthermore, it will explain the the big and bulky design of lock heads.

Thereafter, the focus shifts to the case study used in this research. The northern lock head in Empel is used as a case study. Volkerwessels Infra Competence Centre has provided the calculations and drawings of the northern lock head in Empel.

With the obtained knowledge, different alternatives have been generated to try to increase the sustainability. Each alternative has been compared to the lock head in Empel to test their feasibility. The following alternatives are considered: Inhomogeneous cross section, Prestressing and Hollow sections. Strength, stiffness and stability calculations have been performed for each alternative, while taking into account the cost and MKI.

From the alternative study it becomes clear that none of the alternatives are effective. The alternatives show no significant decrease in cost and MKI. Therefore, the alternatives are neglected in the remainder of the research. Based on this conclusion the following question arises: Is it possible to increase the sustainability of a lock head design based on commonly used design rules?

In the next step of the research a parametric model is developed in order to answer this question. The parametric model design is based on the rules prescribed by the 'Handboek voor het ontwerpen van Schutsluizen' (Ontwerp van Schutsluizen, 2000) and the 'Richtlijnen Vaarwegen 2017' (Richtlijnen vaarwegen 2017, 2017). The parametric model takes into account two types of gates, being a single leaf gate and a mitre gate. Again, the lock head in Empel has been used to validate the parametric model.

From the parametric model it follows that in general a mitre gate is more cost effective and sustainable than a single leaf gate. This is because a mitre gate is generally shorter than a single leaf gate, so less materials are used and the construction pit can be smaller.

Furthermore, the parametric model shows that the global stability check horizontal bearing capacity is a key parameter in the design of a lock head. To account for the horizontal bearing capacity the length and the weight of the lock head are important factors. In case the horizontal bearing capacity becomes

critical, the difference between a mitre gate and single leaf gate diminishes. This is due to an increase in length of the mitre gate to account for the horizontal bearing capacity, becoming approximately as long as a single leaf gate.

The next step is to compare the lock head designs from the parametric model with the lock head design in Empel. The lock head design in Empel deviates from the rules prescribed by the 'Handboek voor het ontwerpen van Schutsluizen' (*Ontwerp van Schutsluizen*, 2000). By deviating from the rules a more cost effective and sustainable design is acquired than both the designs from the parametric model. The lock head in Empel is shorter and lighter than the lock head designs from the parametric model. However, from the parametric model it followed that the length and the weight of the lock head play an important role to fulfill the horizontal bearing capacity. So, how can the lock head in Empel be shorter and lighter and still meet the horizontal bearing capacity requirement? This is due to the fact that the lock head in Empel derives its horizontal bearing capacity from the lock chamber, which is in contradiction with the 'Handoek voor het Ontwerpen van Schutsluizen' (*Ontwerp van Schutsluizen*, 2000). The 'Handoek voor het Ontwerpen van Schutsluizen' states that the lock head has to provide enough horizontal bearing capacity on its own.

In order to design a more cost effective and sustainable lock head it is advised to incorporate the lock chamber in the stability calculations. Hereby a shorter lock head can be achieved.

When the shortening of the lock head results in the gate extending the length of the lock head in open position, the gate should be protected by a wooden guidance wall placed in the approach area. Per case it should be investigated if the the guidance walls is able to replace the function of the lock head to protect the gate against collisions with vessels.

Contents

1

Introduction

On Wednesday the thirteenth of March 2019, the Dutch Ministry of Economische Zaken en Klimaat announced the plans to increase the CO_2 taxes for companies, starting in 2021. The current distribution in CO_2 taxes between households and companies is $50/50$. By increasing the taxes for companies, the distribution shifts to $33/66$. With this measure, the government forces producing companies to decrease their CO_2 release and at the same time increase their sustainability.
According to the Dutch Planbureau voor de Leefomgeving, the CO_2 taxes are most efficient when they are equally distributed over all the sectors (*Uniforme CO2-prijs meest kostenefficiënt*, 2019). This means that all companies have to deal with the CO_2 taxes and not only the polluting companies.
Companies are allowed to emit a certain amount of CO_2. When the threshold is exceeded, 30€ per ton CO_2 needs to be paid. This amount will increase to 150€ over a period from 2021 to 2030. The threshold has not yet been set by the government. With this measure the government hopes to reduce the CO_2 emission caused by the industry to 35.7 Megaton in 2030 (*Effect kabinetsvoorstel CO2-heffing industrie*, 2019).

A sector that produces a lot of CO_2 is the concrete sector. The Netherlands produces about 4.7 million ton cement per year (Cement&BetonCentrum, 2020). Per ton cement produced in the Netherlands, $750 kg \, CO_2$ is is released (Cement&BetonCentrum, 2019). Worldwide the total concrete production contributes for 9.5% to the total CO_2 emission. (Olivier et al., 2014).
Concrete used in the infrastructure causes roughly one third of the total environmental impact during the construction, use and maintenance of a project (*Duurzaam GWW aanbesteden*, 2019).
Structures that contain a lot of concrete are lock heads. Lock heads are big and bulky structures in order to fulfill all the strength, stiffness and stability requirements.
In this research the design of lock heads is optimised to increase the sustainability, while taking into account the cost.

The thesis has been divided in three different sections, see Figure 1.1. The first section is the introduction. The introduction touches upon sustainability. It clarifies the problems around sustainability and concrete, how it is measured and what measures already have been taken by the Dutch government. Furthermore, the introduction discusses the functional and structural requirements of lock heads. The requirements are mainly based on the 'Handboek voor het ontwerpen van Schutsluizen' by the 'Ministerie van Verkeer en Waterstaat' (*Ontwerp van Schutsluizen*, 2000) and the 'Richtlijnen Vaarwegen 2017' (*Richtlijnen vaarwegen 2017*, 2017). In addition, the big and bulky design of lock heads is explained.
In the next section the northern lock head in Empel is discussed. This lock head serves as a case study. Volkerwessels Infra Competence Centre provided the drawings and calculations.
The introduction finalises with the problem definition, objectives, methodology and scope.

The next section deals with the conceptual design of lock heads. In this section different constructive alternatives are elaborated. With the obtained knowledge from the introduction and information about the current innovations in the lock head design, different ideas will be generated in the preliminary

study to implement in the lock head design. These ideas are principles that are not commonly used in the current lock head design. The alternatives are applied to the northern lock head in Empel in order to test their feasibility. Strength, stiffness, stability, cost and MKI calculations are made to check whether the ideas are promising or not. The conceptual design finalises with a decision to further investigate the alternatives or to neglect them.

The last section is the advanced analysis. The path of the advanced analysis is determined by the results of the preliminary design. In case one or more alternative(s) is/are promising, it/they is/are further elaborated. In case none of the alternatives are promising, they will all be neglected. In this case it is tried to increase the sustainability of lock heads by optimising the current design. A parametric model is made based on the design rules from the 'Handboek voor het ontwerpen van Schutsluizen' (*Ontwerp van Schutsluizen*, 2000) and the 'Richtlijnen Vaarwegen 2017' (*Richtlijnen vaarwegen 2017*, 2017). The lock head in Empel is used to validate the parametric model.
The advanced analysis finalises with the results from the research.

Main report

Preface

Summary

Table of Content

Introduction
- Announcement Subject Underlying Report
- Reader

Introduction

Sustainability
- Concrete
- Measuring Sustainability
- Measurements Taken

Navigation Locks
- Maritime and Inland Navigation Locks
- Lay-out
- Lock Heads

Lock Head Empel
- Geometry
- Foundation
- Results
- MKI
- Cost
- Discussion

Problem Definition
- Problem Statement & Objective
- Methodology
- Scope

Preliminary Study

Alternatives
- Idea Generation
- Inhomogeneous Cross Section
- Prestressing
- Hollow Sections
- Conclusion

Alternatives are promising?

Advanced Analysis   Yes   No

Further Analysis of the Alternative(s)

Parametric Model
- Model Lay-out
- Model Overview
- Validation
- Limitations

Results (CEMT class IV)
- Influence Water Head
- Influence Thickness
- Influence Concrete
- Comparison Empel
- Conclusion

Discussion

Conclusions & Recommendations

References

Appendices

Appendix

Explanation Indicators LCA and the MKI Conversion Factors

Structural Design Lock Heads
- Loads
- Load Factors and Combinations
- Strength and Stability
- Global Stability

Calculations Lock Head Empel
- Loads
- Strength
- Stiffness
- Stability
- Cost & MKI

Innovations in Lock Head Design

Calculations
- Strength
- Stiffness
- Global Stability
- Cost & MKI

Parametric Model
- Explanation UML
- Matrix Method
- Validation

Results
- CEMT Class I, II, III, V, VI
- MKI Factor

Figure 1.1: Thesis outline

2

Sustainability

This chapter will discuss the need for a more sustainable design of concrete structures. It will explain what the effect of concrete is on the environment and how it is measured.
The chapter closes with an overview of measures taken by the government to reduce the pollution and their influence on the construction industry.

2.1. Concrete Structures

Concrete is one of the most important construction materials worldwide and is used for all kind of structures.
Concrete is made by mixing aggregates, water and cement (Neville and Brooks, 2010). Concrete consists approximately of 15% cement (Cement&BetonCentrum, 2019). The production of cement, especially the production process of clinker, contributed to about 4.8% of the global CO_2 emission in 2014 (Olivier et al., 2014). The most common type of cement used is Ordinary Portland Cement. Ordinary Portland Cement is produced by heating and mixing the materials limestone and clay in a kiln. The resulting product is clinker. Gypsum is added to the clinkers and hereafter the clinkers are grinded to form the Ordinary Portland Cement. In the kiln the raw materials are mixed at a temperature of $1450°$, where the following reaction takes place:

$$CaCO_3 \rightarrow CaO + CO_2$$
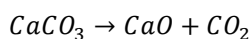
The chemical process in the kiln is the main contributor to the CO_2 emission, the 4.8% mentioned earlier. When including the combustion, the CO_2 emission increases to about 9.5% of the total global CO_2 emission (Olivier et al., 2014). This is an increase of 7.4% relative to 2013. The increase in CO_2 from 2012 to 2013 was 4.8% (Olivier et al., 2014). The increase in the total global CO_2 emission due to cement clinker production is mainly due to an increase in concrete production of 9.3% in China. China is accountable for more than half of the total production (Olivier et al., 2014), Figure 2.1.
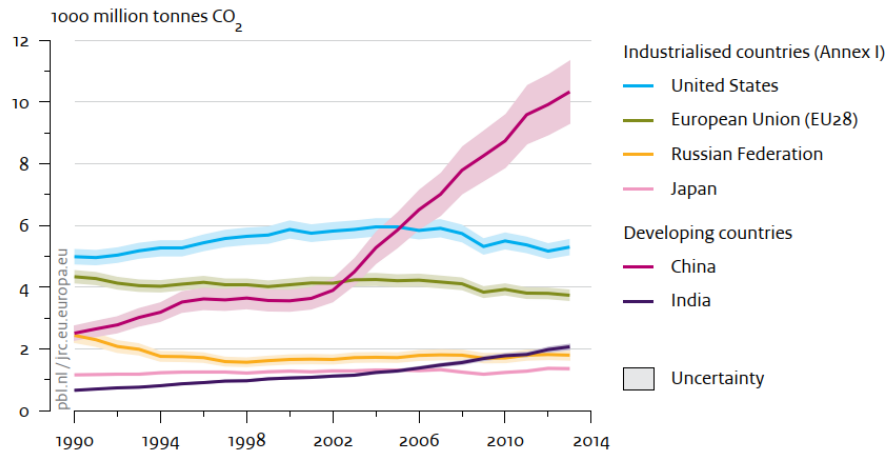
Figure 2.1: CO_2 production top 5 emitting countries and EU (Olivier et al., 2014)

The difference in CO_2 emission per country due to concrete production does not only depend on the volume produced, but also on the clinker content in the concrete. Figure 2.2 shows the clinker content in concrete produced in different countries.

According to Cement & Beton Centrum 1 ton cement produced in Europe causes on average $750kgCO_2$ equivalent (Cement&BetonCentrum, 2019). This number includes the carbonation, combustion, transportation and electricity usage, see Figure 2.3. The cement produced in Eastern Europe causes on average $70kg/ton\ CO_2$ equivalent more than cement produced in Western Europe. The cement produced in the USA produces $927kg/ton\ CO_2$ (NRMCA, 2008). Cement produced in China causes even $970kg/tonCO_2$ equivalent (Cement&BetonCentrum, 2019).
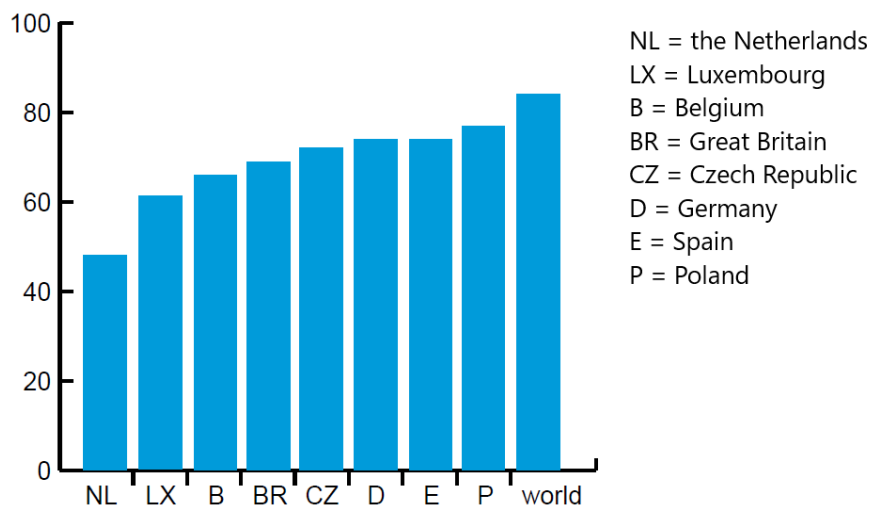
Figure 2.2: Clinker content used in concrete per country (Cement&BetonCentrum, 2019)
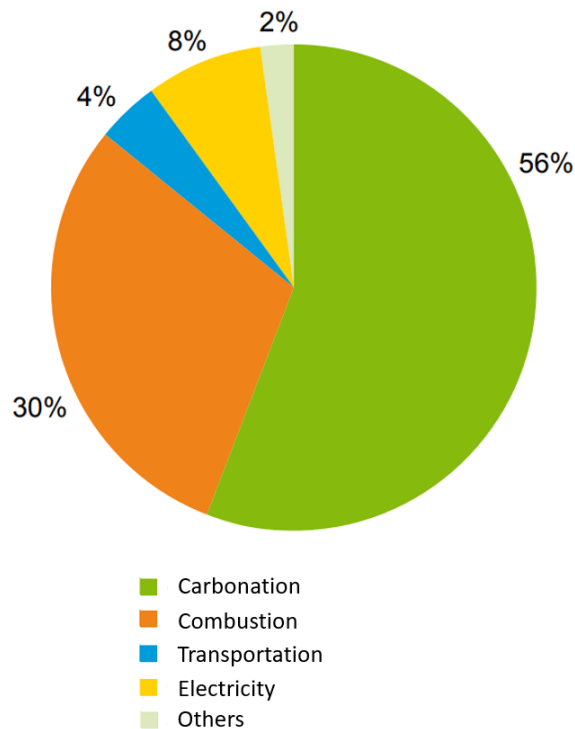
Figure 2.3: CO_2 distribution European cement production (Cement&BetonCentrum, 2019)

2.2. Measuring Sustainability

Sustainability is the development that meets the needs of the present without compromising the ability of future generations to meet their own needs (Keeble, 1988). Durability is the ability of a product to perform its required function over a lengthy period under normal conditions of use without excessive expenditure on maintenance or repair (Cooper, 1994). In the Netherlands sustainability and durability are both covered by the term 'duurzaamheid'. However, this report will namely concentrate on sustainability.

To measure the sustainability of construction works the Dutch government uses the so called Milieu Kosten Indicator. The following section will go into more detail.

2.2.1. MKI

To get an indication into how sustainable a building or structure is, a MKI (Milieu Kosten Indicator) can be calculated. The MKI indicates the costs to society to undo the negative consequences of a functional unit. To calculate the MKI, a Life Cycle Assessment (LCA) has to be assessed. An LCA is a method to quantify all input and output flows related to an assessed item based on researched information and estimations. It has a descriptive or comparing nature and does not judge but quantifies the flows. It is an instrument to screen flows and identify optimisation potential (Hildebrand, 2014). ISO 14040 and 14044 describes how to execute an LCA. The steps to perform a LCA are goal and scope definition, Life cycle inventory analysis (LCI), life cycle impact assessment (LCIA) and interpretation.

Goal and Scope Definition

The goal and scope definition is the first step of performing an LCA. The goal and scope define the layout of the LCA. First the functional unit has to be described. The functional unit can be a product, service or company. The functional unit in this research is a lock head. The next step is to define the life cycle phases, Figure 2.4. The different phases that can be considered are from cradle-to-gate, from gate-to-gate, from gate-to-grave or from cradle-to-grave (Hildebrand, 2014). From cradle-to-gate takes into account the life cycle from the resource extraction to the use phase. The gate-to-gate phase considers the manufacturing process of the functional unit. The gate-to-grave phase considers the life cycle of functional unit from the manufacturing phase all the way up to the disposal phase. The cradle-to-grave phase takes into account the whole life cycle of a functional unit.

The system borders of the assessed item have to be defined. The system borders indicates what parameters are included and what parameters are excluded. This is important when different functional units are compared.
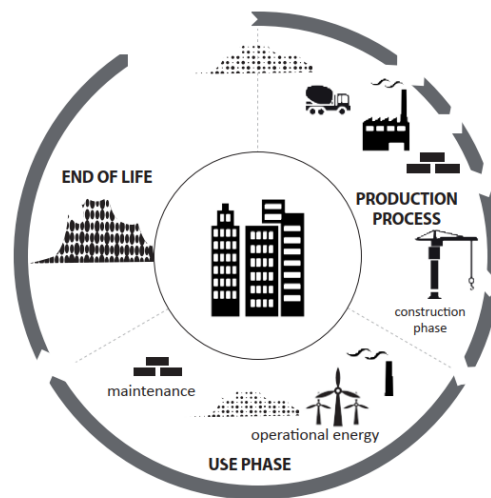
Figure 2.4: Life cycle of a functional unit (Hildebrand, 2014)

Life Cycle Inventory Analysis
The LCI identifies and quantifies all processes related to a particular product. The input and output are identified and quantified into different groups (Hildebrand, 2014):

- Energy inputs, raw material inputs, ancillary inputs, other physical inputs

- Products, co-products and waste

- Releases to air, water and soil

- Other environmental aspects

Life Cycle Impact Assessment
The LCIA assigns ecological impact categories to the LCI results. The LCI results are organised by their impact on the environment and are summarised in an impact category (Hildebrand, 2014). The ISO 14040 divides the requirements for an LCIA in three steps:

- selection of impact categories, category indicators and characterisation models;

- assignment of LCI results to the selected impact categories (classification);

- calculation of category indicator results.

Interpretation
The LCI or LCIA can be followed by an interpretation which identifies the significant results according to the goal and scope defined in the first steps (Hildebrand, 2014).

After a LCA has been performed, the functional unit has up to eleven different values with their corresponding unit based on the different indicators. The 'milieu kosten indicator' is used in the Netherlands to assign one value to a functional unit with the unit euro. Appendix A gives the different conversion factors and their meaning. The MKI value takes into account more negative effects besides the CO_2 emission.

For this report DuboCalc will be used to calculate the MKI value to get an indication of the sustainability. DuboCalc is a program of Rijkswaterstaat and calculates the MKI value based on the LCA.

The lock head in this thesis will be assessed form cradle to grave with a lifetime of 100 years. The system borders are formed by the concrete, reinforcement, the under water concrete floor and the foundation piles.

The MKI calculations take all the eleven indicators into account, see Appendix A.

2.3. Measures taken
Various measures have already been taken to lower the CO_2 emission. This section will give an overview of measures that are applicable to the Netherlands and the construction industry.

2.3.1. Klimaatakkoord
In 2015, 195 countries signed the Paris Agreement. Article 2 of The Paris Agreement of the United Nations states that holding the increase in the global average temperature to well below 2°C above pre-industrial levels and pursuing efforts to limit the temperature increase to 1.5°C above pre-industrial levels (*The Paris Agreement*, 2015).

In order to reach the goals set by the Paris Agreement, the Dutch government has set up its own agreement, the Klimaatakkoord. The Klimaatakkoord states that the emission of greenhouse gasses has to be lowered with 49% before 2030 in comparison with 1990 (*Klimaatakkoord*, 2019). The whole Dutch community has to attribute to reduce the emission of green house gasses, so also the construction companies. Agreements that are part of the Klimaatakkood and are applicable to contractors are the Betonakkoord and Nederland circulair in 2050.

2.3.2. Betonakkoord
The Betonakkoord is an agreement signed by the minister of Infrastructuur en Waterstaat, the minister of Economische Zaken en Klimaat, the minister of Landbouw, Natuur en Voedselkwaliteit, Secratary of State of Binnenlandse Zaken en Koninkrijkrelaties, different municipalities, Prorail, producers of concrete and contractors whom VolkerWessels is one of.

The goal of the Betonakkoord is to improve the collaboration within the concrete chain to increase the sustainability, to use sustainable concrete, to reduce the CO_2 emission with 30% relative to 1990, to make the life-cycle of concrete more circular by means of a circular design, an increase in the lifetime and re-use of materials and to promote innovations (*Betonakkoord*, 2018).

The CO_2 reduction is the most important goal of the Betonakkoord in order to reach The Paris Agreement.

The production of cement is the most polluting factor of the concrete chain, as was mentioned in the previous section. However, according to the Betonakkoord Dutch concrete has a lower clinker content in comparison to concrete produced in the rest of the world, $50-55\%$ vs 80%. This means that the CO_2 emission is already half of the worldwide average emission. Cement & Beton Centrum even states that the Netherlands produces concrete with the lowest clinker content (Cement&BetonCentrum, 2019), Figure 2.2.

The CO_2 emission due to materials has already decreased with 10% over the period from 1990 to 2010. The CO_2 emission due to transport has decreased with 45% over the same period. This means a total reduction of about 13% (*Betonakkoord*, 2018).

2.3.3. Nederland Circulair in 2050
The aim of the document 'Nederland circulair in 2050' by the dutch government is to create a circular economy before the year 2050 and to use up to 50% less raw materials by 2030. Due to the increasing population, the demand in raw materials also increases. Besides, the Netherlands imports 68% of its raw materials form elsewhere (CirculaireEconomie, 2016). The exploitation and transportation of raw materials causes CO_2 emission. The document therefore also takes Article 2 of The Paris Agreement into account. By making the construction process more circular, the Netherlands tries to fulfill in the increasing demand, be less dependable on other countries and to decrease the CO_2 emission.

3

Navigation Locks

This chapter will give an overview of navigation locks. The main focus of this chapter are the lock heads. The structural elements of lock heads will be discussed, as well as the functional requirements. Furthermore the big and bulky design of lock heads is explained.

3.1. Maritime and Inland Navigation Locks

A distinction can be made between maritime navigation locks and inland navigation locks. Maritime locks are used to eliminate tidal effects in harbours and canals adjacent to the sea to keep navigation possible. Due to the tidal effects, maritime locks have to be able to retain water in both directions. For this reason, sea locks are often equipped with two sets of gates at each lock head.

The dimensions of the navigation lock mainly depend on the types of vessels using the navigation lock. A classification for maritime navigation does not exist. The dimensions often depend on a normative sea vessel. This vessel uses the lock occasionally, so most of the time the lock is used to transfer various smaller vessels at once.

For inland navigation, vessels have been classified in different CEMT classes, see Table 3.1. The CEMT classification divides the classes into standard inland navigation vessels. The standard vessels are Peniche (I), Campinois (II), DEK-schip (Dortmund-Ems-Canal) (III), RHK-schip (Rhine-Herne-Canal) (IV), GRS-schip (Big Rhine barge)(Va) and push barge (Va,b, single barge and VIa,b,c > single barge). This study only takes into account minimum navigation locks for inland navigation. With the term minimum navigation lock a reference is made to a navigation lock able to handle one normative vessel at a time (*Richtlijnen vaarwegen 2017*, 2017).

Table 3.1: CEMT class vessels (*Ontwerp van Schutsluizen*, 2000)

CEMT class	Type vessel	Length L (m)	Width B (m)	Draught T (m) empty	Draught T (m) loaded	Clearance H (m)
I	Peniche	39	5.1	1.2	2.2	5.0
II	Campinois	55	6.6	1.4	2.5	6.0
IIa**	Hagenaar	56 or 67	7.2	1.4	2.5	6.3
III***	Dortmunder	67 or 80	8.2	1.5	2.5	6.3
IV	Rhine-Herne-Canal	85	9.5	1.6	2.8	6.7
Va	Big Rhine barge	110	11.4	1.8	3.5	6.7/8.8*
Vb	Pushed convoy	186.5	11.4	1.8	4.0	8.8
VIa	Side-by-side formation	110	22.8	1.8	4.0	8.8
VIb	Pushed barge train	186.5	22.8	1.8	4.0	8.8

3.2. Lay-out

The main function of a navigation lock is to make ship navigation possible between two different water bodies with a difference in water level. The maximum and minimum water levels between which lock operation is possible are called respectively maximum and minimum schutpeil *Richtlijnen vaarwegen 2017* (2017). Navigation locks are most of the time part of a flood defence system. The second function of a navigation lock is therefore water retention.

The structural elements of a navigation lock are the bottom and bank protection, the guide walls, the berthing facilities, the filling and emptying systems, the lock gates, the lock heads, the lock chamber and the seepage cut-off screens. An overview of a lock is given in Figure 3.1.

1. Waiting- or lay-by berths
2. Guard- or guide wall or lead-in jetty
3. 'Closing elements' – lock gates
4. Lock heads
5. Lock chamber
6. Filling and emptying system
7. Cut-off walls and screens (sheetpiles) to prevent piping
8. Bottom protection
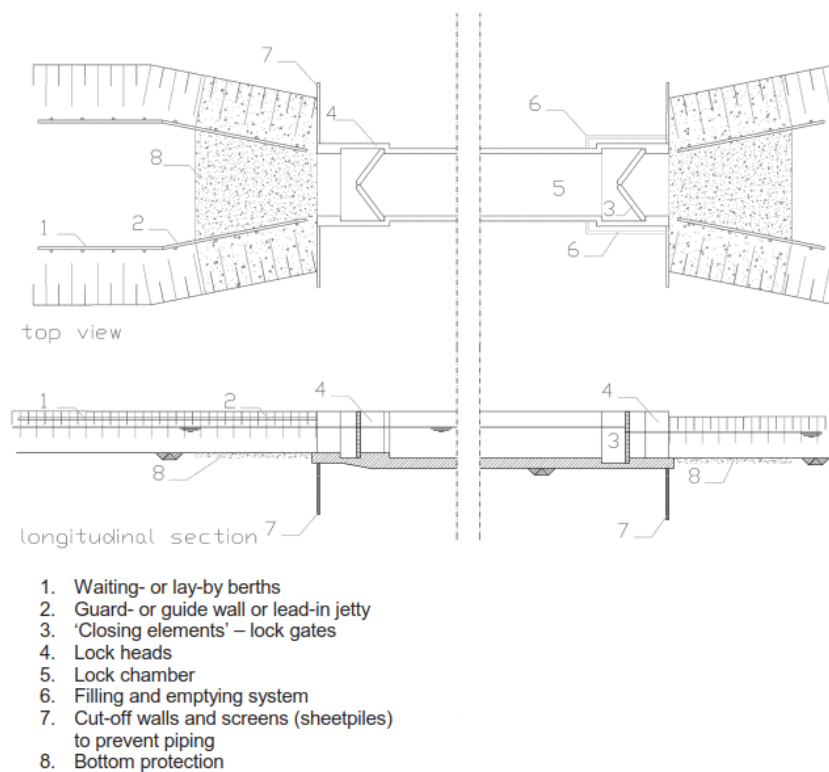
Figure 3.1: Overview of a Lock. (Molenaar, 2011)

The process of a vessel moving from a water plane to another water plane with different water levels is as follows; A vessel approaches the lock and may have to wait at the berthing facilities in case the lock is occupied. The water level in the lock is levelled out with the water level in the adjacent water body via filling and emptying systems. When the water levels are equal, the lock gate can be opened. The lock gate is supported by the lock head. The vessel may now enter the lock chamber. When the vessel has entered the lock chamber, the lock gate is closed. The water level inside the lock is now adjusted to the water level of the other water plane via filling and emptying systems. Once the water levels are levelled out, the gate is opened and the vessel can leave the lock. During this process extra propeller forces may be required for manoeuvring. Therefore, bottom and bank protection are applied at both ends of the lock.

3.3. Lock Heads

The three main functions of a lock head are to support the opening and closing gate, retain water as well as groundwater and to transfer the loads via the walls and the floor to the foundation. The dimensions of the lock head therefore depend on the type of vessel entering the lock, the type of gate being installed and the order of magnitude of the (ground)water pressure and soil pressure. Appendix B gives a detailed description of all the loads acting on the lock head. Besides, the lock head has to be stiff enough to minimise the displacements. Big displacements of the lock head can hamper the gate

from opening and closing. This criteria is gate dependent, since some gate types are more sensitive to displacements than others. Besides, the displacement between the lock head and lock chamber has to be minimal to secure a watertight connection.

Due to all the loads acting on lock heads and the displacement requirements, lock heads end up being designed and constructed in a robust way.

3.3.1. Lay-out

For this section general reference is made to the 'Handboek voor het ontwerpen van Schutsluizen' (*Ontwerp van Schutsluizen*, 2000). The different parts of a lock head are the gate, the gate chamber and gate recess, bearings to support the gate, operating systems to open and close the gate and stop log recess for maintenance. The lay out of a lock head with a single leaf gate or mitre gate will be discussed.

The minimum length of the lock head mainly depends on the type of gate. For a single leaf gate a distinction can be made between the wall with the gate chamber and the wall with the gate recess. When the gate is in an open position the gate vanishes in the gate chamber where it is protected against collisions with vessels and an easy passage for the vessel is provided. In a closed position the gate closes against the gate recess to secure a watertight connection, see Figure 3.2. The 'Handboek voor het ontwerpen van Schutsluizen' provides the following rules of thumb to determine the dimensions of the gate chamber and gate recess for a single leaf gate:

- Gate thickness is $\frac{1}{6}/\frac{1}{8}$ of the free width clearance

- Distance between the wall and the gate is 0.4 times the gate thickness (a in Figure 3.2)

- Distance between the wall and the end of the gate is 0.8 times the gate thickness (b in Figure 3.2)

- the length of the gate recess is half the length of the gate chamber

A lock head with a mitre gate is symmetrical. It has a gate chamber on both sides of the lock head. In closed position the two parts of the mitre gate close against each other with an angle of $1:3$. The dimensions prescribed by the 'Handboek voor het ontwerpen van Schutsluizen' are:

- Gate thickness is $\frac{1}{16}/\frac{1}{20}$ of the free width clearance

- Distance between the wall and the gate is 0.4 times the gate thickness (a in Figure 3.2)

- Distance between the wall and the end of the gate is 0.8 times the gate thickness (b in Figure 3.2)

The width of the lock head is mainly determined by the type of vessel (CEMT class). The depth of the lock head depends on the minimum water level at which lock operations are possible, the loaded draught of the vessel and a prescribed margin set to $0.7m$.

For commercial shipping, the top of the lock head has to be $2.5m$ above the highest possible water level, called maatgevend hoogwater (MHW) (*Richtlijnen vaarwegen 2017*, 2017). Other factors that determine the top of the lock head are the sea level rise, the settlements of the lock head, wind setup, wave overtopping and seiches.
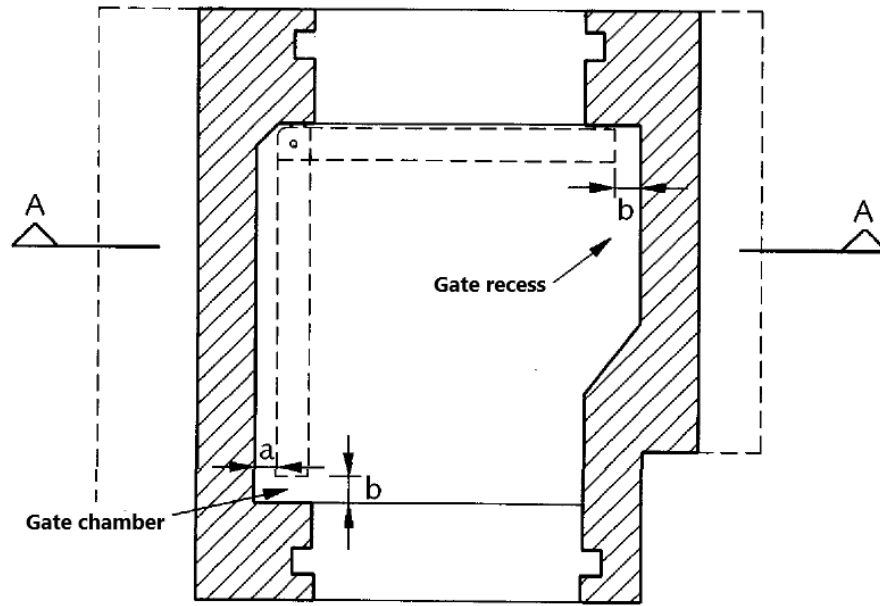
Figure 3.2: Lock Head Lay-out (*Ontwerp van Schutsluizen*, 2000)

3.3.2. Type of Lock Heads

In general there are five different main types of lock heads. The standard U-shape lock head is the most common lock head and is built in-situ. This type will be considered in this research. The remaining four lock heads are based on the standard U-shape. The second option is a pneumatically immersed lock head. These kind of lock heads are applied when there is only little construction space. The third option is a stripped U-shaped head. This lock head is built in a dry dock and shipped to the desired location where it is immersed onto a prepared gravel bed. Using this lock head minimises the hindrance at the desired location. The previous mentioned types of lock heads were all based on a monolithic U-shape to minimise the displacements. It is also possible to construct the lock head out of different parts that have to be connected on site. This kind of lock head is only used for lock heads with a great width. In Figure 3.3 the different kind of lock heads are shown.

Standard U-shaped lock head build in-situ	
Pneumatically immersed lock head	
Stripped U-shaped head, floated in	
U-shape lock head with a construction joint in the middle	
U-shape lock head with two construction joints	
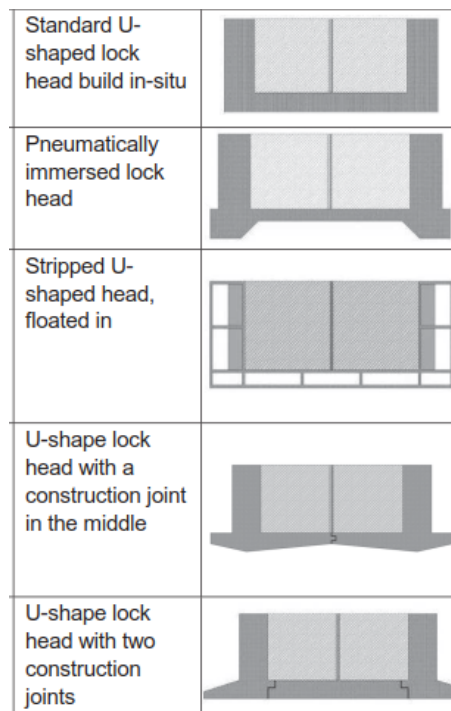
Figure 3.3: Different Lock Heads. (Molenaar, 2011)

3.3.3. Type of Gates

Lock gates are the movable parts of navigation locks and are supported by the lock heads. When closed, the gates ensure a watertight connection between the lock chamber and the adjacent water bodies. When opened, the vessels can enter and leave the navigation lock.

The most common lock gates in the Netherlands are: single leaf gates, mitre gates, rolling gates and lift gates. What gate to choose depends on location dependent parameters and gate dependent parameters. The location dependent parameters are the head difference, the dimensions of the navigation lock, the retention of water in one or both directions, the conditions in which the gate has to operate and the area available around the lock. The gate dependent parameters are the cost, the maintenance, the durability, the locking capacity, the usability and the impermeability, see Appendix B.

Single Leaf Gates

A single leaf gate turns around a vertical axis. When closed, the position of the gate is perpendicular to the main axis of lock. The forces due to a water head difference are transferred via the gate bearings to the walls of the lock head. In open position the gates disappear in a gate recess for safe passage of vessels. The advantages of single leaf gates are:

- Suitable for locks with smaller widths due to easy construction and operation.

- No air draught limitations.

- Retention of water is possible in both directions when special measurements have been taken at the free end.

The disadvantages of a single leaf gate are:

- The gate recesses are long, thus requiring longer lengths for the lock heads.

- Opening and closing of the gate results in a lot of water displacement.

- Only applicable for small widths.

- Vulnerable for ice and debris.

- Large forces on the bearings.

Figure 3.4: Single leaf gate Empel (VHBInfra, 2014)

Mitre Gates

Mitre gates are the most commonly applied lock gates. Mitre gates consist of two leaf gates which turn around a vertical axis. When closed, the gates form an obtuse angle. The two leaf gates point in the direction of the higher water level. Mitre gates are used for water retention in one direction. With special measurements water retention in both directions is possible to a certain extend. Both parts of mitre gates disappear in the gate recesses on both sides of the lock head. The advantages of mitre gates are:

- No air draught limitations.

- Low cost due to relatively light gate structure.

- Opening and closing takes a short time.

The disadvantages of mitre gates are:

- The gate recesses are long, thus requiring longer lengths for the lock heads.

- For water retention in both directions an extra set of gates is needed.

- Sensitive to ice and debris.

- Gates can not be opened or closed under a head difference.

- Precise measures are needed.

Figure 3.5: Mitre gate Lith (*Ontwerp van Schutsluizen*, 2000)

Rolling Gates

To open the gate, the gate moves on a rails or a sliding track in horizontal direction perpendicular to the main axis into a gate recess. The width of the lock head is more than twice the width of the gate. A rolling gate is able to retain water in both directions. The advantages of rolling gates are:

- Able to span large widths.

- No air draught limitations.

- Able to retain water in both directions.

- Easy to maintain.

The disadvantages are:

- Only applicable when space is available next to the lock head.

- Large gate recess structures are needed.

- Gate can not be opened or closed under a head difference.

Figure 3.6: Rolling gates Panama (Iv-Groep, 2016)

Lift Gates

A lift gate is positioned perpendicular to main axis of the lock. The loads due to a head difference are directly transferred to the walls of the lock head. A lift gate is able to retain water in both directions. To open the gate, the gate is lifted in vertical direction by two lifting towers. Counterweights are added to reduce the force needed to lift the gate. The advantages of lifting gates are:

- Lock heads are short.

- Possible to retain water in both directions.

- Easy to maintain.

- Not sensitive to ice and debris.

- Possible to open the lock gate under a head difference.

The disadvantages of lifting gates are:

- Air draught limitations.

- The lifting structures are large, heavy and expensive.

Figure 3.7: Lifting gate Weurt (*Ontwerp van Schutsluizen*, 2000)

3.3.4. Filling and Emptying Systems

Gravity is used to fill and empty a lock. To fill the lock, water from the upper reach of a canal or a river is transferred into the lock chamber. To empty a lock, water in the lock chamber is transferred to the lower reach of a canal or a river. The amount of water that has been displaced during this process is equal to the the area of lock chamber x the head difference.

The most important parameter when choosing a filling and emptying system are: the required lift, the filling and emptying times, the hawser forces and the cost. The time needed to fill and empty the lock chamber should be as short as possible. This has a positive influence on the capacity of the lock. However, a shorter filling time has a negative influence on the hawser forces. To reduce the filling and emptying time, the dimensions of the culverts increases, introducing an increase in dynamic energy of the water. The hawser forces are higher during filling of the lock chamber than during emptying. During filling of the lock, the dynamic energy of water creates surges. Stilling basins are used to reduce the dynamic energy during the filling of the lock chamber.

In principle there are two different filling and emptying systems. These are filling and emptying through the heads and filling and emptying through longitudinal culverts.

Through the Heads

This system is the most common and economical, and has been considered in this research. The systems is used for lifts up to $10m$. Valves are placed at the bottom of the gate and baffle plates are placed to reduce the dynamic energy. During the filling of the lock chamber at the upper lock head a wave propagates to the downstream end. At the downstream end the wave is reflected creating an uninodal wave. This results in a change in the hawser forces in value and in direction.

Figure 3.8: Openings at the bottom of the gate for the lock head in Empel (WillemsUnie, 2014)

Through Longitudinal Culverts

When lifts higher than $15m$ are required, the through longitudinal culverts system provides a good solution. The flow is distributed over the length of the lock chamber to create a better flow distribution. Culverts are constructed around the upper lock head. At the end of the culverts, stilling chambers are placed to reduce the dynamic energy of the water. The openings of the culverts are distributed over the length of the lock chamber.

3.3.5. Construction Method

The construction method depends on the dimensions of lock head and the area bound parameters being; the soil properties, the workspace available, the groundwater level and the possibilities for drainage.

There are five different construction methods. These five methods are discussed in Appendix B. This thesis will only take into account a construction pit consisting out of a dry cofferdam with an under water concrete (UWC) floor with fundation piles, see Figure 3.9. The sheet piles are placed in an impermeable layer. The UWC floor is secured with foundation piles to prevent the UWC floor from hydraulic bursting. The foundation piles are continued in the floor of the lock head. The area between the sheet piles and the walls of the lock head is filled with sand and has a constant groundwater level.
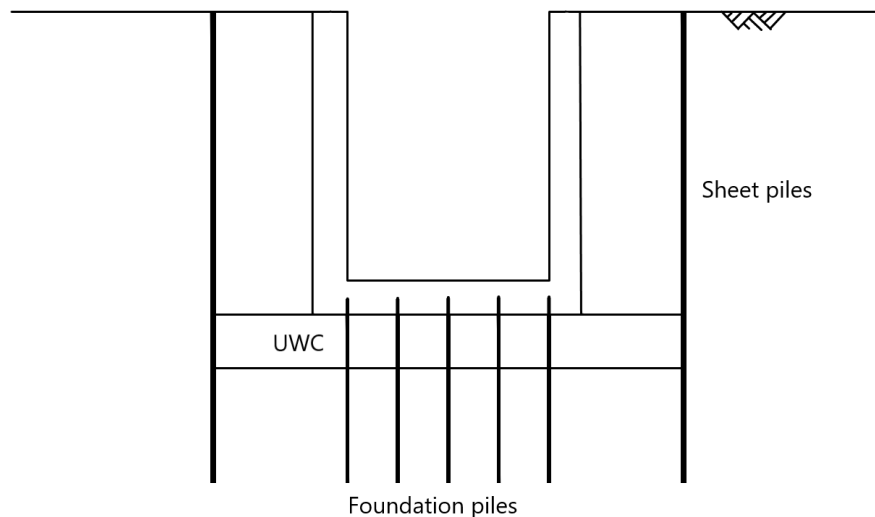
Figure 3.9: A dry cofferdam with sheetpiles, UWC and foundation piles

3.3.6. Functional Requirements

For the functional requirements of lock heads general reference is made to the 'Handboek voor het ontwerpen van Schutsluizen' (*Ontwerp van Schutsluizen*, 2000) and the 'Richtlijnen vaarwegen 2017' (*Richtlijnen vaarwegen 2017*, 2017) by Rijkswaterstaat. The function requirements applicable for lock heads are:

- The lock heads have to enclose the area through which the vessels can easily and safely sail into the lock chamber. The dimension of the lock head depend on the type of vessels entering the lock. A distinction can be made between maritime navigation, inland navigation and recreational navigation. The most common classification is the CEMT (Conference Europeene des Ministres de Transport). Table 3.1 gives the different dimensions. The sections of the lock head, connected to the lock chamber, are used for mooring the vessels during lowering and raising the water level in the lock.

- The lock heads have to provide enough space for vessels to pass the lock heads when the gates are opened and the chance on collision has to be minimised. When the gates are closed, the load on the gates has to be transferred to the lock heads. The connection between the gate and the lock head has to be watertight. Beside the operating systems for the opening and closing of the gate, pivots and trunnions have to be installed for mitre gates and single leaf gates. For lifting gates and rolling gates guiding facilities have to be installed.

- In most cases lock heads are provided with facilities to empty the lock head for maintenance. The lock heads can be emptied with the help of stop logs. For the stop logs, slots are installed into the lock heads. In case the lock head is emptied, the lock head has to be checked on hydraulic bursting.

- In case of a water level difference between the adjacent water bodies of $6m$, the filling and emptying of the chamber has to be done with culverts. The lock heads have to provide space for the filling and emptying systems. In some cases, the upper lock head is equipped with stilling chambers to dissipate the energy of the incoming water.

- When salt and fresh water need to be separated, lock heads have to be accommodated with services to support pneumatic barriers.

- It is not uncommon to construct a movable bridge across a lock head. Most of the time the bridge is constructed across the lower lock head. This is because of the greater head clearance. The bridge can also be constructed across the upper lock head when the lock is located in a tidal area or due to infrastructural requirements.

- The lock has to be able to withstand the forces due to water and soil pressure, operating mechanisms, navigation and land traffic. The navigation loads include the hawser forces and impact from vessels.
  The strength, stability and stiffness of the lock head has to be checked in perpendicular and longitudinal direction.
  The foundation of a lock head can be a shallow foundation or a pile foundation.
  The lock heads have to be rigid to minimise the displacements. Big displacements can hamper the gates and the operating mechanism from working.

- Lock heads need to be soil and watertight. The requirement of water tightness does not apply to chambers with water resistant operating mechanism.

- The surface of lock heads which is exposed to possible damage from passing vessels needs to be executed as smooth as possible. Sharp corners need to be smoothed and provided with steel protection. The concrete cover of the lock heads is thicker to protect the reinforcement after collision with a vessel.

- The difference of settlements between the lock head and lock chamber, each having a different stiffness, can not result in big risks.

- Mooring facilities need to be installed for vessels in case of installation, reparation and maintenance of the lock gates.

- In case the lock chamber is permeable, piping becomes a specific requirement for lock heads. Cut-off screens are installed at the location of the lock heads.

- The navigation lock may be part of a coastal defense or flood protection system. This has an influence on the top of structure level and the decision to apply a back-up gate.

- The distance between the gate recess and the beginning of the lock chamber is $1m$ for mitre gates CEMT classes I & II. For the rest of the classes this distance is $2m$. For a single leaf gate this distance is always $2m$. The distance can be bigger, depending on the type of filling and emptying system.

- The hawsers are placed in a vertical row with a minimal distance of $1.5m$. The lowest hawser is placed $1.5m$ above the lowest water level, but minimal $1.75m$ above the minimum schutpeil. The highest hawser is placed as close to the top of the lock head as possible.

- The gates need to be protected against collisions with vessels. The gates are expensive in construction and maintenance and have a big influence on the design of the lock heads.

4

Lock Head Empel

The navigation lock in Empel is located in the Maximakanaal. Both the navigation lock and the Maximakanaal are constructed in 2014. The Maximakanaal is a canal between the Maas and the Zuid-Willemsvaart. The Maximakanaal is constructed to redirect vessels on the Zuid-Willemsvaart. The Zuid-Willemsvaart is part of the main navigation routes in the Netherlands. This means that it should be able to handle vessels of CEMT class IV. However, the Zuid-Willemsvaart passes the city center of 's-Hertogenbosch. At this location the Zuid-Willemsvaart is only able to handle vessels of CEMT class II. By constructing the Maximakanaal bigger vessel are able to use the waterway between the Maas and Veghel. In the Maximakanaal two navigation locks are constructed, being the navigation lock in Empel and the navigation lock in Hintham. An overview of the situation is given in Figure 4.2.

The navigation lock in Empel is located at the side of the Maas. The water level on the Maas fluctuates between $-0.50 mNAP$ and $+4.40 mNAP$. The water level in the Maximakanaal is constant at a water level of $2 mNAP$. The navigation lock has to retain water in both direction due to the fluctuating water level on the Maas. The gates installed in the lock heads are single leaf gates. The leaf gates can retain water in both directions. The navigation lock in Hintham has to retain water in one direction and is equipped with mitre gates.

The navigation lock in Empel has two functions, these are ship passage and water retention. The lock is designed for ships of CEMT class IV. The lock is able to process one vessel of CEMT class IV within 10 minutes. The lock is part of dijkring 36 which has a probability of exceeding of 1/1250 years.

The navigation lock in Empel, as well as the navigation lock in Hintham, are passed by 9292 vessels per year for commercial shipping and 2023 vessels per year for recreational boating (*Deelrapportage Vaarwegen voor de Nationale Markt- en Capaciteitsanalyse (NMCA)*, 2017). These numbers are small relative to other navigation locks in the Netherlands that are part of the main navigation routes, see Appendix C. The lifetime of the lock heads and the lock chamber is 100 years.

In the remainder of this chapter the structural design of the upper lock head in Empel will be discussed.

Figure 4.1: Navigation Lock Head Empel (Rijkswaterstaat, 2015)
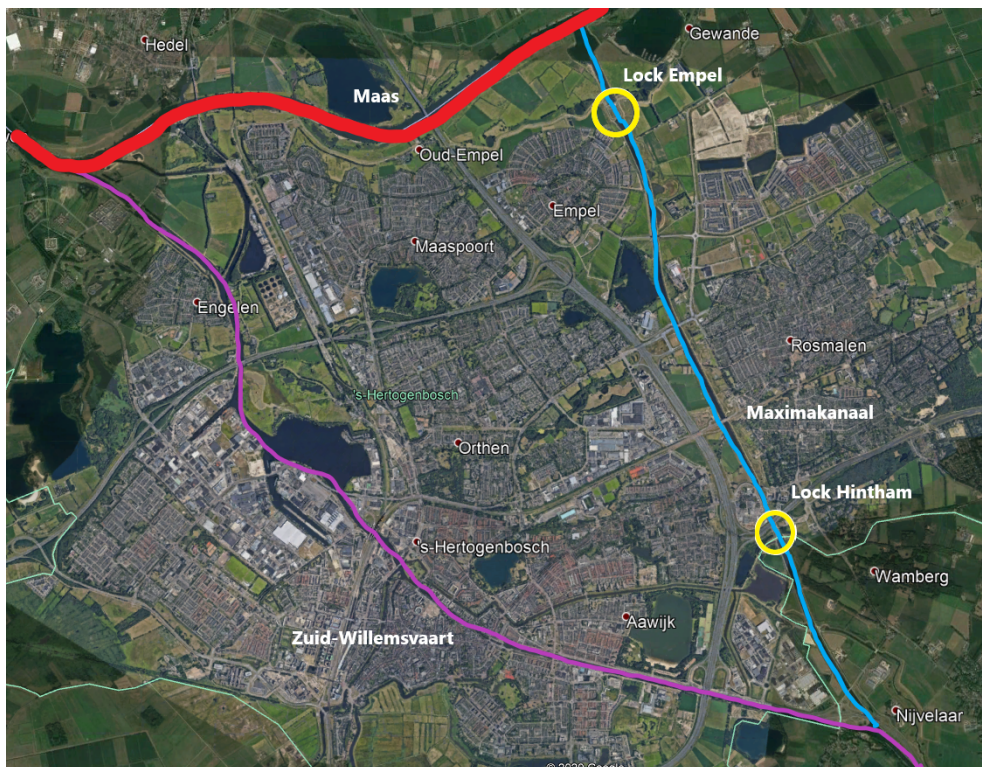
Figure 4.2: Overview of the situation (GoogleMaps, 2019)

4.1. Geometry

The dimensions of the northern lock head are given in Figure 4.3, 4.4 & 4.5. The top of the lock head is at $+8.18mNAP$. The top of the lock chamber is at $+5.90mNAP$. An earth-retaining wall is placed at the transition between the lock head and the lock chamber. The top of the floor is at $-4.60mNAP$. The floor is $2.0m$ thick. The floor is constructed on top of underwater concrete with a thickness of

$2.1m$. The concrete floor and the underwater concrete are connected to sheet piles and GEWI piles. The sheet piles are installed from $+5.0mNAP$ to $-13.5mNAP$. The area between the walls of the lock head and the sheet piles is filled with sand. The groundwater level between the walls of the lock head and the sheet piles is constant at a height of $+5.0mNAP$. The groundwater level outside the cofferdam fluctuates between $+6.68mNAP$ and $-0.50mNAP$.
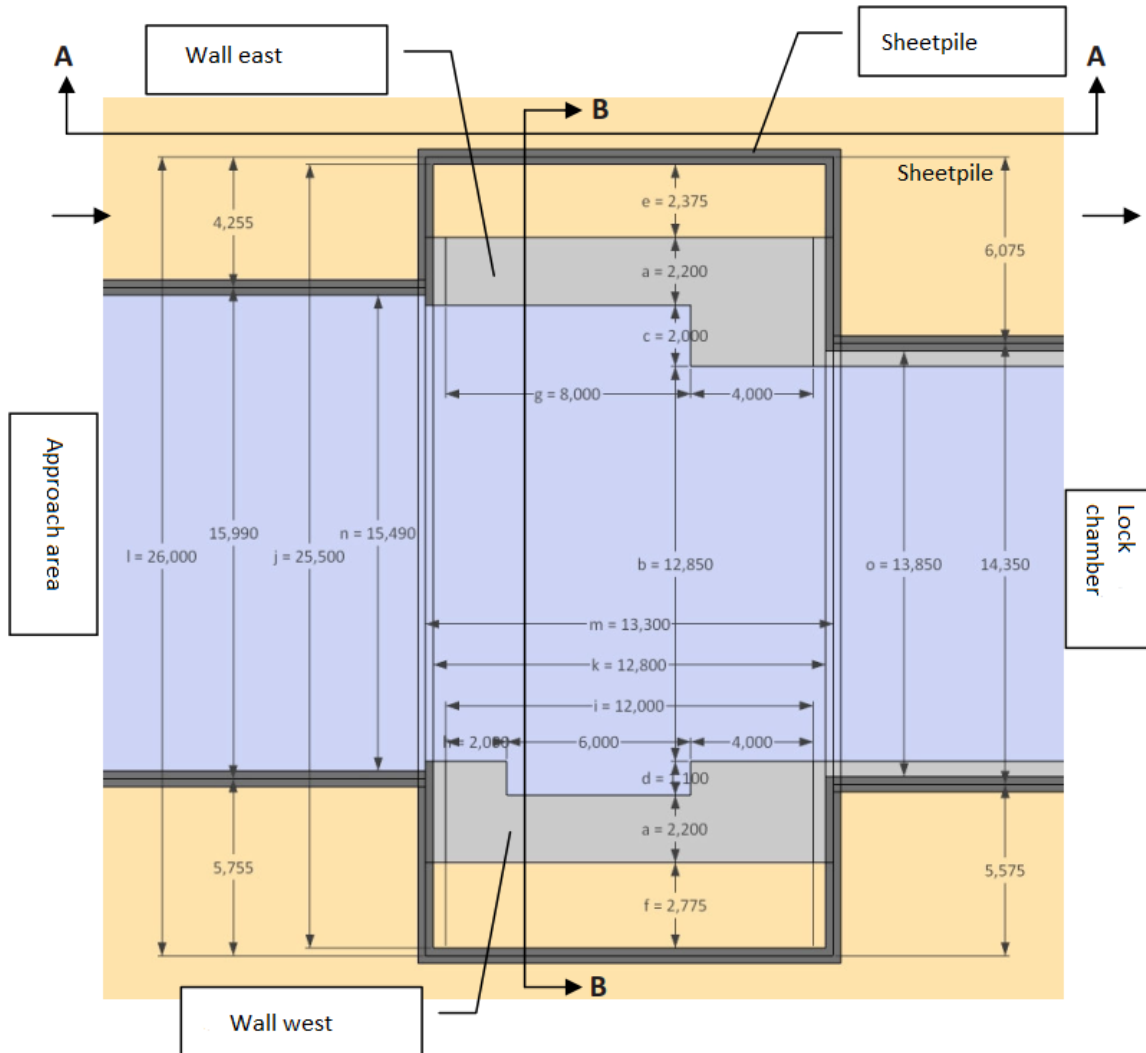
Figure 4.3: Top view northern lock head
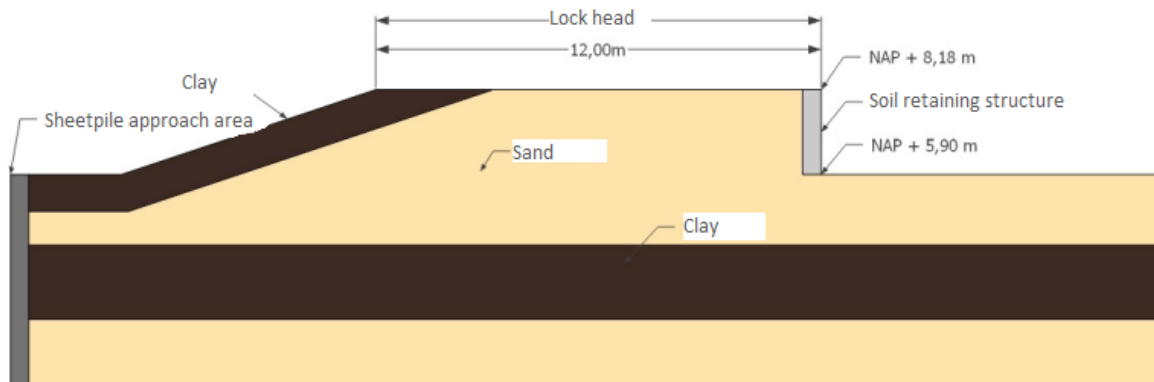
Figure 4.4: Cross section A-A
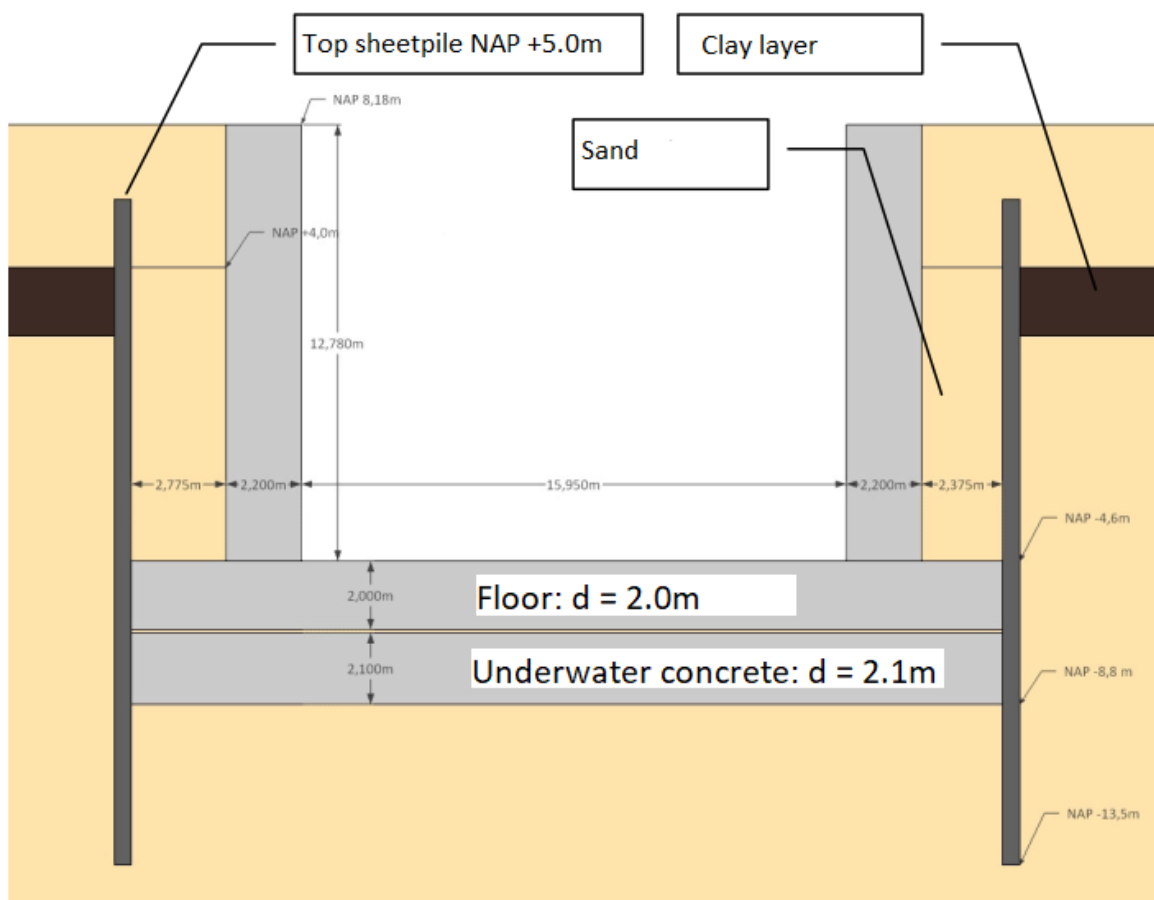
Figure 4.5: Cross section B-B

4.2. Applied Materials

The concrete class applied in the structure is C28/35. The Miliueklassen to be used according to EN 1992-1-1 are XC4 and XF3 for the floor. For the wall up to $+2.30 mNAP$ XC4, XD3 and XF2 have to be used. Above $+2.30 mNAP$ XC4, XD3 and XF4 have to be used.
The reinforcement in the concrete is FeB500.

4.3. Soil Properties

The properties of the soil are given in table 4.1. The area between the wall and sheet pile is filled with sand.

Table 4.1: Soil structure lock head north

Top of layer [mNAP]	Bottom of layer [mNAP]	Soil layer	γ_{dry} [kN/m^3]	γ_{nat} [kN/m^3]	ϕ'_{rep} [°]	c'_{rep} [kN/m^2]
5.9	4.0	Sand	18	20	30	0
4.0	3.0	Clay, brown	18.5	18.5	25	4
3.0	2.0	Clay, grey	17	17	20.5	5
2.0	-9.0	Sand, loose	17	19	30	0
-9.0	-9.75	Clay, deep	18	18	25	5
-9.75	-13.0	Sand, moderate	18	20	32.5	0
-13.0	-14.0	Clay, deep	18	18	25	5
-14.0	max	Sand, moderate	18	20	32.5	0

4.4. Water Levels & Groundwater Levels

Volkerwessel Infra Competence Centre has defined various (ground)water levels. The most important ones are MHW and droogzetten. The different situations and their corresponding (ground)water levels are given in Table 4.2 & 4.3.

Table 4.2: Groundwater levels

Groundwater level	$mNAP$
MHW	+6.68
max schutten	+3.93
min schutten	-0.01
MLW	-0.33
Calamiteit Berlicum	+0.19
Calamiteit Empel	-0.50
GHG	+2.10
GG	+1.65
GLG	+1.35
droogzetten	+1.84

Table 4.3: Water levels

Water level	$mNAP$
MHW-calamiteit	+8.28
MHW	+7.83
max schutpeil	+4.40
kanaalpeil-calamiteit	+3.00
kanaalpeil	+2.00
min schutpeil	-0.50
MLW	-0.90

4.5. Foundation

The lock head is founded on a shallow foundation, sheet piles and GEWI piles. Sheet piles are installed from $5mNAP$ to $-13.5mNAP$. The soil is excavated to a depth of $-8.8mNAP$. GEWI piles are drilled into the soil. GEWI piles are anchors needed during the construction to prevent the floor of the lock

head from hydraulic bursting. During the operational phase the GEWI piles act as foundation piles. The piles have a diameter of $63.5mm$. The pile configuration is 4x7. 4 piles parallel to the navigation lock with a center to center distance of $3.25m$ and 7 piles perpendicular to the navigation lock with a center to center distance of $2.40m$, see Figure 4.6. Underwater concrete with a thickness of $2.10m$ is poured at the bottom of the cofferdam. Hereafter, the water is pumped out of the cofferdam to create a dry working space. On top of the underwater concrete a sand layer of $0.1m$ is placed to account for unevenness of the UWC floor. The sheet piles, GEWI piles and the underwater concrete are part of the final structure.
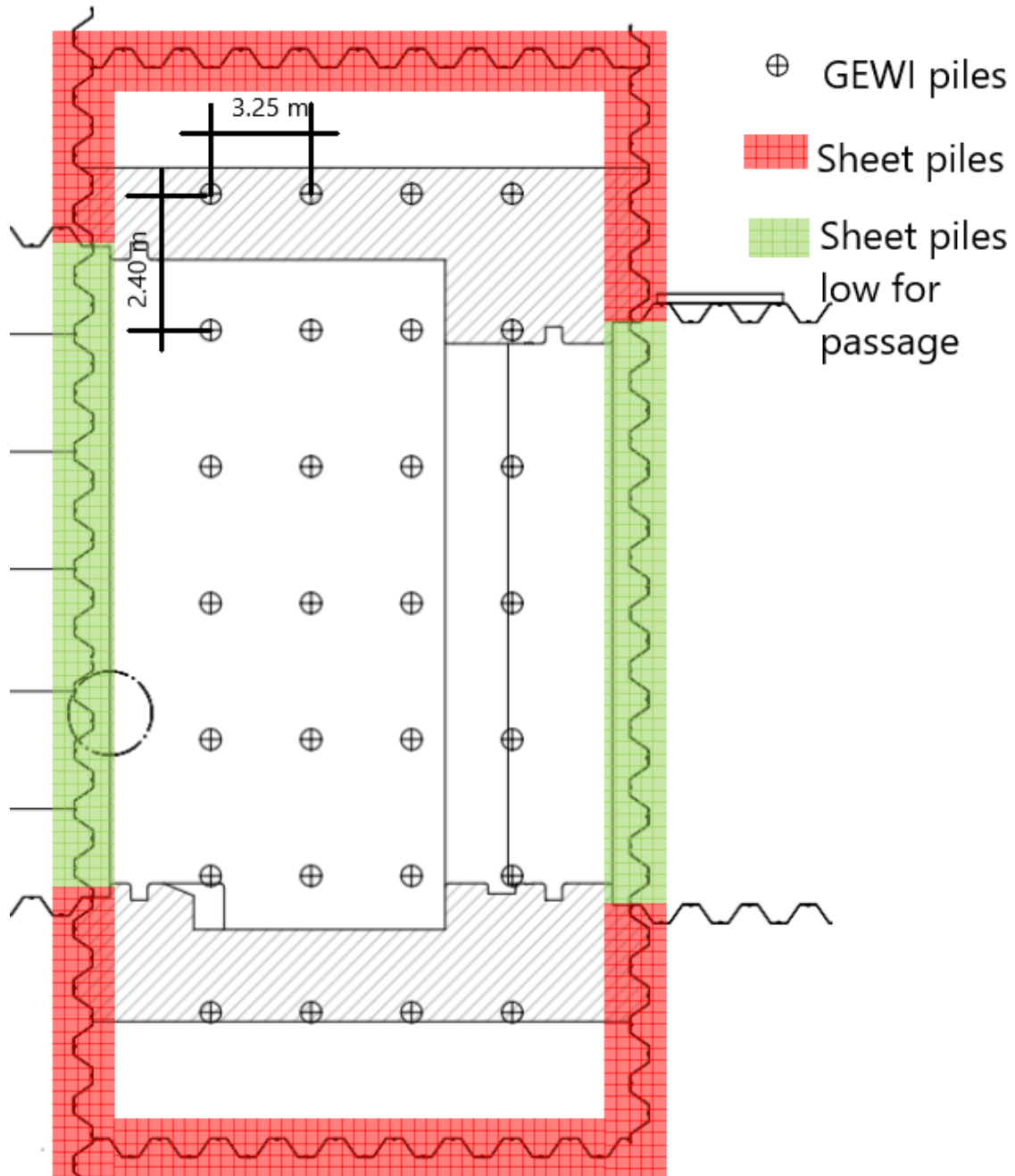
Figure 4.6: Foundation lock head Empel

4.6. Horizontal Bearing Capacity

In case the water level of the Maas is higher than the water level of the Maximakanaal, the horizontal bearing capacity of the lock head is provided by the friction between the walls of the lock head and the soil, the UWC floor of the lock chamber and the soil and the walls of the lock chamber at the location of the UWC floor and the soil, see Figures 4.7 & 4.8.

In case the water level of the Maas is lower than the water level of the Maximakanaal, the horizontal bearing capacity is only provided by the friction between the walls of the lock head and the soil.
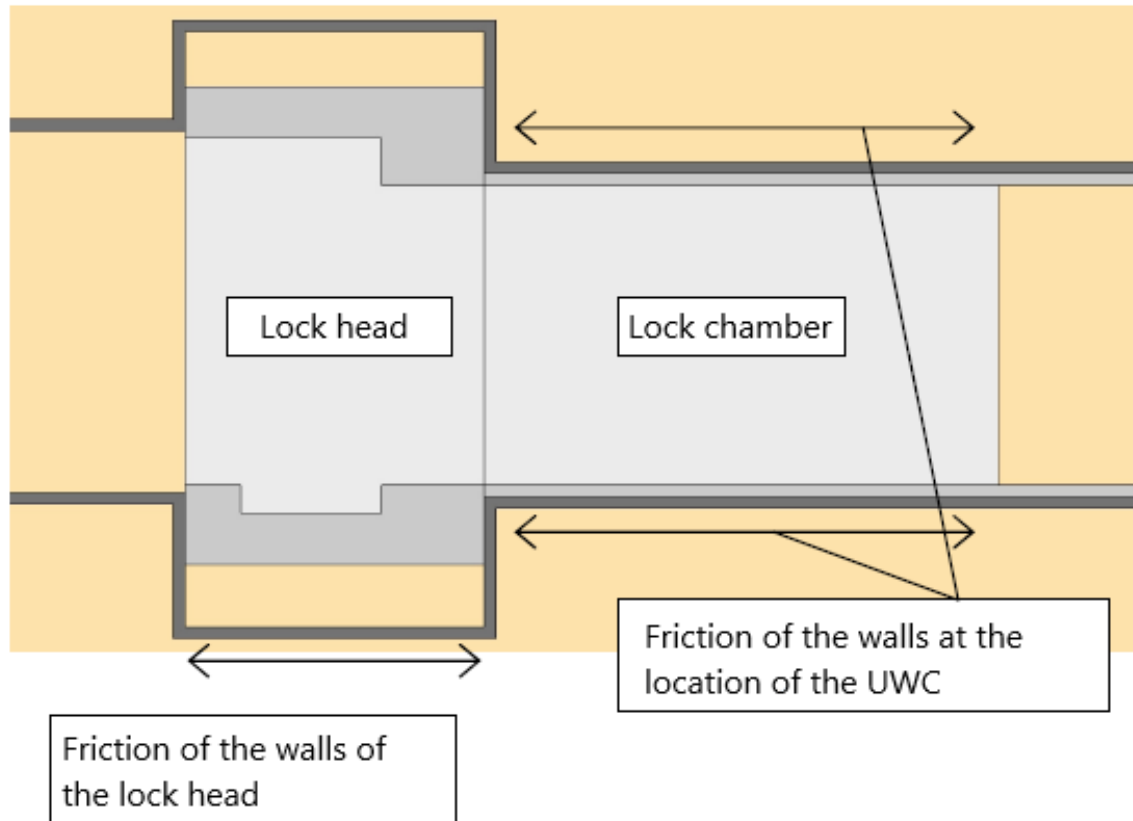
Figure 4.7: Horizontal bearing capacity top view
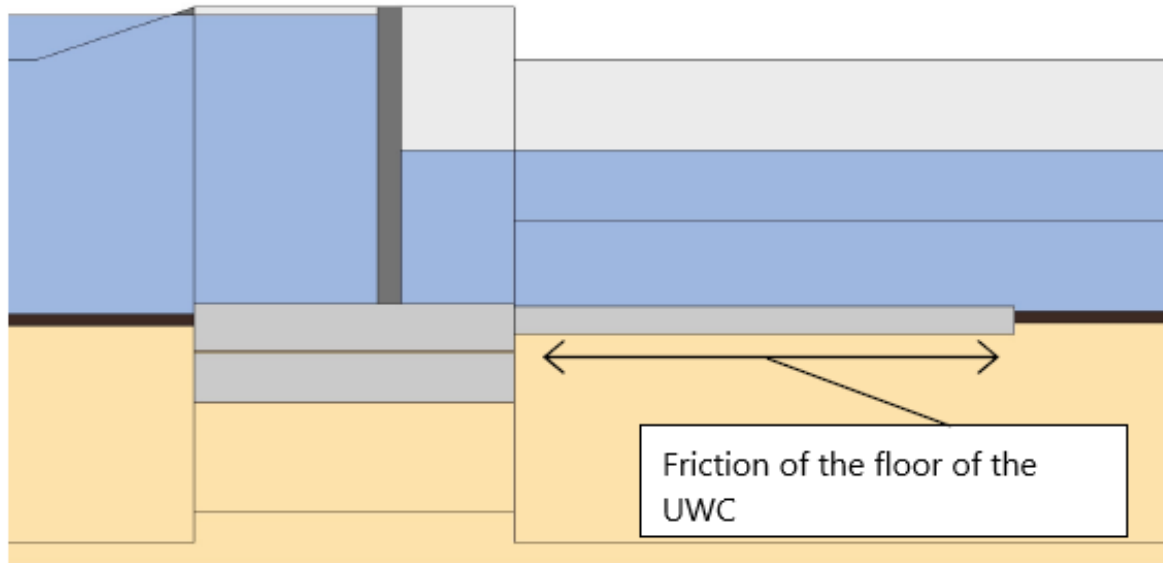
Figure 4.8: Horizontal bearing capacity side view

4.7. Load Cases

The loads acting on the lock head are permanent loads and live loads and are further divided in different load cases. For the calculations of the load cases, see Appendix C

4.7.1. Permanent Loads

- LC1, LC1c and LC2: Own weight concrete structure

- LC1a and LC1b: Own weight gate
  The steel gate has a weight of $850kN$. The load on the trunnion and the neck in x and y direction are respectively $605kN$ and $-605kN$. The door is modelled in open (LC1a) and in closed (LC1b) condition. The load of the door is not combined with the load of a crane.

- LC3: Underwater concrete
  Underwater concrete has a volumetric weight of $23kN/m^3$.

- LC4 and LC5: Soil and water pressure perpendicular to the walls of the lock head
  The soil between the sheet piles and the walls exists of sand. The groundwater level is constant at a level of $+5.0mNAP$.

- LC7, LC8, LC11 and LC12: Soil and water pressure in parallel direction of the navigation lock at the approach are and the lock chamber
  The width of the lock head under influence of the soil pressure at the approach area is $4.255m$ at the eastern wall and $5.755m$ at the western wall. The width at the lock chamber is $6.075m$ at the eastern wall and $5.575m$ at the western wall, see Figure 4.3. The ground level at the location of the lock chamber is $+5.9mNAP$. The ground level at the lock head is $+8.18mNAP$ and decreases under a slope towards the waiting berths to $+5.9mNAP$, see Figure 4.4. The ground level has been averaged to $+7.0mNAP$ for the calculation of the soil pressure at northern part of the lock head. LC7 and LC8 take into account the soil and water pressure at the northern side of the lock head. LC11 and LC12 take the soil and water pressure at southern end of the lock head in to account.

4.7.2. Live Loads

- LC6: Water pressure under the floor
  The water level in the navigation lock fluctuates. The different water levels are shown in Table

4.2. The bottom of the floor is at $-6.60mNAP$.

- LC15: Difference in water pressure due to different water levels
  A water level of MHW at the approach area and 'kanaalpeil' in the chamber is normative for horizontal equilibrium, see Table 4.3.

- LC16: Free water board (LC16)
  The top of the floor is located at $-4.60mNAP$. The sill is the separation line between the water level in the chamber and the water level at the side of the approach area. The difference in water level causes a moment around the y-axis.

- LC9, LC10, LC13 and LC14: Soil and water pressure at the approach area and the lock chamber MHW
  The pressure differences are calculated in comparison with LC7, LC8, LC11 and LC12. Due to a water level of MHW, the water on top of the watertight clay layer at $+2.0mNAP$ introduces a distributed load. The groundwater table during MHW at the approach area of the lock head is $+6.77mNAP$. The ground water table at the lock chamber is $+6.60mNAP$.

- LC17: Wave loads
  The wave loads are calculated according to Goda-Takahashi. The wave loads for different water levels in the Maas and their respective point of gravity are given in Table 4.4. The given loads act in the direction from the Maas on to the northern lock head.

Table 4.4: Wave loads

Water level $[mNAP]$	$F_{h,rep}$ $[kN/m]$	z_c $[mNAP]$
-0.90	7.7	-2.00
-0.50	12.1	-1.65
-0.28	13.2	-1.49
2.00	27.0	0.17
4.40	39.9	1.80
5.86	45.9	2.81
7.83	50.0	3.74

The wave load acting from the canal on the lock head is $F_h, rep = 11.6kN/m$. The point of gravity is $z_c = 0.83mNAP$.

- LC18: Traffic loads
  Traffic causes a horizontal load on the lock head. A distributed load of $20kN/m^2$ is taken into account. This load is situated at the eastern and western part of the lock head (LC18a and LC18b). During construction and maintenance the load due to a crane on the eastern part of the lock head has to be taken into account (LC18c). LC18c and LC18a can not act on the lock head at the same time. The type of crane is a Liebherr LTM 1500-8.1. The maximum force on the outrigger plates is $1730kN$. Sand has an soil stress friction angle of $30°$. This results in a lateral earth pressure of 0.5 at rest. The horizontal force becomes $865kN$ and acts at a distance of $3.81m$ below the top of the structure.

- LC19: Temperature loads

- LC21: Mooring forces (LC21)
  The mooring force is 200 kN. The most unfavourable condition is a mooring force is combination with an empty lock head. The mooring force acts at $NAP + 3.55m$.

- LC22: Ice loads (LC22)
  The ice loads act on the doors and perpendicular to the lock head at a water level of minimum schutpeil and maximum schutpeil, see Table 4.3. The horizontal component is $50kN/m$ and the vertical component is $10kN/m$.

4.8. Load Combinations

Different load combinations are being considered for horizontal equilibrium, strength calculations and displacements. Eight load combinations exist for horizontal equilibrium, twelve for strength calculations and eight for displacements, see Appendix C. The abbreviations used are E (empty lock head), GW (groundwater), G (gate), T (traffic) and C (crane).

4.8.1. Strength

The normative load combinations for strength calculations are:

- SLS MHW2; A water level of the Maas of $7.83mNAP$ and a water level of the canal of $7.83mNAP$ in combination with a minimum soil pressure.

- ULS MHW1; A water level of the Maas of $7.83mNAP$ and a water level of the canal of $2.00mNAP$ in combination with a minimum soil pressure.

- ULS MHW2; A water level of the Maas of $7.83mNAP$ and a water level of the canal of $7.83mNAP$ in combination with a minimum soil pressure.

- ULS MHW3; A water level of the Maas of $7.83mNAP$ and a water level of the canal of $2.00mNAP$ in combination with a maximum soil pressure.

- SLS E3; Low soil pressure and high groundwater pressure for the maximum moment at the centre line of the floor.

- ULS E1; High soil pressure and traffic loads for the maximum moment at the eastern wall.

- ULS E2; High soil pressure and traffic loads for the maximum moment at the western wall.

- ULS E3; Low soil pressure and high groundwater pressure for the maximum moment at the centre line of the floor.

4.8.2. Displacements

The normative load combinations for displacements are:

- SLS E + min GW + G + T; A minimum groundwater level of $0.17mNAP$ with traffic loads acting on the walls and a closed gate.

- SLS E + min GW + C; A minimum groundwater level of $0.17mNAP$ with traffic loads acting on the western wall and a crane load acting on the eastern wall.

- SLS MHW2; A water level of the Maas of $7.83mNAP$ and a water level of the canal of $7.83mNAP$, the gate is open.

4.9. Results

The walls of the lock head have varying thicknesses over the length. The thicknesses are $2.20m$, $3.30m$ and $4.20m$. The concrete class used for the walls is C28/35. The concrete cover at the sides in contact with the soil is $50mm$ thick. The concrete cover at the sides in contact with the water are $60mm$ thick, of which $10mm$ is due to protection against possible collisions with ships. Reinforcement is placed in horizontal and in vertical direction. The following reinforcement is applied at the eastern wall; $\phi25 - 100 + \phi20 - 100$ at the soil side and $\phi25 - 200$ at the water side, both in vertical direction (Figure 4.9). In horizontal direction the reinforcement is $\phi25 - 140$ or $\phi20 - 90$. The reinforcement at the western wall is as follows; $\phi25 - 100 + \phi20 - 100$ at the soil side and $\phi25 - 200$ at the water side, both in vertical direction (Figure 4.10). The horizontal reinforcement is $\phi25 - 140$. The floor has a thickness of $2m$. The concrete class is C28/35. The concrete cover at the bottom is $50mm$. The concrete cover at the bottom is $60mm$. Reinforcement is placed parallel and perpendicular to the axis of the navigation lock. The reinforcement at the top of the floor is $\phi25 - 200 + \phi16 - 200$. The reinforcement at the bottom is $\phi25 - 100 + \phi20 - 100$, see Figure 4.11. The shear reinforcement in the floor is $\phi16 - 400/500$.
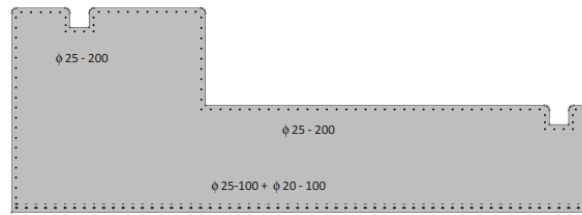
Figure 4.9: Reinforcement eastern wall
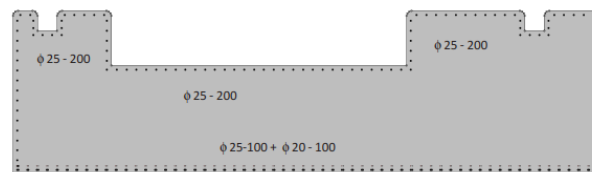
Figure 4.10: Reinforcement western wall
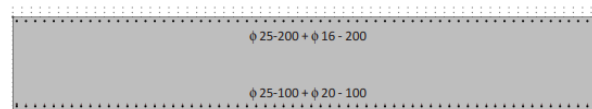
Figure 4.11: Reinforcement floor

4.10. MKI

The total MKI-value of the lock head north is €56372, −. The program DuboCalc is used to calculate the MKI. The MKI value of the lock head north has been calculated based on the amount of concrete, reinforcement, UWC floor and GEWI piles. These materials will be analysed in the remainder of the research.

As was mentioned before the concrete class used for the lock head is $C28/35$. However, $C28/35$ is replaced for $C30/37$, since $C28/35$ is not produced anymore. The lifetime of the structure is 100 years and the MKI is performed from cradle to grave.

4.11. Cost

The total cost of the lock head based on only concrete, reinforcement, UWC and GEWI piles is €419209, −. The cost calculations are based on values used by Van Hattum en Blankevoort. The values include the cost of the materials and the processing cost. The values have been increased with 5% to represent a more accurate value in the current economy.

4.12. Discussion

By studying the lock head in Empel, three design decision made by Volkerwessels Infra Competence Centre stand out. These are the configuration of the lock head, the horizontal bearing capacity of the lock head and the UWC floor of the lock head. The decisions will be discussed in the following section.

4.12.1. Lock Head Configuration

The lock head configuration of Empel with a single leaf gate differs from a lock head configuration prescribed by the 'Handboek voor het Ontwerpen van Schutsluizen' (*Ontwerp van Schutsluizen*, 2000). The difference in configuration is displayed in Figure 4.12. The red part above the horizontal line in Figure 4.12 is missing in Empel. The length of the lock head in Empel is approximately 40% shorter than a single leaf gate designed according to the rules prescribed by the 'Handboek voor het Ontwerpen van Schutsluizen.

The gate extends the length of the lock head in open position. The 'Handboek voor het Ontwerpen

van Schutsluizen' (*Ontwerp van Schutsluizen*, 2000) states that the gate should fully disappear in the gate chamber in open position to provide a safe passage of a vessel while the gate is protected against collisions with vessels. The gate in Empel is protected by wooden guideworks which are placed in front of the lock head, see Figure 4.13.
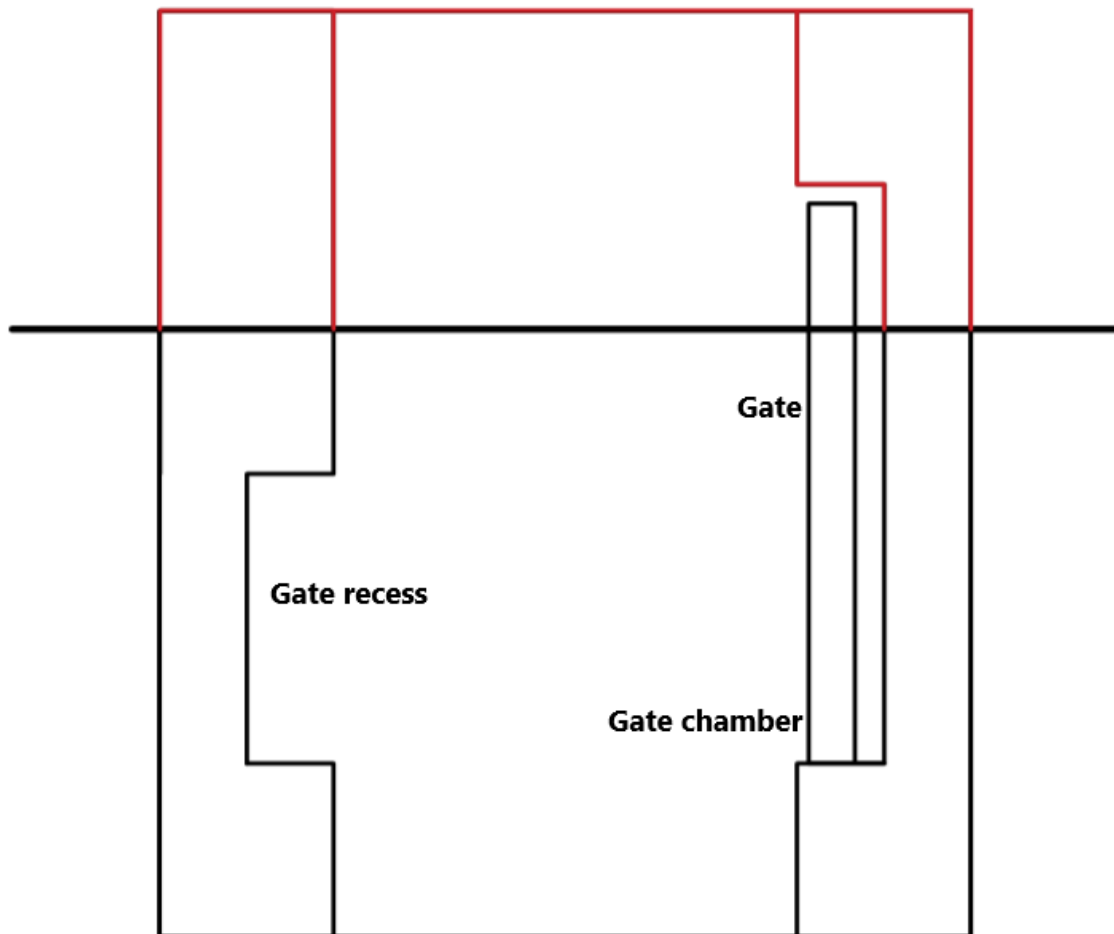
Figure 4.12: Difference in lock lay out between Empel and a standard lock head with a single leaf gate
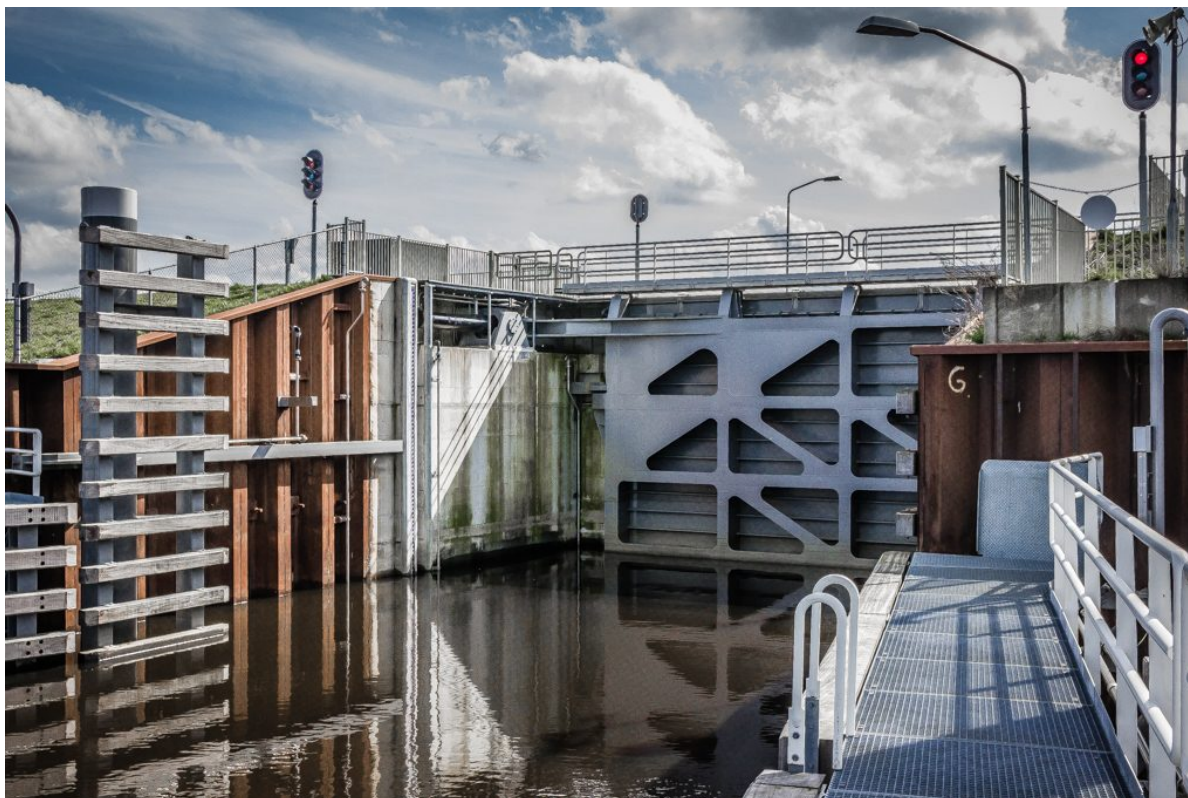
Figure 4.13: Protection of the Gate by Wooden Guideworks (Ropstar, 2016)

4.12.2. Horizontal Bearing Capacity

The 'Handboek voor het Ontwerpen van Schutsluizen' (*Ontwerp van Schutsluizen*, 2000) states that the lock head itself has to be able to generate enough friction to prevent horizontal bearing failure. However, the lock head in Empel derives part of the horizontal bearing capacity from the lock chamber. Besides the friction between the floor of the lock head and the soil has been neglected. Therefore the horizontal bearing capacity of the lock head in Empel is independent of the weight of the lock head. By incorporating the lock chamber in the design of the horizontal bearing capacity calculations, a more cost effective design is achieved.

In Appendix C the horizontal bearing capacity of the lock head is calculated, based on the rules prescribed by the 'Handboek voor het Ontwerpen van Schutsluizen'. From the calculations it follows that the lock head in Empel does not suffice. However if the lock head would be designed according to the design rules in the 'Handboek voor het Ontwerpen van Schutsluizen' (Figure 4.12), the lock head suffices. This is due to an increase in length, generating more friction between the walls and the soil. In reality the upper lock head is always supported by the lock chamber and is therefore not likely to fail due to horizontal bearing capacity. This is also stated by the 'Handboek voor het Ontwerpen van Schutsluizen' (*Ontwerp van Schutsluizen*, 2000). The lower lock head however is not supported by the lock chamber. To provide enough horizontal bearing capacity for the lower lock head in Empel an UWC floor has been placed in the approach area.

4.12.3. UWC Floor

Another interesting aspect of the lock head in Empel is the thickness of the UWC floor. In common engineering practice the UWC has a thickness of around $1.2m$ and the centre to centre distance of the GEWI piles is around $2m$. The question arises why the UWC floor for Empel deviates from this. According to the calculations both configurations suffice, see Appendix C. The configuration applied in Empel is 0.2% more expensive, this difference can be neglected. An increase in thickness however gives more certainty against leakage.

5

Problem Definition

5.1. Problem Statement & Objective

Sustainability is a hot topic. Countries all over the world have signed the Agreement of Paris (*The Paris Agreement*, 2015) to reduce the global warming and to reduce the emission of greenhouse gasses. The Dutch government has composed its own agreement to meet the goals of The Agreement of Paris, the Klimaatakkoord (*Klimaatakkoord*, 2019). Agreements that arise from the Klimaatakkoord and are applicable to the construction industry are the Betonakkoord (*Betonakkoord*, 2018) and Nederland Circulair in 2050 (CirculaireEconomie, 2016).

One of the main materials contractors use is concrete. During the production and transportation of concrete 9.5% of CO_2 is emitted into atmosphere (Olivier et al., 2014).

The main construction material of lock heads is concrete. Lock heads are big and bulky structures since they have to resist big forces, displacements have to be minimal and global stability checks have to be met. The objective of this research is to find out if it possible to increase the sustainability of lock heads. The northern lock head of Empel will be used as a case study during the research.

The main research question is: *How can the design of lock heads be optimised to increase the sustainability?*

To derive the answer to the main research questions, the following sub-question have to be answered:

- How can sustainability be measured?

- What are new possible options to make lock heads more sustainable, what is/are the best option(s) and how do they compare to the original design of a lock head?

5.2. Methodology

To answer the main research question, the sub-questions first have to be answered. The sub question *How can sustainability be measured?* has already been answered in the introduction. The sub-question *What are new possible options to make lock heads more sustainable, what is/are the best option(s) and how do they compare to original design of a lock head?* will be answered in the preliminary study. Different alternatives will be implemented to the lock head in Empel. Strength, stiffness, stability, cost and MKI calculations will be performed to check the feasibility of each alternative.

The results of the preliminary study determine the path of the advanced analysis. The alternatives proposed in the preliminary study will be further elaborated in the advanced analysis of the research in case they are promising. The alternatives will be neglected in case they show no real potential to increase the sustainability, while taking the cost into account. In this case the following sub question will be answered:

How can the sustainability of lock heads increase based on well known design rules?

For this purpose a parametric model will be made in the advanced analysis. The parametric model will be based on the current design rules for lock heads according to the 'Handboek voor het ontwerpen van schutsluizen' (*Ontwerp van Schutsluizen*, 2000) and the 'Richtlijnen Vaarwegen 2017' (*Richtlijnen vaarwegen 2017*, 2017). The case lock head Empel will be used as a reference project to validate the parametric model.

5.3. Project Scope

This research will only take into account the upper lock head. Other parts of the navigation lock are not taken into consideration. The type of lock head is a standard U-shaped lock head build in-situ. The study only considers inland navigation locks with single leaf gates or mitre gates. The construction material will be concrete. Two types of foundations will be considered, a shallow foundation and a pile foundation. The parametric model only takes into account the normative load cases based on the northern lock head in Empel. The construction method of the lock head taken into consideration is a cofferdam with sheet piles, UWC and foundation piles to prevent hydraulic bursting during the construction phase.

6

Alternatives Lock Head Design

The chapter will start with an idea generation based on knowledge from Chapters 2 & 3 and innovations that have been applied in the working field. Three different constructive principles follow from the idea generation. The constructive alternatives are Inhomogeneous Cross Section, Prestressing and Hollow Sections. With the term inhomogeneous cross section, a reference is made to a cross section consisting of different concrete classes, see Figure 6.3.

To see whether the proposed solutions will work in reality, they have been implemented to a real case, being the northern lock head in Empel. The results of the calculations are shown in this chapter. The detailed calculations can be found in Appendix D. Cross section calculations have been performed for the floor under the eastern wall, see Figure 6.1.

To get an indication of the displacements, the total structure has to be considered. The displacements for the load combination SLS DZ1 (Chapter 4) are shown in Figure 6.2.

Cost and MKI calculations have been performed for each alternative per m. The calculations take into account the material cost and labour cost. The MKI value has been multiplied with a factor of 0.2 to make a fair comparison between the cost and the MKI (*Duurzaam GWW aanbesteden*, 2019).
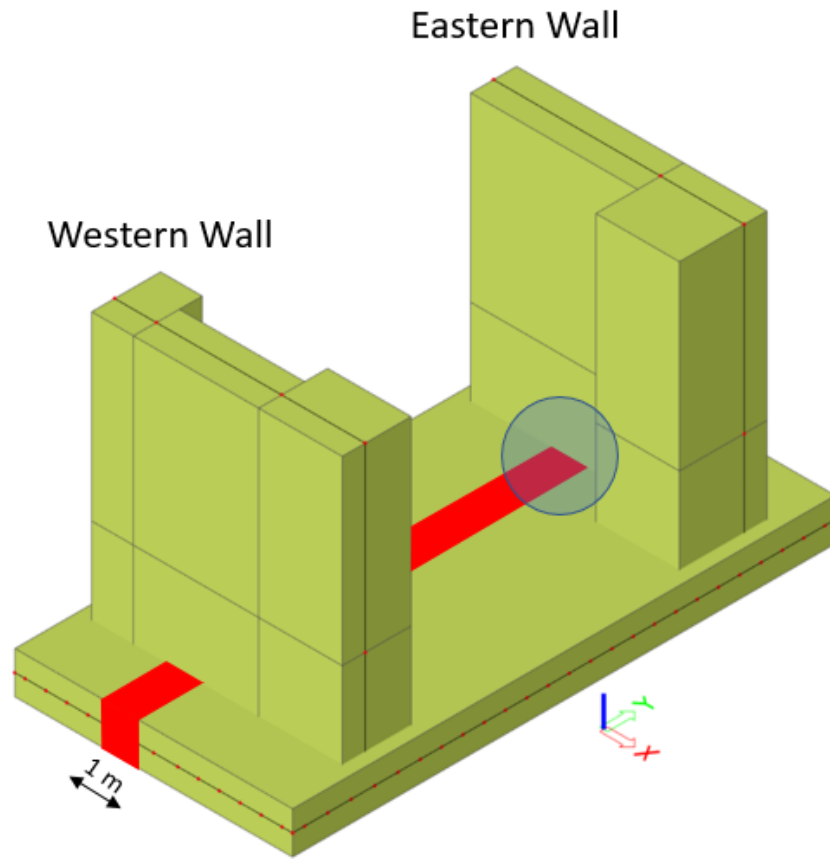
Figure 6.1: Location of the cross section calculations
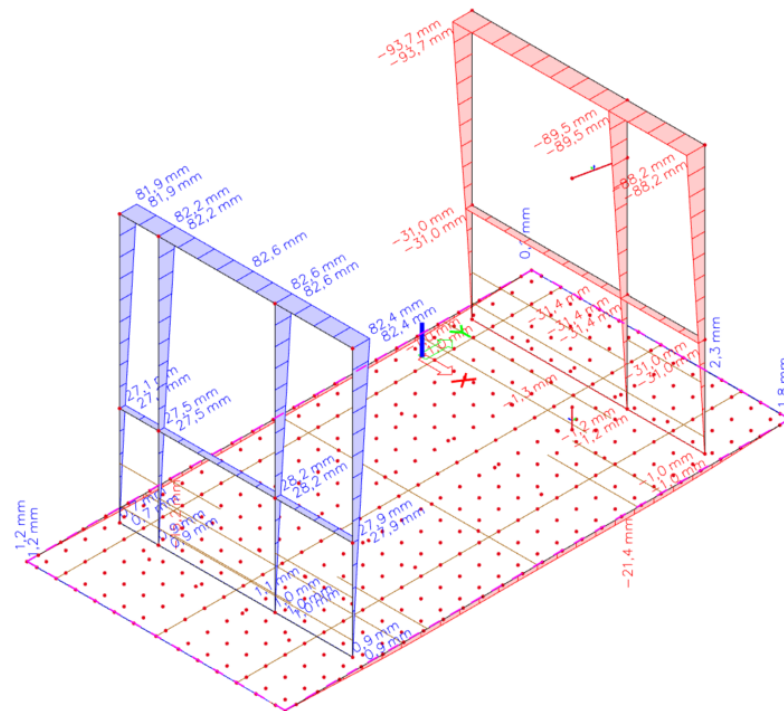
Figure 6.2: Displacements original lock head Empel, BGT DZ1

6.1. Idea Generation

The first step in the research is to generate ideas. To come up with ideas and to learn more about innovations in the field of lock design, the PIANC: Innovation in Navigation Lock Design - 2009 (PIANC, 2009) has been studied. Some important innovations can be found in Appendix D. The information from Chapter 2 and the design principles from Chapters 3 are taken into account during the idea generation.

Cement is the most contributing factor of concrete to the high MKI value. This is due to the burning at high temperatures of raw materials into clinkers and the carbonation. The strength and durability of concrete is determined by the water cement ratio. The lower the water cement ratio the higher the concrete strength. A high concrete strength class therefore uses more cement. The idea is to use less cement in the cross section by applying the higher strength concrete at the outside of the cross section for strength and durability reasons and to use a lower strength concrete in the core of the cross section. The MKI of different concrete classes are shown in Table 6.1. What stands out is the difference in MKI between $CEMI$ and $CEMIII$. This is due to the higher clinker content in $CEMI$. The clinker content in $CEMIII$ is much lower due to the addition of blast furnace slag. The blast furnace slag is able to partially replace and take over the function of the Ordinairy Portland Cement (Tsakiridis et al., 2007). The difference in MKI between different concrete classes with the same cement type is much smaller. As was mentioned in Chapter 2, the Dutch contractors mainly use $CEMIII$. Therefore only this cement type is taken into consideration.

Prestressing has already been applied to several offshore structures due to good corrosion resistance and water tightness. By applying prestressing, more slender structures can be realised. This means a saving in concrete use. In general the deformations increase, the more slender the structure becomes. However, when a structure is fully prestressed it shows no cracks under SLS load combinations. Therefore a higher E-modulus can be used for deformation calculations than for non prestressed structures, where it is assumed that cracks have formed under SLS load conditions.

The idea behind the alternative Hollow Sections is to save concrete without losing too much stiffness. Hollow sections are often applied in bridges where own weight plays a dominant role in the design requirements.

6.2. Inhomogeneous Cross Section

The strength of concrete is mainly determined by the water to cement ratio. The lower the water cement ratio, the higher the strength of the concrete. Concrete classes of higher strength have a higher cement ratio and thus a higher MKI value, see Table 6.1.

Table 6.1: MKI different concrete classes

Concrete class	MKI Materials & Processes [€/m^3]	MKI total [€/m^3]
C12/15 CEMI	28.66	38.78
C12/15 CEMIII	18.65	25.77
C20/25 CEMI	31.50	42.50
C20/25 CEMIII	20.20	27.80
C30/37 CEMI	32.19	43.37
C30/37 CEMIII	20.30	27.92
C35/45 CEMIII	20.71	28.48

6.2.1. Setup

The objective is to check whether it is possible to design a lock head constructed out of different concrete classes (Appendix D.2.1). For this purpose the cross section from Figure 6.1 is composed out of two different concrete classes, being $C30/37$ and $C20/25$. The concrete class $C30/37$ is used for the lock head in Empel, the concrete class $C20/25$ is the lowest concrete class used for constructive purposes. The concrete class $C30/37$ is located at the outside of the cross section and has a height of $l_2 = 500mm$. The core of the cross section is made out of $C20/25$ and has a height of $l_1 = 1000mm$.

An overview of the cross section is given in Figure 6.3.
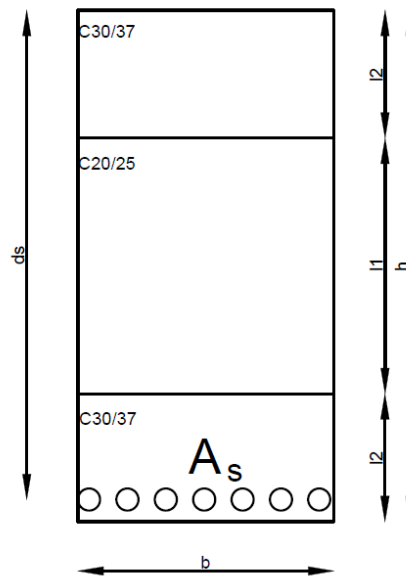
Figure 6.3: Inhomogeneous cross section

6.2.2. Strength Calculations

The cross section is subjected to pure bending. Table 6.2 gives the resulting moments. The cross section is able to resist the maximum moment which occurs in the floor. Figure 6.4 gives the $M - \kappa$ diagram of the inhomogeneous cross section.

No extra shear reinforcement is needed since the amount of shear reinforcement does not depend on the concrete class.

Table 6.2: Moment-Curvature diagram

	M [kNm]	$\kappa * 10^-3$ [m^-1]
Start	0	0
Rupture moment M_r	1435	0.27
Yielding moment M_y	4249	1.64
Stuik moment $M_{c,pl}$	5777	5.48
Ultimate moment M_{Rd}	5852	16.43
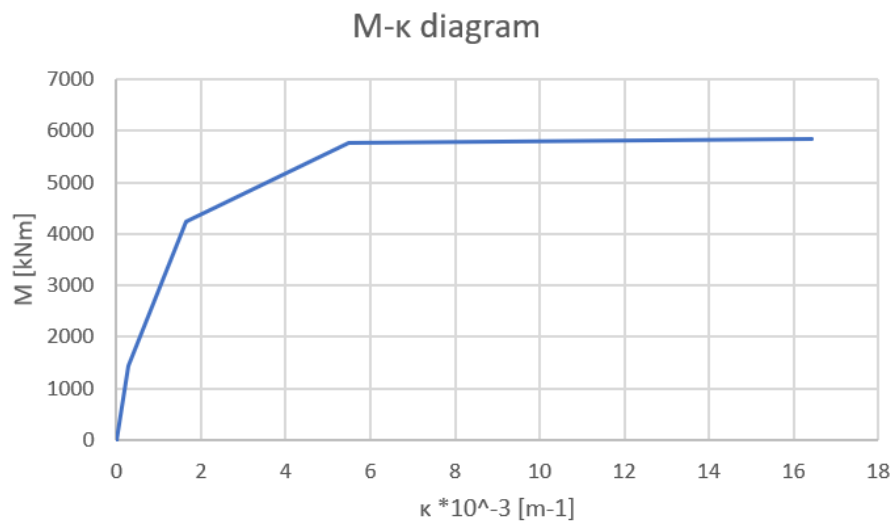
Figure 6.4: Moment Curvature diagram

6.2.3. Stiffness Calculations

The original displacement of lock head Empel are shown in Figure 6.2. The same model will be used to calculate the displacements, but now the concrete class of the structure has been changed to $C20/25$. NEN 6270 Table 15 gives the formula to calculate the fictive E-modulus (Appendix D.2.1). For the concrete class $C20/25$ the formula is as follows:

$$E_f = 2500 + 5500\omega_o$$

Where $\omega_o = 0.446$, according to the calculations done for lock head Empel. This results in an $E_f = 4950 N/mm^2$. The displacements of the lock head made out of concrete class $C20/25$ are shown in Figure 6.5. The change in E-modulus is 10%. The change in displacements is also roughly 10%, which is to be expected. The actual displacements of the inhomogeneous cross section will be somewhere in between.

Figure 6.5: Displacement lock head Empel with concrete class $C20/25$

It is expected that the crack width at the surface area is roughly the same as the original cross section, since the crack width mainly depends on the stresses in the reinforcement steel. The stresses in the reinforcement steel do hardly change. Cracks in the core of the concrete due to the difference in creep and shrinkage of the different concrete classes require further research.

6.2.4. Global Stability
Global stability issues are not to be expected since the dimension of the lock head do not change.

6.2.5. Cost & MKI
The cost and MKI calculations only take the concrete into consideration. Other aspects of the lock head do not change. The cost for $C20/25$ is $98.55€/m^3$, the cost for $C30/37$ is $104.5€/m^3$. The difference in cost between the original lock head and the design with the Inhomogeneous cross section is -2.85%. The difference in MKI between the original floor and the Inhomogeneous floor is -0.21%. To make a fair comparison with the cost difference, a weighing factor has been applied. The MKI difference after applying the weighing factor from literature is -0.04%. When applying the weighing factor from the calculations the MKI difference becomes -0.06% (Appendix D.2.1). The values do not include possible increases in MKI and cost during the construction process, since extra measures are necessary to pour two different concrete classes.

6.2.6. Points of Attention
The interaction forces due to the difference in creep and shrinkage behaviour of the different concrete classes have not been taken into account, as well as the additional construction cost.

6.3. Prestressing
Concrete is a material that is strong in compression and weak in tension. An option to improve the strength and stiffness properties of concrete is to introduce an external force to reduce the tensile stresses. This principle is called prestressing. There are three methods to prestress an element. These

are Prestressing between fixed points, Pre-tensioning and Post-tensioning with bonded tendons or unbonded tendons (Walraven and Braam, 2018). The advantage of using prestressing instead of reinforcement is that more slender structures can be designed. This reduces the use of concrete.

When applying the principle of prestressing, different mechanism have to be taken into account. As stated above, the structure becomes more slender when applying prestressing. Does the structure still meet the requirements for deflection as a result of this? Does the prestressing steel not corrode and lose all its strength when it is applied in a lock head exposed to water? In SLS the formation of cracks in strongly reduced when using prestressing. This is an advantage with respect to water tightness and corrosion resistance. Therefore, offshore structures are often prestressed (Walraven and Braam, 2018). However, prestressing is more expensive and labour intensive than the traditional reinforcing steel (Walraven and Braam, 2018).

6.3.1. Setup

Assumed is a prestressing cable of Y1860S7: $A_p = 2000mm^2$, $E_p = 195 * 10^3 N/mm^2$, $\sigma_{p,\infty} = 1080N/mm^2$, $\sigma_{pm,\infty} = 1080 * 0.98 = 1058N/mm^2$ and $f_{pd} = 1522N/mm^2$. The distance from the top fibre to the centre of the tendon is $d_p = 1000mm$. The tendon profile is straight and has been applied in the middle of the cross section, see Figure 6.6. The tendon profile does not cause additional tensile stresses since it has been applied in the core of the cross section. The detailed calculation can be found in Appendix D.2.2.
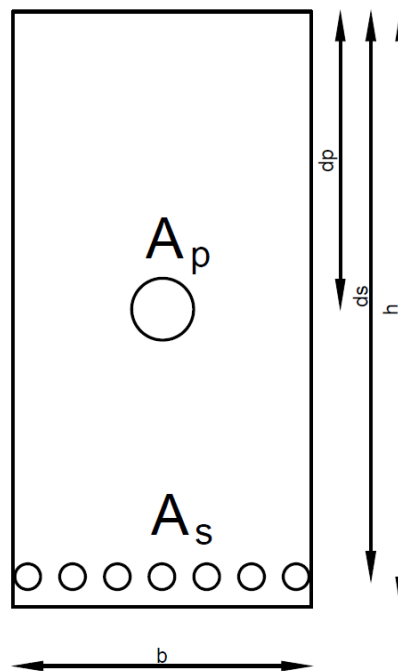
Figure 6.6: Cross section

6.3.2. Strength Calculations

The resulting moment resistance is $M_{Rd} = 7146kNm$. The height of the structure can be reduced to $1.6m$. The moment resistance of the cross section with the new height is $M_{Rd} = 5669kNm$.

No additional shear force reinforcement is needed in case of prestressing.

6.3.3. Stiffness Calculations

The displacements are proportional to the change in E-modulus. A fully prestressed slab does not crack under SLS load combinations. What E-modulus can be used, requires further research. The

displacements of the lock head with an E-modulus of $33000N/mm^2$ and a floor thickness of $h = 1.6m$ is shown in Figure 6.7.
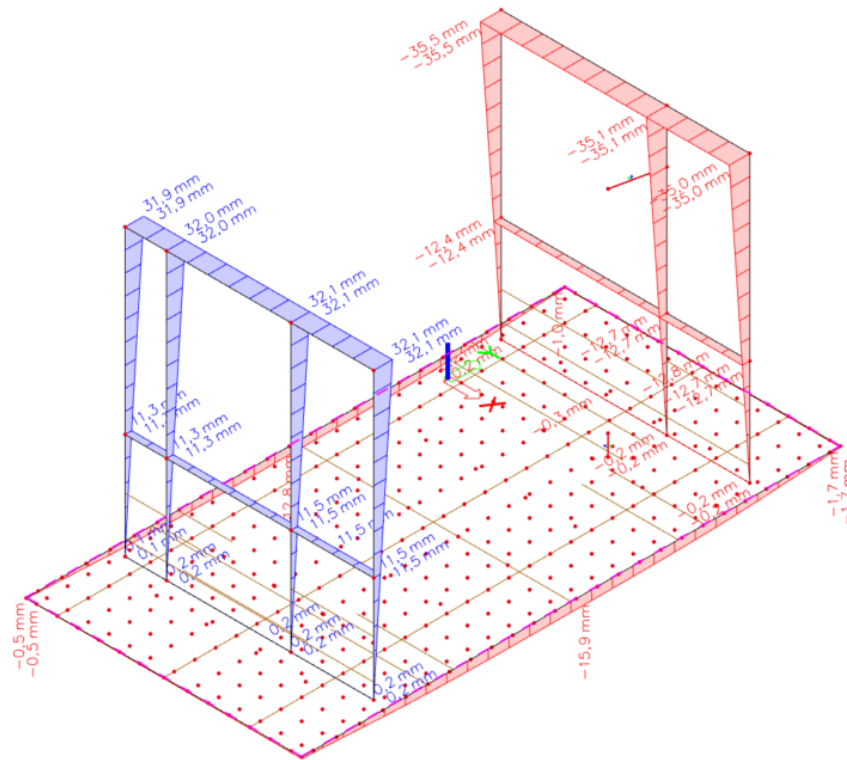
Figure 6.7: Displacements lock head with $E = 33000N/mm^2$ and a floor thickness of $h = 1600mm$

The crack width is reduced to $0.24mm$, so no extra measures are necessary.

6.3.4. Global Stability
The structure becomes lighter. The horizontal bearing capacity of the lock head may be a problem during the use phase. The horizontal bearing capacity of the lock head in Empel however is independent of the weight of the lock head, see Chapter 4.

6.3.5. Cost & MKI
The cost and MKI calculations include concrete, reinforcement and prestressing steel. The MKI value of prestressing is $115.14€/ton$. For preliminary calculations it is assumed that prestressing is three times more expensive than applying reinforcement, $3378€/ton$. The cost increases with 2.3% relative to the original design. The MKI decreases with -15.8%. After applying the weighing factor from literature the MKI decrease becomes -3.2%. The decrease in MKI multiplied with a weighing factor according to the calculations is -1.5%.

6.3.6. Points of Attention
The tendon profile is assumed to be straight for preliminary calculations. The method of prestressing can be optimised by applying a curved tendon profile. This has an influence on the force distribution in the beam. The tendon will cause an additional external moment in the beam.
By applying prestressing the floor becomes more slender. This has a negative influence on the stiffness of the floor. This means that the deflections of the lock head will increase. However, prestressing has a positive influence on crack formation. Therefore a higher E-modulus can be used for deflection calculations.

6.4. Hollow Sections

The idea of the Hollow Sections is to save concrete without losing stiffness. This in order to minimise the increase in displacements.

6.4.1. Setup

A cross section like the one in Figure 6.8 is chosen, see also Appendix D.2.3. The dimensions are $h = 2000mm$, $b = 1000mm$, $t_f = 300mm$ & $t_w = 300mm$. The concrete class is $C30/37$.
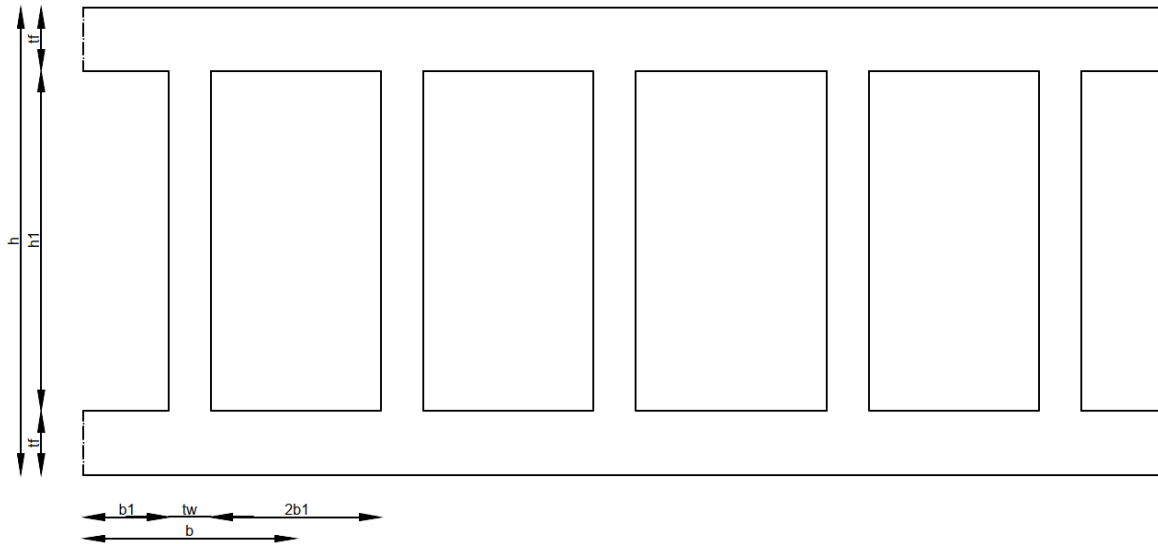
Figure 6.8: Hollow section

6.4.2. Strength Calculations

The resulting moments are given in Table 6.3. The cross section is able to withstand M_d without any extra measures.

Table 6.3: Moment-Curvature diagram

	$M \ [kNm]$	$\kappa * 10^{-3} \ [m^{-1}]$
Start	0	0
Rupture moment M_r	2457	0.26
Yielding moment M_y	6992	1.54
Stuik moment $M_{c,pl}$	7241	5.83
Ultimate moment M_{Rd}	7341	20.10

Figure 6.9: Moment Curvature diagram

The shear force resistance of the hollow section is not sufficient and the shear force reinforcement has to increase from $1005mm^2/m$ to $2116mm^2/m$.

6.4.3. Stiffness Calculations

SCIA Engineer is again used to get an indication of the displacements. The lock head is modelled as separate 2D plate elements. The thickness of the plates has been reduced to an equivalent thickness with the same moment of inertia as an hollow section. The displacements are shown in Figure 6.10. The displacements increase with approximately 10%.

Figure 6.10: Displacements lock head with hollow sections

The crack width calculations result in a crack width of $0,34mm$, which is below the prescribed crack width of $0,40mm$. No extra measures are necessary.

6.4.4. Global Stability

By applying Hollow Sections, the own weight of the structure decreases. The horizontal bearing capacity of the lock head may be a problem during the use phase. However, as was shown in Chapter 4, the horizontal bearing capacity of the lock head in Empel is independent of the weight of the lock head.

6.4.5. Cost & MKI

The cost and MKI calculations include concrete, additional shear reinforcement and additional reinforcement in the x-direction of the lock head. The cost decreases with -3.3% relative to the original design. The MKI decreases with -31.9%. The decrease in MKI after applying the weighing factor from the literature is -6.4%. The decrease in MKI after applying the weighing factor according to the calculations is -3.0%. The MKI and cost do not take extra construction cost into account due to the laborious cross section.

6.4.6. Points of Attention

The cross section with hollow sections can be schematised as in Figure 6.11, where the webs represent the supports and the flange represents the beam. The cross section is loaded by a water level of MHW in the lock head. This leads to the moment distribution and shear force distribution in Figure 6.12 & 6.13. As a result, extra reinforcement needs to be applied in the flanges of the cross section.
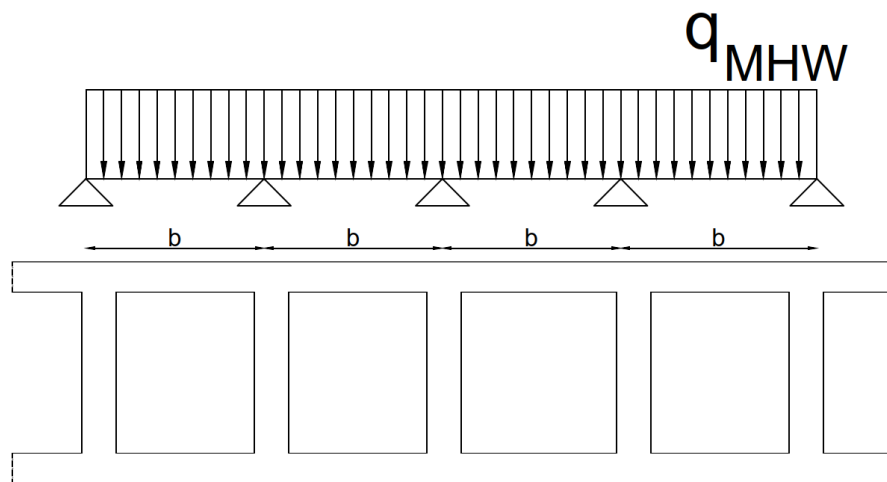
Figure 6.11: Schematization of the hollow cross section in the length direction of the lock head
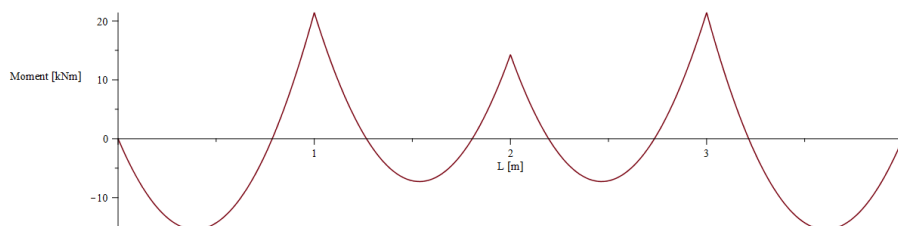
Figure 6.12: Moment distribution due to a water level of MHW
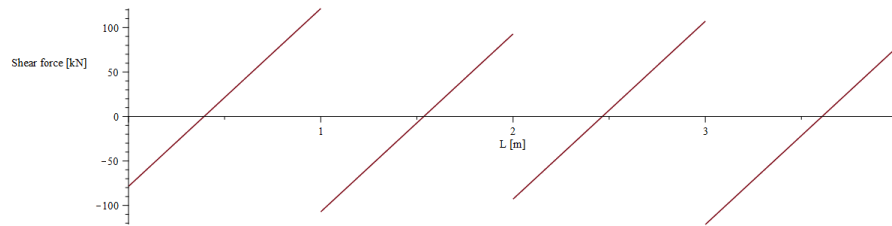
Figure 6.13: Shear force distribution due to a water level of MHW

6.5. Conclusion

Tables 6.4 & 6.5 give an overview of the different alternatives and the respective gain/lose in MKI and cost expressed in percentages relative to the original design of the lock head in Empel. A − sign means a decrease. A + sign indicates an increase.

The alternative Inhomogeneous Cross Section is not a viable option. Although it fulfills the strength, stability anf global stability calculations, the decrease in MKI is negligible. This was to be expected since the Dutch construction sector mainly uses $CEMIII$. This cement type already contains a lower clinker content than $CEMI$. The cost savings are also negligible. Besides, the MKI and cost calculations only take into account labour cost and material cost. Additional construction cost due to the laborious cross section are not taken into account. The difference in shrinkage and creep between the two concrete classes is not taken into account.

The option Prestressing is also neglected. The option Prestressing fulfills the strength requirements. More research is needed for displacement calculations, especially the determination of the E-modulus. The crack width is no problem.
In general the horizontal bearing capacity may be an issue during the use phase, due to a lighter construction. However, the horizontal bearing capacity of the lock head in Empel is independent of the weight.
The gains in MKI only based on material use are relatively small.

The option Hollow Sections seems the most promising option out of the three options. Additional shear reinforcement is needed according to the strength calculations. Additional reinforcement is needed in the flanges in the length direction of the lock head.
In general the horizontal bearing capacity may be an issue during the use phase, due to a lighter construction. The horizontal bearing capacity of the lock head in Empel is independent of the weight.

It has to be concluded that none of the above options reduce the MKI of an lock head significantly. Besides, all the options are laborious and require more attention during the construction. This will likely increase the cost and MKI.
In the advanced analysis of the research the above mentioned alternatives will be neglected. A parametric model will be made in order to try to optimise the design of lock heads based on well established rules from the 'Handboek voor het Ontwerpen van Schutsluizen' (*Ontwerp van Schutsluizen*, 2000) and the 'Richtlijnen Vaarwegen 2017' (*Richtlijnen vaarwegen 2017*, 2017).

Table 6.4: Comparison different alternatives strength, stiffness and stability

Alternative	Strength	Stiffness	Stability
Inhomogeneous cross section	OK	OK	OK
Prestressing	OK	Displacements require more research	Horizontal bearing capacity
Hollow sections	Additional (shear) reinforcement	OK	Horizontal bearing capacity

Table 6.5: Comparison different alternatives cost and MKI

Alternative	Cost [%]	MKI [%]	MKI, factor from literature[%]	MKI, factor from calc.[%]
Inhomogeneous cross section	-2.9	-0.2	-0.04	-0.06
Prestressing	2.3	-15.9	-3.2	-1.5
Hollow sections	-3.3	-31.9	-6.4	-3.0

7

Parametric model

This chapter will elaborate how the parametric model works. It will clarify the input parameters, show what happens inside the parametric model and show some output. The calculations and the results will be compared to the design calculations of the northern lock head in Empel (Chapter 4) to validate the model.

The calculations and functional requirements of the lock head used in the model are based on the rules prescribed by the 'Handboek voor het ontwerpen van Schutsluizen' (*Ontwerp van Schutsluizen*, 2000) and the 'Richtlijnen vaarwegen 2017' (*Richtlijnen vaarwegen 2017*, 2017).

The model only takes into account the operation phase of the lock head. The construction phase is not taken into account.

Based on the given input parameters, the parametric model comes up with a preliminary design for a single leaf gate lock head and/or mitre gate lock head.

7.1. Model Lay-out

The model is built up out of different classes, being a Wall class, Floor class, Section Class, Gate class, Soil class, Load class, Vessel class, Concrete class, Reinforcement class, Cost class, MKI class and a Lock head class. The Lockhead class is the main class, which combines all the others. The unified modeling language diagram (UML) of the parametric model is given in Figure 7.1 (Appendix E) and shows the relation between the classes.

The main class, the Lockhead, combines all the information of the different classes. The global stability checks of the lock head are calculated in this class. The final dimensions are based on the information from the global stability checks and the strength and stability calculations. The total cost and MKI of the lock head are calculated in this class as well.

The five classes Cost, MKI, Reinforcement, Concreteclass and Vessel only contain information. Information of these classes is accessed via the Lockhead class.

The Cost class contains the cost of the materials used, based on material cost and installation cost. The model takes the following materials into account: concrete, reinforcement, tension piles and foundation piles, and under water concrete (UWC).

The MKI class contains the MKI values of concrete, reinforcement, tension piles and foundation piles, and UWC.

The Concrete class contains the concrete properties of the different concrete classes, being $C20/25$, $C30/37$ and $C35/45$.

The Reinforcement class contains the reinforcement properties.

The Vessel class contains the width and the loaded draught of the different CEMT vessels.

The classes Floor, Wall, Gate, Load and Soil have a one to one relation with the Lockhead class. The classes not only contain information, but calculations as well.

The Wall class and Floor class determine the initial length and width of the structure based on the

information from the Gate class, Vessel class and the water levels, specified in the Lockhead class. The Wall class initiates a left wall and a right wall.

After the initial geometry is determined, the external moment distribution, shear force distribution and the displacements are calculated. The values depend on the loads from the Soil class, Gate class and Load class, and on the type of foundation. The type of foundation is determined in the Lockhead class itself.

The Wall class and Floor class are each related to a Section class. The walls and the floor can each be divided in a Head section, Chamber section and Tail section, see Figures 7.2 & 7.3. For each section the amount of reinforcement and shear reinforcement is calculated per meter.

The Gate class determines the dimensions of the gate based on the design rules in Chapter 3 and the dimensions of the vessel specified in the Vessel class. The vertical load and horizontal load of the gate are also calculated in this class. The Gate class can be further divided into a Gatemitre class and a Gatesinglehead class. This depends on what lock configuration is possible.

In the Soil class the groundwater levels and different soil layers and their properties are specified. Based on this information, the soil loads and groundwater loads are calculated. For each soil layer, an instance is created.

The remaining loads are specified in the Load class. The loads specified are the hawser force, crane load, traffic load and the water load. The Load class also contains the load factors of the different loads.

By using classes, a lot of repetitive coding is avoided. Besides, numerous scripts written for the parametric model are coded individually and only depend on the right input parameters. These scripts can be used for other parametric models. Examples of these scripts are the strength and stiffness calculations (moment resistance, shear resistance and crack width), the matrix method calculations, the script that is able to find intersection points and the script that calculates the soil and ground water load. These scripts will be further discussed in the following sections.

Section

+StructurePart(lockhead): void
+ length: float
- concrete cover: float

+ oppervlak(): float

FloorSection

+ Floor = floor

+ thickness(): float
+ krachten_per_meter(): list
+ results(): list

WallSection

+ Wall = wall

+ thickness(): float
+ krachten_per_meter(): list
+ results(): list

Gatemitre()

+ Gatemitre(lockhead): void
+ width: float
- length: float

Gatesingleleaf()

+ Gatesinglelead(lockhead): void
+ width: float
- length: float

Soillayer

+ Soillayer(soil, top_layer, bottom_layer, type_soil): void
- soil_properties: float

+ thickness(): float
+ vert_pressure(z): float
- f_soil_horizontal(): float, float, float

Floor

+ Floor(lockhead): void
- thickness: int

+ BK_vloer(): float
+ OK_vloer(): float
+ width(): float
- moment_shearforce_floor: list, list

Wall

+ Wall(lockhead, location): void
- thickness: int

+ length(): float
+ width(): float
+ moment(): list
- shearforce(): list

Wall left   Wall right

Gate

+ Gate(lockhead): void

+ location_taats(): float
+ location_halsp(): float
+ weigth(): float
- f_gate(): float, float

Load

+ Load(lockhead): void
+ trafficload: float
- craneload: float

+ f_hawser(): float, float
+ f_traffic(): float, float
+ f_crane(): float, float
- f_water(): float, float

Soil

+ Soil(lockhead): void
+ soillayers
- groundwaterlevels

+ f_groundwater(): float, float
+ f_soil(): float
- water_pressure(z): float

Lockhead

+ Lockhead(vessel, concreteclass, gatetype): void
+ waterlevels: float
- top_structure: float

+ scewing_up(): boolean
+ vertical_bearing_capacity(): string
+ rotation(waterlevel_1, waterlevel_2): boolean
- horizontal_beraing_capacity(waterlevel_1, waterlevel_2): boolean

Cost

+ cost_reinforcement: float
+ cost_gewi: float
- cost_foindationpile: float

Vessel

+ Vessel(CEMT_klasse): void
+ width: float
- draught: float

MKI

+ MKI_gewi: float
+ MKI_foundationpile: float
- MKI_reinforcement: flaot

Reinforcement

+ Reinforcement(lockhead): void
+ fyd: float
+ Es: float
+ epsc3: float
+ theta: list
- EG: float

Concreteclass

+ Concreteclass(strengthclass): void
+ fck: float
+ fcd: float
+ fctm: float
+ Ecm: float
+ cost: float
- MKI: float

Figure 7.1: UML diagram of the parametric model

7.2. Model Overview
7.2.1. Input
In order to get a design of a lock head, the user needs to specify the input parameters. The six input parameters are:

- the water levels

- the groundwater levels

- the concrete class

- the soil properties

- the type of vessel

- the top of the structure

- the direction of water retention

Water Levels

The model includes the following water levels, being:

- MHW (maatgevend hoog water), this is the maximum occurring water level

- Max schutpeil, this is the maximimum water level at which the lock can operate

- Kanaalpeil, this is the water level in the adjacent canal

- Min schutpeil, this is the minimum water level at which the lock can operate

- MLW (maatgevend laag water), this is the minimum occurring water level

Groundwater Levels

A distinction can be made between the groundwater level within the construction pit and a groundwater level outside the construction pit. It is assumed that the groundwater level inside the construction pit does not vary. The groundwater level inside the construction pit is used for strength and stability calculations. The groundwater level outside the construction pit varies and depends on the occurring water level. The groundwater levels outside the construction pit are used for the global stability checks. The following groundwater levels have been used in the model:

- MHW

- Max schutpeil

- Min schutpeil

- MLW

- Droogzetten, this is the groundwater level when the lock is emptied for maintenance.

Concrete Class

The concrete class has to be specified upfront. The concrete classes incorporated in the model are $C20/25$, $C30/37$ and $C35/45$. The concrete class $C12/15$ is not incorporated in the model since it is hardly used for constructive purposes (Braam and Lagendijk, 2011). The concrete class $C35/45$ is mostly used for prefab elements (Braam and Lagendijk, 2011). This research only considers lock heads built in-situ. Therefore, the concrete classes $C35/45$ is not likely to be used, however it is incorporated in the model.

Soil Properties

The model takes into account the soil types sand, clay and peat. The soil properties used in the model are given in Table 7.1. The user only has to specify the soil type and the top and bottom of each layer relative to NAP.

Table 7.1: Soil properties model

type of soil	γ_d $[kN/m^3]$	γ_s $[kN/m^3]$	ϕ'_{rep} [°]	c'_{rep} $[kN/m^2]$
Sand	18	20	30	0
Clay	18	18	25	5
Peat	11	11	20	5

Type of Vessel

The type of vessel mainly determines the width of the lock head and the bottom of structure. The model only accounts for inland navigation vessels. The classification and properties of the different vessels can be found in Table 3.1.

Top of Structure

The top of the structure depends on MHW, the sea level rise, the settlements of the lock head, wind setup, wave overtopping and seiches. The exact values of all these factors are very location dependent. The determination of the top of structure is outside the scope of this research. For this reason the top of structure is set as an input parameter.

Direction of Water Retention

The direction of water retention can be in one or in both directions. The width of the lock head and the direction of retention determine the type of gate, see Table 7.2. In some cases both type of gates are possible. In this situation the model considers both types of gates.

Table 7.2: Gate type (*Ontwerp van Schutsluizen*, 2000)

Direction of retention	width [m]	Mitre gate (one direction)	Mitre gate (both directions)	Single leaf gate (one direction)	Single leaf gate (both directions)
One direction	4 - 6			x	
	6 - 10	x		x	
	10 - 16	x			
	16 - 24	x			
Both directions	4 - 6				x
	6 - 10		x		x
	10 - 16		x		x
	16 - 24		x		

7.2.2. Parametric Model

This section will explain what happens within the parametric model. It will explain the calculations and the order of execution.

Lock Configuration

Based on the input parameters, the model first determines what kind of lock configurations are possible. Two lock configurations are possible: a lock head with a single leaf gate and/or a lock head with a mitre gate, see Figure 7.2 & 7.3 . What configuration is possible depends on the width of the lock head, and therefore the type of vessel and the direction of water retention, see Table 7.2.
Based on the input parameters, the model first determines the initial geometry of the lock head. The wall left and wall right are symmetrical for a lock head with a mitre gate. The dimensions of the wall left and wall right for a lock head with a single leaf gate differ. A distinction can be made between the wall with a gate chamber and the wall with a gate recess. The gate chamber protects the gate in open position. The gate recess provides a watertight connection in closed position.
As can be seen in Figure 7.2 & 7.3, the thickness of the walls varies over the length of the lock head. The thickness of wall number 2 (Chamber) has an initial width. The thickness of wall number 1 (Head) & 3 (Tail) depend on the thickness of wall number 2 and the dimensions of the gate. For a lock head with a mitre gate and the wall left for a lock head with a single leaf gate, the thickness of wall number 1 & 3 is equal to the thickness of wall number 2 plus the thickness of the gate and the prescribed distance between the gate and wall 2 in open position, see Chapter 3. The thickness of wall right number 1 & 3 for a single leaf gate is equal to the width of wall number 2 plus the distance between the top of the gate and wall 2 in closed position and the overlay, set to $0.5m$, see Chapter 3.
The length of wall number 1 for the mitre gate and wall left of the single leaf gate has a length of $1m$. The length of wall 1 for wall right of a single leaf gate is equal to half the length of the gate chamber plus $1m$.
The length of wall 2 for a mitre gate and wall left for a single leaf gate is equal to the length of the gate chamber. The gate chamber has a length equal to the gate length plus the prescribed distance between the top of the gate and wall 1 in open position, see Chapter 3. The length of wall right number 2 for a single leaf gate is equal to length of the gate recess, which is equal to half the length of the gate chamber.

The length of wall 3 is the same for wall right and wall left. The length depends on the CEMT class and the type of gate. The length is $1m$ for a mitre gate for CEMT classes I and II. For the other situations, the length is $2m$.

The thickness of the floor also varies over the length of the lock head. The top of the hatched area is $0.5m$ lower than the top of the rest of the floor. This is done to secure a watertight connection between the gate and the lock head, and to keep sediment out of the lock head, which can hamper the gate from opening and closing.

In the remainder of this research, number 1 will be referred to as 'Head', number 2 as 'Chamber' and number 3 as 'Tail'.
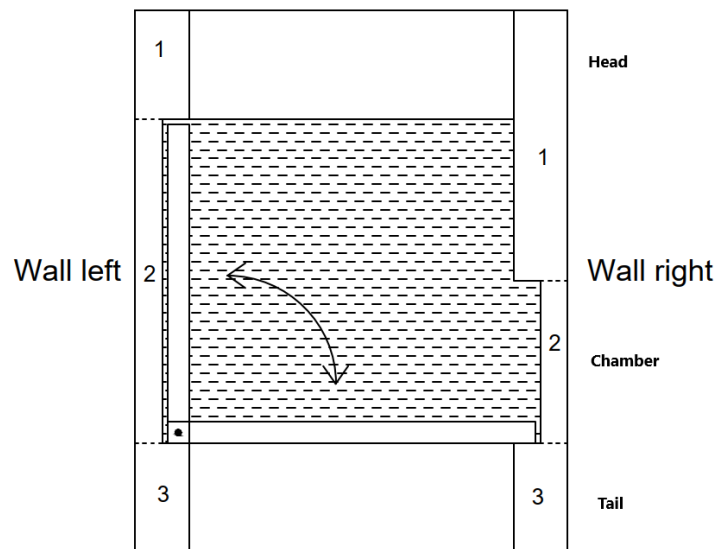
Figure 7.2: Lock configuration with a single leaf gate
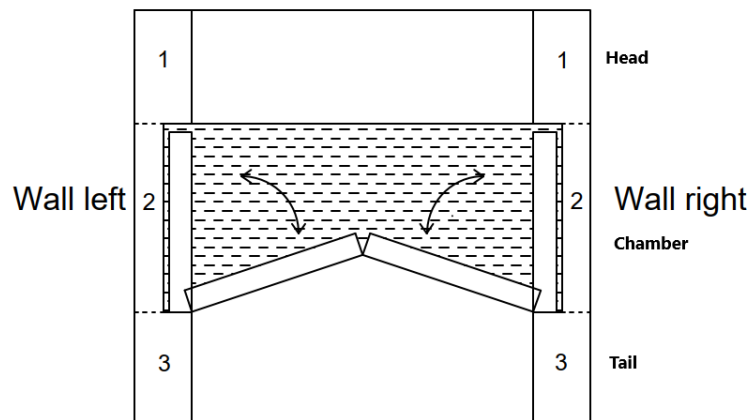
Figure 7.3: Lock configuration with a mitre gate

Foundation

The model assumes two types of foundation, being a shallow foundation and a pile foundation. The type of foundation depends on the input parameters. The model only takes the construction method discussed in Chapter 3 into account. This construction method consists out of a cofferdam with sheet piles and an UWC floor.

First the shallow foundation is being considered. GEWI piles are installed to prevent the UWC floor from

hydraulic bursting. The UWC floor has a thickness of $1.2m$. The centre to centre distance between the piles is set to a maximum of $2m$. The diameter of the the GEWI piles is $63.5mm$. The bearing capacity is assumed to be $1500kN$, based on the calculations done for Empel.

In case of a pile foundation, it is assumed that the foundation piles provide enough resistance to prevent the UWC floor from hydraulic bursting. Assumed is a foundation pile of $C45/55$ with a length of $15m$, a surface area of $450x450mm^2$ and a bearing capacity of $1000kN$. The distance between the foundation piles is set to: $\geq 6D_{eq}$ (NEN-EN 1997-1).

The UWC floor is checked on hydraulic bursting, fracture of the floor and fracture of the floor between the floor and the tension piles, see Appendix C. As was mentioned before the UWC floor has a thickness of $1.2m$. The distance between the piles depends on the type of foundation. The model checks if the UWC floor fulfills all the checks mentioned above. In case one of the check does not meet the requirements, the thickness of the floor is increased with $0.1m$, until the requirements are met, see Figure 7.4.
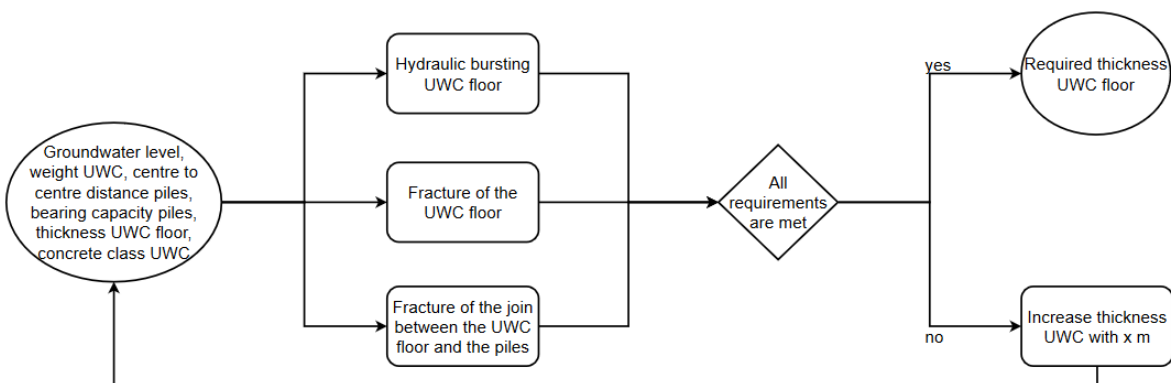
Figure 7.4: Determination of the thickness of the UWC floor

Loads

The loads acting on the lock head can be divided in three main groups: loads acting on the wall in perpendicular and in parallel direction and loads acting on the floor. The loads included in the model can all be found in Appendix B. It is important to note that most of the loads depend on the geometry of the lock head.

The hawser force depends on the type of vessel, see Table 7.3. The crane load used in the model is based on a Liebherr LTM 1500-8.1. The traffic load is set to $20kN/m$.

Figures 7.5, 7.6 & 7.7 give an overview of the loads incorporated in the model and their dependence.

Table 7.3: Hawser force (*Richtlijnen vaarwegen 2017*, 2017)

CEMT class	Hawser force [kN]
I	150
II	150
III	200
IV	200
V	250
VI	300
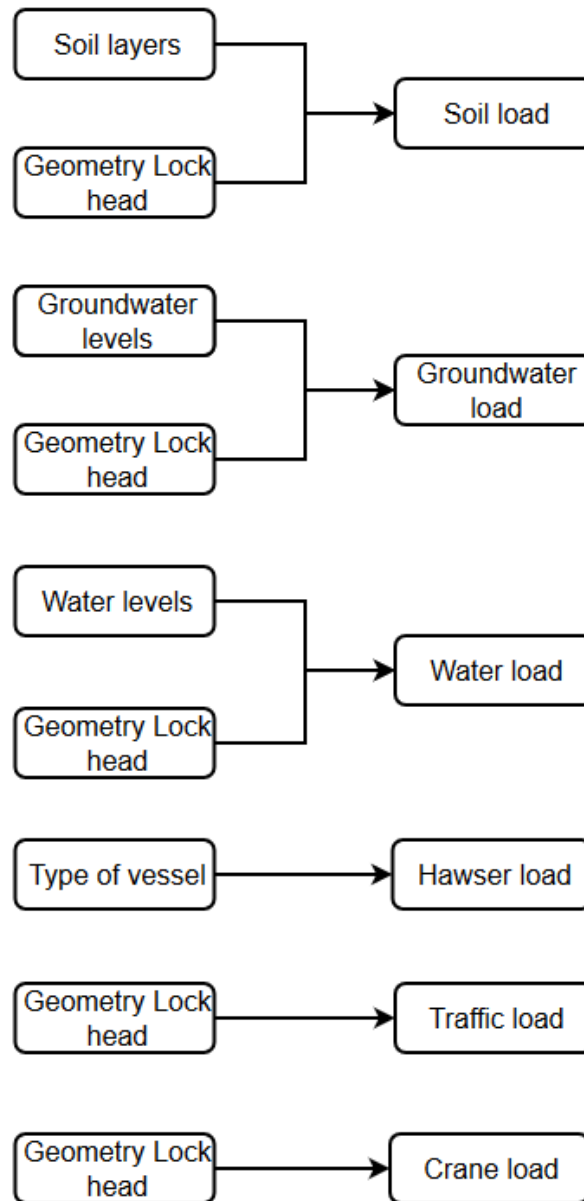
Figure 7.5: Loads on the wall in perpendicular direction
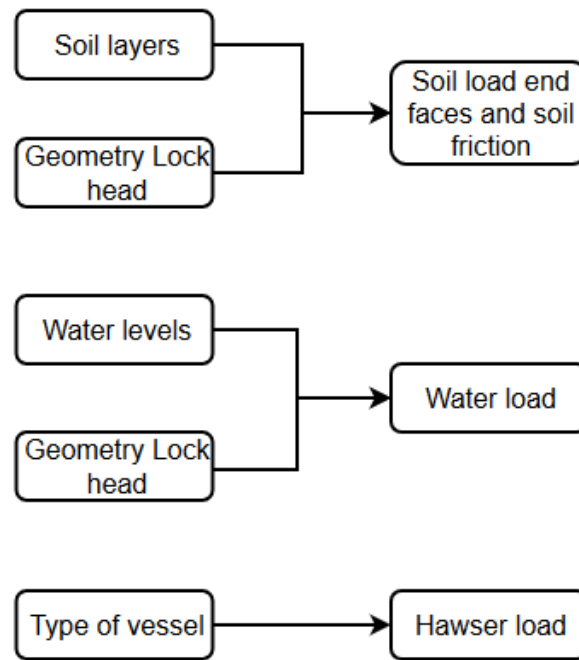
Figure 7.6: Loads on the wall in parallel direction
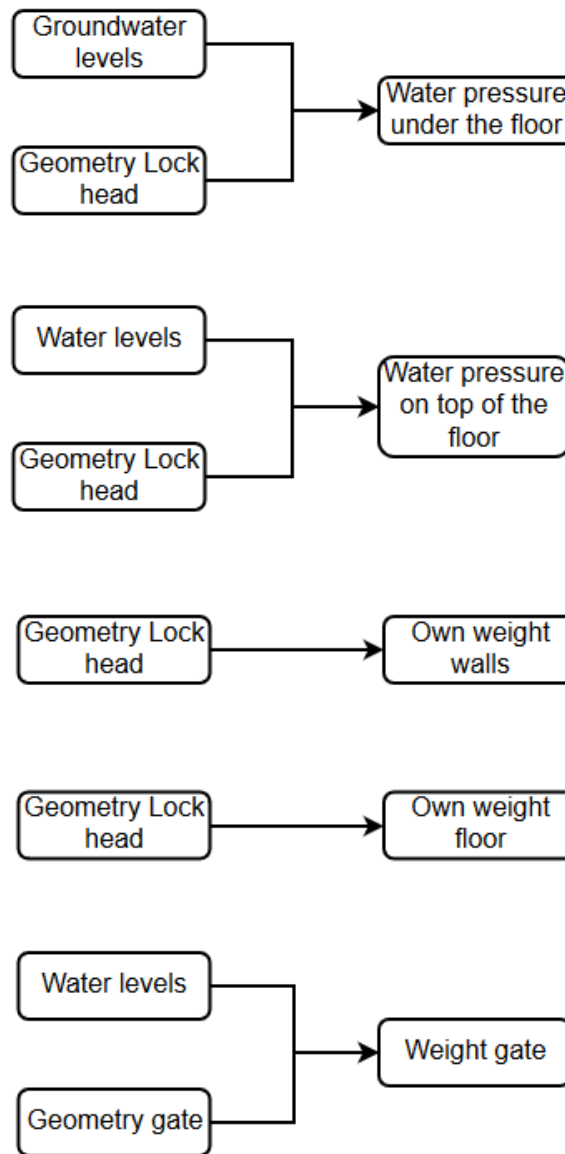
Figure 7.7: Loads on the floor

Load Factors and Combinations

What load factors to use can be found in Table B.1. The load combinations have been calculated according to Appendix B. The load factor for the horizontal soil force is multiplied with a factor λ, since the soil is subjected to fluctuating temperatures and groundwater levels (NEN6740).

Not all load combinations are incorporated into the parametric model. Based on the calculations done for the lock head Empel, two normative load combinations have been selected for both ULS and SLS. The normative load combinations in ULS and SLS are both for the case when the lock head is empty for maintenance. The main difference between the load combinations is the incorporation of the gate. The load combinations are:

- $ULS1 = \gamma_f F_{ownweight} + \gamma_f F_{soil} + \gamma_f F_{groundwater} + \gamma_f F_{traffic} + \gamma_f F_{crane} + \gamma_f F_{boulder}$

- $ULS2 = \gamma_f F_{ownweight} + \gamma_f F_{soil} + \gamma_f F_{groundwater} + \gamma_f F_{traffic} + \gamma_f F_{gate} + \gamma_f F_{boulder}$

- $SLS1 = F_{ownweight} + F_{soil} + F_{groundwater} + F_{traffic} + F_{crane} + F_{boulder}$

- $SLS2 = F_{ownweight} + F_{soil} + F_{groundwater} + F_{traffic} + F_{gate} + F_{boulder}$

Moment & Shear Force Distribution

The external moment and shear force distribution are calculated over the total length of the left wall, right wall and the floor. The moment and shear force distribution of the floor depend on the type of foundation.

The moment and shear force distribution for the walls is easily calculated by schematising the wall as a beam rigidly connected at the intersection of the wall and the floor.

Both the moment and shear distribution of the floor on a shallow foundation and a pile foundation are solved with the help of an ordinary differential equation. To solve the ordinary differential equation, the matrix method is used, since it is convenient to model. The principle of the matrix method is shown in Figures 7.8 & 7.9. Figure 7.8 gives an overview of the degrees of freedom and the forces acting on the beam. Figure 7.9 shows the stiffness matrix and the load vector in order to solve the unknowns.
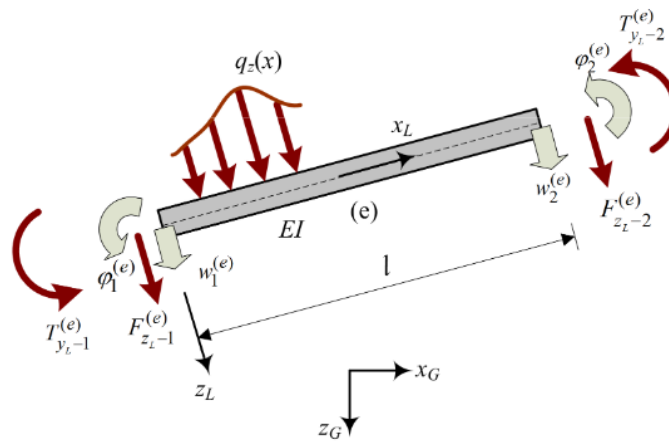
Figure 7.8: Schematisation of a beam with the matrix method (Welleman, 2018)

$$
\begin{bmatrix} F^{(e)}_{z_L-1} \\ T^{(e)}_{y_L-1} \\ F^{(e)}_{z_L-2} \\ T^{(e)}_{y_L-2} \end{bmatrix} = \begin{bmatrix} \frac{12EI}{l^3} & -\frac{6EI}{l^2} & -\frac{12EI}{l^3} & -\frac{6EI}{l^2} \\ -\frac{6EI}{l^2} & \frac{4EI}{l} & \frac{6EI}{l^2} & \frac{2EI}{l} \\ -\frac{12EI}{l^3} & \frac{6EI}{l^2} & \frac{12EI}{l^3} & \frac{6EI}{l^2} \\ -\frac{6EI}{l^2} & \frac{2EI}{l} & \frac{6EI}{l^2} & \frac{4EI}{l} \end{bmatrix} \begin{bmatrix} w^{(e)}_1 \\ \varphi^{(e)}_1 \\ w^{(e)}_2 \\ \varphi^{(e)}_2 \end{bmatrix} - \begin{bmatrix} \frac{1}{2}q_o l \\ -\frac{1}{12}q_o l^2 \\ \frac{1}{2}q_o l \\ \frac{1}{12}q_o l^2 \end{bmatrix}
$$

Figure 7.9: Matrix for an Euler Bernoulli beam without normal force (Welleman, 2018)

With the matrix method only the unknowns at the nodes can be solved. The displacement, rotation, moment and shear force distribution between the nodes can be solved with the information from the nodes and the following formulas respectively:

$$w = \frac{qx(L^3 - 2Lx^2 + x^3)}{24EI}$$

$$\phi = \frac{-q(L^3 - 6Lx^2 + 4x^3)}{24EI}$$

$$M = \frac{qx(-x+L)}{2}$$

$V = \frac{q(-2x+L)}{2}$

where:

q = the distributed load $[kN/m^2]$
L = the length of the beam segment $[m]$
EI = the bending stiffness $[kN/m^2]$
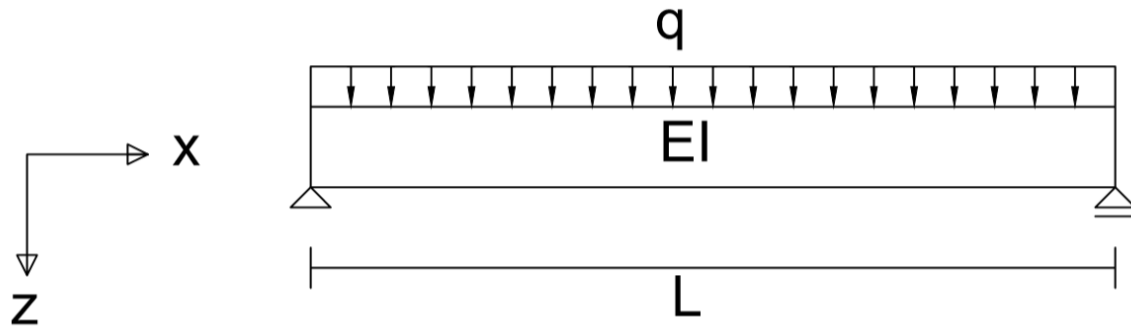
Figure 7.10: coordinate system

In case of a shallow foundation, the floor is schematised as a beam supported by the elastic soil and the GEWI piles. The subgrade modulus for sand is $c = 10^4 kN/m^3$, and for clay and peat $c = 10^{-1} kN/m^3$. The spring stiffness of the GEWI piles is set to $k = 5 * 10^4 kN/m$, based on the GEWI piles used for lock head Empel.

In case of a pile foundation, the amount of foundation piles and the spring stiffness of the foundation piles has to be determined, see Appendix B. The floor is again schematised as a beam supported by the elastic soil and springs which represent the foundation piles.

To solve this problem, the stiffness matrix and the load vector from Figure 7.9 have to be adjusted to account for the elastic soil, see Appendix E.

Now that the stiffness matrix and load vector have been adjusted to account for the elastic soil, the problem can be solved. The floor is divided into different segments, depending on the pile configuration, see Figure 7.11. However, as was mentioned before, the downside of the matrix method is that it only gives the solutions at the prescribed nodes, so in this case at the locations of foundation/GEWI piles. Normally, the above mentioned formulas can be used. However, the floor of the lock head is also supported by the non linear elastic soil. This means that the above mentioned formulas do not apply anymore. A trick has to be applied to overcome this problem. This is done by dividing the segments between the foundation/GEWI piles in even smaller sub segments, see Figure 7.12. This way an approximation of the displacement, rotation, moment and shear force distribution is acquired. The accuracy depends on the amount of sub segments. The more sub segments, the more accurate the answer becomes, however the longer the calculations take. The amount of sub segments can be specified by the user.

For each sub segment the stiffness matrix and force vector is set up. The next step is to assemble the total stiffness matrix of the system. This is simply done by adding the individual matrices at the location of the corresponding nodes. At the locations of the vertical degree of freedom of the foundation piles the spring stiffness of the foundation pile is added to the main diagonal of the total stiffness matrix. The external loads are added to the force vector. The external loads are added to the first two and last two entries of the load matrix, since the floor of the lock head is mainly loaded at the location of the first and last node by a bending moment and a shear force caused by the walls.

Now that the total system is assembled, the matrix can be solved. The results are the displacements and the rotations at the nodes. The support reactions can now easily be found by multiplying the displacements and rotations with the original stiffness matrix, without the spring stiffness, and subtract the force vector, without the external loads.
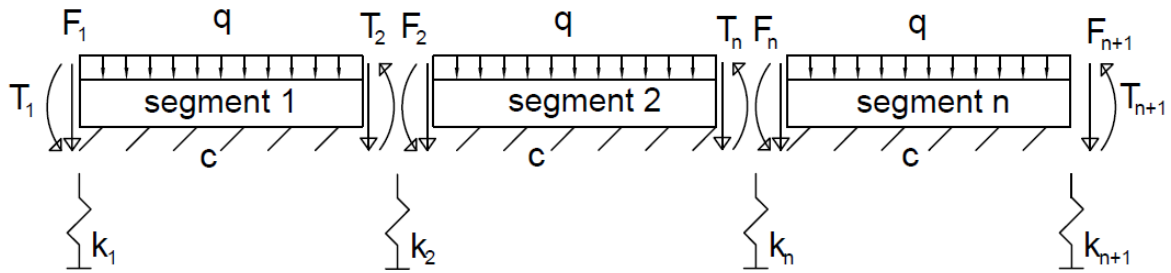
Figure 7.11: The floor divided in different segments
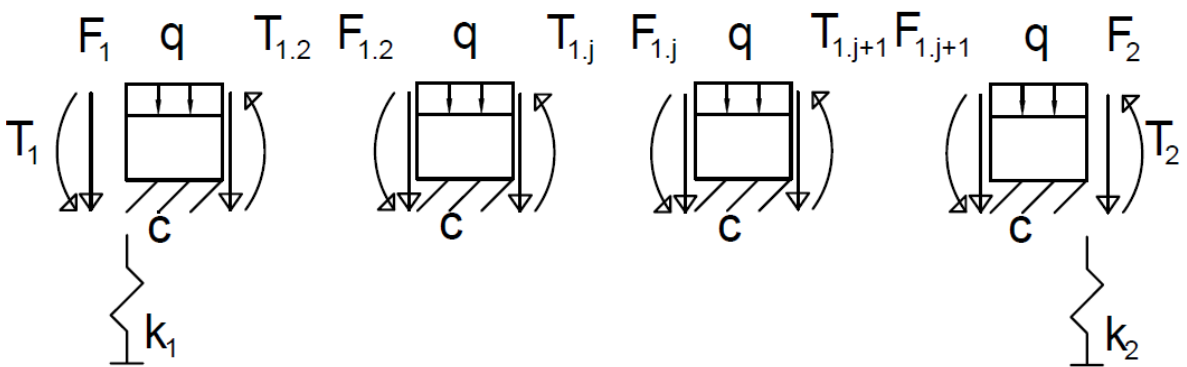
Figure 7.12: Segment 1 is further divided in sub segments

To proceed with the strength and stiffness calculations, the forces per meter need to be known. The external moment and shear force are now divided over the sections Head, Chamber and Tail for the walls and the floor.

The first step is to calculate the centre of gravity for the walls and floor, this is the dashed line in Figure 7.13. With this information the moment of inertia of the total cross section can be calculated. The next step is to calculate the stress distribution over the cross section, see also Figure 7.13:

$$\sigma = \frac{M_{ext} y}{I}$$

where:

M_{ext} = the external bending moment over the total wall or floor $[kNm]$
I = the moment of inertia of the total wall or floor $[m^4]$
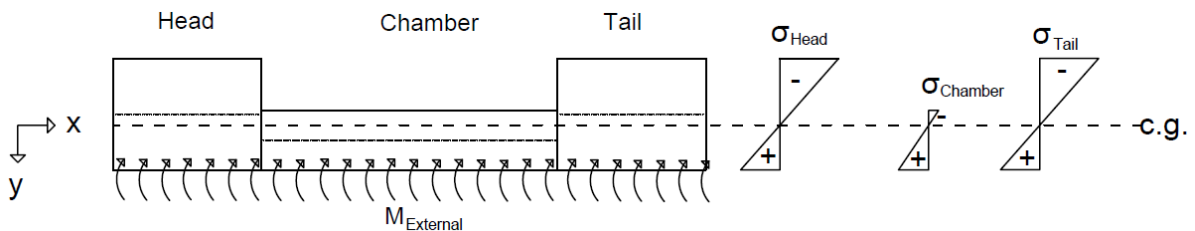
Figure 7.13: Stress distribution over the total length of the wall or floor due to the external moment

The stress distribution can be divided in a stress distribution due to pure bending and due to a normal force. Figure 7.14 shows this principle for the Head.

The moment per section due to pure bending follows from:

$$M_M = \sigma_M W$$

where:

σ_M = the stress distribution per section due to pure bending $[kN/m^2]$
W = the moment of resistance per section $[m^3]$

The moment per section due to the eccentricity of the resulting normal force follows from:

$$M_N = \sigma_N A e$$

where:

σ_N = the stress distribution per section due to a normal force $[kN/m^2]$
A = the surface area per section $[m^2]$
e = the distance between the centre of gravity of the total wall or floor (dashed line) and the centre of gravity of each section (dotted line) $[m]$
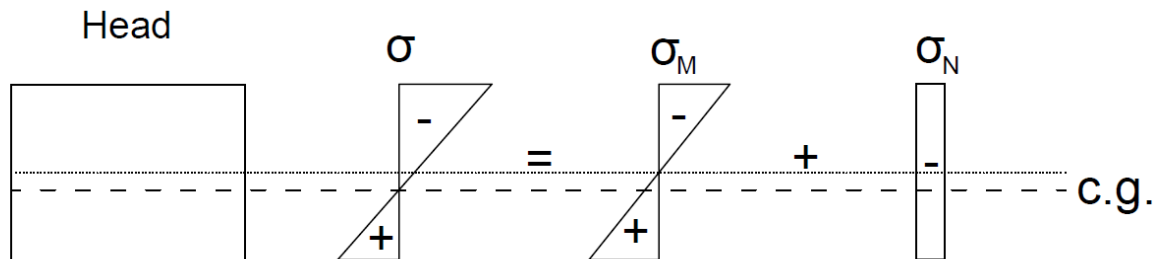
Figure 7.14: Stress distribution due to pure bending and due to a normal force for the Head

A flow chart of the process is given in Figure 7.15.
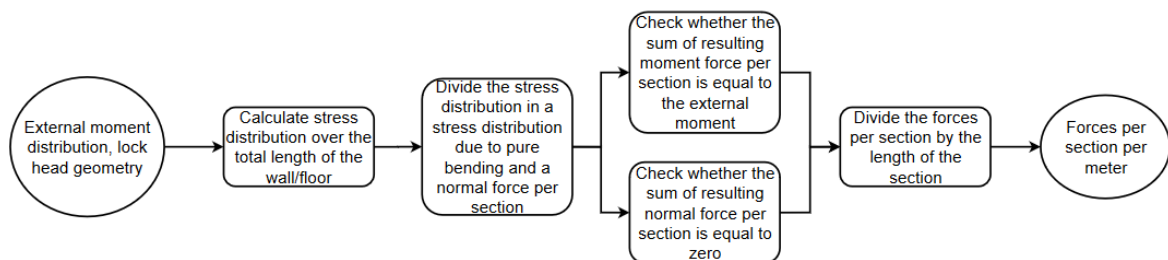
Figure 7.15: Forces per section

Strength & Stiffness

The strength & stiffness calculations: moment resistance, shear force resistance and crack width have been performed for each section per meter. The displacements have been calculated for the total structure. The calculations take into account the moment resistance for ULS, the shear force resistance for ULS, the crack width for SLS and deflections for SLS.

The moment resistance depends on the moment distribution per section per meter, the reinforcement ratio, the height of the cross section and the concrete class.

The reinforcement is a variable in the model. Based on the cross section properties the model determines the minimum and maximum reinforcement ratio according to NEN-EN 1991-1-1. The minimum reinforcement follows from the minimum of the following two formulas:

$$A_s = \frac{M_{cr}}{0.9 d f_{yd}}$$

where:

M_{cr} = the rupture moment $[kNm]$
d = effective height $[m]$
f_{yd} = design yielding moment of the reinforcement $[MPa]$

$$A_s \sigma_s = k_c k f_{ct,eff} A_{ct}$$

where:

σ_s = the maximum allowable stress in the reinforcement right after the first crack $[MPa]$
$k_c = 0.4 [-]$
$k = 0.65 [-]$

The maximum reinforcement follows from:

$$A_s = 0.02 A_c$$

where:

A_c = the area of concrete $[m^2]$

With the obtained information a list of reinforcement ratios can be generated. Due to reasons of practicability the maximum reinforcement ratio in the cross section is set to 2%, according to the Eurocode the maximum allowable reinforcement ratio is 4%.

To calculate the ultimate bending moment it is assumed that $\epsilon_{cu3} = 3.5‰$. The reinforcement in the tension zone and in the compression zone are yielding. The amount of reinforcement in the compression zone is 20% of the reinforcement in the tension zone. From horizontal equilibrium the compression height can be calculated according to:

$$N_c + N_{s,compression} - N_{s,tension} - N_{Ed} = 0$$

$$\frac{3}{4} b x f_{cd} + A_{s,compression} f_{yd} - A_{s,tension} f_{yd} - N_{Ed}$$

where:

A_s = surface area of the reinforcement $[m^2]$
f_{yd} = the design yielding stress $[MPa]$
x = concrete compression height $[m]$
b = the width of the cross section $[m]$
f_{cd} = the compression strength of concrete $[MPa]$

The ultimate bending moment for each reinforcement ratio is calculated according to:

$$M_{Rd} = N_c * (\frac{h}{2} - \frac{7}{18} x) + N_{s,compression}(\frac{h}{2} - (h - d)) + N_{s,tension}(\frac{h}{2} - (h - d))$$

where:

d = effective height $[m]$
h =the height of the cross section $[m]$

Figure 7.16 gives an overview of the process. The model calculates the required reinforcement ratio for several thicknesses, by searching for the intersection point (Figure 7.17). The model repeats this process n times. n is set to 16 in the parametric model. After each loop the model increases the thickness with x mm, in this case $x = 100mm$.
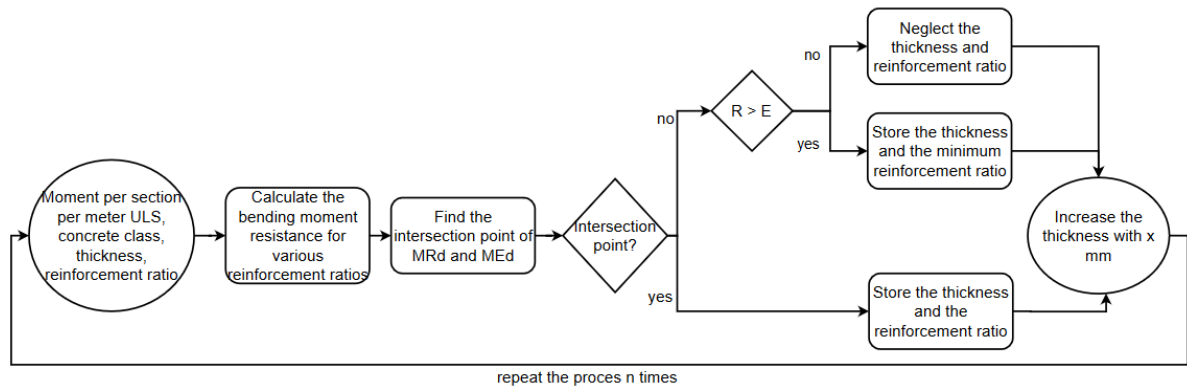
Figure 7.16: Moment resistance
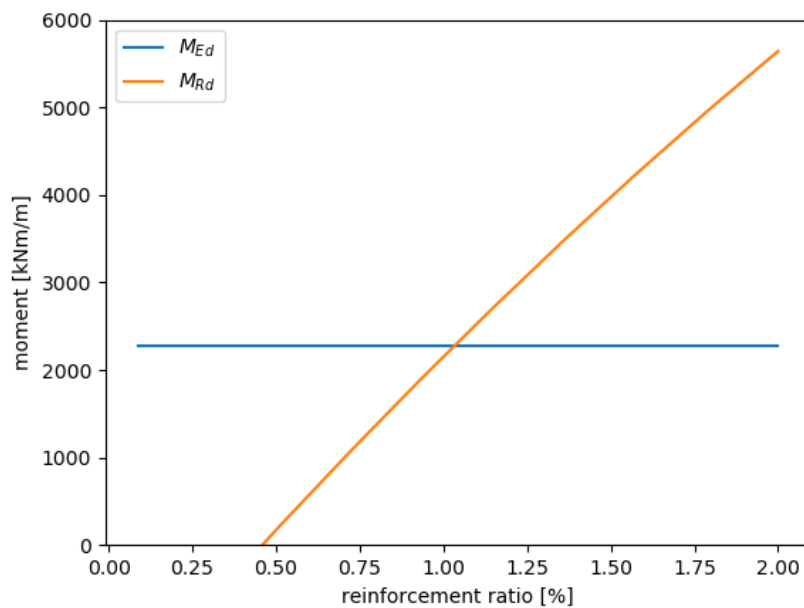
Figure 7.17: Moment resistance versus the bending moment wall left section Chamber per meter

The shear force resistance has been calculated according to NEN-EN 1991-1-1. First the shear resistance of an element without shear reinforcement has been checked according to the following formula:

$$V_{Rd,c} = [C_{Rd,c}k(100\rho_l f_{ck})^{1/3} + k_1\sigma_{cp}]b_w d$$

with a minimum of

$$V_{Rd,c} = [v_{min} + k_1\sigma_{cp}]b_w d$$

where:

$$C_{Rd,c} = 0.12[-]$$
$$k = 1 + \sqrt{\frac{200}{d}} \leq 2[-]$$
$$\rho_l = \frac{A_{sl}}{b_w d} \leq 0.02[-]$$
$$\sigma_{cp} = N_{Ed}/A_c < 0.2f_{cd}[MPa]$$
$$b_w = \text{the smallest with of the cross section under tension }[mm]$$
$$k_1 = 0.15[-]$$
$$v_{min} = 0.035k^{3/2}f_{ck}^{1/2}$$

In case $V_{Rd,c} \leq V_d$ shear reinforcement has to be applied. The diameter of the shear reinforcement in the model is $16mm$ with a varying distance between the shear reinforcement of $100mm$ to $1000mm$. Assumed are vertical reinforcement bars and θ is assumed to be $45°$. To calculate the shear resistance with shear reinforcement, V_{Rd} is the minimum of the following two formulas:

$$V_{Rd,s} = \frac{A_{sw}}{s}zf_y d * cot\theta$$

and

$$V_{Rd,max} = a_{cw}b_w zv_1 f_c d/(cot\theta + tan\theta)$$

where:

A_{sw} = surface area of the shear reinforcement $[m^2]$
s = centre to centre distance of the shear reinforcement $[m]$
f_{yd} = the yielding point of the reinforcement $[MPa]$.
$z = 0.9 * d[m]$
$v_1 = 0.6[-]$
$a_{cw} = 1 + \frac{\sigma_{cp}}{f_{cd}}$ if $0 \leq \sigma_{cp} \leq 0.25f_{cd}$
$a_{cw} = 1.25$ if $0.25f_{cd} \leq 0.5f_{cd}$
$a_{cw} = 2.5(1 + \frac{\sigma_{cp}}{f_{cd}})$ if $0.5f_{cd} \leq 1.0f_{cd}$

Figure 7.18 gives an overview of the process. For each thickness the model searches for the accompanying centre to centre distance of the shear reinforcement. When no shear reinforcement is needed according to the calculations, a c.t.c. between the shear reinforcement of $1000mm$ is applied.
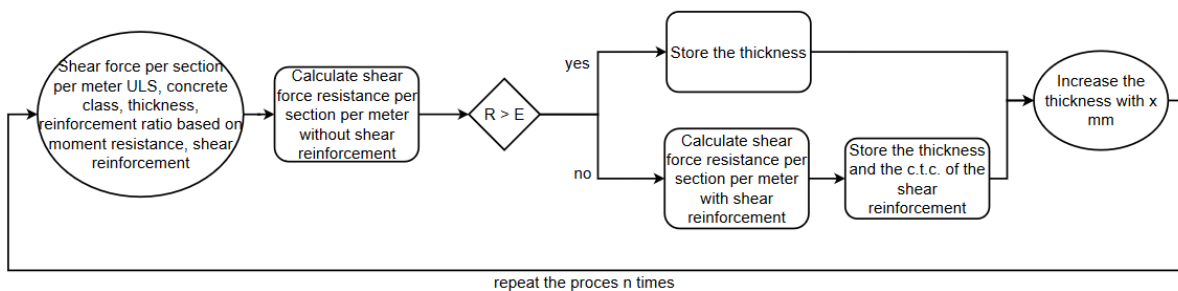
Figure 7.18: Shear force resistance

The crack width is calculated according to NEN-EN 1992-1-1 in the serviceability limit state (SLS). The formula used to calculate the crack width is:

$$w_{max} = \frac{1}{2} \frac{f_{ctm}}{\tau_{bm}} \frac{\phi}{\rho} \frac{1}{E_s} (\sigma_s - \alpha \sigma_{sr} + \beta \epsilon_{cs} E_s)$$

where:

σ_s = the steel stress in a crack under external tensile load $[MPa]$
σ_{sr} = the maximum steel stress in the crack formation stage $[MPa]$
ϵ_{cs} = the shrinkage of the concrete
ρ = the reinforcement ratio
f_{ctm} = the mean tensile strength of concrete $[MPa]$
$\tau_{bm} = 2 * f_{ctm}$ E_s = modulus of elasticity of steel $[MPa]$
$\alpha = 0.5$ for this study
$\beta = 0$ for this study

The crack width depends on the diameter of the reinforcement. The diameters incorporated in the model are $\phi = 16, 20, 25, 32mm$. In case different reinforcement diameters have been used in the cross section, an equivalent diameter has to be calculated according to:

$$\phi_{eq} = \frac{n_1 \Theta_1^2 + n_2 \Theta_2^2}{n_1 \Theta_1 + n_2 \Theta_2}$$

Figure 7.19 gives an overview of the process. This process looks a lot like the moment resistance. The big difference are the different reinforcement diameters and the multiple intersection points, see Figure 7.20. The maximum allowable crack width is set to $0.4mm$, based on information from the lock head in Empel. The user is able to change the maximal allowable crack width.
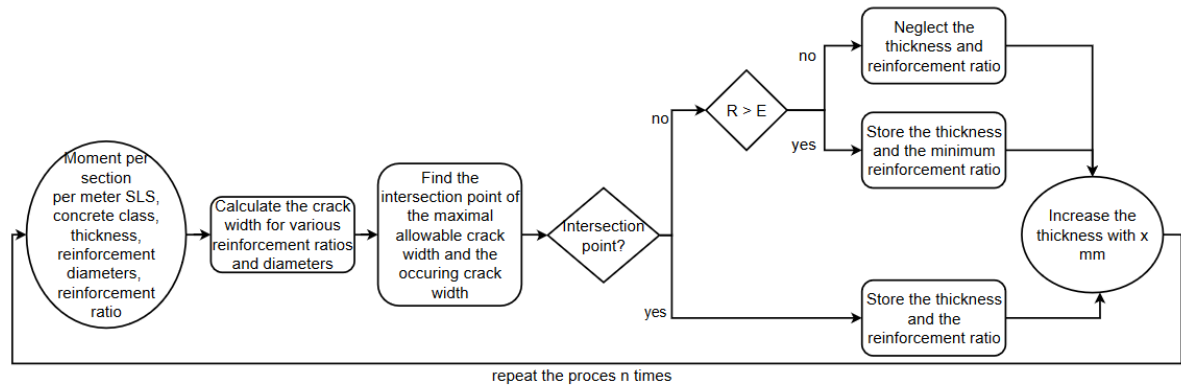
Figure 7.19: Crack width
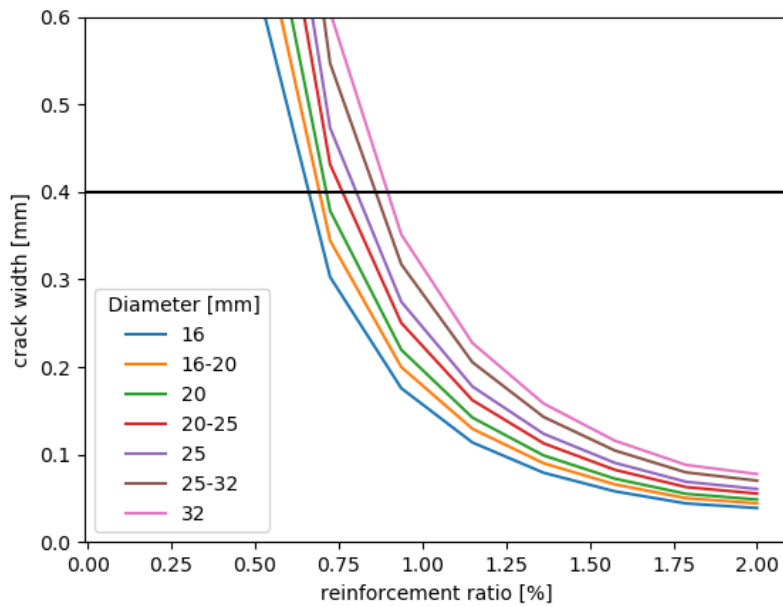
Figure 7.20: Crack width resistance per diameter versus the Maximal allowable crack width wall left section Chamber per meter

The model calculates the displacements based on the normative SLS load combination. The deflections can be divided in a deflection of the wall and a deflection due to the rotation of the floor. The rotation of the floor depends on the type of foundation, see Appendix B. The total deflection of the wall is the sum of the deflection of the wall and and the rotation of the floor. The principle of Euler Bernoulli is used to calculate the deflection of the wall.

$$w = \frac{Fl^3}{3EI}$$

$$\theta = \frac{Fl^2}{2EI}$$

The modulus of elasticity of the concrete is divided by three for the displacement calculations.

Global Stability

The lock head has to be checked on the global stability, being the vertical bearing capacity, horizontal bearing capacity, hydraulic bursting, rotational stability and piping see Appendix B.

The vertical bearing capacity of the soil, the weight of the structure, MHW and the groundwater level determine the type of foundation. The normative situation is a lock head in operation with a water level of MHW and a groundwater level of MHW. All the loads acting in the positive z-direction are multiplied with a factor of $\gamma = 1.1$. The loads acting in the negative z-direction are multiplied with $\gamma = 0.9$. The vertical bearing capacity determines the type of foundation. For a shallow foundation the resultant pressure has to be lower than the bearing capacity of the soil, which is set to $300 kN/m^2$. If this is not the case, a pile foundation is needed.
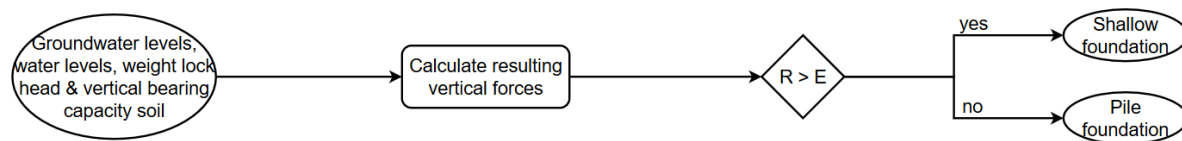
Figure 7.21: Vertical bearing capacity

To check the horizontal bearing capacity of the lock head, the model needs information about the soil properties, water levels, groundwater levels, the weight of the lock head and the length of the lock head. The situations checked in the model are an empty lock with the accompanying groundwater level and a lock head with a water level of Max schutpeil.

Two situations can be distinguished. In the first situation $F_{down} \geq F_{up}$. In this situation the friction force between the bottom of the lock head and the soil contributes to the horizontal bearing capacity. If $F_{down} \leq F_{up}$ there is no friction force between the floor of the lock head and the soil. The horizontal bearing capacity is only provided by the friction between the wall and the soil.

Assumed is a drained situation. The friction force between lock head and the soil follows from:

$$F_{H,friction} = F_{V,res} tan(\delta)$$

where:

$$\delta = \frac{2}{3}\phi$$
phi = angle of internal friction

The loads with a negative influence on the horizontal bearing capacity are multiplied with $\gamma = 1.1$. The loads with a positive influence are multiplied with $\gamma = 0.9$. In case the horizontal bearing capacity is not sufficient, the length of the lock head increases. This is done by increasing the length of the Tail with increments of $0.5m$.
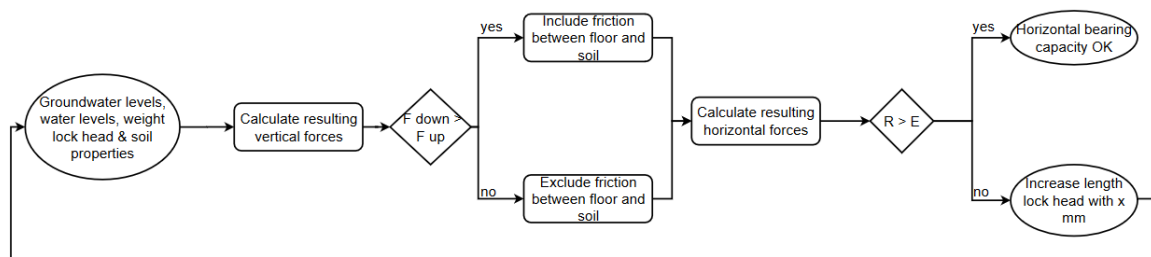
Figure 7.22: Horizontal bearing capacity

For the phenomenon hydraulic bursting the model needs information about the groundwater level and the weight of the lock head. The normative situation for the construction phase is the construction of the floor with a groundwater level of droogzetten. The normative situation for the operation phase is an empty lock for maintenance with a the groundwater level droogzetten. The same safety factors are used as before. When hydraulic bursting is an issue, GEWI piles are installed. It is assumed that when foundation piles are needed, these provide sufficient resistance against hydraulic bursting.
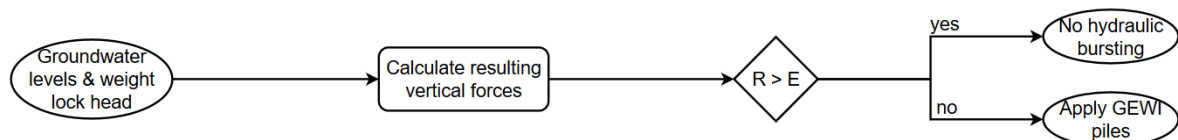
Figure 7.23: Hydraulic bursting

Two normative situations are checked in case of rotational stability. These are a lock head in operation with the biggest water level difference between the gates and an empty lock head with a water level of Max schutpeil. The model needs information about the geometry of the lock head, the water levels and the accompanying groundwater levels. The weight of the gate is also needed in the situation when the lock is in operation.

The geometry of the lock head determines the weight of the lock head, the weight of the gate and the length of the lock head. In case the rotational stability requirement is not met, the length of the lock head has to increase. This is done by increasing the length of the Tail with increments of $0.5m$.
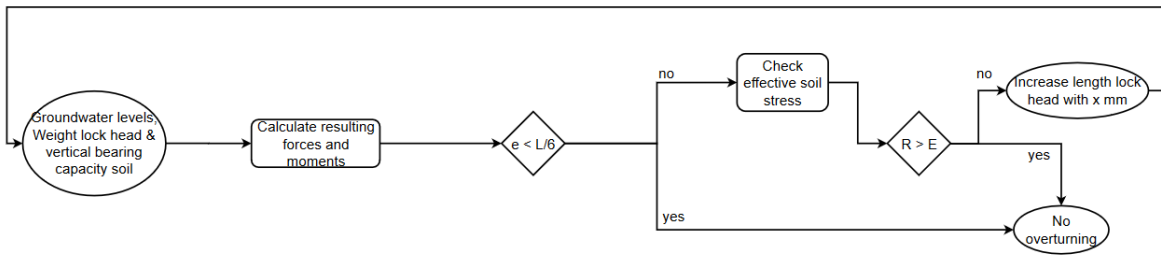
Figure 7.24: Rotational stability

The piping check is not incorporated in the parametric model. It is assumed that the connection between the lock head and lock chamber is watertight. This means that the total length of the navigation lock has to be taken in account for the piping calculations. However, the total length of the navigation lock is not known. The problem of piping can easily be counteracted by placing cut off screens.

Cost & MKI
The cost and MKI calculations are based on the following construction parts in Table 7.4. The costs are based on material cost and installation cost. The cost values are based on information obtained from Volkerwessels Infra Competence Centre. The MKI values are according to values used in DuboCalc. DuboCalc does not provide the MKI value of GEWI piles. To come to a MKI value, the MKI values of reinforcement and a steel foundation pile are combined, see Appendix C.

Table 7.4: Cost and MKI

Construction part	Cost	MKI
Concrete	142 [$€/m^3$]	20 [$€/m^3$]
Reinforcement	1126 [$€/ton$]	106 [$€/ton$]
Tension piles	2584 [$€/pile$]	34 [$€/pile$]
Foundation piles	1100 [$€/pile$]	94.16 [$€/pile$]
UWC floor	134 [$€/m^3$]	25.31 [$€/m^3$]

Iteration
What can be concluded from the above is the fact that a lot of factors depend on the geometry of the lock head. In some cases the dimensions of the lock head have to increase, mainly due to the global stability requirements. This has an influence on the loads, strength and stiffness calculations and the global stability calculations itself. The determination of the geometry of the lock head is therefore an iterative process.

7.2.3. Output
This section will show some output results based on the input parameters of the lock head in Empel. Based on these input parameters, two lock configurations are possible. This means that the output will include the results of the a lock head with a single leaf gate and with a mitre gate. The output of the model includes the following results:

- the geometry

- the moment & shear force distribution

- the moment & Shear force resistance

- the displacements

- the crack width

- the cost

- the MKI

Geometry

The geometry can be divided in five different sections, namely:

- the top of structure

- the bottom of structure

- width structure

- length structure

- thickness floor and wall

The top of the structure is defined as an input parameter. The bottom of the structure depends on type of vessel and its loaded draught and the Min schutpeil. The width of the structure depends on the width of the vessel and the type of gate. The length of the structure depends on the type of gate and the global stability. The thickness of the floor and the wall are variable and depend on the strength and stability calculations and the global stability.

Moment & Shear Force Distribution

The maximum external moment distribution over the total length of the lock head for the left wall are shown in Figure 7.25a & 7.25b. The maximum external moment distribution over the total length of the floor are shown in Figure 7.26a & 7.26b
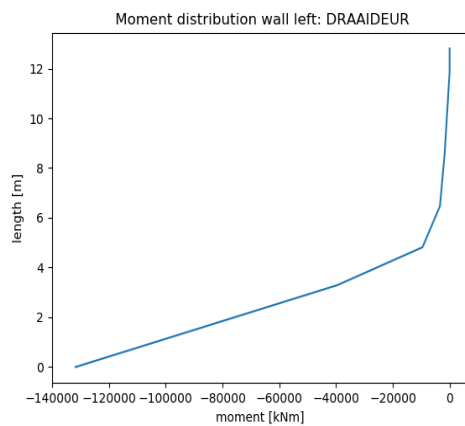
(a) Single leaf gate
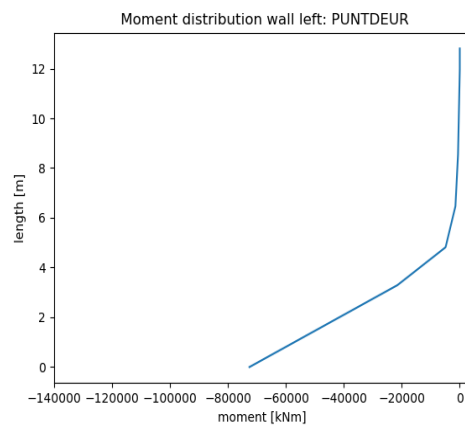
(b) Mitre gate

Figure 7.25: Maximum external moment distribution wall left
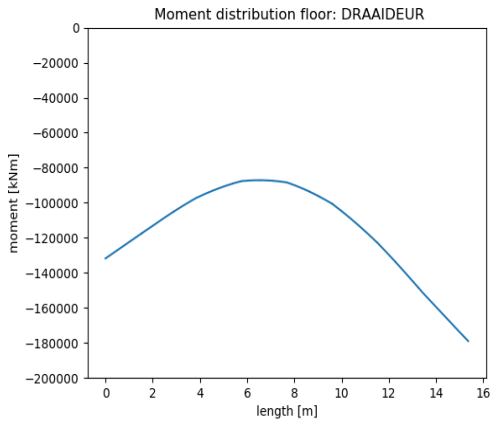
(a) Single leaf gate
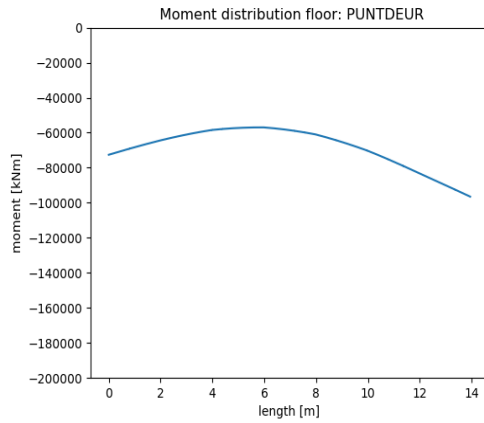
(b) Mitre gate

Figure 7.26: Maximum external moment distribution floor

Figure 7.27a & 7.27b show the maximum external shear force distribution for the wall left. The shear force distribution has a step-wise distribution, since distributed loads have been transformed to point loads. This means that the shear force distribution gives an approximation of the reality.
Figure 7.28a & 7.28b show the maximum external shear force distribution for the floor. One can see a jump in the shear force distribution at the location of the foundation piles.
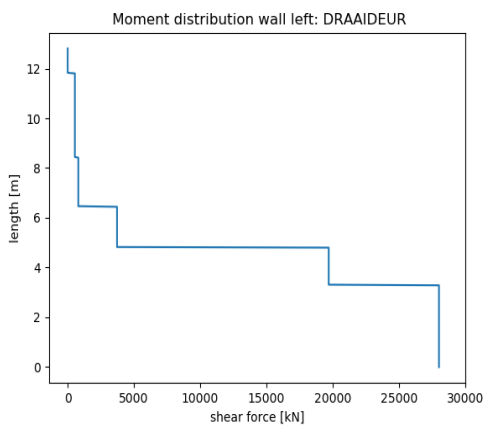
(a) Single leaf gate
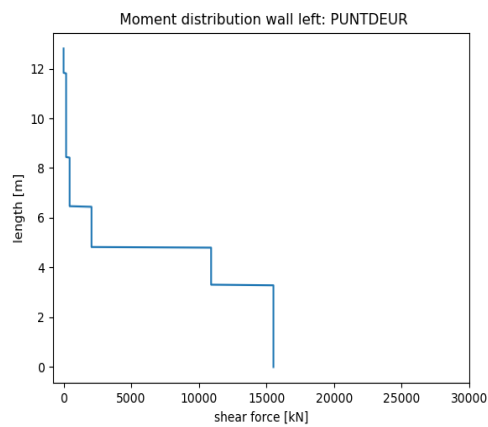
(b) Mitre gate

Figure 7.27: Maximum external shear force distribution wall left
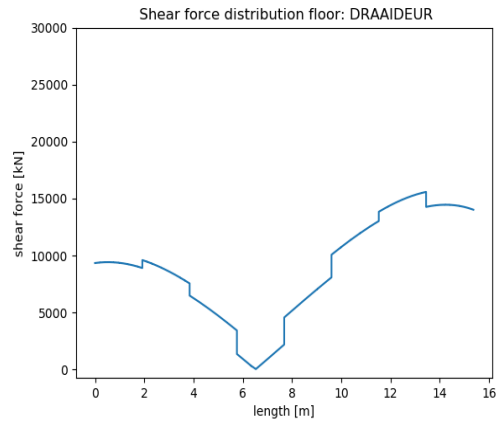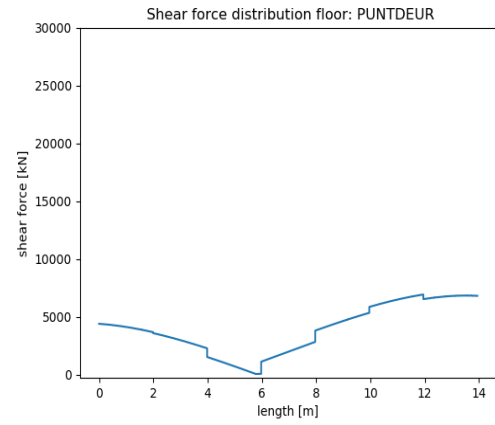
(a) Single leaf gate   (b) Mitre gate

Figure 7.28: Maximum external shear force distribution floor

The maximum moment per meter for the wall left and the floor for the section Chamber are shown in Figures & .
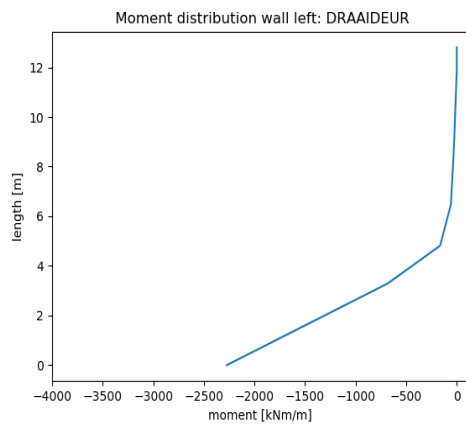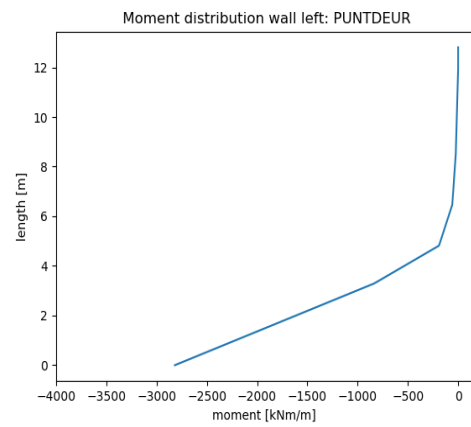
(a) Single leaf gate   (b) Mitre gate

Figure 7.29: Maximum moment distribution wall left section Chamber per meter
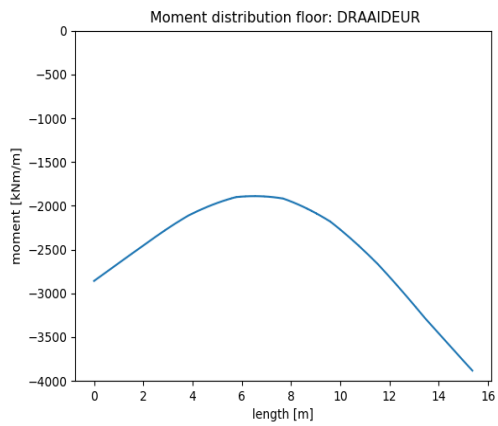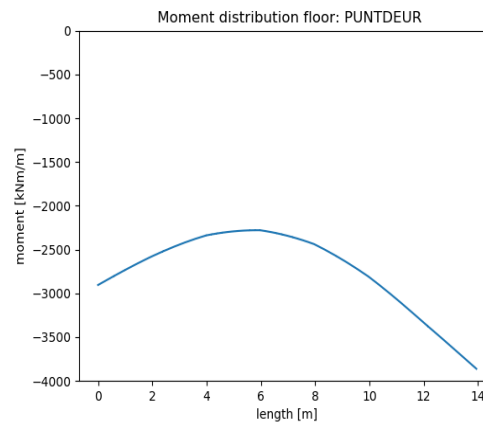
(a) Single leaf gate

(b) Mitre gate

Figure 7.30: Maximum moment distribution floor section Chamber per meter

The maximum shear force distribution per meter for the wall left and the floor for the section Chamber are given in Figure 7.31 & 7.32
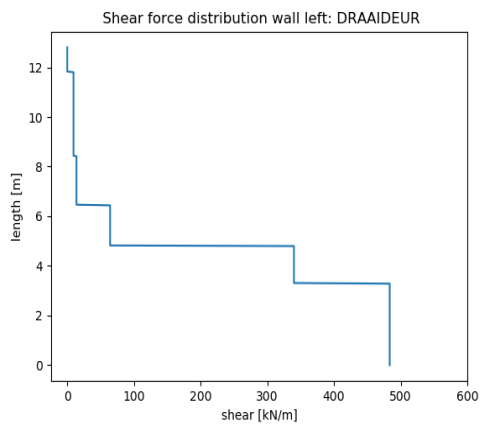
(a) Single leaf gate
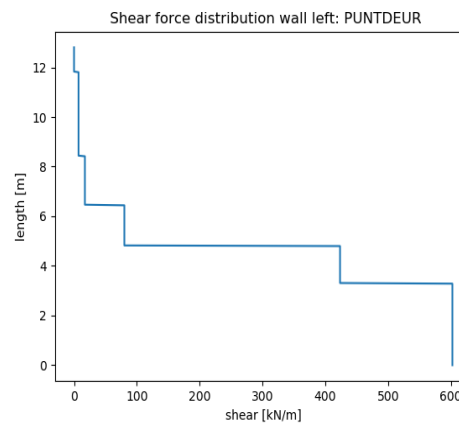
(b) Mitre gate

Figure 7.31: Maximum shear force distribution wall left section Chamber per meter
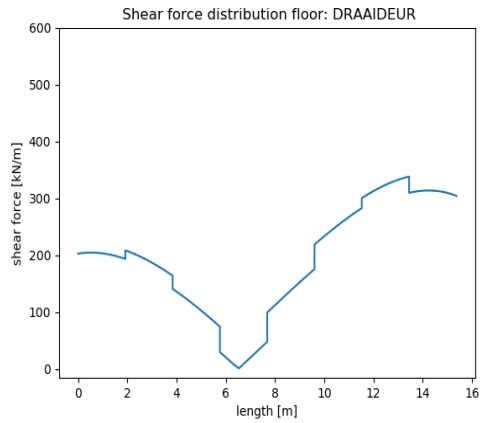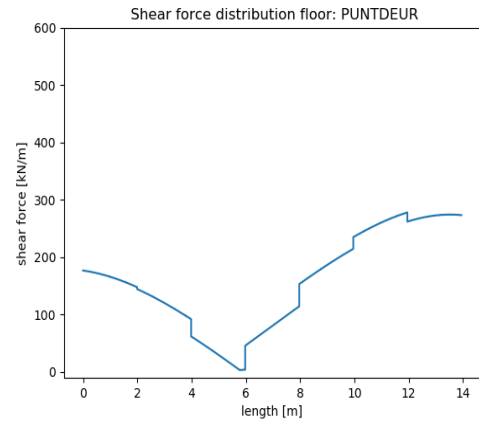
(a) Single leaf gate   (b) Mitre gate

Figure 7.32: Maximum shear force distribution floor section Chamber per meter

Moment & Shear Force Resistance

The model calculates the amount of reinforcement needed to withstand the bending moment per section per meter for several thicknesses by searching for the intersection point. Based on this information the model calculates the accompanying shear reinforcement. This process is repeated for several thicknesses. Keep in mind that for each thickness, the moment and shear force distribution change. Figures 7.33 & 7.34 show the amount of bending reinforcement per thickness for the wall left section Chamber per meter and the floor section Chamber per meter. Figures 7.35 & 7.36 show the centre to centre distance between the shear reinforcement per thickness for the wall left section Chamber per meter and the floor section Chamber per meter.
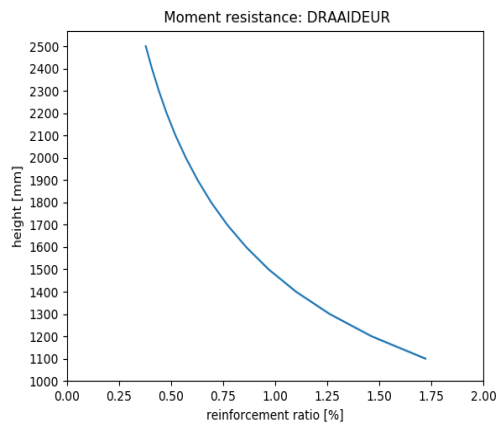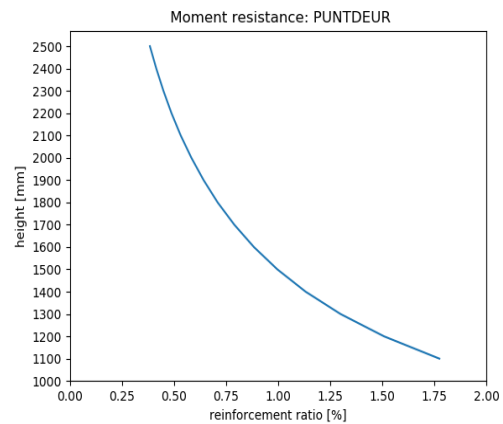
(a) Single leaf gate   (b) Mitre gate

Figure 7.33: Moment resistance wall left section Chamber per meter
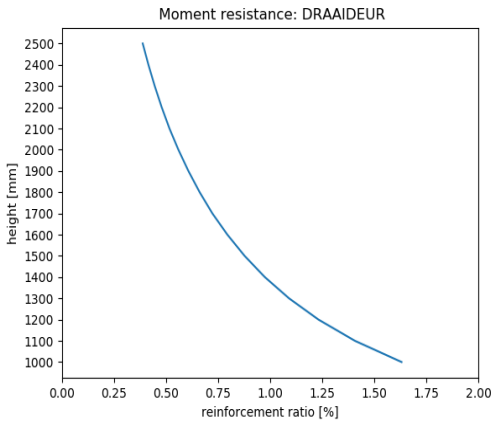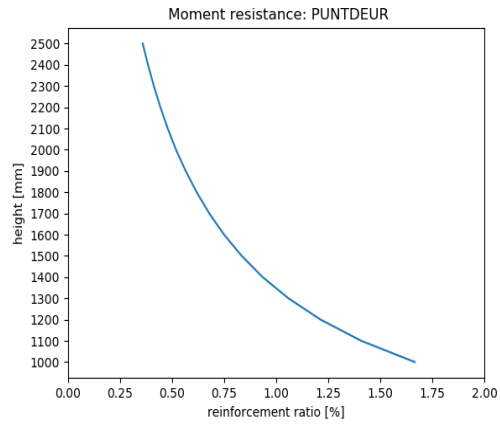
(a) Single leaf gate

(b) Mitre gate

Figure 7.34: Moment resistance floor section Chamber per meter
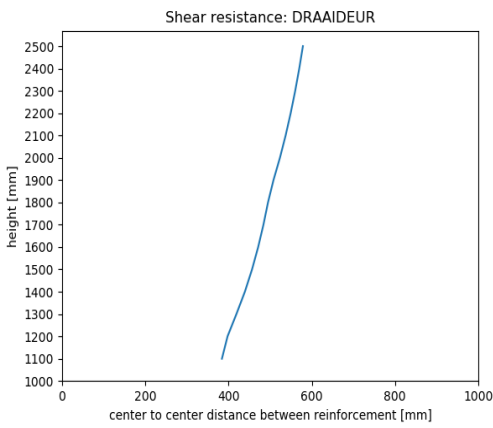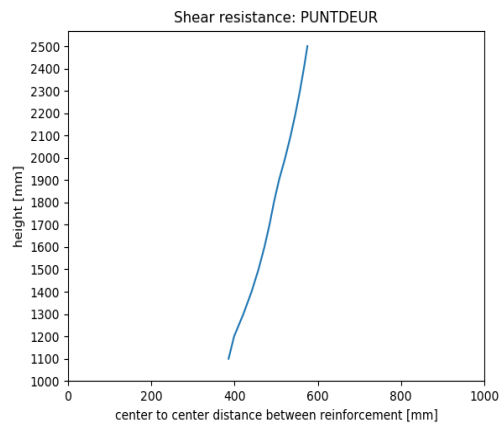
(a) Single leaf gate

(b) Mitre gate

Figure 7.35: Shear force resistance wall left section Chamber per meter
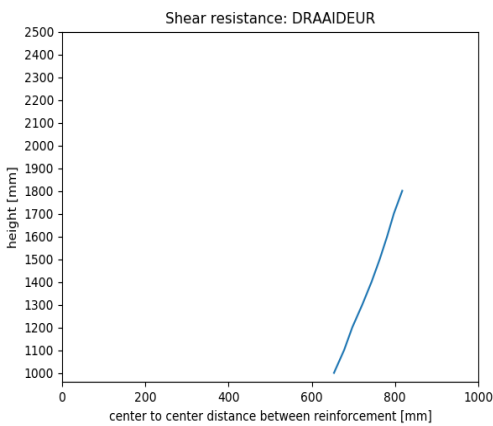
(a) Single leaf gate
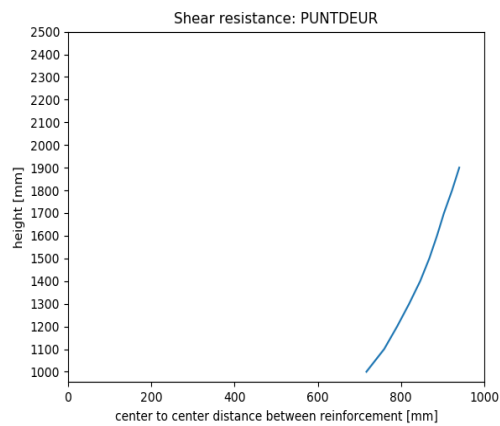
(b) Mitre gate

Figure 7.36: Shear force resistance floor section Chamber per meter

Crack Width

Figures 7.37 & 7.38 give the amount of reinforcement needed for each thickness to stay below the allowable crack width for the wall left section Chamber and the floor section Chamber. The figures show some inaccuracies. This is due to the package that has been used to solve the problem. The package used is called scipy optimize. The two unknowns x (concrete compression height) and ϵ_s (the strain in the reinforcement) are found on trial and error, by solving the horizontal equilibrium and moment equilibrium. The more tries the package need, the more inaccurate the answer becomes.
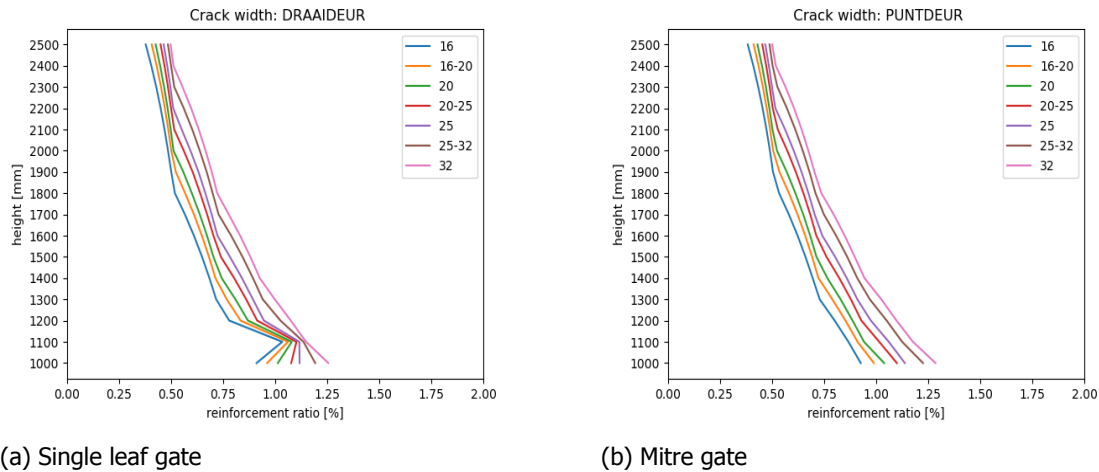
(a) Single leaf gate   (b) Mitre gate

Figure 7.37: Crack width wall left section Chamber per meter
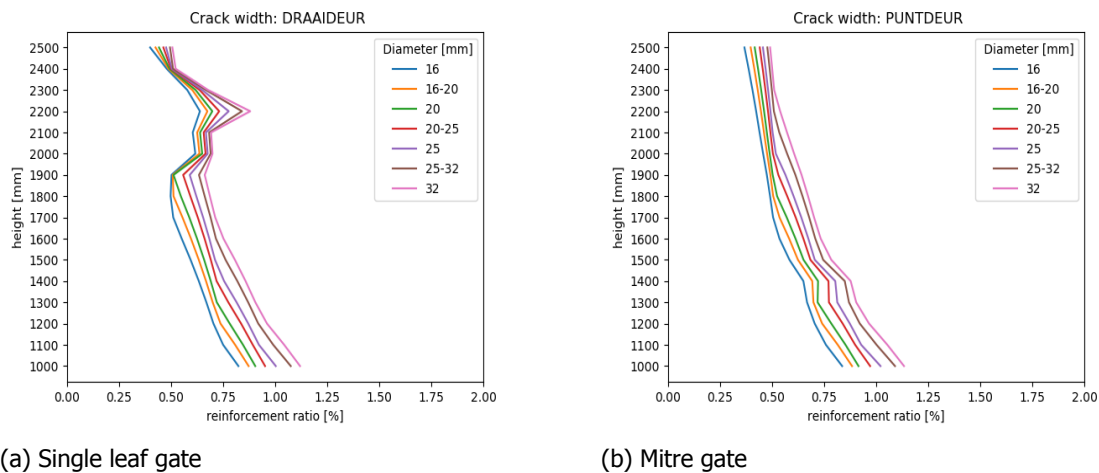
(a) Single leaf gate   (b) Mitre gate

Figure 7.38: Crack width floor section Chamber per meter

Displacements

Figures 7.39 & 7.40 give the displacements over the total length of respectively the wall left and the wall right. The difference in displacement between the single leaf gate and the mitre gate is due to the gate type. The thickness of the single leaf gate is $\frac{1}{6}/\frac{1}{8}$ of the free width clearance. The thickness of a mitre gate is $\frac{1}{16}/\frac{1}{20}$ of the free width clearance. This means automatically that the thickness of the wall section Head and Tail for the single leaf gate is greater than for a mitre gate. This results in a stiffer construction for a single leaf gate and therefore smaller displacements.
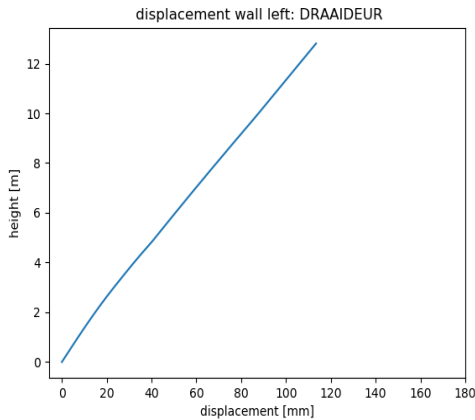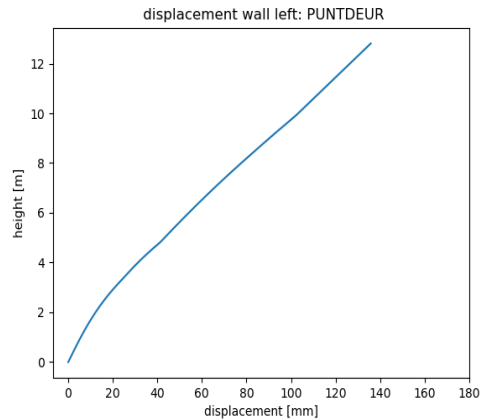
(a) Single leaf gate   (b) Mitre gate

Figure 7.39: Displacements wall left
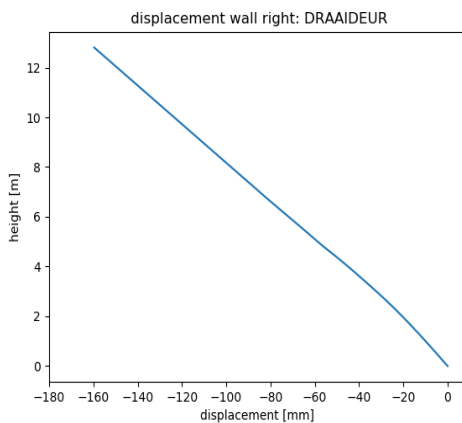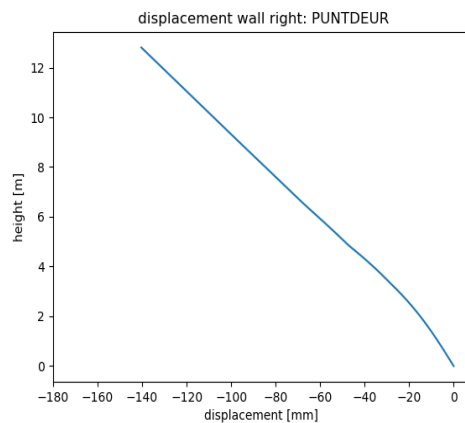
(a) Single leaf gate   (b) Mitre gate

Figure 7.40: Displacements wall right

Cost and MKI
The cost and MKI will be elaborated in Chapter 8.

7.3. Validation

The parametric model has been validated with the help of results from the calculations done for the lock head in Empel, hand calculations, SCIA Engineer calculations and Maple. An one to one comparison with the lock head in Empel is not possible since the lock head configuration of Empel differs from the lock head configuration of the model, see Figures 7.2 & 7.3 and Chapter 4. The gate of the lock head in Empel is secured at the Wall east. In open position the gate extends the length of the lock head, see Figure 4.12. The model always accounts for a protection fully provided by the lock head itself, see Figure 7.2. This results in different dimensions in the x-direction of the lock head.

7.3.1. Loads
To validate the loads, the design parameters of the lock head in Empel have been applied to the parametric model. An one to one comparison of the loads is possible since the loads are calculated per meter. Table 7.5 & 7.6 give the values of the loads and their lever arms. The soil load, groundwater load, hawser load and traffic load according to the parametric model match the values calculated by

Volkerwessel Infra Competence Centre.

The crane load and the gate load differ. Volkerwessel Infra Competence Centre has calculated the horizontal crane load by dividing the vertical crane load by 2, see Appendix C. The parametric model calculates the horizontal crane load according to the guidelines prescribed by the 'Handboek voor het Ontwepren van Schutsluizen' (*Ontwerp van Schutsluizen*, 2000), see also Appendix B.

The load of the gate in the parametric model is based on information from different gates, see Appendix E. To calculate the load of the gate, the length and the width of the gate are needed. The dimensions of the gate depend on the type of vessel entering the lock. In this case the type of vessel is of CEMT-class IV. This results in an inner width of the lock head of $10.5m$. However, the inner width of the lock in Empel is $12.85m$. This explains the difference in gate load.

Table 7.5: Forces Empel & model

	Soil $[kN/m]$	Groundwater $[kN/m]$	Hawser $[kN]$	Traffic $[kN/m]$	Crane $[kN]$	Gate $[kN]$
Empel	550	460	200	130	865	605
Model	541	451	200	127	709	495

Table 7.6: Lever arms Empel & model

	Soil $[m]$	Groundwater $[m]$	Hawser force $[m]$	Traffic $[m]$	Crane $[m]$	Gate $[m]$
Empel	4.86	3.50	8.40	6.51	9.22	10.47
Model	4.82	3.30	8.43	6.47	9.88	11.81

7.3.2. Matrix Method

To validate the matrix method used for the floor, Maple has been used. For this purpose a beam of $10m$ has been modelled both in Python and in Maple. The beam has two equal spans of $5m$ and is supported by three springs. A vertical force and a bending moment have been applied at both ends of the beam. A detailed description is given in Appendix E. Figures 7.41 & 7.42 show the moment and shear force distribution respectively obtained with Maple and Python.
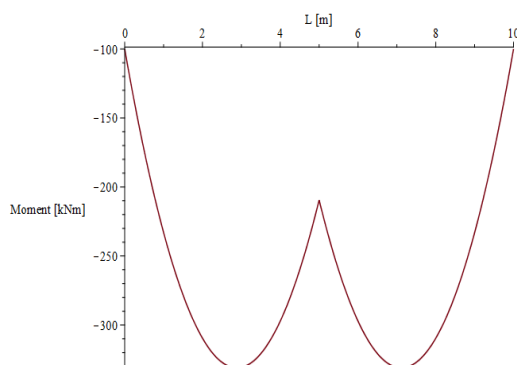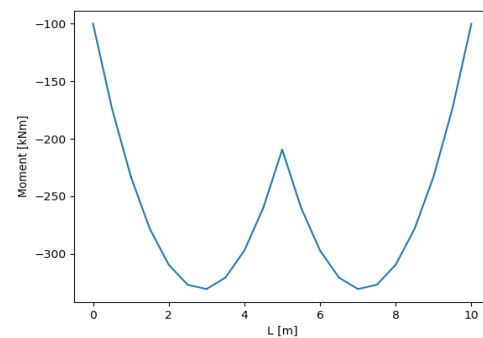
(a) Solving the ODE with Maple   (b) Matrix method with Python

Figure 7.41: Moment distribution
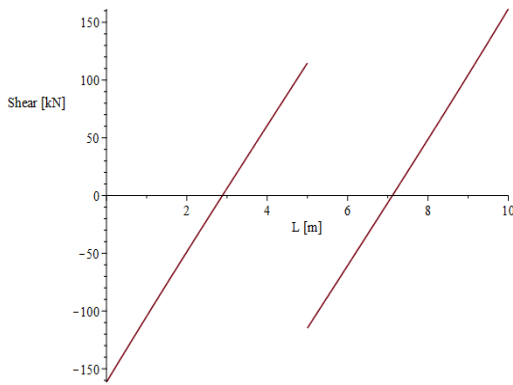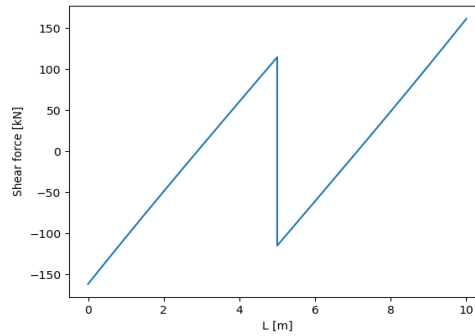
(a) Solving the ODE with Maple   (b) Matrix method with Python

Figure 7.42: Shear force distribution

7.3.3. Moment Distribution

The parametric model calculates the external moments over the total length of the walls and floor. The next step is to divide the external moment over the different sections of the lock head. Since the dimension in x-direction differ, an one to one comparison is not possible. Therefore, the external moment following from load combination ULS DZ1 acting on Wall west of the lock head Empel has been used to validate the calculations in the parametric model.

Volkerwessels Infra Competence Centre has used SCIA Engineer to determine the bending moments per section. To implement this principle to the model, the rules of mechanics have been applied . The results of the calculations can be found in Table 7.7. For a detailed description of the calculations see Appendix E.

Table 7.7: Bending moment per section western wall lock head Empel

	Section Head [kNm]	Section Chamber [kNm]	Section Tail [kNm]	Total [kNm]
SCIA	24615	33554	42134	103781
Hand calculations	25488	27316	50976	103781

The moment distribution of the section Head corresponds with the results of the SCIA model. The results of the section Chamber and section Tail differ with respectively -20% and 20%. This is mainly due to the fact that the concentrated load of the crane and the boulder act on these sections. The sum of the individual sections corresponds with the external moment.

7.3.4. Moment Resistance

Volkerwessel Infra Competence Centre uses Dako to calculate the bending resistance, crack width and shear force resistance (Appendix E). At the time of the design phase of the lock head in Empel, old design rules were applied to the shear force resistance and crack width calculations. Therefore, the shear force resistance and crack width calculations have not been validated, but are based on current rules from the Eurocode. The bending moment resistance has been validated. For this purpose a bending moment resistance calculation is compared to a hand calculation for an identical cross section, see Table 7.8

Table 7.8: Validation bending moment resistance

	Bending moment resistance [kNm]
Dako	5821
Hand calculation	5852

7.3.5. Displacements

The maximum displacement for the wall without the gate for load combination SLS DZ1 according the SCIA calculations is $82.6mm$, see Figure 6.2. To validate the displacements, the thicknesses of the walls and the floor in the parametric model have been set to the thicknesses of lock head Empel. The same load combination has been applied. The wall without the gate in the parametric model is the wall left. The maximum displacement of the wall left is $72.0mm$, see Figure 7.43. This is only a difference of $1cm$. The difference is explained by the fact that the Head part of Empel is missing. Therefore, the total structure is less stiff.
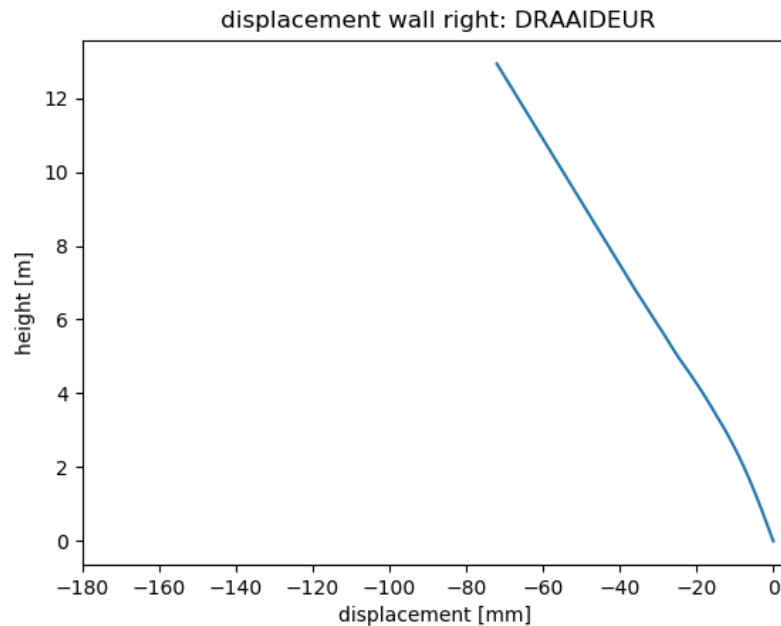
Figure 7.43: Displacements wall left SLS DZ1 parametric model

7.4. Limitations

Only the lock head is taken into account. In order to make the parametric model more relevant, the total navigation lock should be incorporated in the parametric model.

The parametric model only accounts for a lock head with a single leaf gate and a mitre gate. This is because the lock configuration, the gate mechanisms and the loads acting on the structure are very alike. To make a fair comparison between all the lock heads, the lifting gate and rolling gate should also be incorporated in the model.

The parametric model always design a lock head according to a standard configuration prescribed by the rules from the 'Handboek voor het Ontwerpen van Schusluizen' (*Ontwerp van Schutsluizen*, 2000) and the 'Richtlijnen Vaarwegen 2017' (*Richtlijnen vaarwegen 2017*, 2017), see Figures 7.2 & 7.3. To deviate from this configuration is not possible, as is the case for lock head Empel.

The gate choice is only based on the width of the lock head an the direction of water retention. The choice is independent of the construction cost, the maintenance, the reliability, the durability, the locking capacity, the impermeability and the usability.

The gate operating systems are not incorporated in the model. The load of the gate is based on the dimensions of three different gates, being the two gates for the Reeve sluis and the gate for the lock in Empel. The detailed calculations at the locations of the gate hinges are not taken into account.

A lock head may retain water in one or in both directions. What configuration is possible follows from Table 7.2. In some situations extra measures are necessary in order to secure retention in both directions. These measures are not taken into account.

The foundation calculations incorporated in the parametric model require further research. For the pile foundation as well as the shallow foundation with GEWI piles the model assumes a standard foundation/GEWI pile. The type and configuration do not depend on probings. For future studies it is advised

to incorporate the probings in the parametric model.

The bearing capacity of the soil is assumed to be $300kN/m^2$. This differs of course per location.

The crack width calculations take up a lot of time. This is due to the fact that two equations with two unknowns have to be solved. The two unknowns in the equation are the compressive concrete height x and the strain of the reinforcement ϵ_s. To solve this problem in Python, the scipy optimize package has been used. The way this package finds the unknowns is by trial and error. It starts with a guess of 1 for both the unknowns. It changes the guesses until they suffice the equations. The longer the calculations take, the more inaccurate the results become. This can be seen in Figure 7.38.

As was already explained, the floor is divided in different segments and even further divided in smaller sub segments. This results in a long calculation time. It is recommended to replace these sub segments for formulas that are able to predict the behaviour of the floor between the foundation/GEWI piles.

8

Results

This chapter will show the results obtained with the parametric model. The results include the MKI, the cost and the MKI + cost of the lock head design. The cost and the MKI take into account the concrete, the reinforcement, the under water concrete floor and the foundation piles. The reinforcement covers the longitudinal reinforcement and the shear reinforcement.

In order to design an economical and sustainable lock head, different parameters have been altered, being the water head, the thickness of the floor and the walls, and the type of concrete. This has been done for different CEMT classes and for a mitre gate and a single leaf gate.

This chapter will show the results of CEMT class IV with the parameters from the lock head in Empel. The other CEMT classes with the same parameters as in Empel will be discussed in Appendix F.

The chapter concludes with a comparison between a single leaf gate and a mitre gate design from the parametric model and the lock head in Empel.

8.1. Influence Difference in Water Head

In this section the influence of the water head on the lock head design has been investigated. For this purpose the water level inside the lock head has been altered. The beginning water level is equal to MHW ($7.83mNAP$). After each run the water level in the chamber is lowered with $1m$, this is done 10 times. The water level outside the lock head in the approach area is equal to the MHW. The thickness of the walls and the floor is set to $2m$.

8.1.1. Single Leaf Gate

The design of the a single leaf gate up to CEMT class IV is independent of the water head (CEMT class V is discussed in Appendix F). Due to the configuration of the single leaf gate, the lock head is long enough to generate enough friction to prevent the lock head from horizontal bearing failure. Figure 8.1 shows the difference in MKI and cost due to the change in water head. The results show that the lock configuration does not change.
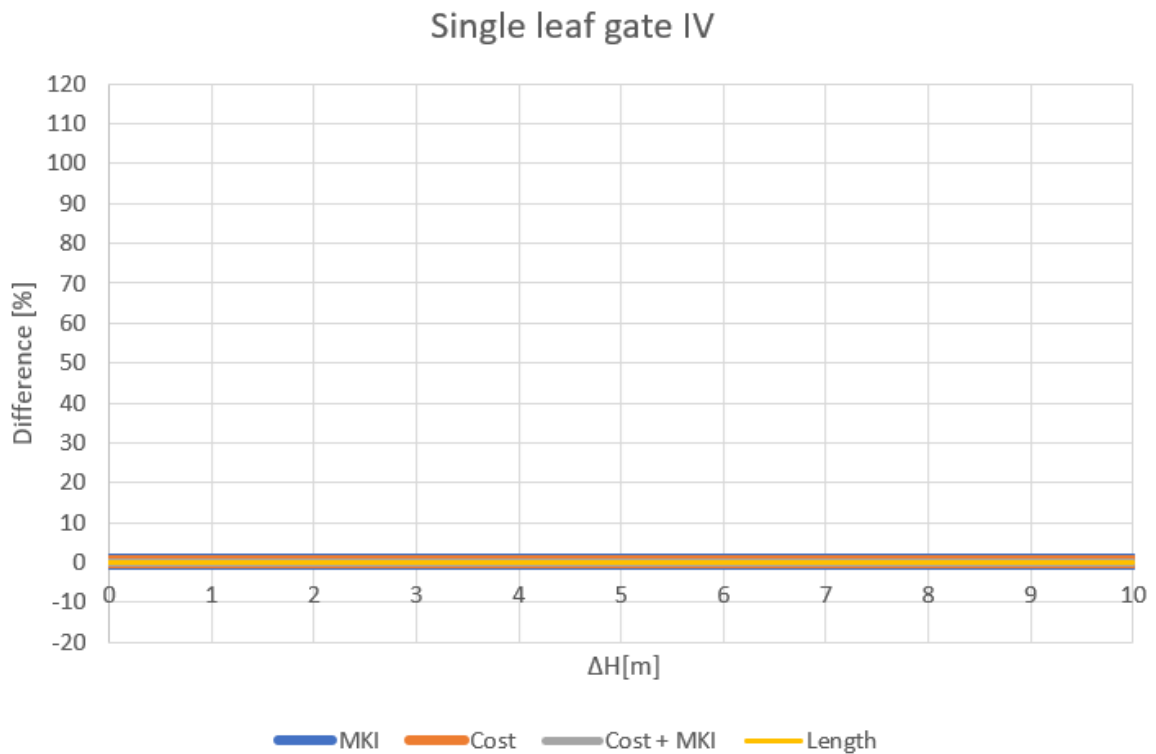
Figure 8.1: Difference in MKI, Cost, Cost + MKI and length for a varying water head

Figure 8.2 shows the the percentage of the reinforcement, concrete, UWC and the GEWI piles on respectively the MKI, the cost and the cost + MKI. The lines are constant, what follows from the fact that the single leaf gate design does not change.

Figure 8.2a shows that concrete has by far the biggest influence on the MKI, abut 70%. Furthermore the GEWI piles have the lowest influence on the MKI (5%), but the biggest influence on the cost (40%). The MKI of GEWI piles is low due to the recycle factor, see Appendix C. However, the GEWI piles have a high unit price.

Figure 8.2c shows that the MKI is about 10% of the total cost, see also Appendix F.

(a) MKI   (b) Cost   (c) Cost + MKI
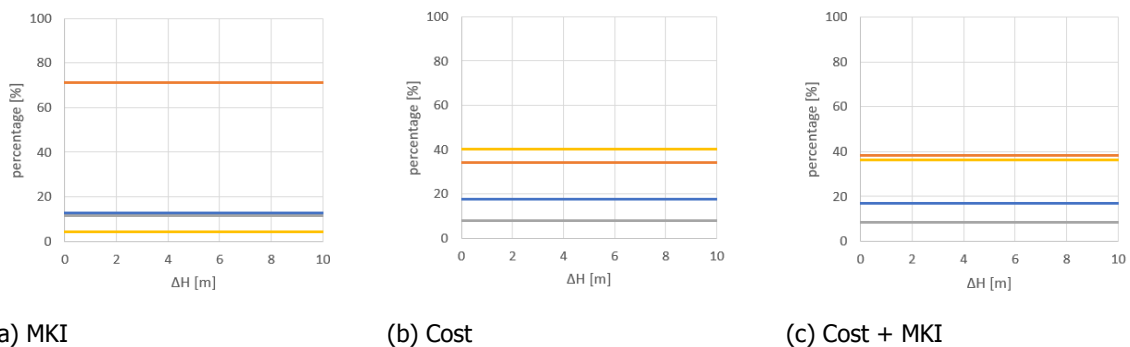
Figure 8.2: Percentage of the materials on the MKI, Cost and Cost + MKI for a single leaf gate with a difference in water head
Blue = Reinforcement, Orange = Concrete, Grey = UWC, Yellow = GEWI

8.1.2. Mitre Gate

Figure 8.3 shows the difference in MKI, cost, cost + MKI and length for a mitre gate due to the difference in water head. From the figure it can be concluded that the mitre gate design depends on the horizontal bearing capacity. When the water head difference increases, the cost, MKI and length increases. Due to the increase in water head difference, the length of the lock head needs to increase

to generate enough friction against horizontal bearing failure.

The lines are not completely straight, as one may expect. This is due to the fact that the parametric model increases the length of the Tail with increments of $0.5m$. Besides the parametric model designs a GEWI pile configuration with a maximum distance between the piles of $2m$. When the threshold of $2m$ is exceeded, the parametric model adds an additional row of GEWI piles. This is mostly seen in the cost line, since the influence of GEWI piles on the cost is approximately 40%, while the influence on the MKI is approximately 5%, see Figure 8.4.
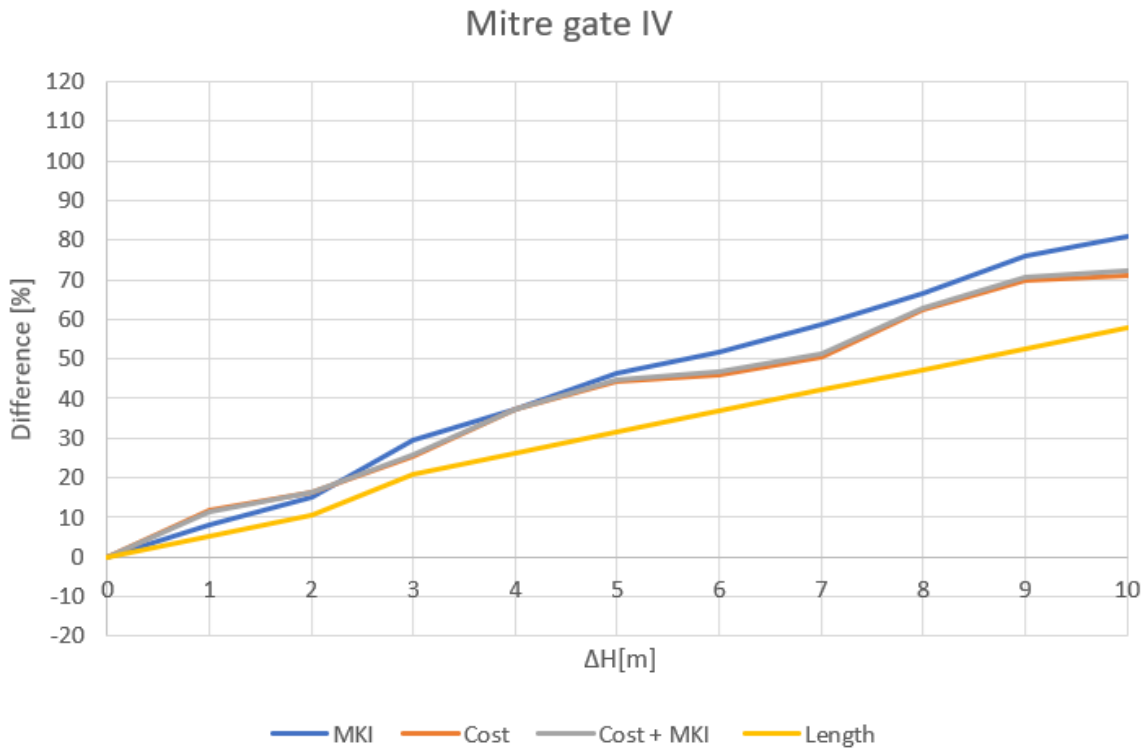
Figure 8.3: Difference in MKI, Cost, Cost + MKI and length for a varying water head

Figure 8.4 shows the the percentage of the reinforcement, concrete, UWC and the GEWI piles on respectively the MKI, the cost and the cost + MKI. The lines are relatively constant. The same can be concluded as for the single leaf gate.

(a) MKI

(b) Cost
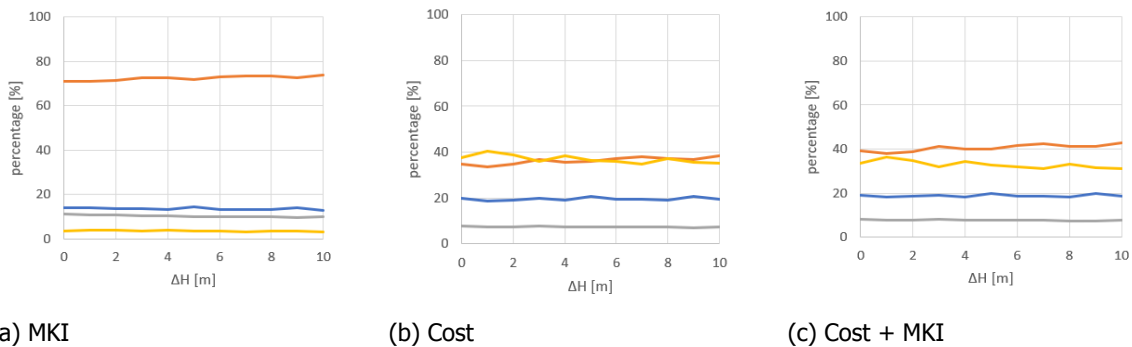
(c) Cost + MKI

Figure 8.4: Percentage of the materials on the MKI, Cost and Cost + MKI for a mitre gate with a difference in water head
Blue = Reinforcement, Orange = Concrete, Grey = UWC, Yellow = GEWI

8.1.3. Comparison

A comparison in the cost + MKI is made between the single leaf gate and the mitre gate. Figure 8.5 shows the ratio between the single leaf gate and the mitre gate. The figure shows that the bigger the difference in water head, the smaller the difference between the single leaf gate and the mitre gate becomes. This is due to the increase in length of the mitre gate. The single leaf gate is already long enough to generate enough friction against horizontal bearing failure due to its standard configuration. The mitre gate becomes approximately as long as a single leaf gate.

The comparison between a mitre gate and a single leaf gate of CEMT classes II, III and V can be found in Appendix F. From the overall results it can be concluded that the influence of the horizontal bearing capacity on the lock head design increases for an increase in CEMT class, see Figure 8.6. This is due to the increase in dimensions per CEMT class. Due to the increase in influence of the horizontal bearing capacity, the difference between a mitre gate and a single leaf gate decreases.
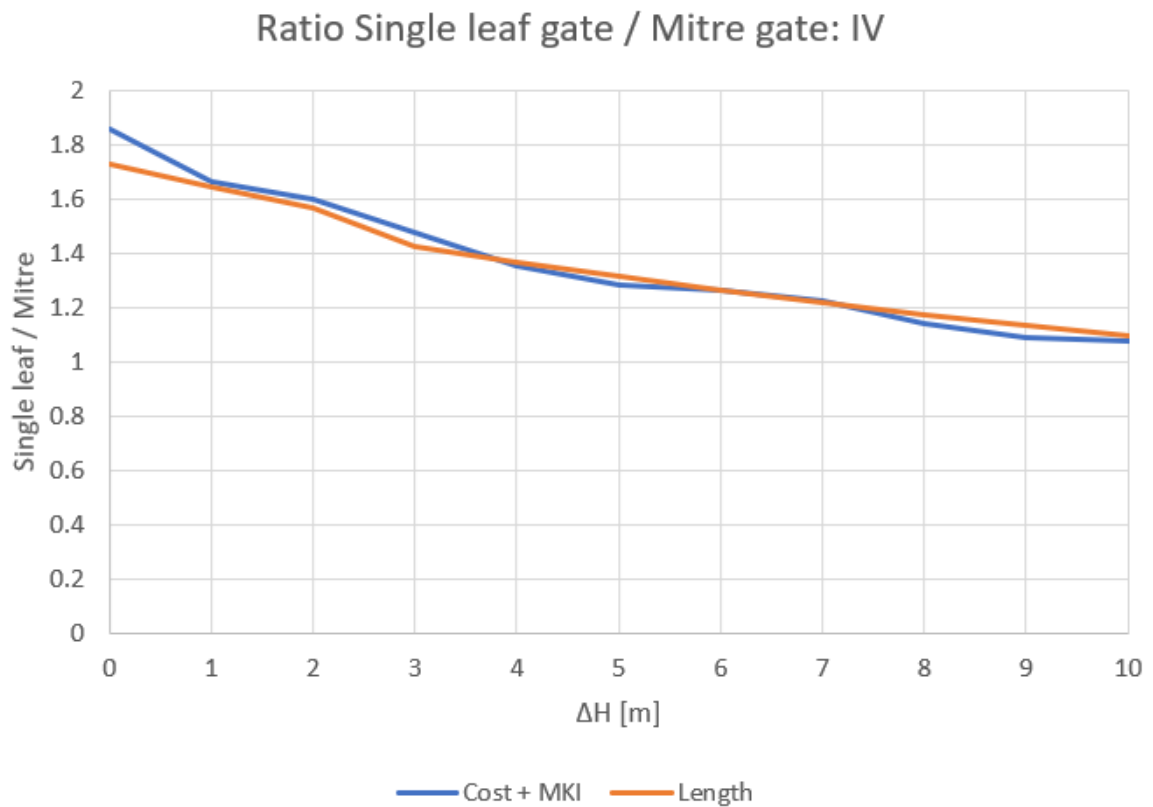
Figure 8.5: Cost + MKI comparison between a mitre gate and single leaf gate with a varying water head
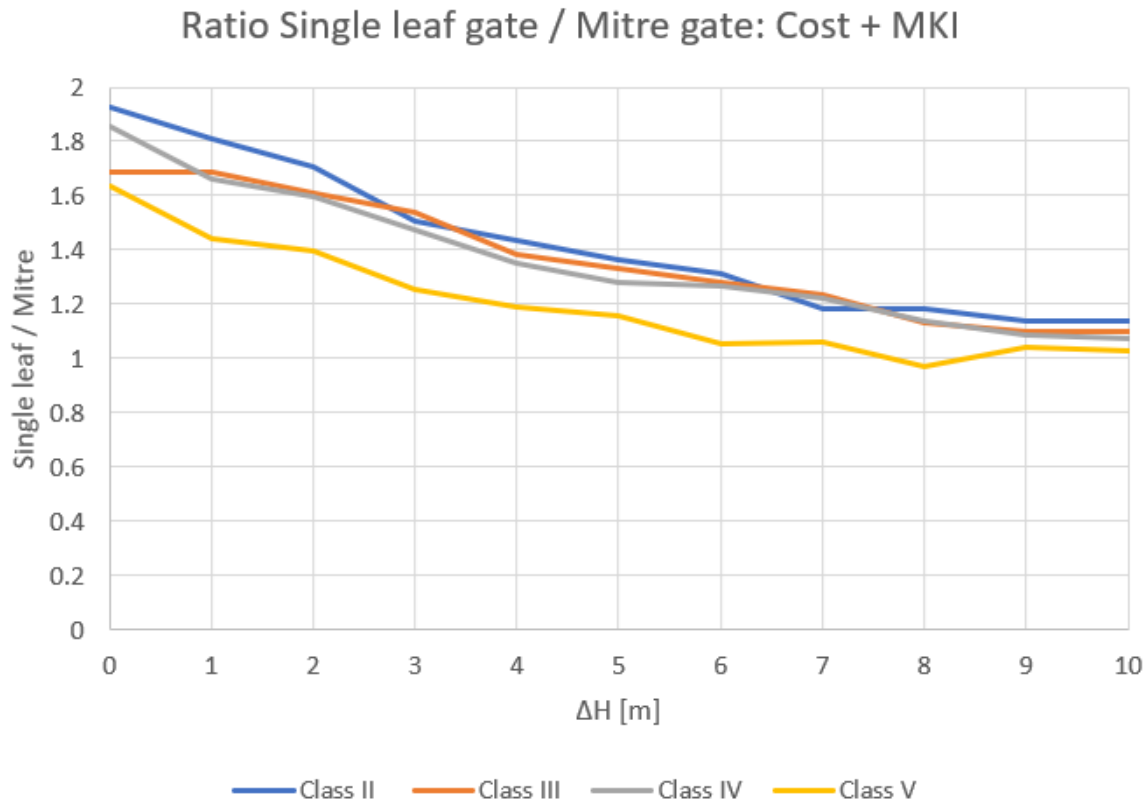
Figure 8.6: Cost + MKI comparison between a mitre gate and single leaf gate with a varying water head for several CEMT classes

8.2. Influence Thickness

In this section the thickness of the section Chamber of the floor and the walls is altered between $1100mm$ and $2500mm$ with steps of $100mm$. The thickness of the sections Head and Tail will change accordingly, see the previous Chapter 7. By increasing the thickness, the weight of the lock head increases. The difference in water head is constant.

8.2.1. Single Leaf Gate

Figure 8.7 shows the difference in cost, MKI and length for a single leaf gate due to the increase in thickness. The lock head design is again independent on the global stability checks, see the constant yellow line. The cost and MKI lines increase due to an increase in thickness. The lines are not completely straight as one may expect. By increasing the thickness of the walls, the width of the construction pit increases. An increase in the construction pit requires more GEWI piles. The parametric model retains a maximum width between the GEWI piles of $2m$. When this is not possible anymore, by for example increasing the width, the model adds an additional row of GEWI piles. This results in a not linear progression of the MKI and cost line. However, the MKI line is more linear because of the small influence of the GEWI piles on the MKI.
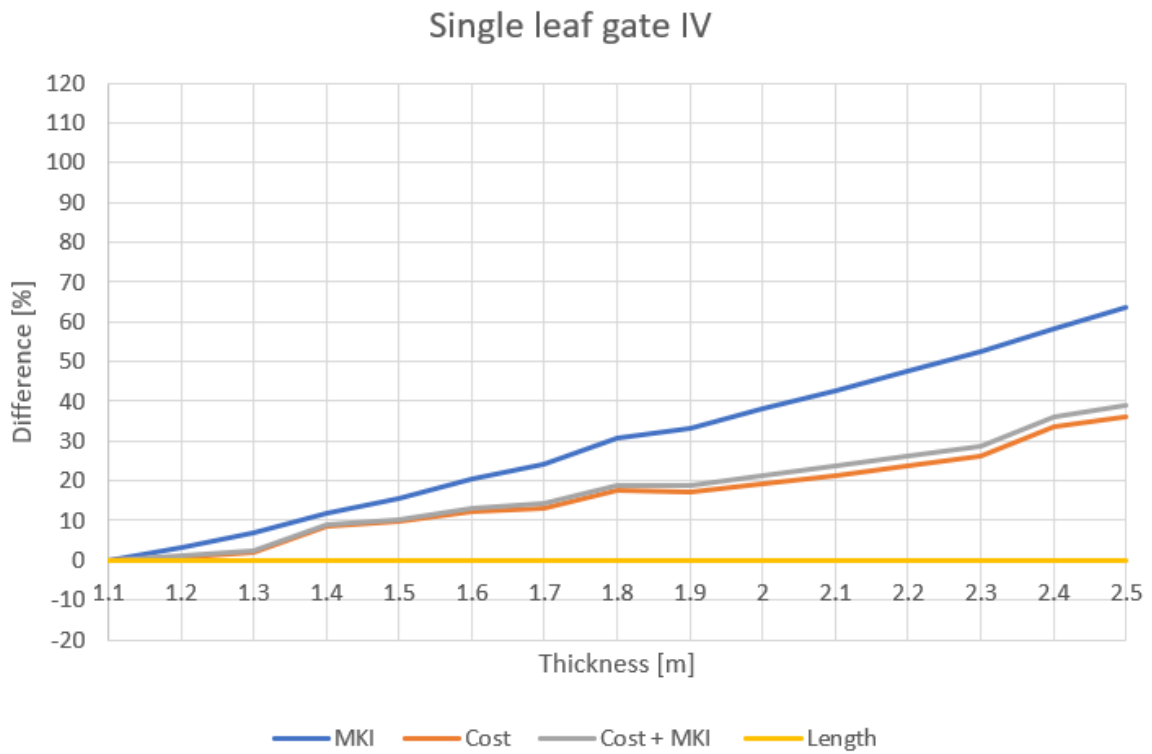
Figure 8.7: Difference in MKI, Cost, Cost + MKI and length with a varying thickness

Figure 8.8 shows the percentage of the reinforcement, the concrete, UWC and GEWI on relatively the MKI, cost and cost + MKI. Again it can be concluded that concrete has the biggest influence on the MKI, Figure 8.8a. Furthermore, the percentage of the concrete increases and the percentage of the reinforcement decreases due to the increase in thickness. The decrease in reinforcement flattens towards the end. This due to the minimum reinforcement that has to be applied in a cross section. The yellow line seems pretty constant in Figure 8.8a. However in Figures 8.8b & 8.8c the yellow line is less constant. This due to the increase in GEWI piles and the high unit price of these.

(a) MKI   (b) Cost   (c) Cost + MKI
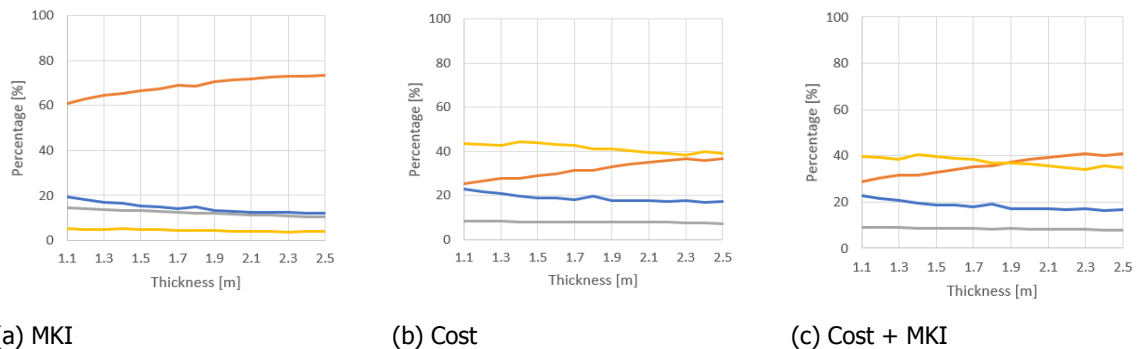
Figure 8.8: Percentage of the materials on the MKI, Cost and Cost + MKI for a single leaf gate with a difference in thickness
Blue = Reinforcement, Orange = Concrete, Grey = UWC, Yellow = GEWI

8.2.2. Mitre Gate
Figure 8.9 shows the difference in cost, MKI and length due to the increase in thickness for a mitre gate. By increasing the thickness of the walls and the floors, the weight of the lock head increases. Therefore, the friction between the floor and the soil increases. This results in a reduction of the length of the lock head. The yellow line is not smooth however. This is due to the parametric model increasing the length of the lock head with increments of $0.5m$ in case the horizontal bearing capacity

or the rotational stability requirements are not met. Would this number be lower, a smooth line is expected.

The grey and orange lines in Figure 8.9 changes suddenly at certain point. This is due to the increase in width of the total structure on the one hand and a decrease in length on the other hand. The length and the width have an influence on the GEWI pile configuration, as is explained before.
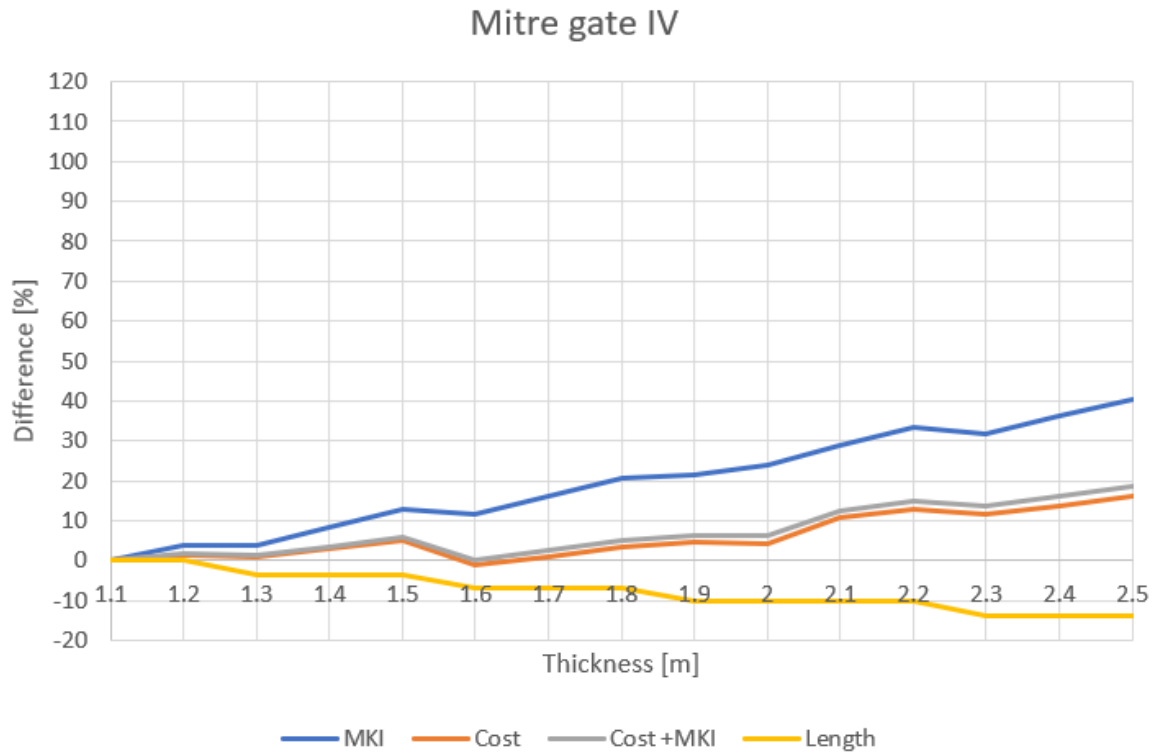
Figure 8.9: Difference in MKI, Cost, Cost + MKI and length with a varying thickness

Figure 8.10 shows the percentage of the reinforcement, the concrete, UWC and GEWI on relatively the MKI, cost and cost + MKI for a mitre gate.
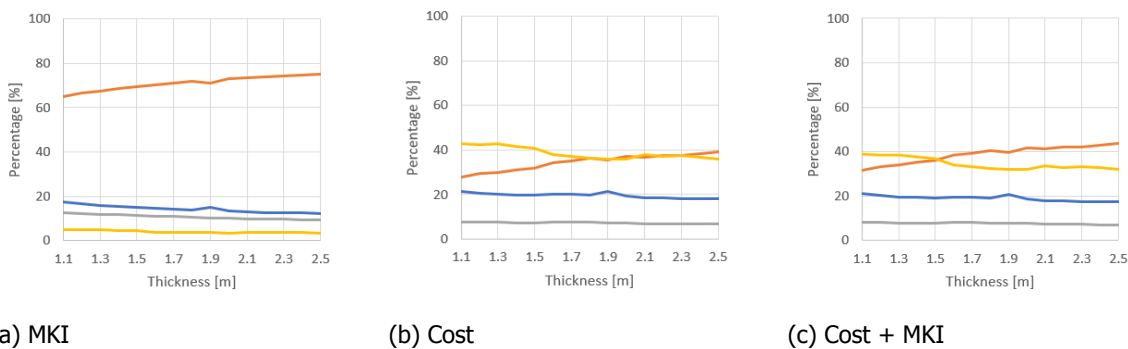
(a) MKI   (b) Cost   (c) Cost + MKI

Figure 8.10: Percentage of the materials on the MKI, Cost and Cost + MKI for a mitre gate with a difference in thickness
Blue = Reinforcement, Orange = Concrete, Grey = UWC, Yellow = GEWI

8.2.3. Comparison

Again a comparison in the cost + MKI is made between the single leaf gate and the mitre gate, see Figure 8.11. In general there is an increase in difference between the mitre gate and the single leaf gate for an increasing thickness. This is because the length of the mitre gate decreases, while the length of the single leaf gate stays the same according to its standard configuration.

The increase is not very consistent. This is due to the interaction between the decrease in length and the increase in width and their influence on the GEWI pile configuration, as is explained in the previous section.

The comparison between a mitre gate and a single leaf gate of CEMT classes II, III and V can be found in Appendix F. From the overall results it can be concluded that the influence of the horizontal bearing capacity on the lock head design increases for an increase in CEMT class, see Figure 8.12. This is due to the increase in dimensions per CEMT class. Due to the increase in influence of the horizontal bearing capacity, the difference between a mitre gate and a single leaf gate decreases.
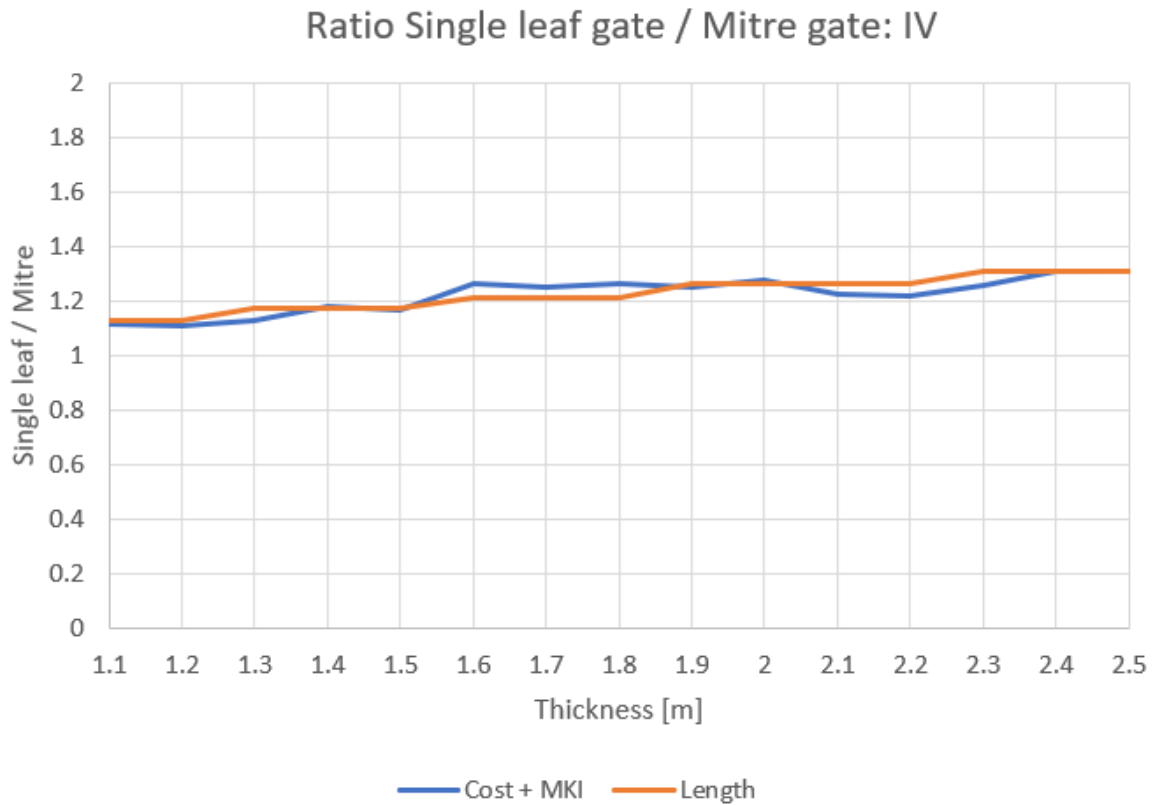
Figure 8.11: Cost + MKI comparison between a mitre gate and single leaf gate with a varying thickness
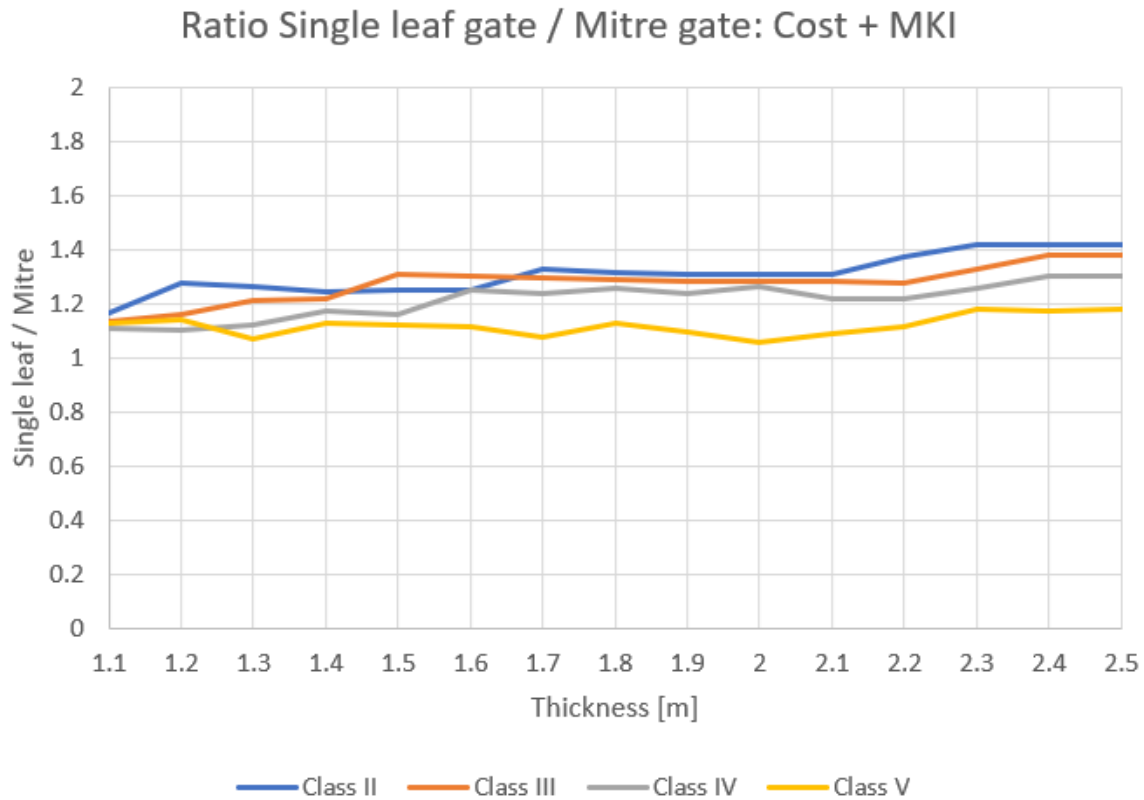
Figure 8.12: Cost + MKI comparison between a mitre gate and single leaf gate with a varying thickness for several CEMT classes

8.2.4. Displacements

The thickness has an influence on the displacements of the lock head. The most important factors that determine the displacement criteria are the water tightness and the operation of the gate. Leakage can occur due to the gate not closing properly and/or a difference in displacement between the lock head and the lock chamber. Besides, the lock gate should be able to operate despite the displacements.

Since the lock chamber is not taken into account in this study it is not possible to say something about the maximum allowable displacements. However, figure 8.13 shows the difference in displacements due to the increase in thickness. The orange line for the single leaf gate shows a nice parabola, as is expected. The blue line, representing the mitre gate, is not consistent. This is due to the variation in the length of the lock head with the mitre gate. The parametric model increase the length of the Tail, making the lock head with a mitre gate stiffer than a lock head with a single leaf gate.
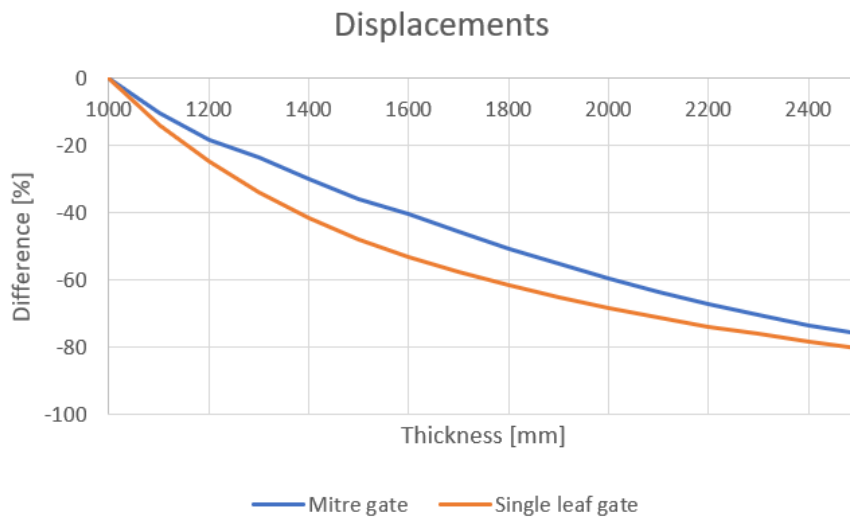
Figure 8.13: Difference in displacement due to a variation in thickness for a single leaf gate and mitre gate

8.3. Influence Concrete

In this section the influence of the concrete class on the cost and MKI is investigated. For this purposes three different types of concrete are used, being $C20/25$, $C30/37$ and $C35/45$. The wall and floor thickness is $2m$ and the difference in water head is constant. The concrete class $C20/25$ is set as default.

8.3.1. Single Leaf Gate

Figure 8.14 shows the difference in cost and MKI between the concrete classes. It can be concluded that the concrete class has no remarkable influence on the cost and MKI.
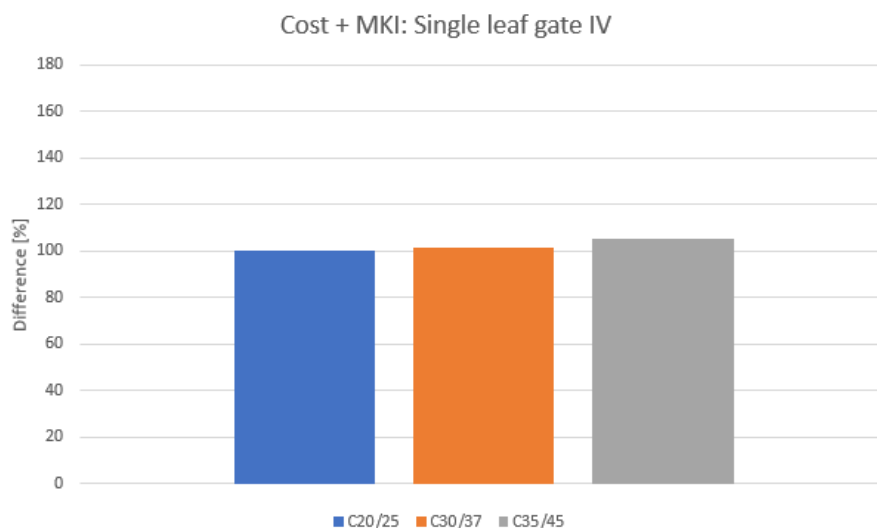
Figure 8.14: Difference in Cost and MKI due to a difference in concrete class

8.3.2. Mitre Gate

Figure 8.15 shows the difference in cost and MKI between the concrete classes. It can be concluded that the concrete class has no remarkable influence on the cost and MKI.
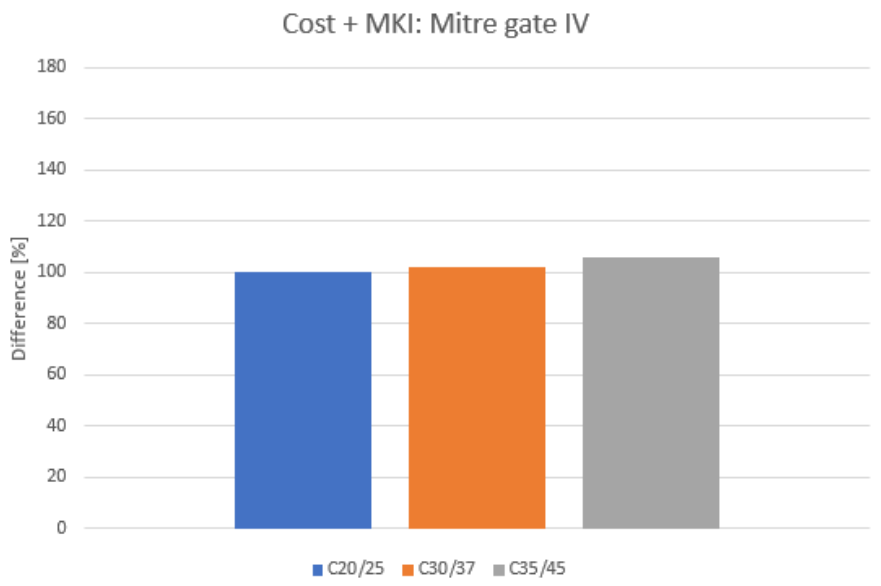
Figure 8.15: Difference in Cost and MKI due to a difference in concrete class

8.4. Empel

In this section a comparison is made between the lock heads designed by the parametric model and the lock head in Empel. From the results it can be concluded that a mitre gate is more cost effective and sustainable than a single leaf gate. The following two question arises:

- Why does the lock head in Empel has a single leaf gate?

- How does the design of Empel compare to the design of a single leaf gate and a mitre gate from the parametric model?

The lock head in Empel has to retain water in both directions. The 'Handboek voor het Ontwerpen van Schutsluizen' has scored both the gates, see Figure 8.16. From both the tables it follows that a single leaf gate is better suited to retain water in both directions.

Aspect	Weighing factor	Two-sided turning mitre gates	Two-sided turning pivot gates	Two-sided turning rolling gates
Construction cost	0.15	9	7	4
Maintenance	0.20	8	9	6
Reliability	0.25	7	8	9
Durability	0.05	9	8	7
Locking capacity	0.10	7	5	8
Environment	0.05	9	7	5
User-friendliness	0.15	7	8	8
Impermeability	0.05	5	9	9
Total score		7.6	7.55	7.1

(a) Gate choice score between 1 and 10

Aspect	Weighing factor	Two-sided turning mitre gates	Two-sided turning pivot gates	Two-sided turning rolling gates
Construction cost	0.15	3	2	1
Maintenance	0.20	2	3	1
Reliability	0.25	1	2	3
Durability	0.05	3	2	1
Locking capacity	0.10	2	1	3
Environment	0.05	3	2	1
User-friendliness	0.15	1	3	2
Impermeability	0.05	1	2	3
Total score		1.8	2.25	1.95

(b) Gate choice score between 1 and 3

Figure 8.16: Gate choice for water retention in both directions (*Ontwerp van Schutsluizen*, 2000)

According to the parametric model, a single leaf gate is more expensive and less sustainable than a mitre gate. To make a fair comparison between the single leaf gate, the mitre gate and Empel, the parameters from Empel have been used. Figure 8.17 shows the difference in cost, MKI, length and weight. The lock head in Empel is set as default. From the figure it follows that the lock head in Empel is the cheapest and most sustainable design. The lock head in Empel is about 40% more cost effective and sustainable than a single leaf gate design from the parametric model, and 20% more cost effective and sustainable than a mitre gate. This is because the lock head in Empel is shorter and lighter than the lock head designs from the parametric model, since the heavy Head part is missing in Empel.
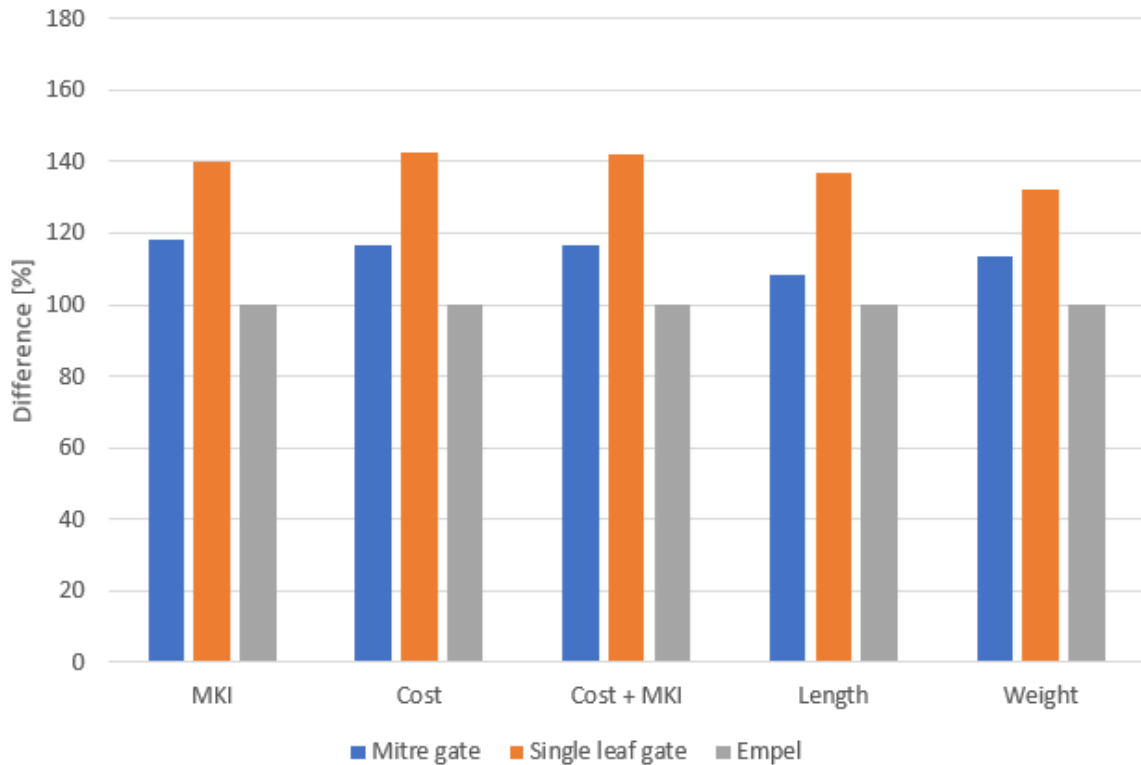
Figure 8.17: Comparison in Cost + MKI between the single leaf gate, mitre gate and Empel

The parametric model designs a lock head that meets the strength, stiffness and stability requirements. From the results it followed that the stability check horizontal bearing capacity has the biggest influence on the lock head design. Important parameters that determine the horizontal bearing capacity are the length and the weight of the lock head. What stands out is that for the same parameters the lock head in Empel is shorter and lighter. So, how can the lock head in Empel be shorter and lighter and still meet the horizontal bearing capacity? Chapter 4 already demonstrated that the lock head in Empel derives its horizontal bearing capacity partially from the lock chamber and that it is independent of its own weight. By involving the lock chamber in the stability calculation a more economical and sustainable lock head design is acquired.

The next step is to make a comparison between the lock head designs from the parametric model and Empel, independent of the horizontal bearing capacity. The lock head designs from the parametric model still have the configuration prescribed by the 'Handboek voor het Ontwerpen van Schutsluizen' (*Ontwerp van Schutsluizen*, 2000). Figure 8.18 shows the results. The difference between the single leaf gate and Empel does not change, since both do not depend on the horizontal bearing capacity. The mitre gate becomes the most sustainable and cost effective option, since the length of the lock head decreases.

The final step is to adjust the lock head configuration of the parametric model according to the design of Empel by removing the Head and part of the Chamber. In this case the gate extends the length of the lock head in open position. Figure 8.19 shows the results. The mitre becomes even more

sustainable and cost effective. The lock head with a single leaf gate from the parametric model becomes approximately as sustainable and cost effective as Empel.
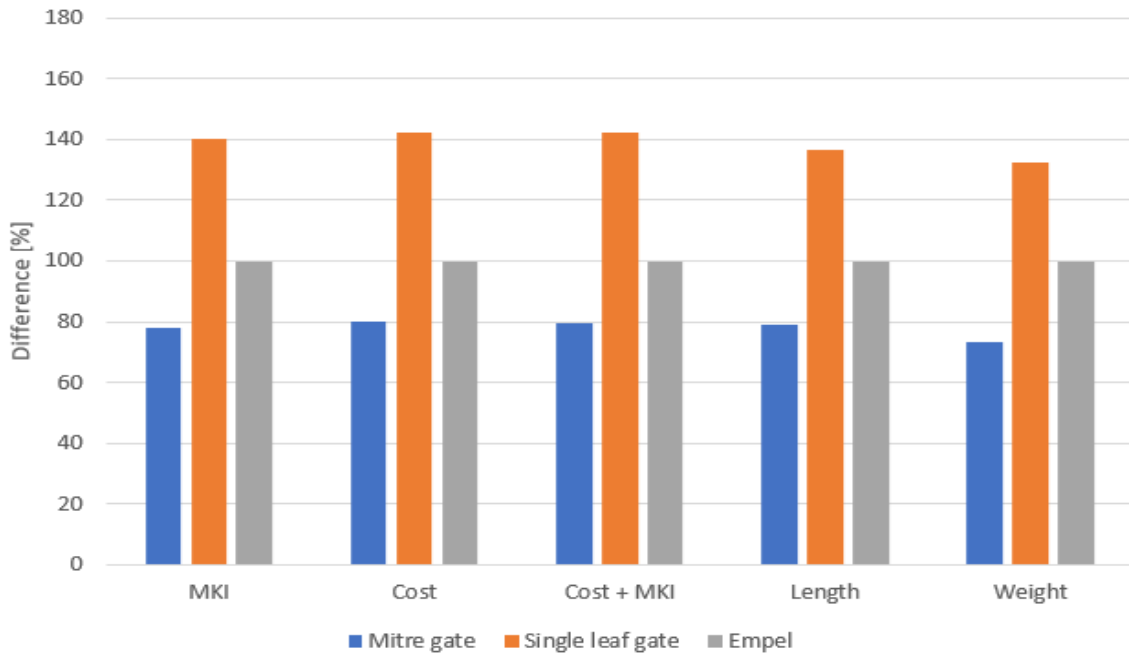
Figure 8.18: Comparison in Cost + MKI between the single leaf gate, mitre gate and Empel independent of the horizontal bearing capacity
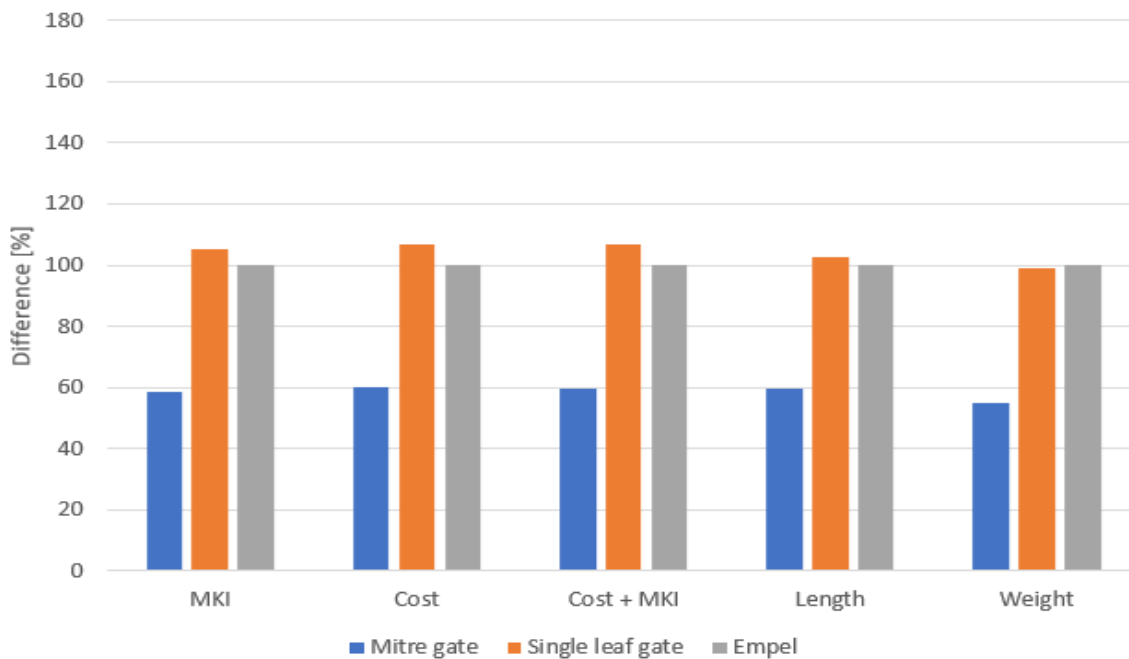
Figure 8.19: Comparison in Cost + MKI between the single leaf gate, mitre gate and Empel independent of the horizontal bearing capacity and adjusted lock head configuration

8.5. Conclusion

From the parametric model it follows that in general a mitre gate is more cost effective and sustainable than a single leaf gate.

Furthermore, the global stability check horizontal bearing capacity has the biggest influence on the cost and MKI of a lock head, especially a mitre gate.

The influence of the horizontal bearing capacity on the lock head design becomes apparent when changing the the difference in water head and the thickness of the walls and the floor and therefore the weight.

By increasing the water head difference, the length of a mitre gate has to increase to account for the horizontal bearing capacity. A single leaf gate already generates enough horizontal bearing capacity due to its standard configuration being longer than a mitre gate. A increase in water head causes the mitre gate to become approximately as long as a single leaf gate, diminishing the difference in cost and MKI between the two.

Due to an increase in thickness, the weight of the lock head increases. Therefore, the friction between the floor and the soil increases. A lock head with a mitre gate is therefore able to decrease in length. A lock head with a single leaf gate is not able to decrease in length, due to its standard configuration. This results in an increasing difference in cost and MKI between the mitre gate and single leaf gate for an increase in thickness.

The influence of the horizontal bearing capacity becomes bigger for an increase in CEMT class, see Appendix F. This can be seen by the decrease in difference between the mitre gate and single leaf gate.

From Figures 8.2, 8.4, 8.8 & 8.10 it can be concluded that indeed the concrete has the biggest influence on the MKI, about 70%. Something else that pops out is the difference in influence of the GEWI piles on the MKI (5%) and Cost (40%). This is mainly due to the recycle factor in the MKI calculations of the GEWI piles, see Appendix C.

From figures 8.2, 8.4, 8.8 & 8.10 it follows that the MKI factor is about 10% of the total cost, see also Appendix F.

From the parametric model it follows that the mitre gate is more economical and sustainable than a single leaf gate. The lock head in Empel invalidates this conclusion. Volkerwessels Infra Competence Centre has designed a lock head that deviates from an original design according to the 'Handboek voor het Ontwerpen van Schutsluizen' by incorporating the lock chamber in the stability calculations. This has resulted in a more economical and sustainable solution. However, when a lock head is designed independent of the horizontal bearing capacity, a lock head with a mitre gate becomes the most sustainable and cost effective option.

9

Discussion

This chapter discusses the results of the research. Furthermore, limitations of the research and the parametric model are discussed, consequences of the research are explained and suggestions are given for future research purposes. The validation of the research is not discussed. The validation of the model can be found in Chapter 7.

9.1. Interpretation of the Results

The results show that in general a lock head with a mitre gate is more cost effective and sustainable than a lock head with a single leaf gate. This result is expected since the lock configuration of a mitre gate is shorter than the lock configuration of a single leaf gate. The 'Handboek voor het Ontwerpen van Schutsuizen' (*Ontwerp van Schutsluizen*, 2000) prescribes that the gate has to vanish in the gate chamber to prevent collisions with vessels. A lock head with a mitre gate consist out of two gates at each side of the lock head. The two gates cover the total width of the lock head. A lock head with a single gate consist out of one gate. The one gate has to cover the total width of the lock head. The single leaf gate is therefore longer than the individual mitre gates. Therefore, the lock head with a single leaf gate requires a longer length of the gate chamber, thus resulting in a longer lock head.

A comparison is made between a lock head with a mitre gate and with a single leaf gate, due to a difference in water head. The difference in cost and MKI between a mitre gate and a single leaf gate decreases due to an increase in difference in water head. The decrease is linear, what is expected. The lock head with a mitre gate has to increase in length to account for the horizontal bearing capacity, while the length of the lock head with a single leaf gate is already sufficient to provide enough horizontal bearing capacity. Meaning that the length of the mitre gate approaches the length of the single leaf gate.

The influence of the water head increases for increasing CEMT classes. This result is expected, since the width and the depth of the lock head also increases. For CEMT classes II, III and IV, a mitre gate will always be more cost effective and sustainable than a single leaf gate. A single leaf gate can only compete with a mitre gate at a difference in water head level that is not likely to occur in reality. For CEMT class V, the difference between a mitre gate and single leaf gate diminishes at a water head difference that is possible in reality. According to the model, the single leaf gate even becomes more cost effective and sustainable than a mitre gate, by increasing the difference in water head. However, the difference can be neglected and is caused by the increment steps of the parametric model. The parametric model increases the length of the lock head with steps of $0.5m$. The difference would be terminated if the increment steps would be smaller.

The CEMT classes I and VI are not mentioned, since for these classes the 'Hand boek voor het Ontwerpen van Schutsluizen' only assigns one type of gate, so a comparison between the two is not possible.

Furthermore, the influence of the thickness on the lock head design for a single leaf gate and a mitre gate has been investigated. The parametric model shows less clear results.

By increasing the thickness of the walls and the floor, the weight of the lock head increases. Therefore,

the friction between the soil and the floor increases. This results in a decrease in length of a lock head with a mitre gate. The standard configuration of a lock head with a single leaf gate is already long enough to generate enough friction. By increasing the weight the lock head with a single leaf gate is not able to decrease in length. Meaning that for an increase in thickness, the difference between a mitre gate and a single leaf gate increases.

For CEMT classes II and III, the results show a linear relationship. For CEMT classes IV and V, this relationship is less significant and contains some deviations.

The deviations can be explained by the increased influence of the horizontal bearing capacity, the configuration of the GEWI piles and the increase/decrease in length of the lock head with steps of $0.5m$. The parametric model designs a GEWI pile configuration with a centre to centre distance between the GEWI piles of maximum $2m$. When this threshold is exceeded, the parametric model adjust the GEWI pile configuration, by adding an additional row. However, the effect of the GEWI piles on the cost is significant.

The deviations would be terminated if the GEWI pile configuration would be constant and the increments with which the lock head increases/decreases were smaller.

Again the CEMT classes I and VI are not mentioned, since for these classes the 'Hand boek voor het Ontwerpen van Schutsluizen' only assigns one type of gate.

Next up, the influence of the concrete class on the cost and MKI has been investigated. The concrete classes taken into account are $C20/25$, $C30/37$ and $C35/45$, since these are used for in-situ structural purposes. The preliminary study already showed that the influence of the concrete class on the cost and MKI is negligible. The results from the parametric model confirm this.

Furthermore, the results highlight the fact that indeed concrete has the biggest influence on the MKI, about 70%. This result is higher than expected. The literature states that the influence of the concrete on the MKI is about one third (*Duurzaam GWW aanbesteden*, 2019). The difference can be explained by different factors. In this research only the concrete, reinforcement, UWC floor and GEWI piles are taken in consideration. The sheet piles for example are left out of the scope. However, it is expected that the influence of the sheet piles on the MKI is small. The sheet piles are made out of steel and therefore have a recycle factor, just like the reinforcement and the GEWI piles. Furthermore, the literature considers infrastructural projects and is not specifically aimed at lock heads. Besides, concrete is by far the highest in volume usage for a lock head.

Another noticeable fact is the difference in influence of the GEWI piles on the MKI and the cost. The influence of the GEWI piles on the MKI is around 5%, while the influence on the cost is approximately 40%. This is due to the recycle factor incorporated in the calculations done for the GEWI piles.

According to literature, the MKI is about 20% of the total cost (*Duurzaam GWW aanbesteden*, 2019). During this research however, a factor of 0.1 is found. The factor from literature is based on a wide variety of different infrastructural projects like road, railroads, bridges and dikes, while the factor from this study is only based on lock heads.

In the last section of the research, the lock head designs from the parametric model have been compared with the lock head design in Empel. In the introduction it was already mentioned that the Head and part of the Chamber are removed from the lock head in Empel. Therefore, it was expected that the lock head in Empel would be more cost effective and sustainable than a lock head design from the parametric model with a single leaf gate.

The lock head in Empel is even 20% more cost effective and sustainable than a lock head design with a mitre gate from the parametric model. Even though the lock head in Empel is only $0.5m$ shorter than the lock head design with a mitre gate. The lock head in Empel is also lighter than the lock head design with a mitre gate from the parametric model. This is because the heavy Head part is missing in Empel. From the introduction it became clear that the horizontal bearing capacity of the lock head in Empel is independent of the weight of the lock head. The horizontal bearing capacity from the lock head in Empel is derived from the length of the lock head and the lock chamber. This is in contradiction with the rule from the 'Handboek voor het Ontwerpen van Schutsluizen' (*Ontwerp van Schutsluizen*, 2000). The 'Handboek voor het Ontwerpen van Schutsluizen' states that the horizontal bearing capacity should be provided by the lock head itself. By deviating from this rule the lock head in Empel is 20% more cost effective and sustainable than a lock head design from the parametric model with a mitre gate.

And 40% more cost effective and sustainable than a lock head design from the parametric model with a single leaf gate. This is mainly due to the difference in length, being the same order of magnitude. The involvement of the lock chamber only applies to the upper lock head. For the upper lock head the water level in the approach area is in general higher than the water level in the lock chamber. For the lower lock head the water level in the lock chamber is higher than the water level in the approach area. The lower lock head is therefore not able to derive the horizontal bearing capacity from the lock chamber.

The upper lock head needs to derive the horizontal bearing capacity on its own when the water level in the lock chamber is higher than the water level in the approach area. This is the case when the lock head needs to retain water in both directions. However, the decay in water level in this direction is much smaller.

9.2. Limitations Research

For the cost and the MKI calculations only the concrete, reinforcement, UWC and GEWI/foundation piles are taken into consideration. Sheet piles, bracing frames, formworks and cooling are left out of the scope.

The gate choice in the parametric model is only based on the width of the lock head and the direction of water retention as prescribed by the 'Handboek voor het Ontwerpen van Schutsluizen'. The choice is independent of the construction cost of the gate, the maintenance, the reliability, the durability, the locking capacity, the impermeability and the usability. Besides, the parametric model does not take into account to what extend water retention in both direction is possible.

The difference in gate only follows from the lock head configuration. Difference in gate mechanisms are not taken into account. In case a gate has to retain water in both directions, extra measures are necessary. These measures are not taken into account.

Furthermore, the research only takes into account the mitre gate and the single leaf gate, since these are the most common used gates in the Netherlands. The rolling gate and lifting gate are left out of the scope.

The parametric model only takes into account the upper lock head. To get a better view on the total situation, the whole navigation lock should be incorporated in the parametric model.

The configuration of the GEWI piles leads to misleading results. The determination of the foundation of the lock head is an interaction between the thickness of the UWC floor and the distance between the GEWI piles. Some assumptions have been made to simplify these calculations.

The length of the lock head is increased with increments of $0.5m$. To obtain better results, this number should be lowered. However, this would increase the calculation time of the parametric model.

9.3. Future of Parametric Design

A parametric model is a good tool to get a quick overview of the basic design in the preliminary design stage. Another advantage of a parametric model is that scripts are easily interchangeable. The scripts only require the right input parameters in order to calculate the answers. Examples are the moment resistance calculations, crack with calculations and shear resistance calculations. However programs already exist that are able to do this.

The parametric model designs a lock head based on prescribed rules and according to a standard configuration. The rules are informative but not binding. This means it is possible to deviate from the rules, in order to optimise the design. The design team from Empel has done this in order to design a more cost effective and sustainable lock head. A parametric model can not deviate from the rules prescribed in the program.

There are many similarities between different projects, but every project is unique. For every project, location dependent boundaries, wishes and demands apply. A parametric model is not able to account for all of these. Therefore, the future is not in parametric modelling.

9.4. Consequences of the Research

The results of the parametric model show that a mitre gate is in general more cost effective and sustainable than a single leaf gate. Does this mean that from now on every lock head will be equipped

with a mitre gate? This is not likely, since the decision of the type of gate depends on more factors than only the cost and MKI.

Besides, Volkerwessels Infra Compentence Centre has showed that it was able to design a more cost effective and sustainable lock head with a single leaf gate than a lock head design from the parametric model with a mitre gate. This result was achieved by incorporating the lock chamber in the design. Therefore, it is advised to take a second look at the rules prescribed in the 'Handboek voor het Ontwerpen van Schutsluizen'.

9.5. Suggestions for Following up Investigations

As was mentioned in the previous section, it is advised to take a second look at the rules prescribed in the 'Handboek voor het Ontwerpen van Schutsluizen'. Especially the rules about the horizontal bearing capacity and the protection of the gate.

The lock head in Empel involves the lock chamber for its horizontal bearing capacity. It would be interesting to investigate under what circumstances this is possible and to what extend. Especially, since there are different types of lock chambers.

For further research it is also suggested to study the protection of the gate. In the original lock head design, the gate is fully protected by the lock head. The gate in Empel exceeds the length of the lock head in open position and is protected by a wooden guidance work placed in the approach area. From the literature study it followed that the lock head in Empel is situated in a waterway with a relatively low intensity. It would be interesting to investigate if the protection measures taken in Empel also suffice for a waterway with a higher intensity.

For further research it is suggested to take the whole navigation lock in consideration. This includes the approach area, the upper lock head, the lock chamber and lower lower lock head. The lock chamber should be incorporated to determine the displacements of the lock head to prevent leakage between the lock head and the lock chamber and to determine the horizontal bearing capacity. The approach area should be incorporated, since the protection of the gate in lock Empel is a function of the approach area in stead of the lock head.

According to literature the MKI is 20% of the total cost and the environmental impact of concrete is about one third of the total MKI (*Duurzaam GWW aanbesteden*, 2019). This research shows that the MKI of the lock head is about 10% of the total cost and the environmental impact of concrete is about 70%. It has to be investigated if these number will approach the results from literature if the whole navigation lock is taken into consideration.

10

Conclusions & Recommendations

10.1. Conclusions

Based on the results from the parametric model it can be concluded that in general a lock head with a mitre gate is more cost effective and sustainable than a lock head with a single leaf gate.

The research also shows that the global stability check: horizontal bearing capacity, has the biggest influence on the lock head design. The importance of the global stability check: horizontal bearing capacity becomes apparent by changing the parameters water head and thickness in the parametric model.

By increasing the difference in water head, the influence of the horizontal bearing capacity increases. In general the length of the lock head has to increase to generate enough bearing capacity to prevent the lock head from sliding.

A lock head with a single leaf gate is in most cases already long enough to generate enough friction to account for the horizontal bearing capacity. This is due to its standard configuration.

A lock head with a mitre gate on the other hand, has to increase in length to provide the horizontal bearing capacity, since the length of a lock head with a mitre gate is shorter than the length of a lock head with a single leaf gate.

The increase in water head diminishes the difference in cost and MKI between a mitre gate and a single leaf gate. This is due to an increase in length of the mitre gate becoming approximately as long as a single leaf gate. For CEMT class up to IV a lock head with a mitre gate is always more cost effective and sustainable than a lock head with a single leaf gate. A lock head with a single leaf only becomes competitive at a difference in water head that is not likely to occur in reality. For CEMT class V, the single leaf gate and mitre gate are much more competitive.

The weight of the lock head also plays an important role in the horizontal bearing capacity. This is showed by altering the thicknesses of the walls and the floors. By increasing the thickness, the weight of the lock head increases. Therefore, the friction between the floor of the lock head and the soil increases.

A lock head with a single leaf gate is already long enough to provide enough horizontal bearing capacity. By increasing the weight of the lock head, the cost and MKI only increase. The length of the lock head with a single leaf gate is not able to decrease due to the standard lock configuration.

A lock head with a mitre gate is shorter than a single leaf gate. To generate enough horizontal bearing capacity, the length of the mitre gate has to increase. However, by increasing the thickness of the walls and the floor, the weight of the lock head increases. Therefore the length of the mitre gate can decrease.

Up to CEMT class III a mitre gate is more cost effective and sustainable than a single leaf gate. The difference will only increase with an increase in thickness. From CEMT class IV the difference between a mitre gate and a single leaf gate is less noticeable and the results show deviations. This is due to the increasing influence of the horizontal bearing capacity and some assumptions that have been made in the parametric model. The overall trend that the mitre gate becomes more cost effective and sustainable than a single leaf gate with an increase in thickness is still noticeable.

From the results it can be concluded that the influence of the horizontal bearing capacity increases by increasing the CEMT class. By increasing the CEMT class, the width and the depth of the lock head increases. The increased influence of the horizontal bearing capacity results in a smaller difference between a mitre gate and a single leaf gate. This is especially noticeable from CEMT class IV.

The parametric model takes into account three different concrete classes, being $C20/25$, $C30/37$ & $C35/45$. For each concrete class a lock head with a single leaf gate and a lock head with a mitre gate has been designed. The difference in cost and MKI due to the a different concrete class is negligible.

The parametric model shows that a lock head with a mitre gate is the most cost effective and sustainable option for the parameters used in Empel. However, the lock head in Empel has a single leaf gate, since the gate choice depends on more parameters than only the cost and sustainability. The navigation lock in Empel has to retain water in both directions. For that purpose a single leaf gate is better suited.
A cost and MKI comparison between the lock head designs from the parametric model and the lock head design in Empel shows that the design of the lock head in Empel is the most cost effective and sustainable option.
The lock head in Empel is shorter and lighter than the lock head designs from the parametric model, what results in less material usage.
From the conclusion above it follows that the horizontal bearing capacity has the biggest influence on the lock head design. Besides, the length and the weight are important factors for this stability check. How can the lock head in Empel still meet the horizontal bearing capacity, while it is shorter and lighter than the designs from the parametric model? The lock head in Empel derives its horizontal bearing capacity mainly from the lock chamber. This is in conflict with the guidelines from the 'Handboek voor het Ontwerpen van Schutsluizen' (*Ontwerp van Schutsluizen*, 2000). The 'Handboek voor het Ontwerpen van Schutsluizen' states that the lock head has to generate enough horizontal bearing capacity on its own without the help of the lock chamber. The horizontal bearing capacity of the lock head in Empel depends on the length of the lock head and the lock chamber and is independent of the weight of the lock head.
By incorporating the lock chamber in the horizontal bearing capacity calculations, a more cost effective and sustainable lock head can be designed.

Furthermore, the study highlights the fact that indeed concrete has the highest influence on the MKI, about 70%. The literature states that this influence is only one third (*Duurzaam GWW aanbesteden*, 2019). The influence of the GEWI piles on the MKI is around 5%, while the influence on the cost is approximately 40%. This is due to the recycle factor incorporated in the calculations done for the GEWI piles.
During the research a MKI factor of 0.1 is found. This means that the MKI is about 10% of the total cost. However, the literature dictates a MKI factor of 0.2 (*Duurzaam GWW aanbesteden*, 2019).

Before the decision was made to make a parametric model, different design alternatives have been investigated in the preliminary study in order to increase the sustainability of lock heads. The alternatives proposed in the preliminary study are Inhomogeneous Cross Section, Prestressing and Hollow Sections.
With the term Inhomogeneous cross section a reference is made to a cross section consisting out of different concrete classes. Each concrete class has a different cement to water ratio. Cement has the biggest influence on the sustainability of concrete. The idea is that by using a lower concrete class in the core of the cross section, less cement is used and thereby a more sustainable construction is achieved. The option Inhomogeneous cross section fulfills all the strength, stiffness and stability requirements. The difference in shrinkage and creep between the different concrete classes is not taken into account. According to the calculations the cost decreases with 3% relative to the original design of Empel and the decrease in MKI is negligible. The results from the parametric model also confirm that the influence of a different concrete class on the cost and MKI is negligible.
The options Prestressing and Hollow sections are both based on the fact to save concrete. Concrete has the highest influence on the sustainability. With the method of Prestressing more slender structures

can be accomplished. With Hollow Sections, concrete can be saved without losing too much stiffness. The option Prestressing is able to meet the strength requirements. The stiffness requirement displacements requires more research. The crack width is no problem. The stability check horizontal bearing capacity requires more research. The cost increases with 2%, while the MKI decrease with 1.5% relative to Empel.

The option Hollow Sections meets the strength and stiffness requirements. The global stability check horizontal bearing capacity requires more research. The cost decreases with 3%. The MKI decreases with 3% relative to Empel.

The options Prestressing and Hollow sections both require more research with regard to the horizontal bearing capacity. From the results it followed that reducing the weight of the lock head requires an increase in length. This would nullify the decrease in MKI. On the other hand, the design of the lock head in Empel is independent on the weight of the lock head.

The proposed options all seem to have no real future to be implemented in the lock head design. The decrease in cost and MKI are negligible. The more laborious construction processes are not taken into account. These will most likely further reduce the gain in sustainability. Therefore, the advanced analysis does not further elaborate the alternatives and further investigation in the horizontal bearing capacity of the options Prestressing and Hollow Sections would be meaningless. Instead a parametric model is made based on well known design rules from the 'Handboek voor het ontwerpen van Schutsluizen' (*Ontwerp van Schutsluizen*, 2000) and the 'Richtlijnen Vaarwegen 2017' (*Richtlijnen vaarwegen 2017*, 2017).

10.2. Recommendations

To increase the sustainability of the lock head design, it is recommended to involve the lock chamber in the horizontal bearing capacity. This way, the horizontal bearing capacity of the lock head becomes less dependent on the weight and the length of the lock head. Meaning that less materials are needed and the construction pit can be smaller. When decreasing the length of the lock head it is advised to remove the Head and part of the Chamber. The length of the Tail can not change and follows from rules in the 'Richtlijnen voor Vaarwegen 2017', (*Richtlijnen vaarwegen 2017*, 2017).

To what extend the lock chamber can be involved in the horizontal bearing capacity calculations should be investigated.

When a shorter lock head results in the gate extending the length of the lock head, the protection of the gate should be provided by a wooden guidance wall, placed in the approach area. Per case it must be demonstrated that the wooden guidance wall can replace the function of the lock head to protect the gate.

The research recommends to use a MKI factor of 0.1 for lock heads, instead of the factor of 0.2 from literature (*Duurzaam GWW aanbesteden*, 2019). Research is required if the factor of 0.1 is also applicable to the whole navigation lock.

Bibliography

Betonakkoord (2018), Technical report, Rijksoverheid.

Bouwbesluit 2012 (2012), Technical report, Rijksoverheid.

Braam, C. and Lagendijk, P. (2011), *Constructieleer Gewapend Beton*, 7 edn, Aeneas.

Calle, E. and Weijers, J. (1994), Technisch rapport voor controle op het mechanisme piping bij rivierdijken, Technical report, Grondmechanica Delft.

Cement&BetonCentrum (2019), Brochure.

Cement&BetonCentrum (2020), http://www.cementenbeton.nl.

CirculaireEconomie (2016), Nederland circulair in 2050, Technical report, Rijksoverheid.

Cooper, T. (1994), Beyond recycling, Technical report, The New Economics Foundation.

Deelrapportage Vaarwegen voor de Nationale Markt- en Capaciteitsanalyse (NMCA) (2017), Technical report, Rijkswaterstaat.

Duurzaam GWW aanbesteden (2019), Technical report, Advies van de Stuurgroep Duurzaam GWW.

Effect kabinetsvoorstel CO2-heffing industrie (2019), https://www.pbl.nl/.

GoogleMaps (2019), http://maps.google.com/.

Hildebrand, L. (2014), Strategic investment of embodied energy during the architectural planning proces, Technical report, TU Delft.

Iv-Groep (2016), https://iv-groep.nl/.

Keeble, B. (1988), The brundtland report: 'our common future, Technical report, Medicine and War.

Klimaatakkoord (2019), Technical report, Rijksoverheid.

Molenaar, W. (2011), *Hydraulic Structures Locks*, TU Delft.

Molenaar, W. and Voorendt, M. (2016), *Manual Hydraulic Structures*, TU Delft.

Neville, A. and Brooks, J. (2010), *Concrete Technology*, 2 edn, Pearson.

NRMCA (2008), Technical report, National Ready Mixed Concrete Association.

Olivier, J. G., Janssens-Maenhout, G., Muntean, M. and Peters, J. A. (2014), Trends in global co_2 emission, Technical report, PBL Netherlands Environmental Assessment Agency.

Ontwerp van Schutsluizen (2000), Technical report, Bouwdienst Rijkswaterstaat.

PIANC (2009), Innovations in navigation lock design, Technical report, PIANC.

Richtlijnen vaarwegen 2017 (2017), Technical report, Rijkswaterstaat.

Rijkswaterstaat (2015), http://beeldbank.rws.nl/.

Ropstar (2016), http://ropstar.nl/.

techopedia (2019), https://www.techopedia.com/.

The Paris Agreement (2015), Technical report, UNFCCC.

Tsakiridis, P., Papadimitriou, G., Tsivilis, S. and Koroneos, C. (2007), Utilization of steel slag for portland cement clinker production, Technical report, Journal of Hazardous Materials.

Uniforme CO2-prijs meest kostenefficiënt (2019), https://www.pbl.nl/.

VHBInfra (2014), https://vhbinfra.nl/.

Walraven, J. and Braam, C. (2018), *Prestressed concrete*, TU Delft.

Welleman, H. (2018), 'Slender structures load carrying principles', http://icozct.tudelft.nl/.

WillemsUnie (2014), http://willemsunie.com/.

A

Sustainability and Durability

A.1. Indicators

Global Warming Potential (GWP 100)

Life on earth is impossible without greenhouse gasses. The greenhouse gasses reflect the harmful radiation and maintain a moderate temperatures on earth. An increase in layer thickness results in an increase in temperature. Ice melts due a increase in temperature, leading to floods. Carbon dioxide CO_2 is the most common greenhouse gas. Therefore CO_2 equivalent is the reference for this impact category.

Ozone Depletion Potential (ODP)

The ozone layer filters UV radiation and is located in the stratosphere. Because of the depletion of this layer, UV radiation is penetrating the layer more easily. UV radiation not only causes diseases, but also contributes to the global warming. CFC is the most common contributor to the depletion of the ozone layer. The reference indicator is CFK11 equivalent.

Acidification Potential (AP)

Acidification potential is caused by acids emitted in the atmosphere, resulting in acid rains. This affects the water quality and the ecosystem. Sulphur dioxide is the indicator for AP (SO_2 equivalent).

Eutrophication Potential (EP)

Eutrophication happens when due to an increase in fertilizer in bodies of water, algae grow. The algae prevent the sunlight from reaching the deeper water layers. Sunlight is needed for the production of oxygen. Less oxygen means a decrease in vegetation and fish. EP is expressed in phosphate equivalent (PO_4 equivalent).

Photochemical Ozone Creation Potential (POCP)

A complicated chemical process which involves CO_2, SO_4, high temperatures, low air humidity and no air movement results in the production of ozone in the troposhere. It causes harm to vegetation, materials and in high concentrations to human health. POCP is expressed in ethene equivalent (C_2H_4 equivalent).

Abiotic Resource Depletion Potential Material/Energy (ADP)

Abiotic resources refer to non-living resources like for example minerals and fossil fuels. ADP gives an identification of the amount resources used for a material or process.

Human Toxicity Potential (HTP)

This potential takes into account the human health. The assessment is done based on tolerable concentrations in air and water and acceptable daily intake. HTP is expressed in 1.4 dichlorobenzene ($1.4 - DB$ equivalent).

Ecotoxicity to Freshwater, Land and Maritime Water (FAETP, TETP, MAETP)

The emission of toxic substances can have an influence on the ecosystem. The assessment is done based on tolerable concentrations in the different ecosystems. FAETP, TETP, MAETP are expressed in 1.4 dichlorobenzene ($1.4 - DB$ equivalent).

A.2. MKI

Table A.1: MKI conversion factors (*Bouwbesluit 2012*, 2012)

Indicator	Equivalent unit	Conversion factor [€/kg]
Abiotic resource depletion potential material/energy (ADP)	Sb eq	€0.16
Global Warming Potential (GWP 100)	CO_2 eq	€0.05
Ozone Depletion Potential (ODP)	$CFK - 11$ eq	€30
Photochemical Ozone Creation Potential (POCP)	C_2H_4 eq	€2
Acidification Potential (AP)	SO_2 eq	€4
Eutrophication Potential (EP)	PO_4 eq	€9
Human Toxicity Potential (HTP)	$1.4 - DCB$ eq	€0.09
Freshwater aquatic ecotoxicity (FAETP)	$1.4 - DCB$ eq	€0.03
Marine aquatic ecotoxicity (MAETP)	$1.4 - DCB$ eq	€0.0001
Terrestrial ecotoxicty (TETP)	$1.4 - DCB$ eq	€0.06

B

Structural Design

This appendix will give an overview of the differenct construction methods, loads acting on the lock head and the different load factors and load combinations. The two different types of foundations, shallow foundation and pile foundation, are being discussed.

B.1. Construction Methods

There are five main different types of construction methods, as was mentioned in the main report. This section will discuss these five construction methods.

The first method is a construction pit under a natural slope in combination with drainage. The second method is based on method 1, only with the addition of sheet piles. The third option is a dry cofferdam with a relatively thick UWC floor to prevent hydraulic bursting. Alternative four is based on alternative 3. The UWC floor is thinner and foundation piles have been applied to prevent hydraulic bursting. The last method is when a lock head is build in-situ and transported to the desired location where it is pneumatically immersed.

The 'Handboek voor het ontwerpen van Schutsluizen has summarised the construction alternatives and their field of application and their requirements, see Figures B.1 & B.2. A distinction is made in the width of the lock head between Klein (small), (Middel)groot (medium) and Zeer groot (big). The width dimension for Klein are $4 - 6m$, for (Middel)groot are $10 - 24m$ and for Zeer groot $> 24m$.

NUMMER ALTERNATIEF	KENMERKEN		Geschikt voor		Geschikt voor afmeting		
	Def. constructie	Bouwstadium	Kolk	Hoofd	Klein	(Middel-)groot	Zeer groot
1	Gewapend betonnen mono-liet (eventueel paalfundering)	Bouwput, bemaling	X	X	X	X	X
2	ALS 1	Bouwput, bentoniet-cement-schermen tot in ondoorlatende laag	X	X	X	X	X
3	ALS 1 (geen paalfundering)	Damwandkuip, dikke onderwater-betonvloer	X	X	X	X	X
4	ALS 1 (altijd paalfundering)	Damwandkuip, dunne onderwater-betonvloer, trekpalen	X	X	X	X	X
5	ALS 1	Pneumatisch caisson, gebouwd op maaiveld	X	X	X	X	
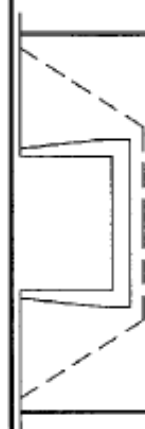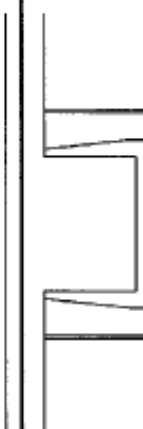
Figure B.1: Different construction alternatives and their field of application (*Ontwerp van Schutsluizen*, 2000)

NR	Kenmerken	2a Bemaling nodig	2b Beperkte bemaling nodig	2c Combinatie bemaling met tour-bemaling denkbaar	3 Beperkte uitvoerings-breedte	K Kolk kan worden droog gezet en vloer is dicht	Opmerkingen
1	Monoliet, bemalen bouwput	X				X	
2	Monoliet, schermen tot in ondoor-latende laag		X	X		X	X(2b) kan zinnig zijn om toch gebruik te kunnen maken van een te hoog gelegen laag. X(2c) is dan zeer wel denkbaar
3	Monoliet, damwandkuip met onverankerde o.w.-betonvloer		X	X	X	X	X(2b) kan zinnig zijn om een dunnere o.w.-vloer te krijgen. X(2c) is dan zeer wel denk-baar.
4	Monoliet, damwandkuip met o.w.-betonvloer en trekpalen				X	X	
5	Monoliet, pneumatisch caisson				X	X	

Figure B.2: Different construction alternatives and their requirements (*Ontwerp van Schutsluizen*, 2000)

B.2. Type of Gate

The type of gate depends on the head difference, the dimensions of the lock head, the direction of water retention, the area available around the lock and the cost, see Figures B.3, B.4 & B.5.

Type sluis	Sluisbreedte	Eenzijdig kerende puntdeuren	Dubbel stel puntdeuren	Tweezijdig kerende puntdeuren	Eenzijdig kerende draaideur	Tweezijdig kerende draaideur	Tweezijdig kerende roldeur	Eenzijdig kerende hefdeur	Tweezijdig kerende hefdeur
Tweezijdig kerende zeevaartsluis	Klein 6-10 m		X	X					
	Middelgroot 10-16 m		X	X		X			
	Groot 16-24 m		X	X		X	X		
	Zeer groot > 24 m						X		
Tweezijdig kerende binnenvaartsluis	Zeer klein 4-6 m		X	X		X			
	Klein 6-10 m		X	X		X			
	Middelgroot 10-16 m		X	X		X			
	Groot 16-24 m						X		X
Eenzijdig kerende binnenvaartsluis	Zeer klein 4-6 m				X				
	Klein 6-10 m	X			X				
	Middelgroot 10-16 m	X						X	
	Groot 16-24 m	X						X	

Figure B.3: Type of gate as function of the type of navigation lock and the width (*Ontwerp van Schutsluizen*, 2000)

Aspect	Weegfactor	Eenzijdig kerende puntdeuren	Eenzijdig kerende draaideuren	Eenzijdig kerende hefdeuren
Bouwkosten	0.15	9	7	5
Onderhoud	0.20	7	8	5
Bedrijfszekerheid	0.25	7	8	9
Duurzaamheid	0.05	9	8	7
Schutcapaciteit	0.10	7	5	9
Milieu	0.05	7	8	5
Gebruiksgemak	0.15	9	7	8
Waterdichtheid	0.05	5	9	9
Totaalscore		7.6	7.45	7.15
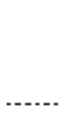
Figure B.4: Decision matrix for a navigation lock with a width of $10 - 16m$ for water retention in one direction (*Ontwerp van Schutsluizen*, 2000)

Aspect	Weighing factor	Two-sided turning mitre gates	Two-sided turning pivot gates	Two-sided turning rolling gates
Construction cost	0.15	9	7	4
Maintenance	0.20	8	9	6
Reliability	0.25	7	8	9
Durability	0.05	9	8	7
Locking capacity	0.10	7	5	8
Environment	0.05	9	7	5
User-friendliness	0.15	7	8	8
Impermeability	0.05	5	9	9
Total score		7.6	7.55	7.1

Figure B.5: Decision matrix for a navigation lock with a width of $10 - 16m$ for water retention in both directions (*Ontwerp van Schutsluizen*, 2000)

B.3. Loads

B.3.1. Loads on the Wall

The loads acting on the wall can be divided in three components:

- Horizontal, perpendicular to the wall

- Horizontal, parallel to the wall

- Vertical

Horizontal Perpendicular

- Water load inside the lock head:

$$f = \frac{1}{2}\gamma_w(h_k - z_k)^2$$

where:

γ_w = weight water $[N/m^3]$
h_k = water level in the lock $[mNAP]$
z_k = top lock head floor $[mNAP]$
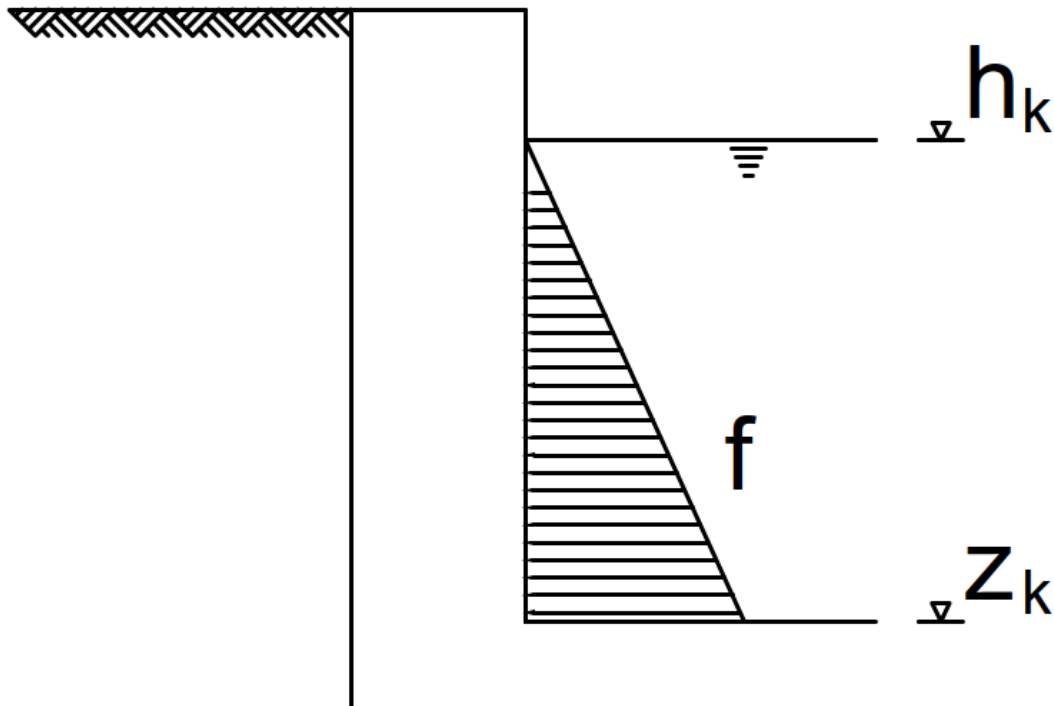
Figure B.6: Water load

- Soil load:
  The neutral lateral earth pressure is used for the calculations since the walls of the lock head hardly deform. The horizontal soil load for a homogeneous soil is given by

$f = 1 : \frac{1}{2}K_0\gamma_{dr}(h_b - h_g)^2 +$
$\quad\ \ 2 : K_0\gamma_{dr}(h_b - h_g)(h_g - z_k) +$
$\quad\ \ 3 : \frac{1}{2}K_0(\gamma_{sat} - \gamma_w)(h_g - z_k)^2 +$
$\quad\ \ 4 : \frac{1}{2}\gamma_w(h_g - z_k)^2$

where:

K_0 = coefficient neutral lateral earth pressure $[-]$
γ_{dr} = weight dry soil $[N/m^3]$
γ_{sat} = weight saturated soil $[N/m^3]$
γ_w = weight water $[N/m^3]$
h_b = ground level $[mNAP]$
h_g = groundwater level $[mNAP]$
z_k = top lock head floor $[mNAP]$
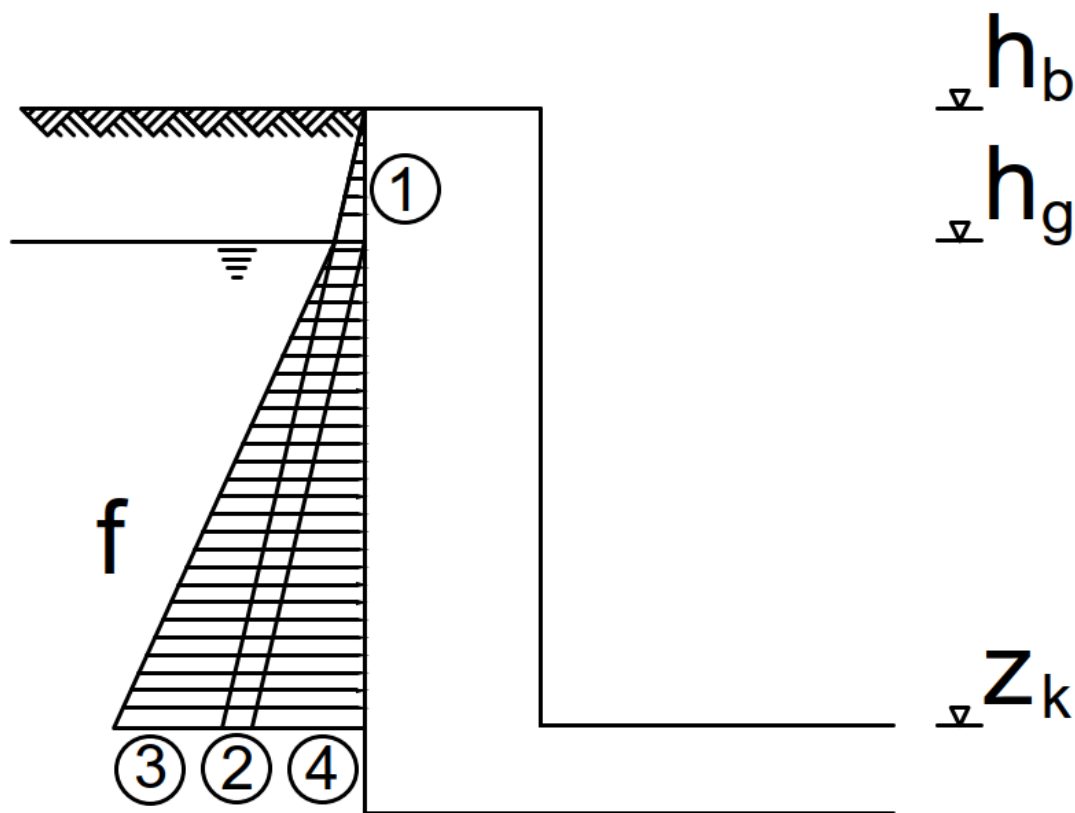
Figure B.7: Soil load

- Traffic load:

$$f = K_0 q_m (h_b - z_k)$$

where:

q_m = distributed traffic load $[N/m^2]$
K_0 = coefficient neutral lateral earth pressure $[-]$

h_b = ground level $[mNAP]$
z_k = top lock head floor $[mNAP]$
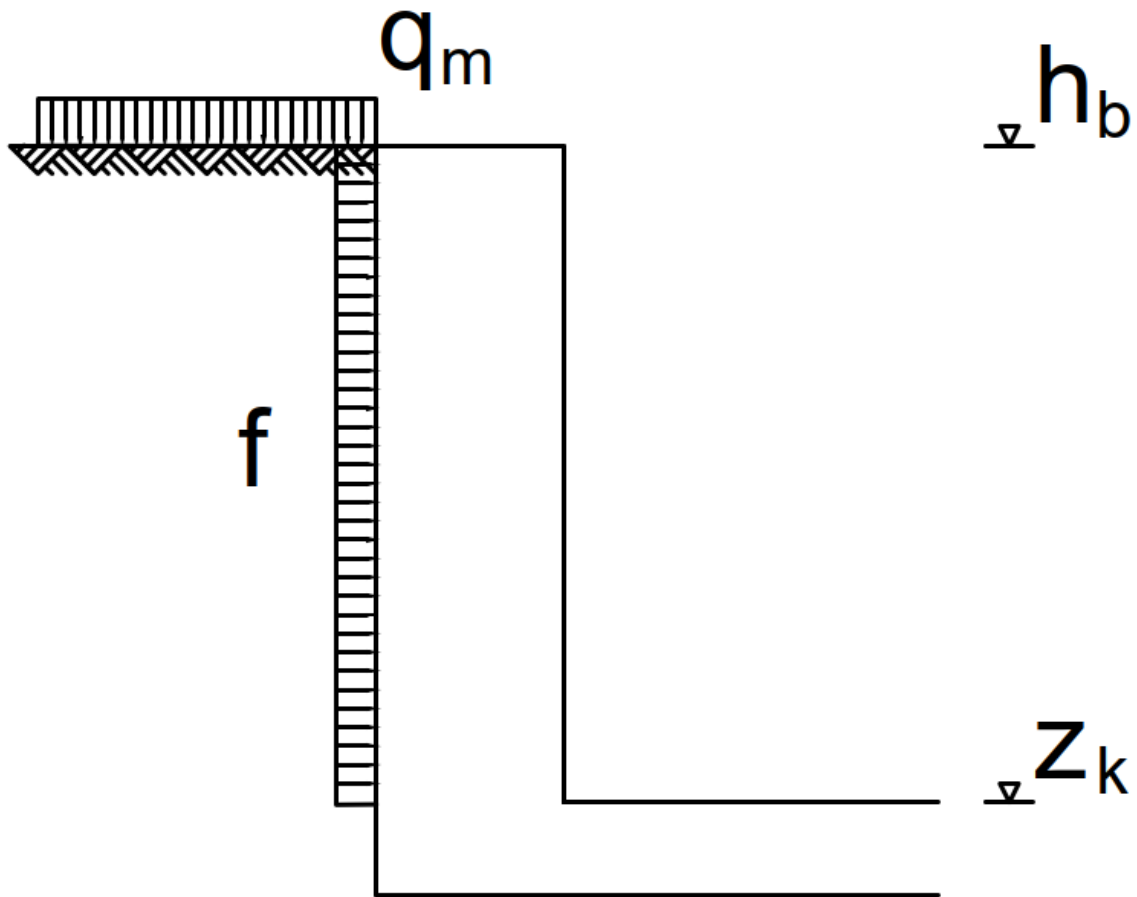
Figure B.8: Traffic load

- Crane load:
  The load acts from z_3 to z_5 in an shape of a triangle, see Figure B.9

  $f = \frac{1}{2}K_0 q_c(z_3 - z_5)l_c/(l_c + 2d_c)$

  where:

  $q_c = \frac{P_c}{l_c b_c}$ crane load $[N/m^2]$
  P_c = concentrated point load $[N]$
  l_c = length stamp $[m]$
  b_c = width stamp $[m]$
  d_c = distance lock head to stamp $[m]$
  K_0 = coefficient neutral lateral earth pressure $[-]$
  $z_3 = tan(\phi) * d_c$ $[mNAP]$
  $z_5 = tan(\frac{\phi}{2} + 45) * (d_c + b_c)$ $[mNAP]$
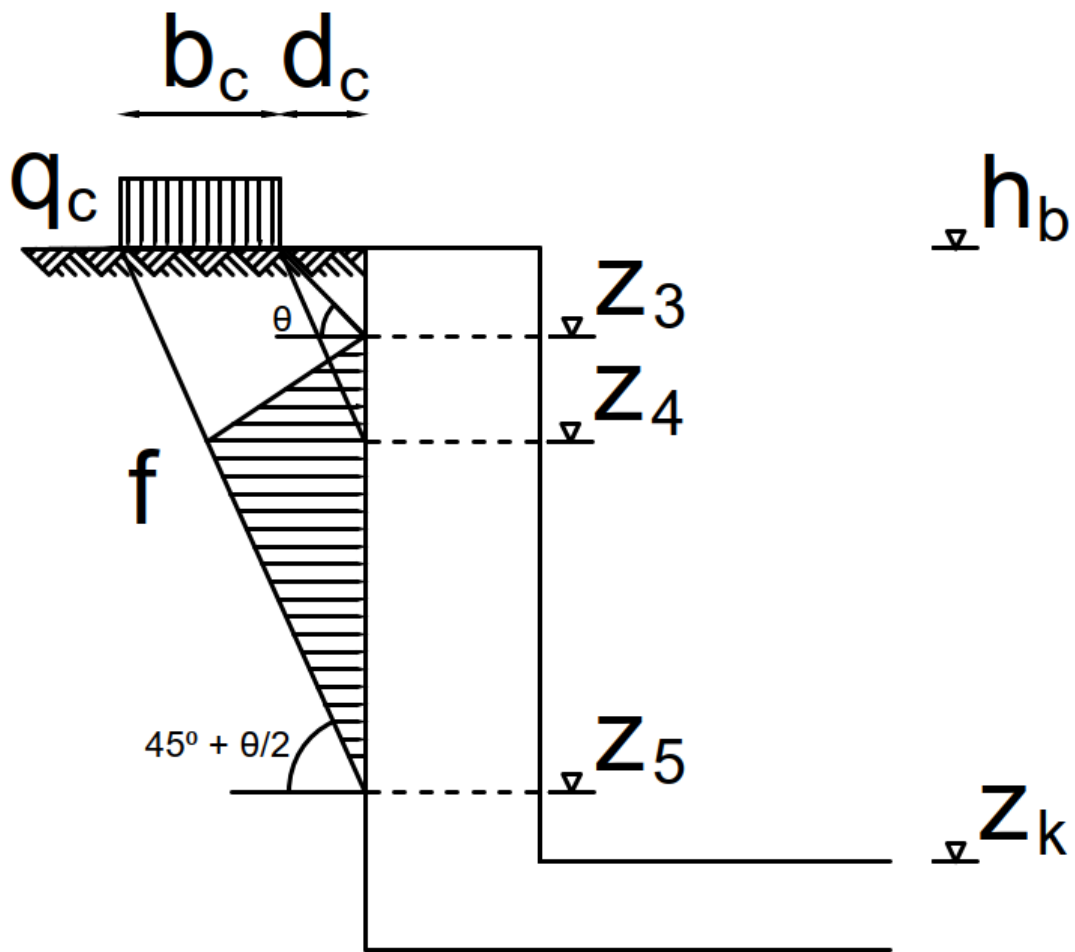
Figure B.9: Crane load

- Hawser load:
  The 'Richtlijnen voor Vaarwegen 2017' prescribes a standard hawser load per CEMT class (*Richtlijnen vaarwegen 2017*, 2017). The hawser load is $200kN$ for classes I & II, $250kN$ for classes III & IV, $250kN$ for class V, $300kN$ for class VIa and $350kN$ for class VIb. The load per meter is:

  $f = F_h/l_h$

  where:

  F_h = load boulder $[N]$
  l_h = effective width $[m]$
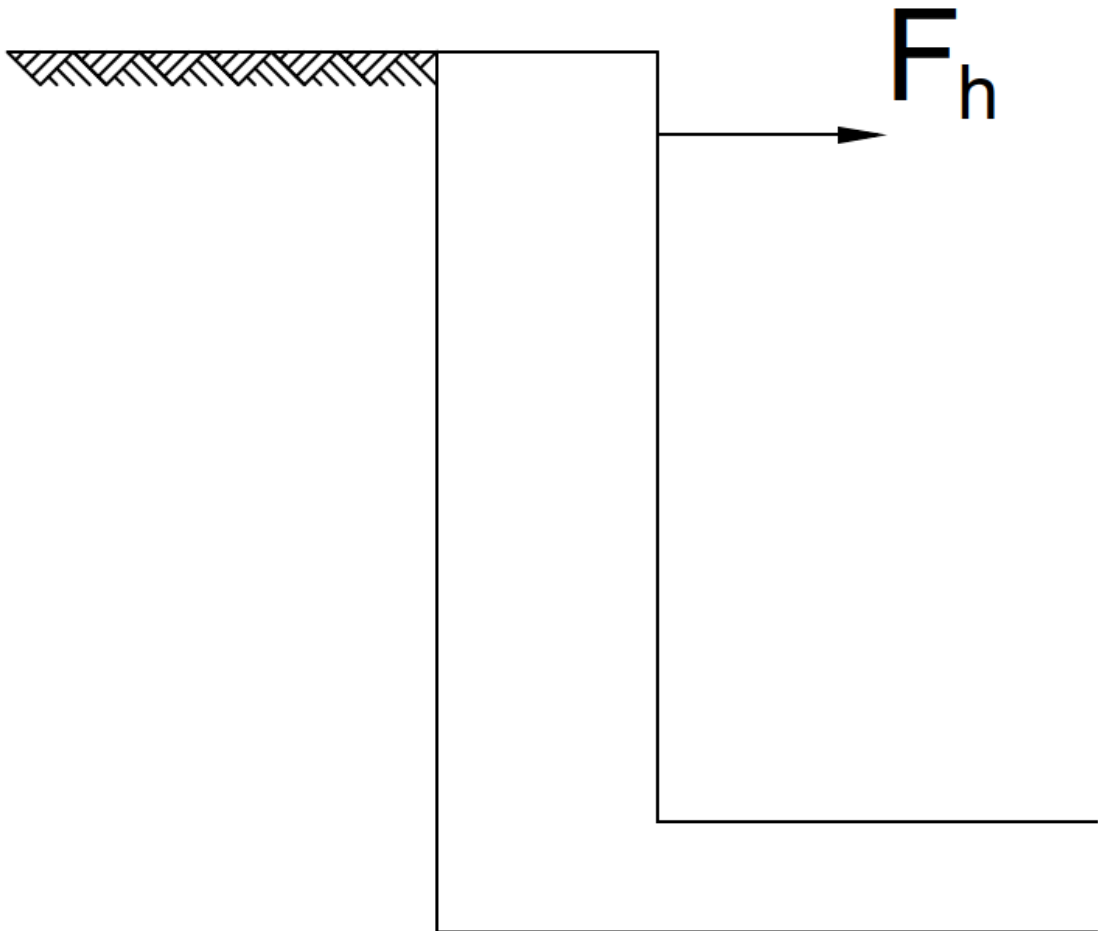
Figure B.10: Hawser load

- Gate load:
  This load only applies to mitre gates. Mitre gates are placed under an angle of $1 : 3$. The force due to different water levels at both sides of the gate is transferred to the walls.

$$F = \frac{F_{water}}{2tan(\alpha)}$$

where:

α = angle of the gates [°]
F_{water} = resultant force in horizontal direction parallel to the lock head due to the difference in water level at both sides of the gate [N].
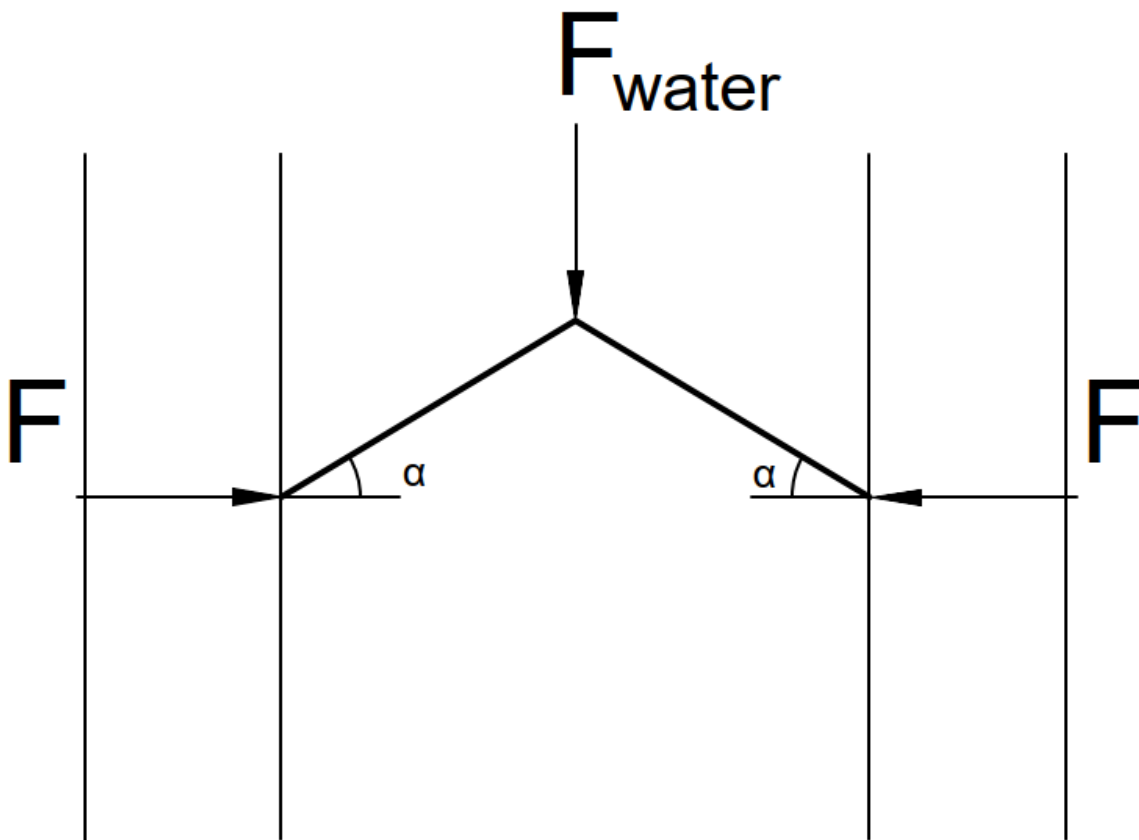
Figure B.11: Mitre gate load

Horizontal Parallel
- Water load due to different water level:

$$F = b[\frac{1}{2}\gamma_w(h_1 - z_k)^2 - \frac{1}{2}\gamma_w(h_2 - z_k)^2]$$

where:

γ_w = weight water $[N/m^3]$
h_1 = high water level $[mNAP]$
h_2 = low water level $[mNAP]$
z_k = top lock head floor $[mNAP]$
b = inner width of the lock head $[m]$
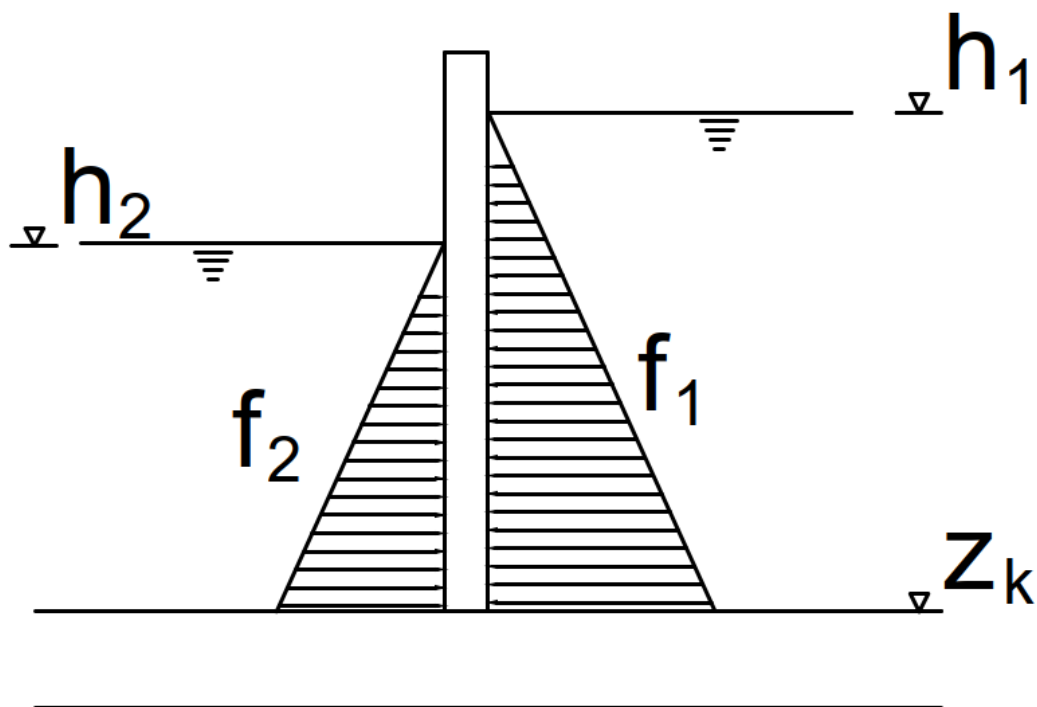
Figure B.12: Water load due to difference in water level

- Soil and (ground)water force at the end faces of the lock head. Depending on the lock head, the force can be a water force or a soil and groundwater force. To calculate the soil force, a neutral lateral earth pressure has to be used.

Vertical
- Own weight walls:
  For this research only the own weight of the walls and the gate are taken in to account. Loads due to lifting towers and bridges have been disregarded.

B.3.2. Loads on the Floor

In total five main loads act on the floor, being:

- Loads acting on the walls. The loads acting on the walls are transferred to the floor due to the rigid connection between the walls and the floor.
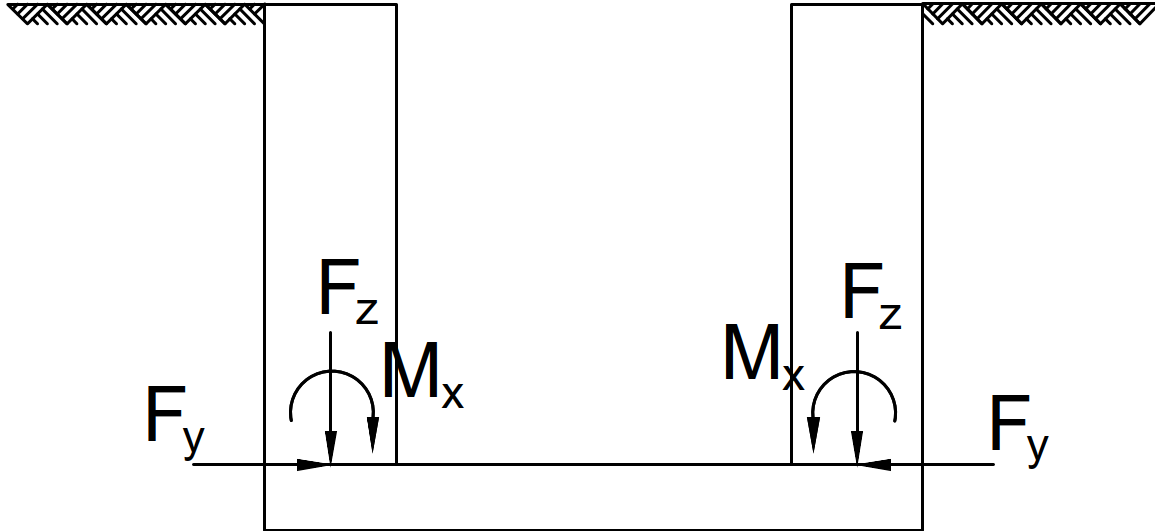
Figure B.13: Loads acting on the walls are transferred to the floor

- Own weight floor

$$f = \gamma_c(z_k - z_b)$$

where:

γ_c = weight concrete $[N/m^3]$
z_k = top lock head floor $[mNAP]$
z_b = bottom lock head floor $[mNAP]$
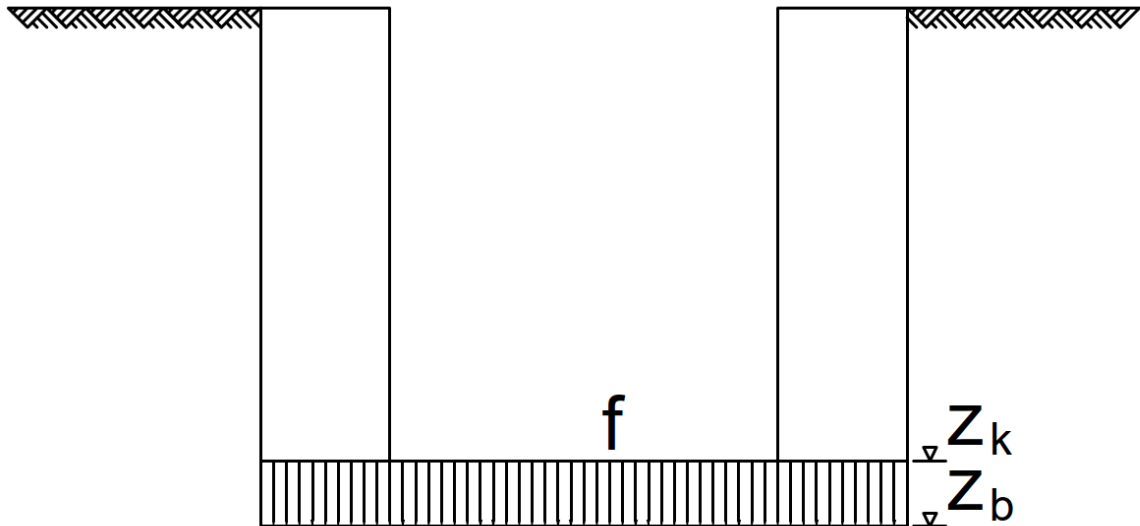
Figure B.14: Own weight floor

- Water load on top of the floor:

$$f = \gamma_w (h - z_k)$$

where:

γ_w = weight water $[N/m^3]$
h = water level in the lock head $[mNAP]$
z_k = top lock head floor $[mNAP]$
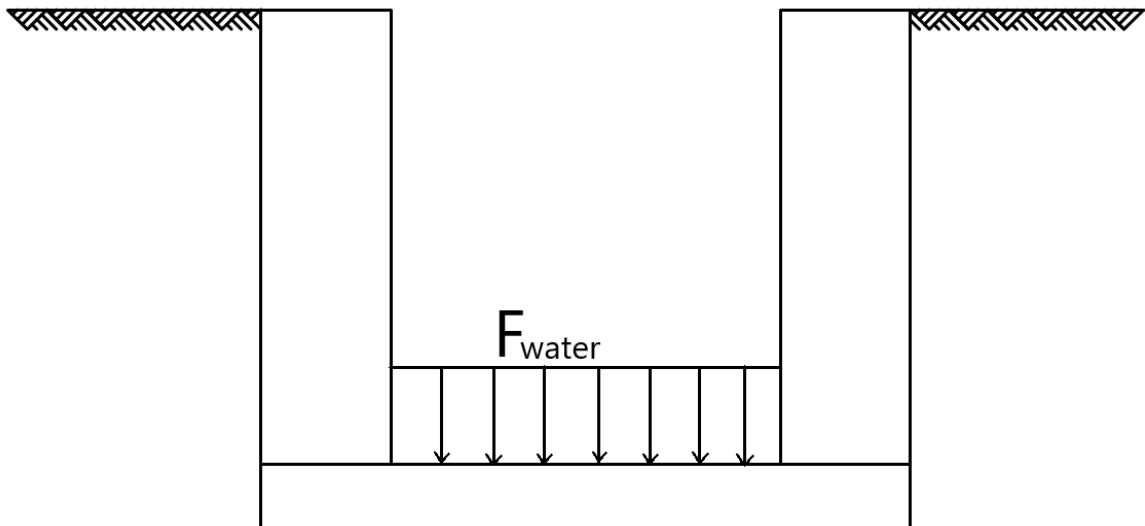
Figure B.15: water load on top of the floor

- Ground water load under the floor:

$$f = \gamma_w(h_g - z_b)$$

where:

γ_w = weight water $[N/m^3]$
h_g ground water level $[mNAP]$
z_b = bottom lock head floor $[mNAP]$
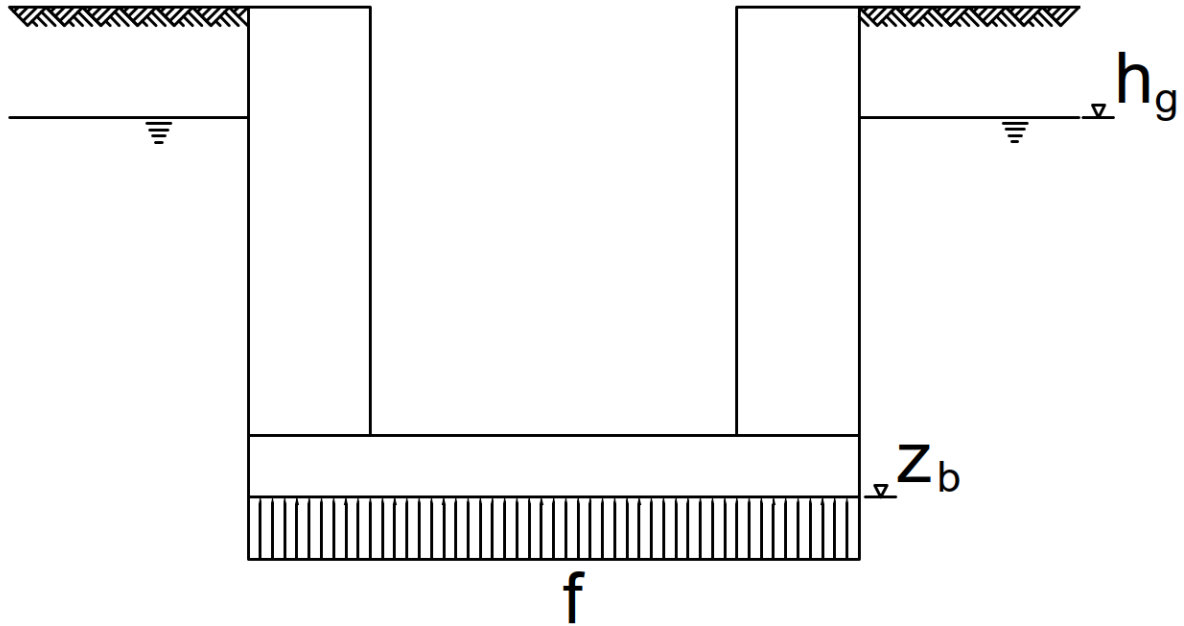
Figure B.16: Ground water load under the floor

- Weight gate:
  In case of a single leaf gate or a mitre gate, the weight of the gate is directly transferred to the floor via the pivot. For a single leaf gate the gate load only acts on one side of the lock head.
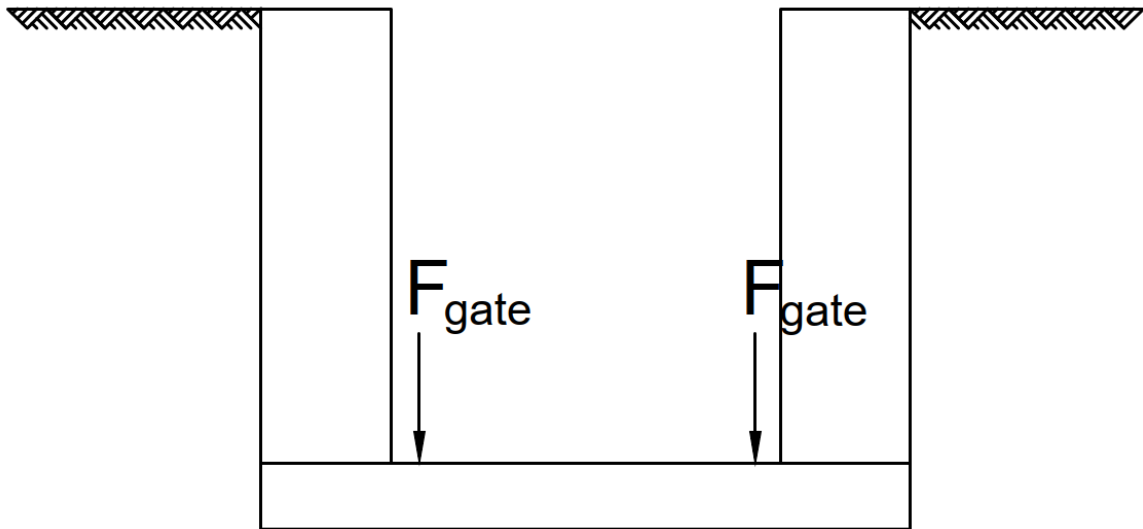
Figure B.17: Gate load

B.4. Load Factors and Combinations

B.4.1. Load Factors

The load factors taken into account in this research are according to Leidraad TAW and are shown in table B.1.

Table B.1: Load factors according to Leidraad TAW

Load	Dominant load	Combination load
Permanent		
Own weight	(1.35 or 1.2 or 1.0 or 0.9) F_{rep}	(1.2 or 1.0 or 0.9) F_{rep}
Soil pressure	(1.2 or 1.0 or 0.9) F_{rep}	(1.2 or 1.0 or 0.9) F_{rep}
Soil water pressure	(1.2 or 1.0 or 0.9) F_{rep}	(1.2 or 1.0 or 0.9) F_{rep}
Variable		
Pressure difference water levels	1.1 F_{norm}	1.25 F_{10}
Pressure difference wind waves	NA	NA
Current	NA	NA
Vessel waves	NA	NA
Vessel current	NA	NA
Boulder loads	1.30 F_{max}	1.30 F_{max}
Wind loads	NA	NA
Temperature loads	NA	NA
Traffic loads	1.5 F_{rep}	1.5 F_{rep}
Exceptional		
Collision	NA	NA
Explosion	NA	NA
Ice	NA	NA

B.4.2. Load Combinations

The load combinations for this research are according the following principle:

$$\gamma_{f;g} G_{rep} + \gamma_{f;g} \psi_t Q_{1;rep} + \Sigma \gamma_{f;q} \psi_i Q_{i;rep}$$

where:

G_{rep} = permanent load
$\gamma_{f;g}$ = load factor for permanent load
$Q_{1;rep}$ = variable load 1
$\gamma_{f;q}$ = load factor for variable load 1
ψ_t = reduction factor
$Q_{i;rep}$ = variable load i
ψ_i = reduction factor i

The value ψ_t is 1 for a reference period of 50 years. The loads taken into account in this research all have a reference period of 50 years or longer.

B.5. Strength & Stiffness

B.5.1. Strength & Stability Walls

The walls can be schematised as a single wall with a rigid connection at the bottom. The forces discussed in the previous section cause a moment at the rigid connection. The moment is taken at $\frac{1}{8} d_{floor}$ under the top of the lock head floor.
The deflection of the wall is the sum of the deflection of the wall itself and the rotation the of the floor.

B.5.2. Strength & Stiffness Floor

A distinction has to be made between a lock head on a shallow foundation or a lock head on foundation piles. In case of a lock head on a shallow foundation, the floor can be schematised as a floor on a elastic soil. In case of a pile foundation, the floor is supported by individual piles which can be schematised as springs.

Shallow Foundation

The floor can be regarded as an Euler Bernoulli beam of $1m$ width supported by an elastic foundation.
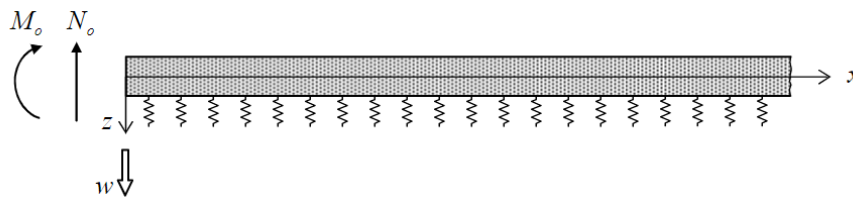
Figure B.18: Slab on an elastic foundation and the sign convention

This research only takes the soil types sand, clay and peat in to account. The subgrade modulus for sand is set to $c = 10^7 N/m^3$ and for clay and peat $c = 10^2 N/m^3$. The deflection of the beam can be can be calculated according to the following formula:

$$w(x) = -\frac{N_0}{2EI\lambda} \exp^{-\lambda x} sin(\lambda x + \frac{\pi}{2})$$
$$w(x) = -\frac{M_0}{EI\lambda^2 \sqrt{2}} \exp^{-\lambda x} sin(\lambda x + \frac{3\pi}{4})$$

The rotation is given by:

$$\phi(x) = \frac{N_0 \sqrt{2}}{EI\lambda^2} \exp^{-\lambda x} sin(\lambda x + \frac{\pi}{4})$$
$$\phi(x) = \frac{M_0}{EI\lambda} \exp^{-\lambda x} sin(\lambda x + \frac{\pi}{2})$$

The moment distribution is given by:

$$M(x) = -\frac{N_0}{\lambda} \exp^{-\lambda x} sin(\lambda x)$$
$$M(x) = -M_0 \sqrt{2} \exp^{-\lambda x} sin(\lambda x + \frac{\pi}{4})$$

The shear force is given by:

$$V(x) = -N_0 \sqrt{2} \exp^{-\lambda x} sin(\lambda x - \frac{\pi}{4})$$
$$V(x) = -2M_0 \lambda \exp^{-\lambda x} sin(\lambda x)$$

where:
N_0 = the weight of the wall $[N]$
M_0 = the moment at the bottom of the wall $[Nm]$
$\lambda = \frac{c}{4EI}^{\frac{1}{4}}$ the characteristic length $[m^{-1}]$

Pile Foundation

The floor is again schematised to an Euler Bernoulli beam of $1m$ width. The beam is supported by several springs which represent the pile foundation. The spring stiffness of the a single pile can be calculated according to the following formula:

$$k_p = \frac{E_c A_c}{(1+\beta) l_p}$$

where:

E_c = the stiffness of the foundation pile $[N/m^2]$
A_c = the surface area of the foundation pile $[m^2]$
l_p = the length of the foundation pile $[m]$
β = a factor varying between the 0.2 and 0.5

B.6. Global Stability

The lock head has to be checked on global stability. This includes the vertical bearing capacity, horizontal capacity, rotational stability, screw up and piping.

B.6.1. Vertical Bearing Capacity

The bearing capacity of the soil determines the foundation of the lock head. An estimate for the bearing capacity of a shallow foundation is $300kN/m^2$ (Molenaar, 2011). In case of a pile foundation an initial pile bearing capacity of $1000kN$ per $450x450mm^2$ pile can be used, provided the pile toe is in a layer where the cone value is around $10N/mm^2$ (Molenaar, 2011). The normative situation is a lock head in operation with the highest water level and the minimum groundwater level.

B.6.2. Horizontal Bearing Capacity

Horizontal equilibrium has to be checked to prevent the lock head from sliding. This is especially important for the lower lock head, since it is not supported by the lock chamber. According to the design rules the upper and lower lock head have to withstand the horizontal shear force caused by the difference in water level, on their own.

A lock head on a shallow foundation gets its resistance from the shear resistance between the floor and soil, the passive soil pressure at the end faces of the lock head and the shear resistance between the walls and the soil.

The shear resistance between the floor and the soil for a drained soil is given by:

$$F_h = F_v tan(\frac{2}{3}\phi)$$

where:

F_v = resultant vertical force $[N]$
ϕ = angle of internal friction $[°]$

This force may only be taken into account when the resulting force F_v is working downwards.
The normative situation is an empty lock head with the highest groundwater level. In case the horizontal bearing capacity is exceeded, the lock head can be made heavier, extended in horizontal direction or more batter piles need to be installed.

B.6.3. Hydraulic Bursting
This phenomenon occurs when the resulting force in upward direction is bigger than the resulting force in downward direction. For a lock head on a shallow foundation it has to be avoided that the soil pressure becomes zero. For a pile foundation it has to be avoided that the tension strength of the piles is exceeded.
The normative situation is an empty lock head with the highest ground water level. Measures to prevent the lock head from screwing up are to make the lock head heavier or to apply tension piles.

B.6.4. Rotational Stability
The rotation of a lock head is mainly caused by the difference in water level at both sides of the lock. In reality only the lower lock head is susceptible to rotation, since it is not supported by the lock chamber. However, both lock heads have to be checked on rotational stability. This is done by calculating the resulting moment around the bottom of the structure at the middle of the floor. The soil has to withstand the resulting moment. However, the soil is only able to resist compression pressure, if it stays below the bearing capacity of the soil.
The next step is to translate the resulting moment to a vertical force with a corresponding lever arm:

$$e = \frac{F_{v,total}}{M_{total}}.$$

When $e \leq \frac{L_{lock}}{6}$, there is no tension. The lock head is not susceptible to rotation. The total lock head stays in contact with the soil. When $e \geq \frac{L_{lock}}{6}$, there is a redistribution of the soil pressure. Now it has to be checked if the effective soil pressure is smaller than the bearing capacity of the soil. When this is not the case, the lock head is susceptible to overturning. To account for this instability, the lock head can be made longer or the gates can be transferred to the lower water side.

B.6.5. Piping
Piping is the ability of a water flow under and around the structure to transport soil particles. It is an self reinforcing process. Piping can be calculated with the formulas of Bligh and Lane. The normative situation is when the water level difference between both sides of the lock head is the greatest. When the lock head and the lock chamber are watertight connected and the lock chamber itself is also watertight, piping is most of the time not a problem. When this is not the case, the lock head has to be checked on piping. Piping is easily prevented by placing cutoff screens.

For the piping calculations the formulas of Bligh and Lane are used.

Bligh: $L_B \geq \gamma C_B \Delta H$

Lane: $L_L \geq \gamma C_L \Delta H$

where:

$\gamma = 1.5$
C_B = Bligh's constant
C_L = Lane's constant
ΔH = head difference over the lock head
$L_B = \Sigma L_{vert} + \Sigma L_{hor}$
$L_L = \Sigma L_{vert} + \Sigma \frac{1}{3} L_{hor}$

The constants are shown in Table (naar de Bijlage)

Table B.2: Constants Bligh and Lane (Calle and Weijers, 1994)

Soil type	Bligh's constant	Lane's constant
Very fine sand	18	8.5
Fine sand	15	7.0
Coarse sand	12	5
Gravel	4-9	4
Clay	3	2

C

Lock Empel

C.1. Vessel Passages Navigation Locks in the Netherlands

Figure C.1 shows the amount of passages per navigation lock per year due to commercial shipping and recreational boating in 2014. The navigation locks are part of the main navigation routes in the Netherlands.

Route*	Sluisnaam	Passages (2014)		Motivatie voor selectie
		Beroepsvaart	Recreatievaart	
ROT-DUI	Amerongen	10.009	6.319	Voor betreffende sluizen geldt: - Liggen op HVWN - Hebben een dominante beroepsvaart-functie (meer dan 10.000 passages per jaar) - Er is nog geen capaciteits-uitbreiding gepland
ROT-LUI	Belfeld	20.521	7.962	
ROT-LUI	Born,	20.878	4.290	
AMS-DEL	Gaarkeukensluis	14.418	5.620	
ROT-LUI	Grave	10.179	9.819	
ROT-ANT	Hansweert	41.112	6.558	
ROT-LUI	Heel	18.930	4.050	
AMS-DEL	Houtribsluizen	37.140	19.192	
ROT-ANT	Krammersluizen	39.666	33.693	
ROT-ANT	Kreekraksluizen	69.058	2.274	
ROT-LUI	Maasbracht	21.726	4.490	
AMS-DEL	Oostersluis	14.102	5.669	
AMS-ROT	Oranjesluizen[9]	47.407	58.394	
AMS-DUI	Pr. Bernardsluis, Tiel	31.970	2.234	
AMS-DUI	Pr. Irenesluis	35.448	1.957	
AMS-DEL	Pr. Margrietsluis	19.405	20.234	
ROT-LUI	Pr. Maximasluizen	13.447	13.605	
ROT-LUI	Sambeek	27.130	10.166	
n.v.t.	Schijndel	12.760	1.797	
ROT-DUI	St. Andries	10.128	4.388	
ROT-DUI	Weurt	29.074	4.544	
AMS-DEL	Zeesluis Farmsum	11.806	5.752	
n.v.t.	Sluis Empel	9.292**	2.023**	Recentelijk geopende sluis met groeipotentie
n.v.t.	Sluis Hintham	9.292**	2.023**	Sluis Empel is identiek aan Hintham in zowel afmeting als aanbod van schepen.
ROT-DUI	Sluis Hagestein	7.906	6.638	Zie toelichting in de hoofdtekst
ROT-DUI	Sluis Delden	7.378	459	
n.v.t.	Sluis Panheel	5.254	2.711	

Figure C.1: Vessel passages per year in 2014 (*Deelrapportage Vaarwegen voor de Nationale Markt- en Capaciteitsanalyse (NMCA), 2017*)

C.2. Parameters Calculations

Table C.1: Geometrical parameters

Top of Structure	8.18	m NAP
Top floor	-4.60	m NAP
Top underwater concrete chamber	-4.70	m NAP
Thickness floor	2	m
Thickness walls	2.2	m
Bottom floor	-6.60	m NAP
Layer thickness between floor and underwater concrete	0.10	m
Thickness underwater concrete	2.1	m
Bottom underwater concrete	-8.80	m NAP
Thickness underwater concrete chamber	1.20	m
Width vessel passage	12.85	m
Depth gate chamber	2.00	m
Depth gate recess	1.10	m
Distance between sheet pile and eastern wall	2.375	m
Distance between sheet pile and western wall	2.775	m
Length gate chamber	8.00	m
Length lock head	12.00	m
Cofferdam c.t.c. width	26.00	m
Cofferdam c.t.c. length	13.30	m
Width approach area north	15.49	m
Width lock chamber	13.85	m
Ground level approach area	7.00	m NAP
Top of sheet pile approach area	5.90	m NAP
Ground level lock chamber	5.90	m NAP
Bottom sheet piles	-13.50	m NAP
Top sheet piles approach area	-5.05	m NAP
Mean High Water	7.83	m NAP
Water level lock chamber	2.00	m NAP
Average highest groundwater level	2.10	m NAP
Weight concrete	25	kN/m^3
Weight underwater concrete	23	kN/m^3
Weigth water	10	kN/m^3
Length underwater concrete floor	22	m

Table C.2: Influence width soil and water pressure approach area and chamber

Location	$b_{gaterecess}$ [m]	sheet pile [m]	$b_{gatechamber}$ [m]	sum [m]
Approach area	5.755	15.990	4.255	26.00
Chamber	5.575	14.350	6.075	26.00

C.3. Load Cases

C.3.1. Load Case 1: Own Weight
The moment M_y is calculated around the centre line of the lock head.
The own weight of the concrete for the floor and walls A1, A2 and A3 is $25kN/m^3$.

The own weight of the concrete for the walls A4 and A5 is $24kN/m^3$.
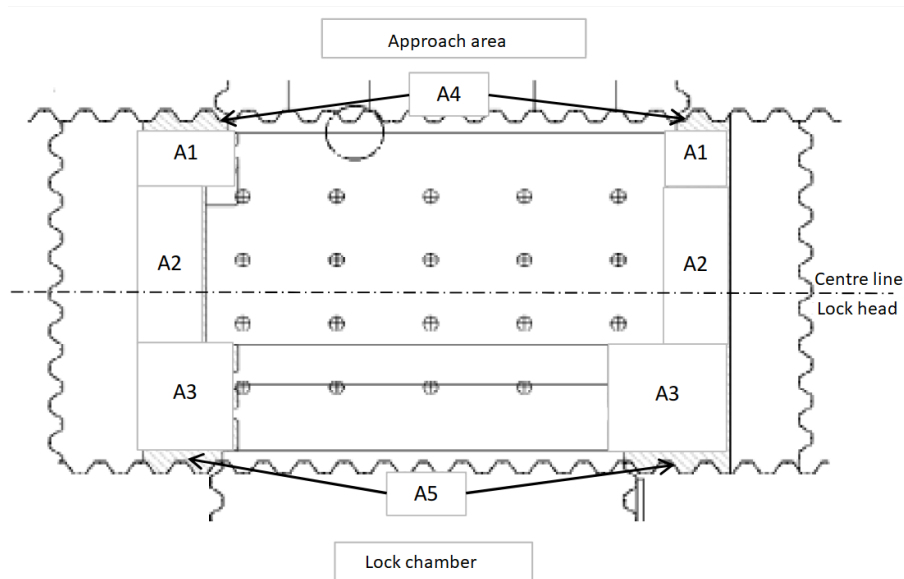
Figure C.2: Load case 1: own weight

The eccentricity of the sum of A1, A2 and A3 has been calculated with the following formula:

$$e = \frac{l_1*b_1*e_1 + l_2*b_2*e_2 + l_3*b_3*e_3}{l_1*b_1 + l_2*b_2 + l_3*b_3}$$

The eccentricity for A4 and A5 has been calculated in a similar fashion.

Table C.3: Influence width soil and water pressure approach area and chamber

Location	l [m]	b [m]	h [m]	e [m]	V [m^3]	F_z [kN]	M_y [kNm]
Floor	13.30	26.00	2	0	694.6	-17290	0
Wall A1	2.00	5.5	12.78	-5	140.58	-3515	-17573
Wall A2	6.00	4.4	12.78	-1	337.392	-8435	-8435
Wall A3	4.00	7.50	12.78	4	383.4	-9585	38340
Sum walls				**0.573**		**-21534**	**12333**
Sum walls and floor LC1						**-38824**	**12333**
Wall A4	0.65	5.5	12.78	-6.325	45.6885	-1097	-6936
Wall A5	0.65	7.5	12.78	-6.325	62.3025	-1495	-9458
Sum walls A4 & A5				**0.973**		**-2592**	**2522**

C.3.2. Load Case 3: Underwater Concrete

Weight underwater concrete: $23kN/m^3$
Weight water: $10kN/m^3$
Net weight underwater concrete: $23 - 10 = 13kN/m^3$

Table C.4: Forces underwater concrete

Location	l [m]	b [m]	h [m]	e [m]	V [m^3]	F_z [kN]	M_y [kNm]
Underwater concrete	13.30	26.00	2.1	0	726.18	**-9440**	**0**

C.3.3. Load Case 4 & 5: Sand between Sheet Piles and Lock Walls

The ground water level is $5.00mNAP$. The ground level is at $8.18mNAP$. The soil properties are:

Table C.5: Soil properties sand between sheet piles and lock walls

Layer	Bottom layer [m NAP]	γ_d [kN/m^3]	γ_s [kN/m^3]	ϕ'_{rep} [°]	c'_{rep} [kN/m^2]	K_0 [−]
Sand	-4.60	18	20	30	0	0.5

The active soil pressure coefficient is calculated with the following formula: $K_0 = 1 - sin(\phi'_{rep})$.

Table C.6: Soil pressures

Level [m NAP]	σ_v [kN/m^2]	σ_w [kN/m^2]	σ_{korrel} [kN/m^2]	σ_h [kN/m^2]
8.18	0.0	0.0	0.0	0.0
5	57.2	0.0	57.2	28.6
-4.6	249.2	96.0	153.2	76.6

Table C.7: Soil forces

Location	l [m]	b [m]	e [m]	A[m^2]	$F_{z,soil}$[kN]	$F_{z,water}$[kN]
A1	13.3	2.625	0	34.9	-5350	-3351.6
A2	13.3	3.025	0	40.2	-6165	-3862.32
Sum					**-11515**	**-7214**

C.3.4. Load Case 6: Groundwater under the Floor

The weight of water is $10kN/m^3$.
The groundwater level is $6.680mNAP$.
The bottom of the floor is at $-6.60mNAP$.
The length of the floor is $13.30m$ and the width is $26.0m$.

Table C.8: Groundwater under the floor

Combination	Waterlevel Maas [mNAP]	Waterlevel canal [mNAP]	GWL [mNAP]	upward pressure [kN/m²]	F [kN]
MHW	7.83	2.00	6.68	132.8	45922
MHW F10	5.86	2.00	5.10	117.0	40459
max schutten	4.40	2.00	3.93	105.3	36413
MLW F10	-0.28	2.00	0.17	67.7	23411
min schutten	-0.50	2.00	-0.01	65.9	22788
MLW	-0.90	2.00	-0.33	62.7	21682
Calamiteit Berlicum	-0.50	3.00	0.19	67.9	23480
Calamiteit Empel	-0.50	-0.50	-0.50	61.0	21094
Empty lock	1.80	2.00	1.84	84.4	28529

C.3.5. Load Case 7 & 8: Soil and Water Pressure Approach Area

Table C.9: Soil properties

Type	Bottom of layer [NAPm]	γ_d [kN/m³]	γ_s [kN/m³]	ϕ'_{rep} [°]	c'_{rep} [kN/m²]
Sand	4.00	18	20	30	0
Clay, brown	3.00	18.5	18.5	25	4
Clay, grey	2.00	17	17	20.5	5
Sand, loose	-9.00	17	19	30	0
Clay, deep	-9.75	18	18	25	5
Sand, moderate	-13.00	18	20	32.5	0

The water level is at $2.1 mNAP$. The ground level is at $7.0 mNAP$. The width at the gate recess is $5.755m$. The width at the gate chamber is $4.255m$.

Table C.10: Soil loads LC7 and LC8

Level [mNAP]	σ_v [kN/m²]	σ_w [kN/m²]	Top [kN/m²]	Bottom [kN/m²]	K_0 [−]	$\sigma'_{h,b}$ [kN/m²]	$\sigma'_{h,o}$ [kN/m²]
7	0	0	0	54.0	0.50	0	27.0
4	54.0	0	54.0	72.5	0.58	31.2	41.9
3	72.5	0	72.5	87.8	0.65	47.1	57.1
2.1	87.8	0	87.8	88.5	0.65	57.1	57.5
2	89.5	1	88.5	156.9	0.50	44.3	78.5
-5.6	233.9	77	156.9	185.7	0.50	78.5	92.9
-8.8	294.7	109	185.7		0.50	92.9	

Vertical soil and water pressure LC7 & LC8
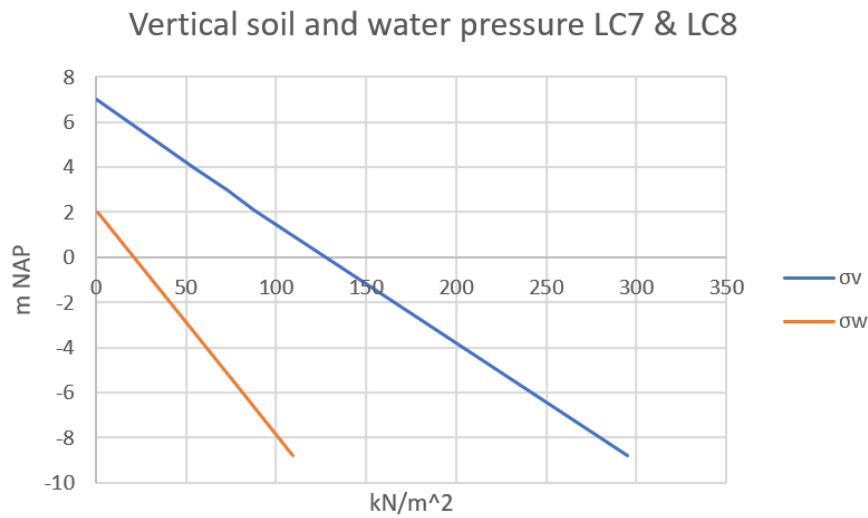
Figure C.3: Vertical soil and water pressure at the approach area

Horizontal soil and water pressure LC7 & LC8
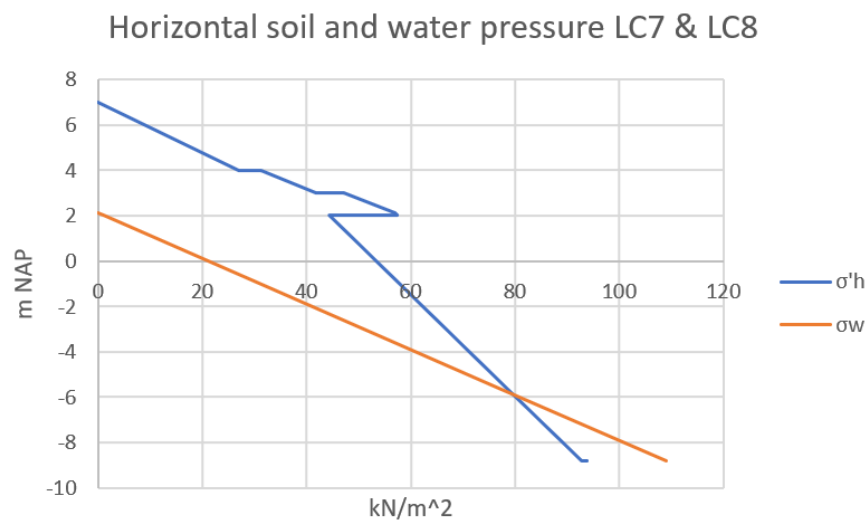
Figure C.4: Horizontal soil and water pressure at the approach area

The load up to $-5.6 mNAP$ has influence on the wall. The load between $-5.60 mNAP$ and $-8.80 mNAP$ acts on the floor and the underwater concrete. The moment is calculated at $-5.60 mNAP$.

Table C.11: LC8 load up to $-5.6 mNAP$

LC8	Gate recess	Gate Chamber	Sum
$F\ [kN]$	1706.07	1261.39	2967
$z\ [mNAP]$	-3.03	-3.03	-3.03
$M\ [kNm]$	4379	3238	7616

Table C.12: LC8 load between $-5.6mNAP$ and $-8.8mNAP$

LC8	Gate recess	Gate Chamber	Sum
$F\,[kN]$	1712.69	1266.29	2979
$z\,[mNAP]$	-7.29	-7.29	-7.29
$M\,[kNm]$	-2897	-2142	-5040

Table C.13: LC8 load total

LC8	Gate recess	Gate Chamber	Sum
$F\,[kN]$	3419	2528	5946
$z\,[mNAP]$	-5.17	-5.17	-5.17
$M\,[kNm]$	-1481	-1095	-2577

Table C.13 is a summation of Table C.11 & C.12.

Table C.14: LC7 load up to $-5.6mNAP$

LC7	Gate recess	Gate Chamber	Sum
$F\,[kN]$	3429	2535	5965
$z\,[mNAP]$	-0.91	-0.91	-0.91
$M\,[kNm]$	16074	11885	27959

Table C.15: LC7 load between $-5.6mNAP$ and $-8.8mNAP$

LC7	Gate recess	Gate Chamber	Sum
$F\,[kN]$	1577	1166	2744
$z\,[mNAP]$	-7.24	-7.24	-7.24
$M\,[kNm]$	-2594	-1918	-4513

Table C.16: LC7 load total

LC7	Gate recess	Gate Chamber	Sum
$F\,[kN]$	5007	3702	8708
$z\,[mNAP]$	-2.91	-2.91	-2.91
$M\,[kNm]$	13480	9966	23446

C.3.6. Load Case 9 & 10: Soil and Water Pressure Approach Area MHW

The bottom of the clay layer at $2mNAP$ is watertight. The water level in and above this layer does not change. The weight on top of the clay layer is added as vertical load. The groundwater level is at $6.77mNAP$. The water level MHW is at $7.83mNAP$. The width at the gate recess is $5.755m$. The width at the gate chamber is $4.255m$.

Table C.17: Soil and water loads LC9 and LC10

Level [mNAP]	σ_v [kN/m²]	σ_w [kN/m²]	Top [kN/m²]	Bottom [kN/m²]	K_0 [−]	$\sigma'_{h,b}$ [kN/m²]	$\sigma'_{h,o}$ [kN/m²]
7.83	0	0	0	34.2	0.50	0	17.1
7	8.3	0	8.3	62.3	0.5	4.15	31.15
4	62.3	0	62.3	80.8	0.58	36.0	46.7
3	80.8	0	80.8	96.1	0.65	52.5	62.4
2.1	96.1	0	96.1	96.8	0.65	62.4	62.9
2	97.8	1	96.8	50.1	0.65	62.9	32.6
2	97.8	47.7	50.1	118.5	0.5	25.1	59.3
-5.6	242.2	123.7	118.5	147.3	0.5	59.3	73.7
-8.8	303	155.7	147.3		0.5	73.65	

The pressure difference with respect to Load case 8 and 9 are calculated.

Table C.18: Pressure difference LC9 and LC10 with respect to LC7 and LC8

Level [mNAP]	σ_w [kN/m²]	$\sigma'_{h,b}$ [kN/m²]	$\sigma'_{h,o}$ [kN/m²]
7.83	0	0	0
7	0	4.2	4.2
4	0	4.8	4.8
3	0	5.4	5.4
2.1	0	5.4	5.4
2	0	5.4	5.4
2	46.7	-19.2	-19.2
-5.6	46.7	-19.2	-19.2
-8.8	46.7	-19.2	
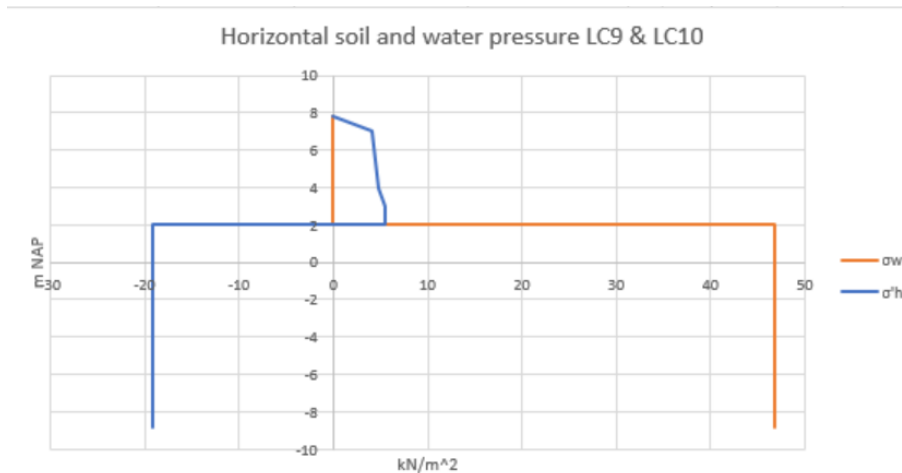
Figure C.5: Horizontal soil and water pressure at the approach area

Table C.19: LC9 load up to $-5.6mNAP$

LC9	Gate recess	Gate Chamber	Sum
$F\ [kN]$	-710	-525	-1234
$z\ [mNAP]$	-2.93	-2.93	-2.93
$M\ [kNm]$	-1893	-1400	-3293

Table C.20: LC9 load between $-5.6mNAP$ and $-8.8mNAP$

LC9	Gate recess	Gate Chamber	Sum
$F\ [kN]$	-354	-261	-615
$z\ [mNAP]$	-7.20	-7.20	-7.20
$M\ [kNm]$	566	418	984

Table C.21: LC9 load total

LC9	Gate recess	Gate Chamber	Sum
$F\ [kN]$	-1063	-786	-1849
$z\ [mNAP]$	-4.35	-4.35	-4.35
$M\ [kNm]$	-1328	-982	2309

Table C.22: LC10 load up to $-5.6mNAP$

LC10	Gate recess	Gate Chamber	Sum
$F\ [kN]$	2042.56	1510.18	3553
$z\ [mNAP]$	-1.80	-1.80	-1.80
$M\ [kNm]$	7762	5739	13500

Table C.23: LC10 load between $-5.6mNAP$ and $-8.8mNAP$

LC10	Gate recess	Gate Chamber	Sum
$F\ [kN]$	860.03	635.87	1496
$z\ [mNAP]$	-7.20	-7.20	-7.20
$M\ [kNm]$	-1376	-1017	-2393

Table C.24: LC10 load total

LC10	Gate recess	Gate Chamber	Sum
$F\ [kN]$	2903	2146	5049
$z\ [mNAP]$	-3.40	-3.40	-3.40
$M\ [kNm]$	6386	4721	11107

C.3.7. Load Case 11 & 12: Soil and Water Pressure Lock Chamber

Table C.25: Soil properties

Type	Bottom of layer [NAPm]	γ_d [kN/m³]	γ_s [kN/m³]	ϕ'_{rep} [°]	c'_{rep} [kN/m²]
Sand	4.00	18	20	30	0
Clay, brown	3.00	18.5	18.5	25	4
Clay, grey	2.00	17	17	20.5	5
Sand, loose	-9.00	17	19	30	0
Clay, deep	-9.75	18	18	25	5
Sand, moderate	-13.00	18	20	32.5	0

The water level is at $2.1mNAP$. The ground level is at $5.9mNAP$. The width at the gate recess is $5.575m$. The width at the gate chamber is $6.075m$.

Table C.26: Soil loads LC11 and LC12

Level [mNAP]	σ_v [kN/m²]	σ_w [kN/m²]	Top [kN/m²]	Bottom [kN/m²]	K_0 [−]	$\sigma'_{h,b}$ [kN/m²]	$\sigma'_{h,o}$ [kN/m²]
5.9	0	0	0	34.2	0.50	0	17.1
4	34.2	0	34.2	52.7	0.58	19.7	30.4
3	52.7	0	52.7	68.0	0.65	34.2	44.2
2.1	68.0	0	68.0	68.7	0.65	44.2	44.6
2	69.7	1	68.7	137.1	0.50	34.4	68.6
-5.6	214.1	77	137.1	165.9	0.50	68.6	83.0
-8.8	274.9	109	165.9		0.50	83.0	
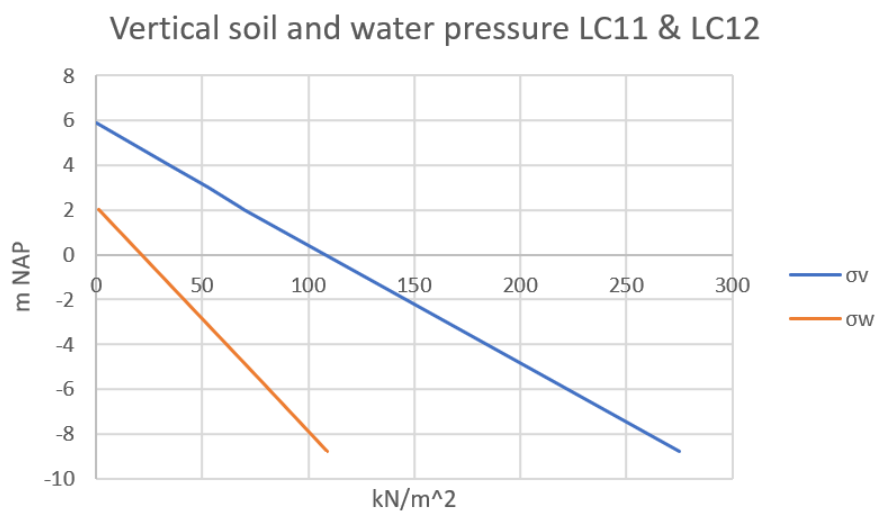
Figure C.6: Vertical soil and water pressure at the lock chamber

Horizontal soil and water pressure LC11 & LC12
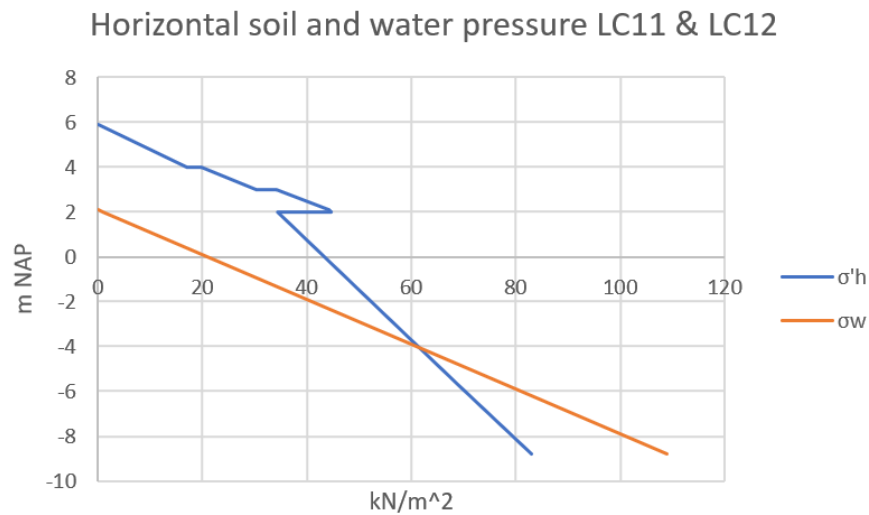
Figure C.7: Horizontal soil and water pressure at the lock chamber

Table C.27: LC11 load up to $-5.6 mNAP$

LC11	Gate recess	Gate Chamber	Sum
$F\ [kN]$	2632	2868	5500
$z\ [mNAP]$	-1.29	-1.29	-1.29
$M\ [kNm]$	11350	12368	23718

Table C.28: LC11 load between $-5.6 mNAP$ and $-8.8 mNAP$

LC11	Gate recess	Gate Chamber	Sum
$F\ [kN]$	1351	1473	2824
$z\ [mNAP]$	-7.25	-7.25	-7.25
$M\ [kNm]$	-2231	-2431	-4661

Table C.29: LC11 load total

LC11	Gate recess	Gate Chamber	Sum
$F\ [kN]$	3983	4341	8324
$z\ [mNAP]$	-3.31	-3.31	-3.31
$M\ [kNm]$	9119	9937	19056

Table C.30: LC12 load up to $-5.6mNAP$

LC12	Gate recess	Gate Chamber	Sum
$F\ [kN]$	1652.71	1800.93	3454
$z\ [mNAP]$	-3.03	-3.03	-3.03
$M\ [kNm]$	4242	4622	8864

Table C.31: LC12 load between $-5.6mNAP$ and $-8.8mNAP$

LC12	Gate recess	Gate Chamber	Sum
$F\ [kN]$	1659.12	1807.92	3467
$z\ [mNAP]$	-7.29	-7.29	-7.29
$M\ [kNm]$	-2807	-3059	-5865

Table C.32: LC12 load total

LC12	Gate recess	Gate Chamber	Sum
$F\ [kN]$	3312	3609	6921
$z\ [mNAP]$	-5.17	-5.17	-5.17
$M\ [kNm]$	1435	1564	2999

C.3.8. Load Case 13 & 14: Soil and Water Pressure Lock Chamber MHW

The bottom of the clay layer at $2mNAP$ is watertight. The water level in and above this layer does not change. The weight on top of the clay layer is added as vertical load. The groundwater level is at $6.60mNAP$. The width at the gate recess is $5.58m$. The width at the gate chamber is $6.08m$.

Table C.33: Soil and water loads LC13 and LC14

Level [$mNAP$]	σ_v [kN/m^2]	σ_w [kN/m^2]	Top [kN/m^2]	Bottom [kN/m^2]	$K_0\ [-]$	$\sigma'_{h,b}$ [kN/m^2]	$\sigma'_{h,o}$ [kN/m^2]
5.9	0	0	0	0	0	0	0
5.9	0	0	0	34.2	0.5	0	17.1
4.0	34.2	0	34.2	52.7	0.58	19.7	30.4
3.0	52.7	0	52.7	68	0.65	34.2	44.2
2.1	68	0	68	68.7	0.65	44.2	44.6
2.0	69.7	1	68.7	23.7	0.65	44.6	15.4
2.0	69.7	46	23.7	92.1	0.5	11.9	46.1
-5.6	214.1	122	92.1	120.9	0.5	46.1	60.5
-8.8	274.9	154	120.9		0.5	60.5	

The pressure difference with respect to Load case 11 and 12 are calculated.

Table C.34: Pressure difference LC13 and LC14 with respect to LC11 and LC12

Level [mNAP]	σ_w [kN/m²]	$\sigma'_{h,b}$ [kN/m²]	$\sigma'_{h,o}$ [kN/m²]
5.9	0	0	0
5.9	0	0	0
4.0	0	0	0
3.0	0	0	0
2.1	0	0	0
2.0	0	0	-22.5
2.0	45	-22.5	-22.5
-5.6	45	-22.5	-22.5
-8.8	45	-22.5	
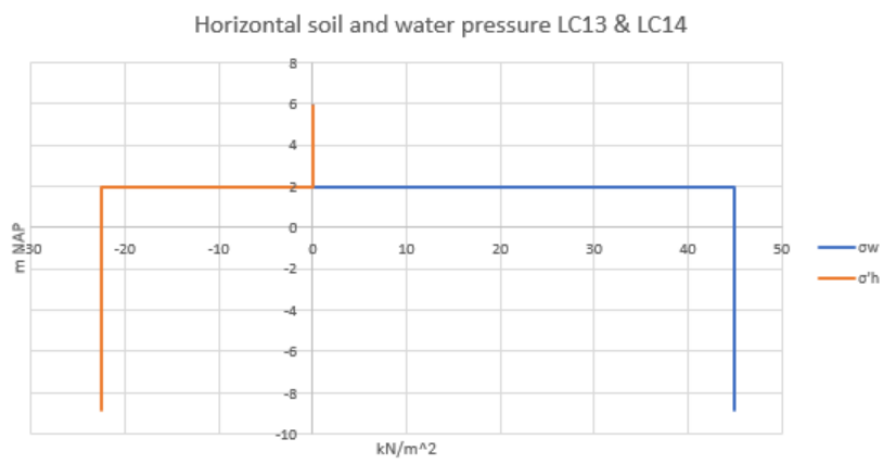
Figure C.8: Horizontal soil and water pressure at the lock chamber

Table C.35: LC13 load up to $-5.6mNAP$

LC13	Gate recess	Gate Chamber	Sum
$F\,[kN]$	-953	-1039	-1992
$z\,[mNAP]$	-1.80	-1.80	-1.80
$M\,[kNm]$	-3623	-3948	-7570

Table C.36: LC13 load between $-5.6mNAP$ and $-8.8mNAP$

LC13	Gate recess	Gate Chamber	Sum
$F\,[kN]$	-401	-437	-839
$z\,[mNAP]$	-7.20	-7.20	-7.20
$M\,[kNm]$	642	700	1342

Table C.37: LC13 load total

LC13	Gate recess	Gate Chamber	Sum
$F\ [kN]$	-1355	-1476	-2831
$z\ [mNAP]$	-3.40	-3.40	-3.40
$M\ [kNm]$	-2980	-3248	-6228

Table C.38: LC14 load up to $-5.6mNAP$

LC14	Gate recess	Gate Chamber	Sum
$F\ [kN]$	1906.655	2077.65	3984
$z\ [mNAP]$	-1.80	-1.80	-1.80
$M\ [kNm]$	7245	7895	15140

Table C.39: LC14 load between $-5.6mNAP$ and $-8.8mNAP$

LC14	Gate recess	Gate Chamber	Sum
$F\ [kN]$	802.80	874.80	1678
$z\ [mNAP]$	-7.20	-7.20	-7.20
$M\ [kNm]$	-1284	-1400	-2684

Table C.40: LC14 load total

LC14	Gate recess	Gate Chamber	Sum
$F\ [kN]$	2709	2952	5662
$z\ [mNAP]$	-3.40	-3.40	-3.40
$M\ [kNm]$	5961	6495	12456

C.3.9. Load Case 15: Pressure Difference due to Water Level

The bottom of the structure is at $-8.80mNAP$. The moment M_y is calculated at $-5.60mNAP$.
The inner width at the lock approach area is $15.99m$. The inner width at the lock chamber is $14.35m$.
The values are calculated as in C.3.5.

Table C.41: Water pressure different water levels

z [mNAP]	$\sigma_{w,MHW}$ [kN/m^2]	$\sigma_{w,MHW,F10}$ [kN/m^2]	$\sigma_{w,max,schut}$ [kN/m^2]	$\sigma_{w,cal,Ber}$ [kN/m^2]	$\sigma_{w,2.0}$ [kN/m^2]	$\sigma_{w,MLW,F10}$ [kN/m^2]	$\sigma_{w,min,schut}$ [kN/m^2]	$\sigma_{w,MLW}$ [kN/m^2]
7.83	0.0	0.0	0.0	0.0	0.0	0.0	0.0	0.0
5.86	19.7	0.0	0.0	0.0	0.0	0.0	0.0	0.0
4.40	34.3	14.6	0.0	0.0	0.0	0.0	0.0	0.0
3.00	48.3	28.6	14.0	0.0	0.0	0.0	0.0	0.0
2.00	58.3	38.6	24.0	10.0	0.0	0.0	0.0	0.0
-0.28	81.1	61.4	46.8	32.8	22.8	0.0	0.0	0.0
-0.50	83.3	63.6	49.0	35.0	25.0	2.2	0.0	0.0
-0.90	87.3	67.6	53.0	39.0	29.0	6.2	4.0	0.0
-4.60	124.3	104.6	90.0	76.0	66.0	43.2	41.0	37.0
-5.60	134.3	114.6	100.0	86.0	76.0	53.2	51.0	47.0
-8.80	166.3	146.6	132.0	118.0	108.0	85.2	83.0	79.0

Table C.42: Loads up to $-5.60\ mNAP$

F_x [kN/m]	901.8	656.7	500.0	369.8	288.8	141.5	130.1	110.5
z [mNAP]	-1.20	-1.78	-2.27	-2.73	-3.07	-3.83	-3.90	-4.03
M_y [kNm/m]	4037	2508	1667	1060	732	251	221	173

Table C.43: Loads between $-5.60\ mNAP$ and $-8.80\ mNAP$

F_x [kN/m]	481.0	417.9	371.2	326.4	294.4	221.4	214.4	201.6
z [mNAP]	-7.26	-7.27	-7.27	-7.28	-7.29	-7.32	-7.33	-7.34
M_y [kNm/m]	-797	-696	-621	-550	-498	-382	-370	-350

Table C.44: Loads up to $-8.80\ mNAP$

F_x [kN/m]	1382.8	1074.6	871.2	696.2	583.2	363.0	344.5	312.1
z [mNAP]	-3.26	-3.91	-4.40	-4.87	-5.20	-5.96	-6.03	-6.17
M_y [kNm/m]	3240	1812	1045	511	233	-131	-149	-177

C.3.10. Load Case 16: Free Water Board
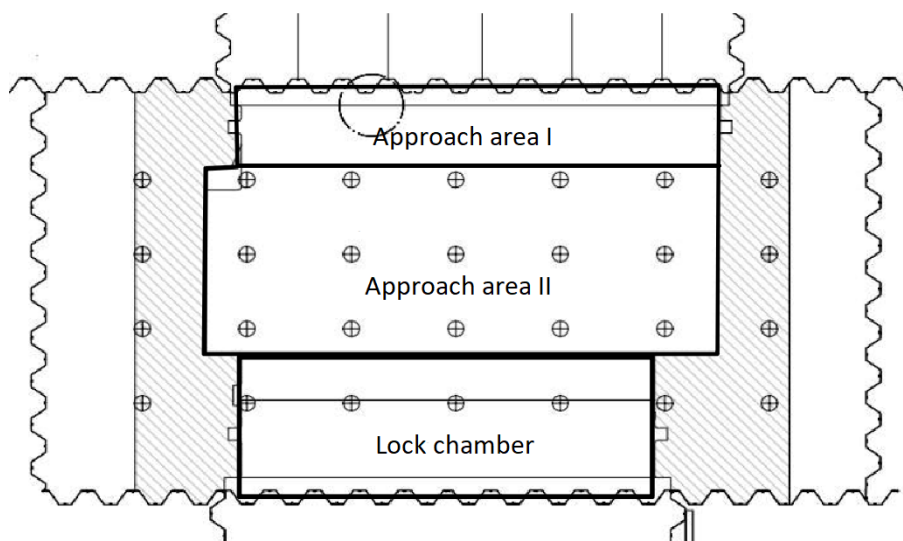
Figure C.9: Overview lock head north

The moment M_y is calculated around the centre line of the lock head.
Weight water: $10 kN/m^3$
The normative situation is MHW. The water level at the approach area is $7.83 mNAP$ and the water level in the lock chamber is $2.00 mNAP$. The top of the floor is at $-4.60 mNAP$.

Table C.45: Forces load case 16

Location	l_x [m]	l_y [m]	A [m]	W [kN/m^2]	F_z [kN]	e [m]	M_y [kNm]
Approach area I	2.65	14.85	39.35	124.3	-4891	-5.325	-26047
Approach area II	6	15.95	95.7	124.3	-11895	-1	-11895
Lock chamber	4.65	12.85	59.75	66	-3944	4.325	17056
Sum					**-20731**		**-20886**

C.3.11. Load Case 17: Wave Loads

The normative situation MHW is further elaborated. The pressure distribution is given in Figure C.10.
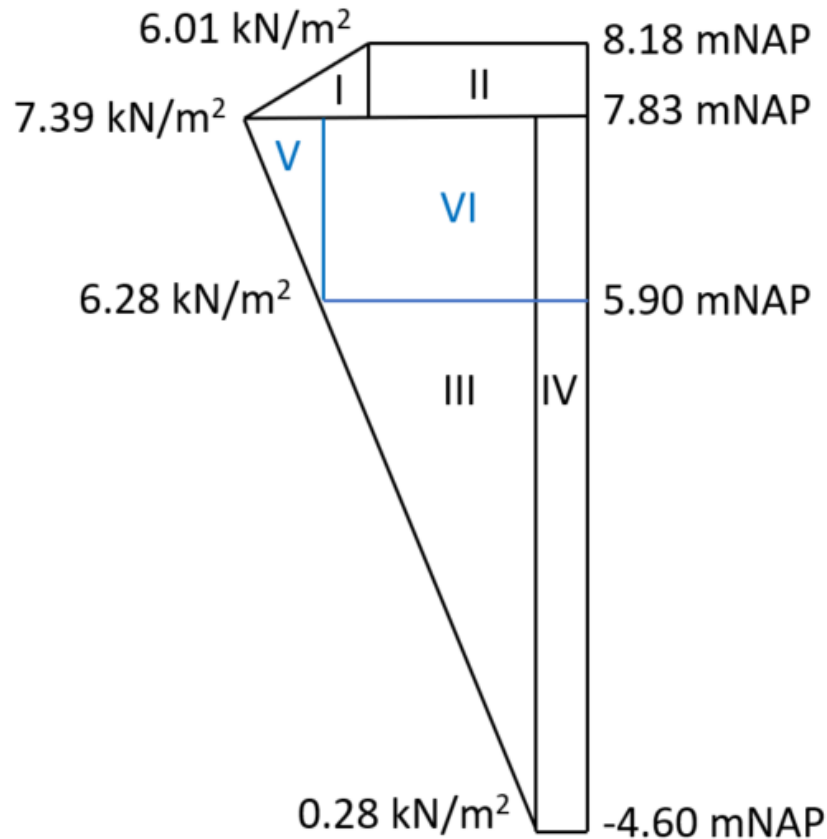
Figure C.10: Pressure distribution MHW

The moment M_y is calculated at $-5.6 mNAP$. The width at the gate recess is $5.755m$. The width at the gate chamber is $4.255m$. The width between the walls is $15.99m$. The pressure distribution acts from $8.18 mNAP$ to $5.9 mNAP$ at the sheet piles. The pressure distribution acts from $8.18 mNAP$ to $-4.60 mNAP$ at the location between the gates.

Table C.46: Load per area

Area	F_x [kN/m]
Area I	0.24
Area II	2.10
Area III	44.13
Area IV	3.48
Area V	1.06
Area VI	12.12

Area I, Area II, Area III and Area IV contribute to the forces acting on the area between the walls. Area I, Area II, Area V and Area VI contribute to the forces acting on the area on the walls in x-direction at the approach area.

Table C.47: Wave loads

	F_y [kN/m]	z [mNAP]	M_y [kNm]
Passage	799.1	3.74	7466
Sheet piles	155.4	7.06	1967

C.3.12. Load Case 18: Traffic Loads

The moment M_x is calculated at $-4.85mNAP$. The traffic load acts at $4.37mNAP$. The distributed traffic load is $20kN/m^2$. The width of the lock head is $12m$. The active soil pressure coefficient is 0.5. The force due to the crane is $1730kN$. This means a force of $865kN$ at each outrigger plate.

Table C.48: Crane loads

	F_y [kN]	e_h [m]	M_x [kNm]
Traffic	1564	6.515	10187
Crane	1730	9.22	15950.6

C.3.13. Load Case: Mooring Forces

The mooring force is $200kN$. The mooring force acts $3.55mNAP$. The moment M_x is calculated at $-4.85mNAP$.

Table C.49: Mooring loads

F_y [kN]	e_h [m]	M_x [kNm]
200	8.40	1680

C.4. Load Combinations

Horizontal equilibrium has to be checked for a water level in the Maas higher than the canal and a water level in the Maas lower than the canal. For both situations the following combinations have been checked in ULS:

- Extreem verval; A water level of the Maas of $7.83mNAP$ and a water level of the canal of $2.00mNAP$. The value of the safety factor $\gamma = 1.10$.

- Extreem verval; A water level of the Maas of $-0.90mNAP$ and a water level of the canal of $2.00mNAP$. The value of the safety factor $\gamma = 1.07$.

- Momentaan verval F_{10}; A water level of the Maas of $5.86mNAP$ and a water level of the canal of $2.00mNAP$. The value of the safety factor $\gamma = 1.25$.

- Momentaan verval F_{10}; A water level of the Maas of $-0.28mNAP$ and a water level of the canal of $2.00mNAP$. The value of the safety factor $\gamma = 1.25$.

- Bijzondere combinatie; A water level of the Maas of $8.28mNAP$ and a water level of the canal of $2.00mNAP$. The value of the safety factor $\gamma = 1.00$. Wave loads are not taken into account.

- Bijzondere combinatie; A water level of the Maas of $-0.50mNAP$ and a water level of the canal of $3.00mNAP$. The value of the safety factor $\gamma = 1.00$. Wave loads are not taken into account.

- Bijzondere combinatie (Ice Loads); A water level of the Maas of $4.40mNAP$ and a water level of the canal of $2.00mNAP$. The value of the safety factor $\gamma = 1.00$

- Bijzondere combinatie (Ice Loads); A water level of the Maas of $-0.50mNAP$ and a water level of the canal of $2.00mNAP$. The value of the safety factor $\gamma = 1.00$.

Twelve load combinations are being considered for strength calculations. Six load combinations for ULS and six load combinations for SLS. For both ULS and SLS; three load combinations in case the lock is emptied and three load combinations in case of MHW. The three combinations for an empty lock are:

- ULS/SLS E1; High soil pressure and traffic loads for the maximum moment at the eastern wall.

- ULS/SLS E2; High soil pressure and traffic loads for the maximum moment at the western wall.

- ULS/SLS E3; Low soil pressure and high groundwater pressure for the maximum moment at the centre line of the floor.

The three load combinations for MHW are:

- ULS/SLS MHW1; A water level of the Maas of $7.83mNAP$ and a water level of the canal of $2.00mNAP$ in combination with a minimum soil pressure.

- ULS/SLS MHW2; A water level of the Maas of $7.83mNAP$ and a water level of the canal of $7.83mNAP$ in combination with a minimum soil pressure.

- ULS/SLS MHW3; A water level of the Maas of $7.83mNAP$ and a water level of the canal of $2.00mNAP$ in combination with a maximum soil pressure.

The displacements are calculated in SLS. The following eight combinations are being considered:

- SLS MHW1; A water level of the Maas of $7.83mNAP$ and a water level of the canal of $2.00mNAP$, the gate is closed.

- SLS MHW2; A water level of the Maas of $7.83mNAP$ and a water level of the canal of $7.83mNAP$, the gate is open.

- SLS MLW1; A water level of the Maas of $-0.90mNAP$ and a water level of the canal of $2.00mNAP$, the gate is closed.

- SLS MLW2; A water level of the Maas of $-0.90mNAP$ and a water level of the canal of $-0.90mNAP$, the gate is open.

- SLS max schutpeil1; A water level of the Maas of $4.40mNAP$ and a water level of the canal of $2.00mNAP$, the gate is closed.

- SLS max schutpeil2; A water level of the Maas of $4.40mNAP$ and a water level of the canal of $4.40mNAP$, the gate is open.

- SLS min schutpeil1; A water level of the Maas of $-0.50mNAP$ and a water level of the canal of $2.00mNAP$, the gate is closed.

- SLS min schutpeil2; A water level of the Maas of $-0.50mNAP$ and a water level of the canal of $-0.50mNAP$, the gate is open.

The displacements have also been checked for an emptied lock in combination with live loads and different groundwater levels. The combinations are:

- E + max GW; A maximum groundwater level of $1.84mNAP$.

- E + min GW; A minimum groundwater level of $0.17mNAP$.

- E + max GW + G; A maximum groundwater level of $1.84mNAP$ with a closed gate.

- E + min GW + G; A minimum groundwater level of $0.17mNAP$ with a closed gate.

- E + max GW + C; A maximum groundwater level of $1.84mNAP$ with traffic loads acting on the western wall and a crane load acting on the eastern wall.

- E + min GW + C; A minimum groundwater level of $0.17mNAP$ with traffic loads acting on the western wall and a crane load acting on the eastern wall.

- E + max GW + G + T; A maximum groundwater level of $1.84mNAP$ with traffic loads acting on the walls and a closed gate.

- E + min GW + G + T; A minimum groundwater level of $0.17mNAP$ with traffic loads acting on the walls and a closed gate.

E: Emptied lock
max. GW: Ground water level of $1.84mNAP$
min. GW: Ground water level of $-0.17mNAP$
G: Gate closed
T: Traffic load on the eastern and western wall
C: Crane load on the eastern wall and traffic load on western wall

C.5. Strength and Stability

The lock head has been modelled in SCIA engineer by VolkerInfra. The maximum values per section are used for further calculations.

C.5.1. Vertical Equilibrium

M_y is calculated around the centre line of the lock head. Loads acting in the negative z-direction (downwards) are multiplied with $\gamma = 0.9$. Loads acting in the positive z-direction (upwards) are multiplied with $\gamma = 1.1$.

Table C.50: Vertical loads

Load case	γ	F_z [kN]	M_y [kNm]
LC1: Own weight floor	0.9	-17290	0
LC1: Own weight walls A1, A2 & A3	0.9	-21534	12333
LC1: Own weight walls A4 & A5	0.9	-2592	2522
LC3: Underwater concrete	0.9	-9440	0
LC4: Soil pressure	0.9	-11515	0
LC5: Water pressure	0.9	-7214	0
LC6: Groundwater under the floor	1.1	45922	0
LC16: Free water board	1.1	-20731	-20886
Sum SLS		**-44394**	**-6032**
Sum ULS		**-34916**	**-9606**

C.5.2. Horizontal Equilibrium

Table C.51: Horizontal loads

Load case	γ	F_x [kN]	e [mNAP]	M_y [kNm]
LC7: Soil pressure approach area	1.0	8708	-2.91	51313
LC8: Water pressure approach area	1.0	5946	-5.17	21605
LC9: Soil pressure approach area MHW	1.1	-1849	-4.35	-8226
LC10: Water pressure approach area MHW		5049	-3.40	27263
LC11: Soil pressure lock chamber	1.0	-8324	-3.31	-45692
LC12: Water pressure lock chamber	1.0	-6921	-5.17	-25145
LC13: Soil pressure lock chamber MHW	1.1	2831	-3.40	15287
LC14: Water pressure lock chamber MHW	1.1	-5662	-3.40	-30574
LC15: Pressure difference due to water level	1.1	13928	-1.96	95299
LC17: Wave loads	1.25	954	4.28	12488
Sum SLS		**14662**		**113617**
Sum ULS		**16330**		**126644**

C.5.3. Wall East

Wall east is divided in section 11 ([-6.0, 8.575, -4.85], [2.0, 8.575, -4.85]) and section 12 ([2.0, 8.575, -4.85], [6.0, 8.575, -4.85]). The maximum moment and normal force are given per section with the corresponding load combination.

Section 11
$F_z = -5674kN$ BGT MHW2
$M_x = 53252kNm$ UGT E1 & $M_x = -2490kNm$ UGT MHW2
$M_y = 9268kNm$ UGT MHW1 & $M_y = -6725kNm$ UGT E2

Section 12
$F_z = -11260kN$ UGT MHW3
$M_x = 55538kNm$ UGT E1 & $M_= -5883kNm$ UGT MHW2
$M_y = 887kNm$ UGT MHW1 & $M_y = -7735kNm$ UGT E1

Sum 11+12
$F_z = -13913kN$ UGT E1
$M_x = 111065kNm$ UGT E1 & $M_x = -8347kNm$ UGT MHW2
$M_y = 44040kNm$ UGT MHW3

C.5.4. Wall West

Wall west is divided in section 13 ([-6.0, -9.575, -4.85], [-4.0, -9.575, -4.85]), section 14 ([-4.0, -9.575, -4.85], [2.0, -9.575, -4.85]) and section 15 ([2.0, -9.575, -4.85], [6.0, -9.575, -4.85]). The maximum moment and normal force are given per section with the corresponding load combination.

Section 13
$F_z = -3821kN$ UGT E1 & $F_z = 1791kN$ UGT MHW1
$M_x = -24615kNm$ UGT E1 & $M_x = 1863kNm$ UGT MHW2
$M_y = 1927kNm$ UGT MHW3

Section 14

$F_z = -4548kN$ UGT MHW2
$M_x = -33554kNm$ UGT E1 & $M_x = 1811kNm$ UGT MHW2
$M_y = 2336kNm$ UGT MHW3 & $M_y = -36kNm$ BGT MHW2

Section 15

$F_z = -10094kN$ UGT MHW3
$M_x = -42134kNm$ UGT E1 & $M_x = 4359kNm$ UGT MHW2
$M_y = -5271kNm$ UGT E1 & $M_y = 1202kNm$ UGT MHW1

Sum 13+14+15

$F_z = -13078kN$ UGT E1
$M_x = -103781kNm$ UGT E1 & $M_x = 7346kNm$ UGT MHW2
$M_y = 41271kNm$ UGT MHW3

C.5.5. Floor next to Wall east V1

The floor next to Wall east V1 is divided in section 21 ([-6.65, 7.75, -5.6], [2.0, 7.75, -5.6]) and section 22 ([2.0, 6.0, -5.6], [6.65, 6.0, -5.6]). The maximum moment and normal force are given per section with the corresponding load combination.

Section 21

$F_y = -15210kN$ UGT E2 & $F_y = 796kN$ UGT MHW2
$M_x = 44686kNm$ UGT E2

Section 22

$F_y = -7537kN$ UGT E1 & $F_y = 372kN$ UGT MHW2
$M_x = 19800kNm$ UGT E2 & $M_x = -1982kNm$ UGT MHW2

Sum 21+22

$F_y = -22726kN$ UGT E2 & $F_y = 1168kN$ UGT MHW2
$M_x = 64486kNm$ UGT E2 & $M_x = -112kNm$ UGT MHW2

C.5.6. Floor next to Wall West V1

The floor next to Wall west V1 is divided in section 23 ([-6.65, -7.788, -5.6], [-4.00, -7.788, -5.6]), section 24 ([2.0, -7.788, -5.6], [6.65, -7.788, -5.6]) and section 25 ([-4.0, -8.75, -5.6], [2.00, -8.75, -5.6]). The maximum moment and normal force are given per section with the corresponding load combination.

Section 23

$F_y = -3891kN$ UGT E1 & $F_y = 81kN$ UGT MHW1
$M_x = 18007kNm$ UGT E2 & $M_x = -7681kNm$ UGT MHW1

Section 24

$F_y = -7572kN$ UGT E2 & $F_y = 251kN$ UGT MHW2
$M_x = 26487kNm$ UGT E1

Section 25

$F_y = -9826kN$ UGT E1 & $F_y = 1441kN$ UGT MHW2
$M_x = 31498kNm$ UGT E1

Sum 23+24+25
$F_y = -21276kN$ UGT E2 & $F_y = 1695kN$ UGT MHW2
$M_x = 75989kNm$ UGT E1

C.5.7. Floor Centre Line V1

Section 26
Section 26 ([-6.65, -0.70, -5.6], [6.65, -0.70, -5.6]) $F_y = -21987kN$ UGT E1 & $F_y = 1266kN$ UGT MHW2
$M_x = -10895kNm$ UGT E3

C.5.8. Floor next to Wall East V2
The floor next to Wall east V1 is divided in section 21 and section 22. The maximum moment and normal force are given per section with the corresponding load combination.

Section 21
$F_y = -15212kN$ UGT E2 & $F_y = 796kN$ UGT MHW2
$M_x = 44364kNm$ UGT E2

Section 22
$F_y = -7530kN$ UGT E1 & $F_y = 374kN$ UGT MHW2
$M_x = 19597kNm$ UGT E2 & $M_x = -1397kNm$ UGT MHW2

Sum 21+22
$F_y = -22721kN$ UGT E2 & $F_y = 1170kN$ UGT MHW2
$M_x = 63961kNm$ UGT E2

C.5.9. Floor next to Wall West V2
The floor next to Wall west V1 is divided in section 23, section 24 and section 25. The maximum moment and normal force are given per section with the corresponding load combination.

Section 23
$F_y = -3826kN$ UGT E1 & $F_y = 107kN$ UGT MHW1
$M_x = 19130kNm$ UGT E2 & $M_x = -7243kNm$ UGT MHW1

Section 24
$F_y = -7531kN$ UGT E2 & $F_y = 266kN$ UGT MHW2
$M_x = 27106kNm$ UGT E1

Section 25
$F_y = -10041kN$ UGT E1 & $F_y = 1365kN$ UGT MHW2
$M_x = 30613kNm$ UGT E1

Sum 23+24+25
$F_y = -21386kN$ UGT E2 & $F_y = 1657kN$ UGT MHW2
$M_x = 76844kNm$ UGT E1 & $M_x = -1838kNm$

C.5.10. Floor Centre Line V2
Section 26
$F_y = -21992kN$ UGT E1 & $F_y = 1264kN$ UGT MHW2
$M_x = -9423kNm$ UGT E3

C.6. Displacements
The displacements of the walls are in y-direction at $8.18mNAP$ at the location of the lock gate.

C.6.1. Variant 1

Table C.52: U_y SLS Variant 1

Location	Displacement [mm]	Load combination
max. displacement east	-71.2	E + min. GW + G + T
max. displacement west	62.8	E + min. GW + C
max. displacement total	-70.5 + 62.8 = 133.3	E + min. GW + C
min. displacement east	-19.5	MHW2
min. displacement west	16.6	MHW2
min. displacement total	-19.5 + 16.6 = 36.1	MHW2

C.6.2. Variant 2

Table C.53: U_y SLS Variant 2

Location	Displacement [mm]	Load combination
max. displacement east	-74.8	E + min. GW + G + T
max. displacement west	66.6	E + min. GW + C
max. displacement total	-74.2 + 66.6 = 140.8	E + min. GW + C
min. displacement east	-24.7	MHW2
min. displacement west	21.5	MHW2
min. displacement total	-24.7 + 21.5 = 46.2	MHW2

C.7. MKI
The total MKI of the northern lock head in Empel is $56372€$, see Table C.54

Table C.54: MKI value lock head Empel

Object	MKI value [€]
Reinforcement	11448
Concrete	29406
UWC	14022
GEWI	1496

The MKI values per m^3 for C30/37 CEMIII and FeB 500 are respectively, €20.30, − and €98.31, − (Table C.55 & C.56). Multiplying these values by the amount of the concerned materials, the MKI value of 'Materialen en Processen' is obtained. To get the total MKI value, the MKI 'Categorieopslag' and 'Afvalscenario' have to be added. The MKI 'Afvalscenario' is given by Dubocalc (Table C.57). The MKI 'Categorieopslag' is calculated as follows:

$MKI_{Categorieopslag} = (MKI_{MaterialenenProcessen} + MKI_{Afvalscenario}) * 0.3$

Table C.55: 30/37 CEMIII per m^3

Object	Percentage of total MKI [%]	Amount	MKI value [€]
Concrete C30/37 CEMIII	64.22	2.395 ton	13.04
Gr. mach. hydr.	1.82	0.04 h	0.37
Betonpomp incl. voertuig	0.02	0.00952 h	0.005
Sloophamer hydr. aanb.	5.7	0.04 h	1.16
Verdichten beton (trilnaad)	0.02	0.4 h	0.003
Gr. mach. hydr.	2.73	0.06 h	0.55
Gr. mach. hydr.	18.17	0.4 h	3.69
Transport bulk	7.33	2.395 tonkm	1.49
Total			20.30

Table C.56: FeB 500 per m^3

Object	Percentage of total MKI [%]	Amount	MKI value [€]
FeB 500	70.06	1 ton	68.88
Kraan hydr. tele. band	2.35	0.37	2.31
Gr. mach. hydr.	6.29	0.67 h	6.18
Sloophamer hydr. aanb.	19.72	0.67 h	19.39
Transport staal	1.58	1 tonkm	1.55
Total			98.31

Table C.57: MKI 'Afvalscenario'

Object	MKI value [€]
Floor	
- C30/37	811.65
- FeB 500	-1708.89
Wall	
- C30/37	1146.90
- FeB 500	-1642.52

The MKI for FeB 500 is negative since it can be recycled.

The MKI of the GEWI piles follow from:

$$MKI_{materialenprocessen} + MKI_{categorieopslag} + MKI_{afvalscenario} = 78.14 + 18.47 - 16.59 = 80.02 €/ton$$

Table C.58: MKI materialen en processen GEWI pile

Object	Indicator [€/ton]
Reinforcement	68.88
Hydr. Trilblok	0.03
Transportation steel	1.55
Dragline	1.89
Gr. Mach. Hydr.	5.76
Total	78

C.8. Cost

The total cost of the lock head is $419209€$. The cost take in to account the concrete, reinforcement, UWC floor and GEWI piles.

Table C.59: Cost lock head Empel north

Object	Quantity	Cost per unit [€]	Total [€]
Reinforcement	108 ton	1126	121608
Concrete	1054 m^3	104	109669
Underwater concrete	554 m^3	134	74236
GEWI	32	2584	113696

C.9. Foundation

As was mentioned in the main report, the UWC floor configuration deviates from the common practice. This section will check the current UWC floor configuration and a configuration according to common engineering, based on the Manual Hydraulic Structures (Molenaar and Voorendt, 2016). For this configuration the UWC floor has a thickness of $1.2m$ and the c.t.c distance between the GEWI piles is $2m$. The UWC floor has to be checked on hydraulic bursting of the floor, fracture of the floor and fracture of the join between the floor and the tension piles.

For the first criterion, hydraulic bursting, the weight of the UWC floor needs to be known, the water pressure under the floor and the maximum tension force of the GEWI piles, $F_u = 1786.4kN$ for Empel. According to the calculations both the configurations meet the criterion of hydraulic bursting, see Table C.60.

Table C.60: Hydraulic bursting UWC

	Empel	Common
Upward load $[kN]$	33566	40445
Downward load $[kN]$	50019	78602

The second check is the fracture of the floor. The first step is to calculate the bending moment. The bending moment is calculated in two directions, since the c.t.c. distance differs for the Empel configuration. The bending moment in the UWC floor follows from:

$$M_d = \frac{1}{10} * q * l^2$$

Now the the stress in the concrete can be calculated according to:

$$\sigma = \frac{M_d}{1/6bh^2}$$

The resulting stress has to be smaller than $0.7 * f_b$. The results are shown in Table C.61. Both the configuration suffice in both directions.

Table C.61: Fracture UWC

	Empel	Common
M_d direction 1 $[kNm]$	103	47
M_d direction 1 $[kNm]$	56	47
σ direction 1 $[kN/m^2]$	139	195
σ direction 2 $[kN/m^2]$	76	195
$0.7f_b [kN/m^2]$	980	980

The last step is to check the fracture of the join between the floor and the GEWI piles, see Table C.62. The shear force is calculated according to:

$$T_d = q * c.t.c._1 * c.t.c._2$$

where:

$c.t.c._1$ = the centre to centre distance in direction 1 $[m]$.
$c.t.c._2$ = the centre to centre distance in direction 2 $[m]$.

The next step is to calculate the resulting stress according to:

$$\tau_d = \frac{T_d}{4 * \theta_{GEWI} * h}$$

where:

θ_{GEWI} = the diameter of the GEWI pile $[m]$

This value needs to be lower than $0.5 * f_b$.

Table C.62: Fracture join

	Empel	Common
T_d $[kN]$	757	468
τ $[kN/m^2]$	199	123
$0.5 f_b [kN/m^2]$	700	700

C.10. Horizontal Bearing Capacity

In the main report it was mentioned that the 'Hanboek voor het ontwerpen van Schutsluizen' (*Ontwerp van Schutsluizen*, 2000) states that the lock head has to provide enough horizontal resistance on its own to prevent the lock head from sliding. The calculations done for the lock head in Empel also take into account part of the lock chamber. If the rules according to the 'Hanboek voor het ontwerpen van Schutsluizen' are applied to the lock head in Empel, the lock head does not meet the horizontal bearing capacity, see Tables C.63 & C.64. For the friction between the walls and the soils the results from Empel are used. The friction between the floor and the soil is calculated according to Appendix B. The horizontal and vertical (ground)water load follow from the calculations done for Empel. The water level MHW is $7.83mNAP$. The water level in the lock is $2mNAP$. The ground water level is $6.68mNAP$.
A measure to solve this problem is to increase the length of the lock head. The lock head configuration of the lock in Empel deviates from the configuration prescribed by the 'Hanboek voor het ontwerpen van Schutsluizen' (*Ontwerp van Schutsluizen*, 2000). When this configuration is applied the length of the lock head increases. An increase in length is in favour of the horizontal bearing capacity. For this reason the horizontal bearing capacity has been checked for and adjusted lock head according to the design rules from the 'Hanboek voor het ontwerpen van Schutsluizen'. The results show that this configuration does meet the horizontal bearing capacity, see Tables C.65 & C.66.

Table C.63: Vertical loads original lock head

	F_v [kN]
Walls	21550
Floor	17300
UWC floor	16702
Water pressure	-50515
Weight water	18658
Weight sand	15511
Total	33651

Table C.64: Horizontal loads original lock head

	F_h [kN]
Friction floor and soil	6730
Friction walls and soil	7567
Water pressure	-16330
Total	-2031

Table C.65: Vertical loads adjusted lock head

	F_v [kN]
Walls	31878.1125
Floor	25415
UWC floor	24551
Water pressure	-74252
Weight water	33853
Weight sand	22800
Total	52675

Table C.66: Horizontal loads adjusted lock head

	F_h [kN]
Friction floor and soil	10535
Friction walls and soil	11124
Water pressure	-16330
Total	5329

D

Alternatives Lock Head Design

D.1. Innovations in Lock Design

Over the years different navigation locks have been designed and constructed, each with their own innovative characteristics. This section will give some important innovations with a corresponding example and how it contributes to the principles of sustainability and durability. The examples are from the PIANC: Innovation in Navigation Lock Design - 2009 (PIANC, 2009).

D.1.1. GFRP Gate: Lock Golbey

The navigation lock located in Golbey, France was equipped with a new type of gates. In 1997 the steel mitre gates were replaced with mitre gates made out of glass fibre reinforced polymers (GFRP). The door is connected with the wall by means of stainless steel hinges and collars. The aim of the new gates was to reduce the maintenance up to 70%. The new materials do not corrode and have good ageing properties. The gates are light, thus reducing friction and handling time.

Figure D.1: GFRP gate lock Golbey PIANC (2009)

D.1.2. Water Retention in Both Directions: Lock Limerick

The lock in Limerick, Ireland was in need of a new lock gate. Due to environmental changes the lock needed to retain a reverse water difference of $1.7m$ from the tidal river Shannon. The originally proposed solution was to install two sets of gates at the end of the river Shannon. However this solution needed a lot of modifications to accommodate the gate. Instead one mitre gate was installed, able to resist water in both direction. The gate is equipped with load bearing hinge points and an independent sealing system. Hydraulic cylinders are used to open and closed the gate. When using this system, less maintenance is needed in the long run. Besides, less material is needed.
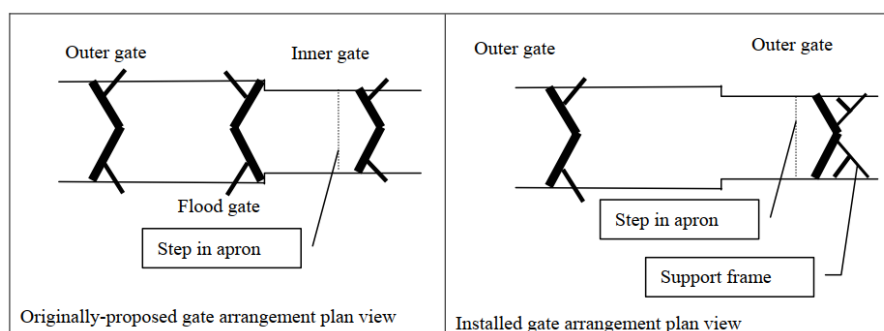
Figure D.2: Lock lay out water retention in both directions PIANC (2009)

D.1.3. Water Saving Basin: Lock Panama Canal

To accommodate for the never ending growing traffic demand, Panama has expanded the capacity of the canal by building a third set of locks. To reduce the water usage of the lock, water saving basins have been constructed. By using the water saving basins the water in Gatun Lake stays fresh water. This has a positive effect on the ecosystem and the consumption of water by humans.

D.1.4. Protecting Gates: Lock Bollène and Châteauneuf

The locks Bollène and Châteauneuf are located in the river Rhône in France. Both these locks only have one gate at the downstream end, which makes them hard to repair. Both the locks are equipped with an intermediate gate, that allow vessels up to $90m$. In case of an incident at the downstream end, the intermediate doors would be closed for maintenance operations. The intermediate gates however are out of date, because the length of the vessel increases. A solution was needed to solve the problem. Three different options were being considered. The first option was to double the lock. The second option was to double the downstream gates. The third option was to protect the existing gates. The chosen option was to install protection measures. The measures taken are: installing an energy absorption system in front of the gate to prevent collision with vessels going upstream, installing safety barriers in front of downstream gate to prevent collision with vessels going downstream and installing a boat detection system to prevent to lock from closing before the vessels have left or entered the lock.

D.1.5. Reinforced Concrete Slab: Lock Dörverden

In 2008 two locks in the Weser river were replaced by one lock to accommodate for the increase in size of the vessels. The innovative design of the lock is the way the lock chamber is constructed. A secant pile wall with a diameter of $1.20m$ is constructed. The secant pile wall consists of primary piles and secondary piles. First the primary piles are constructed. Hereafter the secondary piles are constructed in between the primary piles. The secondary piles are reinforced. The secant pile wall has a load bearing function and is part of the final structure. The secondary piles are anchored to deal with the soil and groundwater pressure. To make the wall watertight and more durable a reinforced concrete slab of $0.40m$ is installed in front of the secant wall. By using a secant pile wall the amount of steel used is reduced. This method however, was only used for the lock chamber. The secant pile wall for the construction of the lock head was only temporary.

D.1.6. Inhomogeneous Cross-section: Lock Uelzen II

The lock Uelzen II was finished in 2006 to increase the capacity of the Elbe-Seiten canal. Besides water saving basins which fill up 70% of the lock and a powerless cable restraining device to protect the lower head against ship impact, the concrete structure of the lock is composed of a slow aging concrete core surrounded by high-class concrete. The cross section is a monolithic structure with integrated water saving basins. To minimise the heat development and the resulting stresses, CEM III is used in the core of the cross section. CEM III has slow heat development. The boundary section with a width of $1m$ are composed of CEM II. CEM II meets the requirements for freezing and thawing, and the mechanical loads.
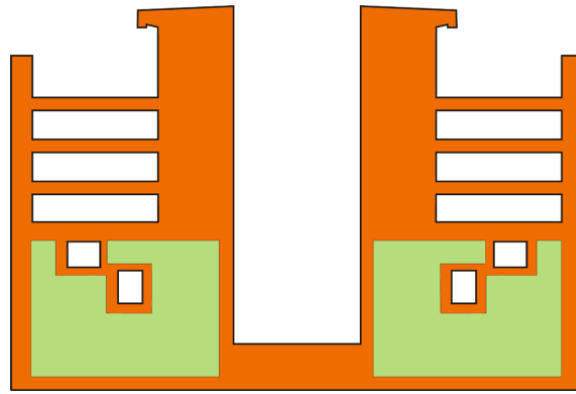
Figure D.3: Cross section with different concrete classes PIANC (2009)

D.2. Alternatives

The alternatives are implemented to Empel. Cross section calculations are performed at the location of the floor under the eastern wall, see Figure D.4. The cross section has a width of $1m$ and a height of $2m$. The chosen cross section is subjected to $M_d = 4500kNm$, $M_{rep} = 3900kNm$ and $V_d = 1563kN$. The reinforcement configuration at the tension side of the cross section consists out of two rows. Row 1 consists out of $\phi35.3 - 200$ and row 2 out of $\phi25 - 200$. The shear reinforcement is $\phi16 - 400$. The reinforcement is made of $B500$. The maximum allowable crack width in the cross section is $0.40mm$.
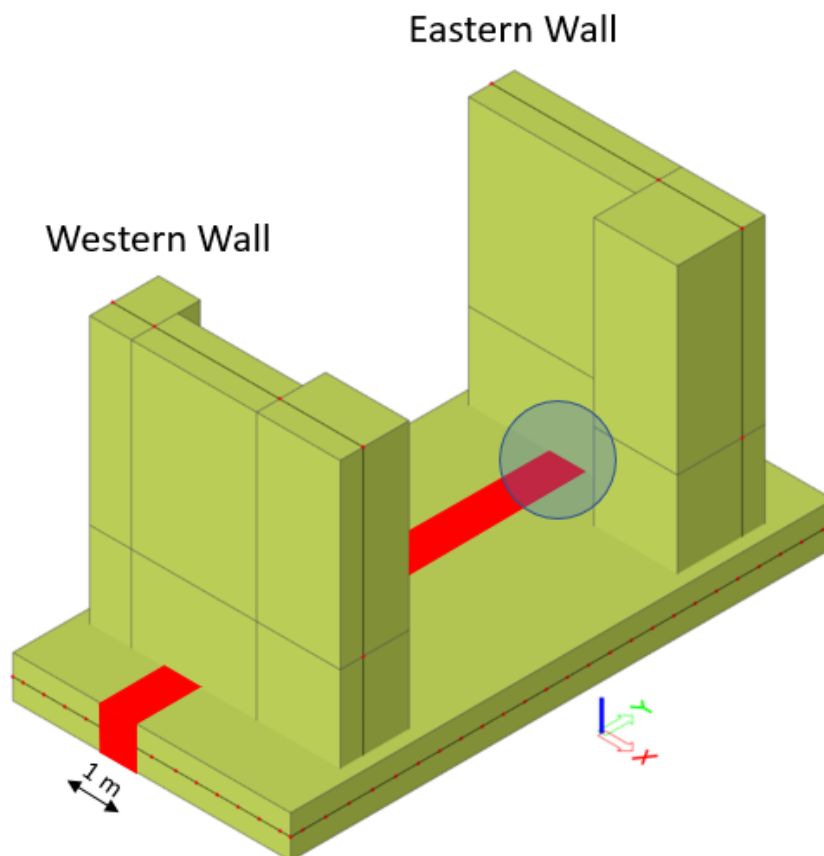
Figure D.4: Location of the cross section calculations

D.2.1. Inhomogeneous Cross Section

Setup

The objective is to check whether it is possible to design a lock head constructed out of different concrete classes. For this reason calculations have been performed for a cross section exposed to pure bending. The situation is similar to the floor of the lock head.

The dimensions of the concrete slab are $h = 2000mm$ & $b = 1000mm$, same as for the floor of the lock head. The cross section is composed out of two different concrete classes, being $C30/37$ and $C20/25$. The concrete class $C30/37$ is located at the outside of the cross section and has a height of $l_2 = 500mm$. The core of the cross section is made out of $C20/25$ and has a height of $l_1 = 1000mm$. Since the concrete slab is exposed to pure bending, only reinforcement is placed at the bottom of the slab. The original reinforcement configuration of the concrete floor for the lock head is $\theta 35.3 - 200$ and $\theta 20 - 200$. The reinforcement configuration has been changed to an equivalent $\theta 43 - 200$ for reasons of simplicity. The reinforcement is located at a distance of $d_s = 1914mm$. The reinforcement is made of $B500$.
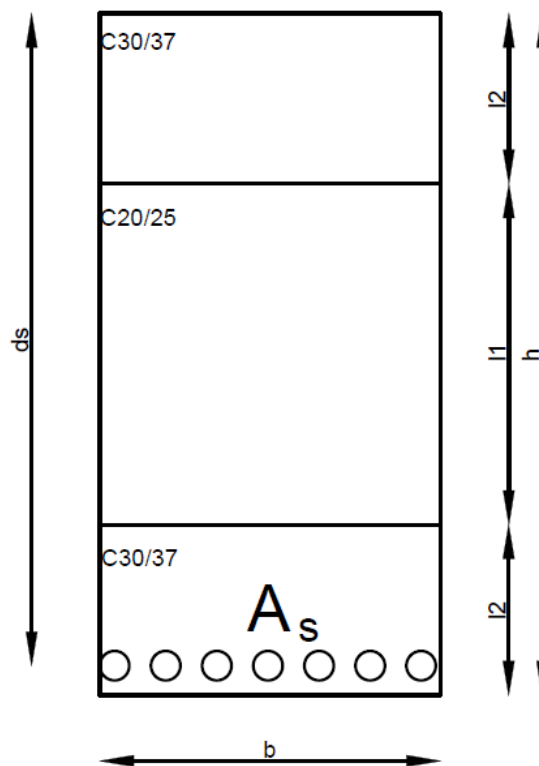
Figure D.5: Cross section

Moment Resistance

Rupture Moment

In a reinforced concrete slab the reinforcement takes on the tension and the concrete the compression. Before the reinforcement is activated the concrete has to crack. This happens when the stresses exceed f_{ctm}. The strain at this location is:

$$\epsilon_{ct} = \frac{f_{ctm}}{E_c} \ [-]$$

The stress strain curve for concrete can be assumed to be linear up to ϵ_c. The elasticity modulus can therefor be calculated according to Hooke's law:

$E_c = \frac{f_{cd}}{\epsilon_c}$ $[N/mm^2]$

The next step is to calculate the height of the uncracked area, $x_{uncracked}$:

$x_{uncracked} = \frac{A_c x_c + \alpha_e A_s x_s}{A_c + A_s}$ $[mm]$

Assumed is that the area of the reinforcement is α_e times bigger:

$\alpha_e = \frac{E_s}{E_c}$.

With $x_{uncracked}$ and ϵ_{ct} the strain distribution can be calculated from which follows the stress diagram (Table D.1).

$\sigma = E_c \epsilon$ $[N/mm^2]$

Table D.1: Strain and Stress distribution Rupture moment

	z $[mm]$	E $[N/mm^2]$	$\epsilon * 10^{-3}$	σ $[N/mm^2]$
Material 2	1000	11429	0.28	3.24
Material 2	914	11429	0.26	2.97
Material 2	500	11429	0.156	1.70
Material 1	500	7600	0.15	1.13
Material 1	0	7600	0.01	0.11
Material 1	-500	7600	-0.12	-0.91
Material 2	-500	11429	-0.12	-1.37
Material 2	-914	11429	-0.23	-2.64
Material 2	-1000	11429	-0.25	-2.90
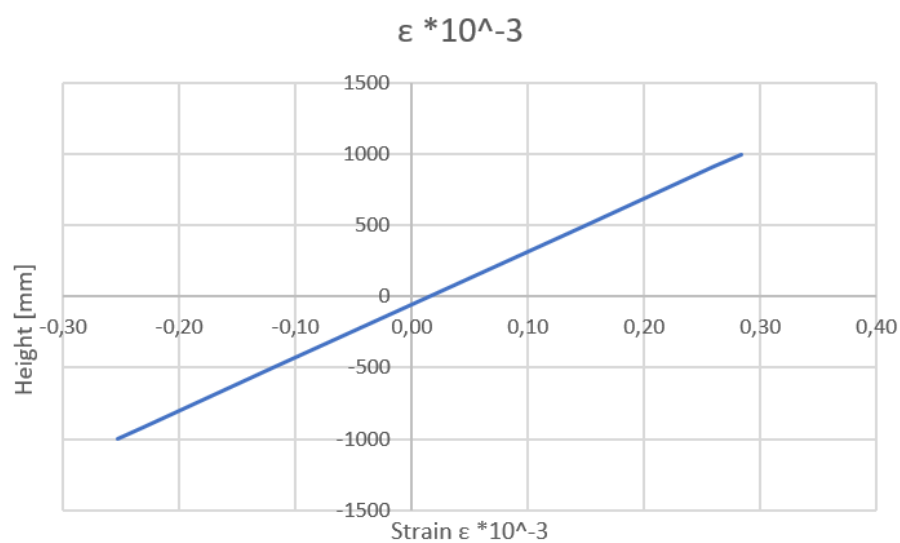
Figure D.6: Strain distribution Rupture moment
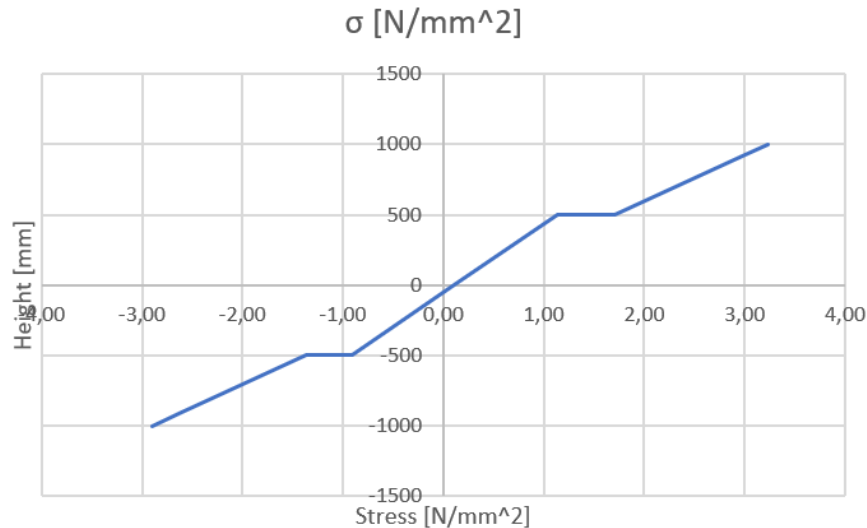
Figure D.7: Stress distribution Rupture moment

The rupture moment is determined by taking the moment around the bottom of the concrete height x. $M_r = A_S * f_y * (h - x - a) + F_{concrete} * z = 1598kNm$.

Yielding Moment
If the load keeps increasing the reinforcement starts to yield. The strain in the reinforcement follows from:

$$\epsilon_s = \frac{f_{yd}}{E_s} = \frac{200000}{435} = 2.175‰$$

To calculate the compression height x, N_c has to be in equilibrium with N_s. The first estimate of the compression height is $x > l_2$. This means that $C20/25$ has to be included in the calculations of N_c. For this reason N_c will be divided in $N_c = N_1 + N_2 + N_3$, see Figure D.8. N_1 and N_2 act over a length equal to l_2. N_3 acts over a length of $x - l_2$, where x is the compression height.

$$N_1 = l_2 * \epsilon_{500} * E_2$$

$$N_2 = \frac{1}{2} * l_2 * E_2 * (\epsilon_{1000} - \epsilon_{500}) \text{ and}$$

$$N_3 = \frac{1}{2} * (x - l_2) * E_1 * \epsilon_{500}$$

where:

E_1 is the modulus of elasticity of $C20/25$ $[N/mm^2]$
E_2 is the modulus of elasticity of $C30/37$ $[N/mm^2]$
ϵ_{1000} is the strain at $z = 1000$
ϵ_{500} is the strain at $z = 500$.
$\epsilon_{1000} = \frac{x}{d_s - x} * \epsilon_s$
$\epsilon_{500} = \frac{x - l_2}{d_s - x} * \epsilon_s$.

By solving the equilibrium, a compression height of $x = 586mm$ is found. Besides it has to be checked if $\epsilon_c \leq 1.75‰$. In this case $\epsilon_c = 1.15‰$, so the calculations can be continued.
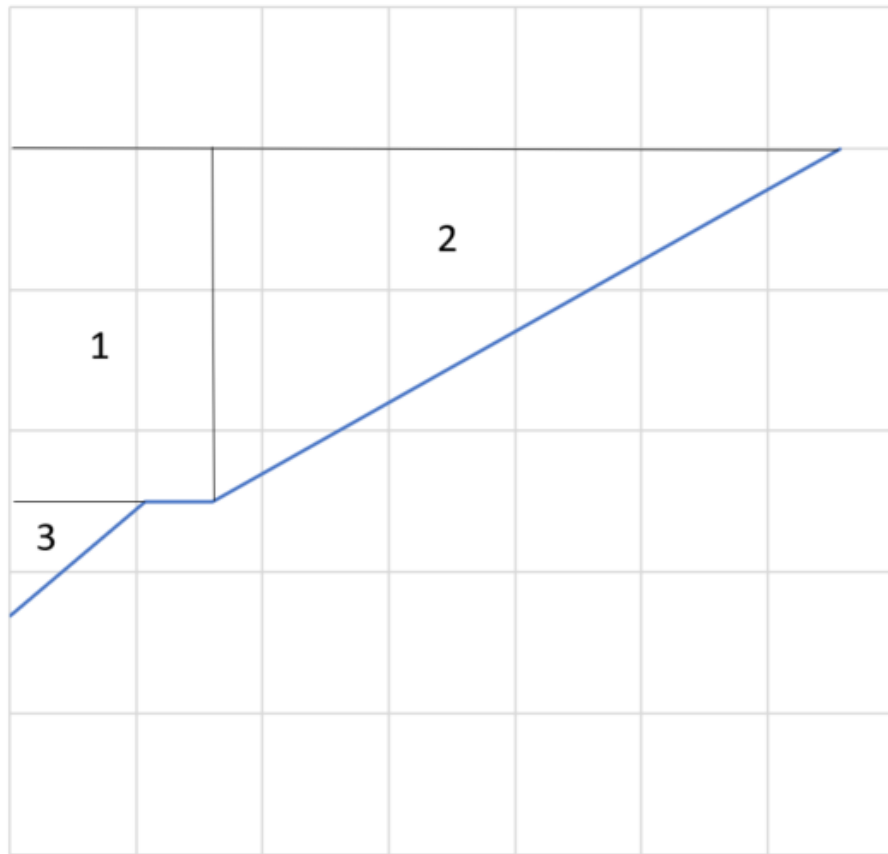
Figure D.8: Calculating N_c

Table D.2: Strain and Stress distribution Yielding moment

	$z\ [mm]$	$E\ [N/mm^2]$	$\epsilon * 10^{-3}$	$\sigma\ [N/mm^2]$
Material 2	1000	11429	0.96	10.98
Material 2	914	11429	0.82	9.37
Material 2	500	11429	0.14	1.62
Material 1	500	7600	0.14	1.08
Material 1	0	7600	-0.68	-5.15
Material 1	-500	7600	-1.50	-11.38
Material 2	-500	11429	-1.50	-17.11
Material 2	-914	11429	-2.18	-24.86
Material 2	-1000	11429	-2.32	-26.47
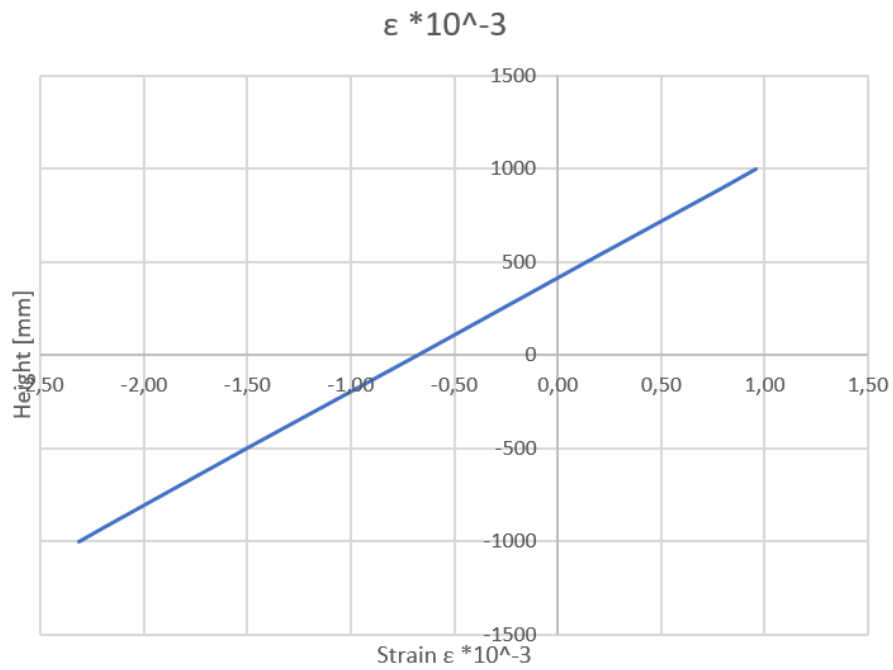
Figure D.9: Strain distribution Yielding moment
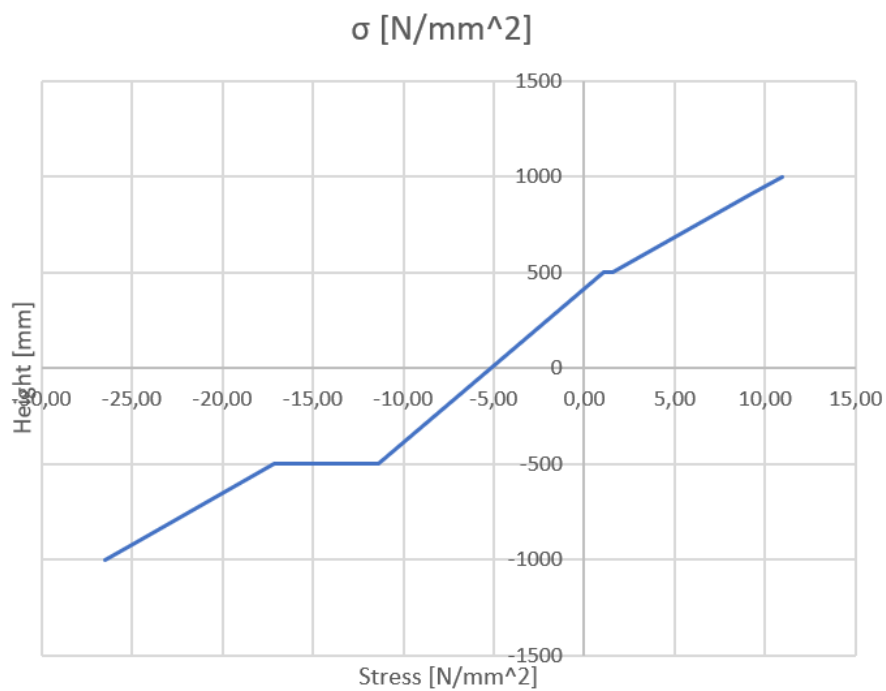
Figure D.10: Stress distribution Yielding moment

The yielding moment is calculated around the N_c, resulting in a yielding moment of $My = 4248kNm$.

Stuik Moment
At this moment the outer strain of the concrete compression zone $\epsilon_c = 1.75\%_0$. The stress is therefore f_{cd}. The strain in the reinforcement is $\epsilon_s > \frac{f_{yd}}{E_s}$. Assumed is that the compression height $x \leq l_2$. The compression height can be calculated from force equilibrium:

$N_c = N_s \Rightarrow \frac{1}{2} bx f_{cd} = A_s f_{yd}.$

The resulting compression height $x = 320mm$. The assumption made is satisfied. The resulting moment $M_{c,pl} = 5777 kNm$.

Ultimate Moment
At this moment the outer strain of the concrete compression zone $\epsilon_c = 3.5\%$. The stress is therefore f_{cd}. The strain in the reinforcement is $\epsilon_s > \frac{f_{yd}}{E_s}$. Assumed is that the compression height $x \leq l_2$. The compression height can be calculated from force equilibrium:

$N_c = N_s \Rightarrow \alpha bx f_{cd} = A_s f_{yd}.$

The resulting compression height $x = 213mm$. The assumption made is satisfied. The resulting moment $M_{Rd} = 5852 kNm$.

Moment-Curvature Diagram
From the four different moments calculated above the moment-curvature diagram can be constructed. The moments have already been calculated. Only the curvatures are needed. The curvatures easily follow from the strain distribution:

$\kappa = \frac{\epsilon_c + \epsilon_s}{d} \ [m^{-1}],$

where d is the distance between the outer concrete fibre in the compression zone to the reinforcement.

Table D.3: Moment-Curvature diagram

	$M \ [kNm]$	$\kappa * 10^{-3} \ [m^{-1}]$
Start	0	0
Rupture moment M_r	1435	0.27
Yielding moment M_y	5665	1.64
Stuik moment $M_{c,pl}$	5777	5.48
Ultimate moment M_{Rd}	5852	16.43
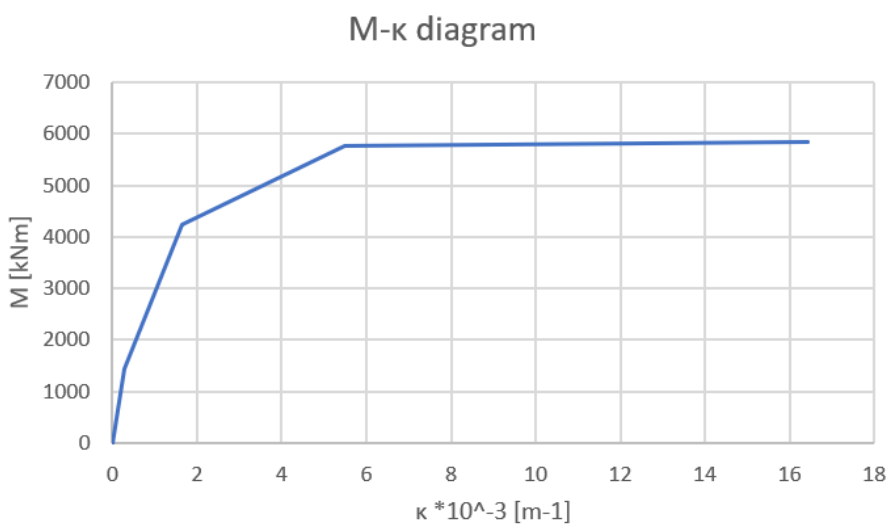
M-κ diagram

Figure D.11: Moment Curvature diagram

Stability

To get an indication of the displacements, the concrete class in the SCIA model has been changed to $C20/25$. The E-modulus used follows from NEN 6720 table 15, see Figure D.12.

Tabel 15 – Fictieve elasticiteitsmodulus E_f

f'_{ck} N/mm²	buiging en normaalkracht symmetrisch gewapende rechthoekige doorsnede		buiging zonder normaalkracht; excentrisch gewapende rechthoekige doorsnede
	$\alpha_n \leq 0,5$	$0,5 < \alpha_n \leq 0,9$	
15	$1300 + 4100\,\overline{\omega}_{ot} + (9000 - 1300\,\overline{\omega}_{ot})\alpha_n \nleq 2900$	$(8700 + 5175\,\overline{\omega}_{ot})(1 - 2/3\,\alpha_n)$	$2200 + 4900\,\overline{\omega}_o \nleq 2900$
25	$1600 + 4200\,\overline{\omega}_{ot} + (14000 - 1600\,\overline{\omega}_{ot})\alpha_n \nleq 3600$	$(12900 + 5100\,\overline{\omega}_{ot})(1 - 2/3\,\alpha_n)$	$2500 + 5500\,\overline{\omega}_o \nleq 3600$
35	$1900 + 4300\,\overline{\omega}_{ot} + (19000 - 1900\,\overline{\omega}_{ot})\alpha_n \nleq 4300$	$(17100 + 5025\,\overline{\omega}_{ot})(1 - 2/3\,\alpha_n)$	$2800 + 6100\,\overline{\omega}_o \nleq 4300$
45	$2200 + 4400\,\overline{\omega}_{ot} + (24000 - 2200\,\overline{\omega}_{ot})\alpha_n \nleq 5000$	$(21300 + 4950\,\overline{\omega}_{ot})(1 - 2/3\,\alpha_n)$	$3100 + 6700\,\overline{\omega}_o \nleq 5000$
55	$2500 + 4500\,\overline{\omega}_{ot} + (29000 - 2500\,\overline{\omega}_{ot})\alpha_n \nleq 5700$	$(25500 + 4875\,\overline{\omega}_{ot})(1 - 2/3\,\alpha_n)$	$3400 + 7300\,\overline{\omega}_o \nleq 5700$
65	$2800 + 4600\,\overline{\omega}_{ot} + (34000 - 2800\,\overline{\omega}_{ot})\alpha_n \nleq 6400$	$(29700 + 4800\,\overline{\omega}_{ot})(1 - 2/3\,\alpha_n)$	$3700 + 7900\,\overline{\omega}_o \nleq 6400$

waarin:

$$\overline{\omega}_{ot} = \frac{A_s + A'_s}{A_b}\,100 \qquad\qquad \alpha_n = \frac{N'_d}{A_b f_b + (A_s + A'_s)\,f_s}$$

waarin:

$$\overline{\omega}_o = \frac{A_s}{A_b}\,100$$

Figure D.12: Table 15 NEN 6720 fictitious E-modulus

Cost

The cost of $C30/37$ is $104.5€/m^3$. The cost of $C20/25$ is $98.55€/m^3$. The cost for the original floor is:

$$691.6 * 104.5 = 72272.2€$$

The cost for the new floor is:

$$345.8 * 104.5 + 345.8 * 98.55 = 70214.69€.$$

This means an decrease in cost of $154.7€$ per meter.

MKI

The total volume of $C20/25$ in the floor is:

$$l * b * l_1 = 13.3 * 26 * 1 = 345.8m^3$$

The Total volume of $C30/37$ is:

$$l * 2 * l_2 = 13.3 * 26 * 2 * 0.5 = 345.8m^3$$

The MKI value of $C20/25$ is $27.80€/m^3$ and $27.92€/m^3$ of $C30/37$. The MKI value of the new floor becomes:

$$345.8 * 27.80 + 345.8 * 27.92 = 19268€$$

The MKI value of the old floor was $191.6 * 27.92 = 19309€$. The decrease in MKI is $3.12€$ per meter. The weighing factor becomes:

$$MKI_{new}/Cost_{new} = 19309/72272.2 = 0.27$$

D.2.2. Prestressing

Setup

To find out if prestressing is a viable option, the moment resistance of a concrete prestressed slab will be checked. The concrete class is $C30/37$ and the dimensions are $h = 2m$ and $b = 1m$.

The original reinforcement configuration exists out of two rows of reinforcement bars on top of each other. For reasons of simplicity the reinforcement has been changed to an equivalent single row with a diameter of $\phi = 43 - 200$. The distance from the top fibre to the centre of the reinforcement is $d_s = 1914mm$. The reinforcing steel is made out of $B500$.

Assumed is a straight prestressing cable of Y1860S7: $A_p = 2000mm^2$, $E_p = 195 * 10^3 N/mm^2$, $\sigma_{p,\infty} = 1080 N/mm^2$, $\sigma_{pm,\infty} = 1080 * 0.98 = 1058 N/mm^2$ and $f_{pd} = 1522 N/mm^2$. The distance from the top fibre to the centre of the tendon is $d_p = 1000mm$. Figure D.13 gives an overview of the cross section.
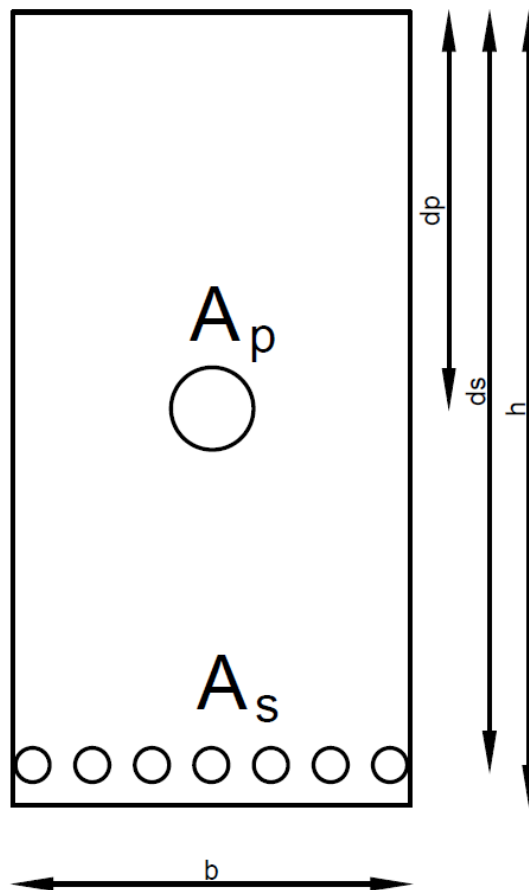
Figure D.13: Cross section

Moment Resistance

The bending moment resistance M_{Rd} has been calculated according to the equilibrium method, see Figure D.14. A straight tendon profile is chosen for preliminary calculations. A straight tendon profile applied in the middle of the cross section does not cause an external moment.
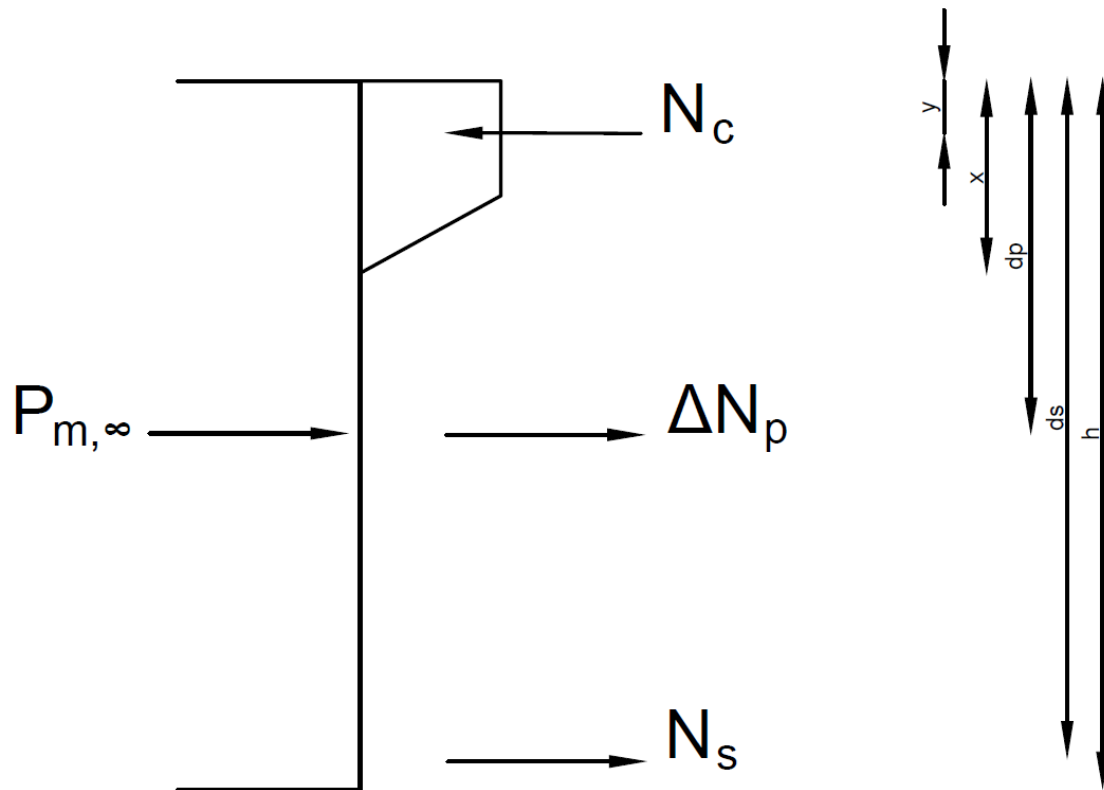
Figure D.14: Equilibrium method

Step 1: Estimation of the Compression Height
The first step is to estimate the compression height x. Assumed is that the concrete has cracked and the reinforcement is yielding. Based on horizontal equilibrium the compression height x can be calculated.

$$N_c = N_s + \Delta N_p + P_{m,\infty}$$

$$\alpha b x f_{cd} = A_s * f_{yd} + A_p(f_{pd} - \sigma_{p,\infty}) + A_p \sigma_{p,\infty},$$

with $\alpha = 0.75$

From this calculation a compression height of $x = 416mm$ follows.

Step 2: Rotational Capacity
The next step is to check the rotational capacity according to the following formula:

$$\delta \geq \frac{f}{500+f} + \frac{x_u}{d},$$

where:

$$f = \frac{(\frac{f_{pk}}{\gamma_s} - \sigma_{pm,\infty})A_p + f_{yd}A_s}{A_p + A_s}.$$

Rewriting the formula results in:

$\frac{x_u}{d} \leq 1 - \frac{f}{500+f}$ [−]

The compression height has to be $x \leq 979mm$, this condition is met.

Step 3: Strain in Reinforcement and Prestressing Steel
The third step is to calculate the strains in the reinforcement and prestressing steel.
The strain in the reinforcement is:

$\epsilon_s = (\frac{d_s}{x} - 1)\epsilon_{cu} = 10.3 * 10^{-3}$.

The increase in strain for the prestressing is:

$\Delta\epsilon_p = (\frac{d_p}{x} - 1)\epsilon_{cu} = 4.9 * 10^{-3}$.

The total strain in the prestressing steel becomes:

$\epsilon_p = \Delta\epsilon_p + \epsilon_{pw} = 0.0049 + \frac{1058}{195000} = 10.3 * 10^-3$.
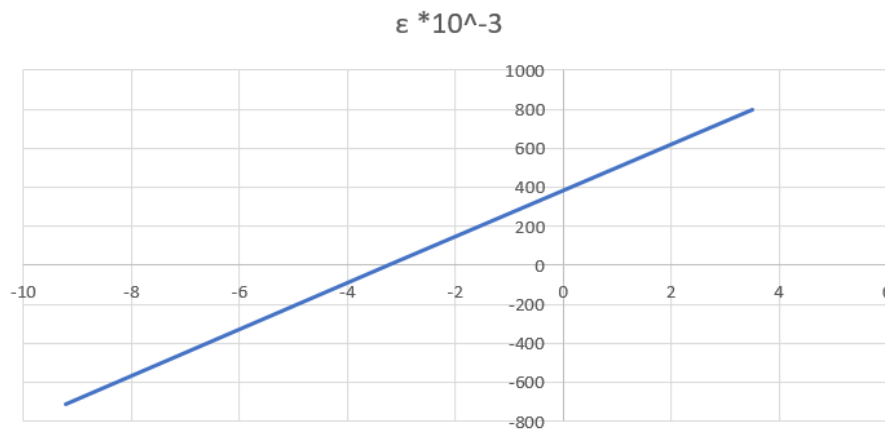
Figure D.15: Strain distribution

Step 4: Forces
From the calculated strains, the forces can be calculated. The force in the reinforcement is:

$N_s = A_s f_{yd} = 3195kN$.

f_{yd} can be used since the strain in the reinforcement has exceeded the value of:

$\frac{f_{yd}}{E_s} = 2.175 * 10^{-3}$.

The increase in prestressing force is:

$\Delta N_p = A_p(\sigma_{pu} - \sigma_{p,\infty}) = 959kN$,

where:

$\sigma_{pu} = \frac{\frac{f_{pk}}{\gamma_s} - f_{pd}}{\epsilon_{uk} - \frac{f_{pd}}{E_p}} * (\epsilon_p - \frac{f_{pd}}{E_p}) + f_{pd} = 1538N/mm^2$
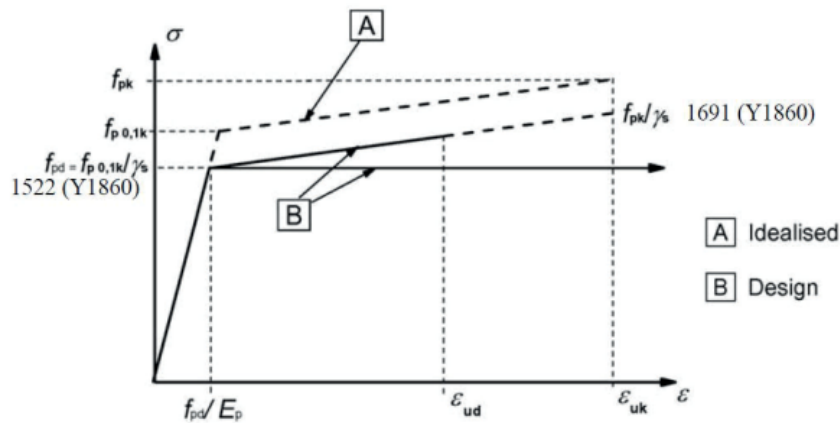
Figure D.16: Stress strain relationship prestressing steel in ULS (Walraven and Braam, 2018)

Step 5: Checking the Compression Height x
It has to be checked if the calculated compression height x is right. There are three different possibilities:

- $|N| < |N_c - P_{m,\infty}|$, the compression height x is too large.

- $|N| = |N_c - P_{m,\infty}|$, the compression height x is correct.

- $|N| > |N_c - P_{m,\infty}|$, the compression height x is too small.

In this case $N = 4154kN$ and $N_c - P_{m,\infty} = 4123kN$, so x is assumed too small. The Steps 1 to 5 have to be repeated with a newly assumed compression height x. The same formula as in step 1 is used, only f_{pd} has been changed to the calculated σ_{pu} in step 4. After two iterations a compression height of $x = 418mm$ is found.

Table D.4: Determining the compression height x

	Start	Iteration 1	Iteration 2
x [mm]	416	418	418
$\epsilon_s * 10^{-3}$	12.6	12.5	12.5
$\Delta\epsilon_p * 10^{-3}$	4.9	4.9	4.9
$\epsilon_p * 10^{-3}$	10.3	10.3	10.3
σ_{pu} [N/mm²]	1538	1537	1537
N_s [kN]	3195	3195	3195
ΔN_p [kN]	959	959	959
N_c [kN]	6239	6270	6270
$P_{m,\infty}$ [kN]	2116	2116	2116
N [kN]	4154	4154	4154
$N_c - P_{m,\infty}$ [kN]	4123	4154	4154

Step 6: Moment Resistance
The moment is calculated around the point where N_c acts on the cross section.

$$M_{Rd} = A_s \sigma su(d_s - y) + A_p(\sigma_{pu} - \sigma p, \infty)(d_p - y) + P_{m,\infty}(\frac{h}{2} - y)$$

where $y = \beta x$.

The resulting bending moment is $M_{Rd} = 7146kNm$.

Shear Force Resistance

To check whether shear force reinforcement is needed the following formula has been used:

$$V_{Rd,c} = [C_{Rd,c} k (100 \rho_l f_{ck})^{1/3} + k_1 \sigma_{cp}] b_w d] = 945 kN \leq 1563 kN$$

This means that shear reinforcement is needed.

Crack Width

The mean concrete compressive stress σ_{cpm} in the cross section due to the prestressing is:

$$\sigma_{cpm} = P_{m\infty}/A_c = 1.32 N/mm^2$$

The cracking moment is:

$$M_c r = W_b (\sigma_{cpm} + f_{ctm}) = 1800 * 10^6 kNm$$

The next step is to calculate the steel stress σ_s. Therefore the internal equilibrium and moment equilibrium are considered:

$$P_{m\infty} + A_p \Delta \sigma_p + A_s \sigma_s - N_c = 0$$

$$P_{m,\infty} + A_p \xi_1 \frac{d-x}{x} \epsilon_c E_p + A_s \frac{d-x}{x} \epsilon_c E_s - \frac{1}{2} \frac{\epsilon_c}{1.75*10^{-3}} f_{cd} b_f x = 0$$

where:

$$\xi_1 = \sqrt{\frac{\tau_{bmp}}{\tau_{bms}} \frac{\Theta_s}{\Theta_p}} = 0.55$$
$$\Theta_p = 1.6 \sqrt{A_p} = 72mm$$

$$M_{max} = N_c e_c + A_s \sigma_s e_s$$

where:

$$e_c = \frac{h}{2} - \frac{x}{3} \; [mm]$$
$$e_s = d_s - \frac{h}{2} \; [mm]$$

By solving the two equilibrium above for $M_m ax = M_{rep}$, ϵ_c and x can be found;

$$\epsilon_c = 1.1 * 10^{-3}$$
$$x = 668mm$$

The steel strain is:

$$\epsilon_s = \frac{d_s - x}{x} \epsilon_c * E_s = 1.40 * 10^{-3}.$$

The same calculation can be performed for a bending moment of $M_{cr} = 1801.6 kNm$.

The crack width follows from:

$$w_{max} = \frac{1}{2} \frac{f_{ctm}}{\tau_{bm}} \frac{\Theta}{\rho_{p,eff}} \frac{1}{E_s} (\sigma_s - \alpha \sigma_{sr}) = 0.24mm$$

where:

$$\alpha = 0.5$$
$$\tau_{bm} = 2 f_{ctm}$$

Cost

The cost calculations are based on concrete cost, prestressing cost and reinforcement cost. The values used, already take into account labour cost. The concrete cost are $104.05€/m^3$. The prestressing cost are approximately three times more expensive than the reinforcement cost. This results in a value of $3378€/ton$.
The reduction in concrete cost is:

$$13.3 * (2 - 1.6) * 26 * 142 = 14392€$$

By adding prestressing the cost increase with:

$$b * l * (h_{old} - h_{new}) * \rho_p * \gamma_s * 3378 = 18339€$$

with:

$$\rho_p = A_p/h_{new} = 0.00154.$$

The total increase in cost due to prestressing is $298€$ per meter.

MKI

The total floor is made out of concrete $C30/37$ $CEMIII$. The MKI value of this type of concrete is $27.92€/m^3$. During he calculations only the floor has been taken into account. The height of the concrete floor is reduced from $2m$ to $1.6m$. The gain in MKI only based on concrete use is:

$$13.3 * 26 * (2 - 1.6) * 27.92 = 3861.90€$$

The MKI of prestressing is $115.14€/ton$. In total $5.4ton$ prestressing steel is used. The amount of prestressing per meter is $A_p = 2000mm^2$. The prestressing ratio per meter is:

$$\rho_p = \frac{A_p}{A_c} = 0.14\%$$

The total amount of prestressing steel used for the floor is:

$$\rho_p * h * l * b = 0.14\% * 1.4 * 13.3 * 26 = 0.69m^3$$

The total decrease in MKI value for the floor is $(625 - 3861)/13.3 = -243€$ per meter.
The weighing factor is:

$$20391.6/173171.8 = 0.12$$

D.2.3. Hollow Sections

The proposed alternation is a cross section made out of I-sections, see Figure D.17.
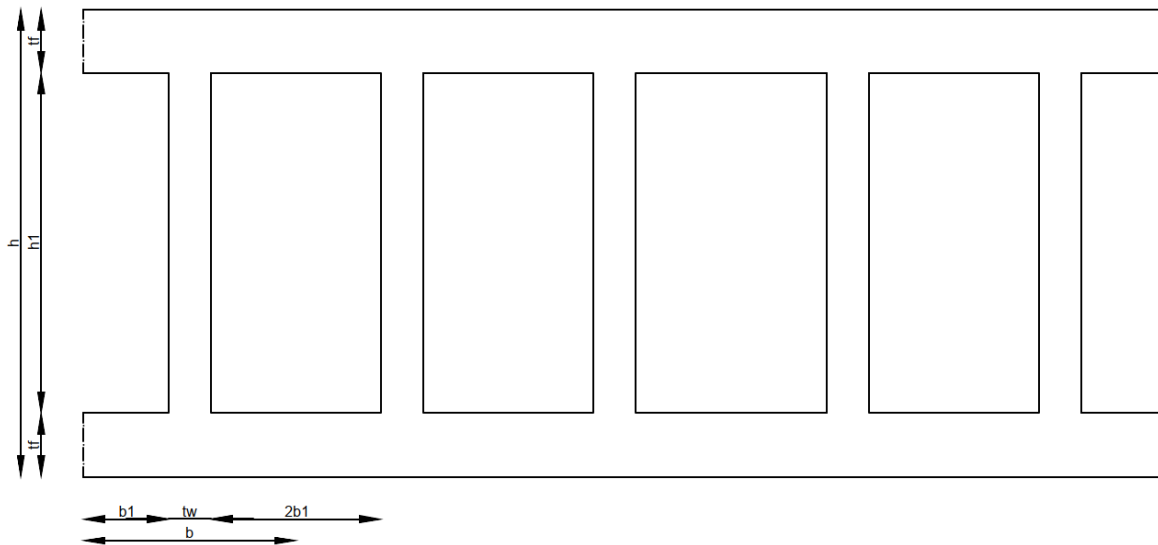
Figure D.17: Cross section wall with hollow sections

Moment Resistance
The moment resistance has been calculated for section 14. Section 14 is situated at the western wall and has a width of $b = 6m$ and a height of $h = 2.2m$ The forces acting on this section are $M_d = 33554kNm$ and $N_d = 1125kN$ (compression). The forces are divided by $6m$ to get the forces per meter, $M_{rep} = \frac{33554}{6} = 5592kNm$ and $N_{rep} = \frac{1125}{6} = 187.5$. Two rows of reinforcement are placed at the tension side of the cross section. Row 1 is $\phi 35.3 - 200$ and row 2 is $28.3 - 200$. As in previous calculations, the reinforcement is combined to one representative $\phi 45 - 200$. The reinforcement at the compression side of the wall is $25 - 200$.
The distance from the top of the wall to the center of the reinforcement is $d_s = 2110mm$. The distance from the top of the cross section to the center of the reinforcement at the compression side is $a = 62.5mm$. Figure D.18 gives an overview of the situation.
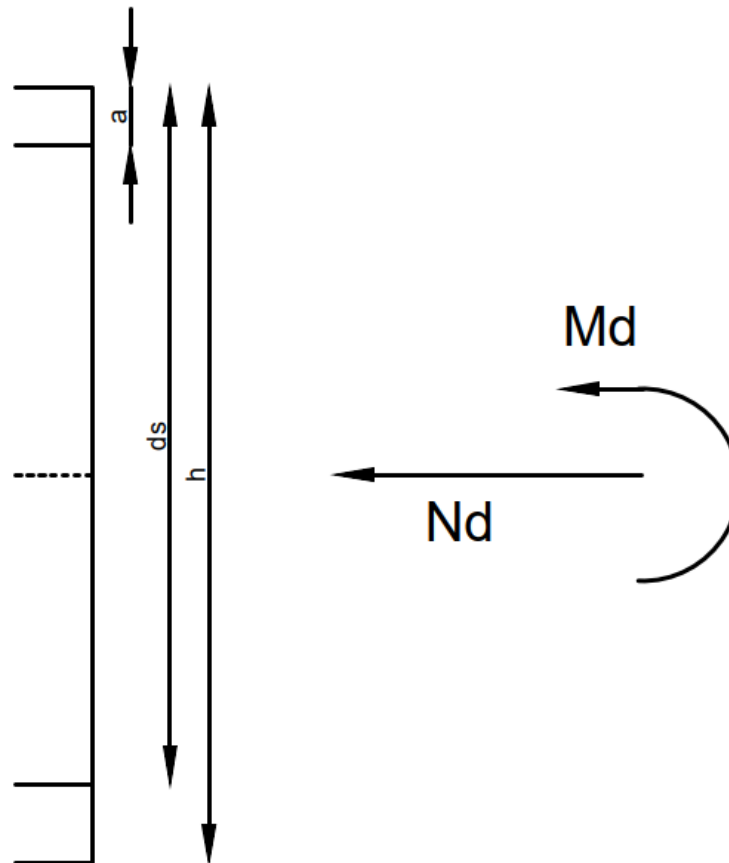
Figure D.18: Overview of the cross section

The same kind of calculations have already been performed in Appendix D.2.1.

Rupture Moment

f_{ctm} is known in this situation. For $C30/37$ $f_{ctm} = 2.9N/mm^2$. The modulus of Elasticity is $E_c = \frac{f_{cd}}{\epsilon_{c3}} = 11429N/mm^2$. Now f_{ctm} and E_c are known, $\epsilon_{c,tension}$ can be calculated:

$\epsilon_{c,tension} = \frac{f_{ctm}}{E_c} = 0.25 * 10^{-3}$.

The forces acting on the cross section are:

- $N_c = \frac{1}{2} * b * x * \epsilon_c * E$, where $\epsilon_c = \frac{\epsilon_{c,tension}*x}{h-x}$.

- $N_{s,compression} = A_{s,compression} * E_s * \epsilon_{s,compression}$,

  where:

  $\epsilon_{s,compression} = \frac{x-a}{h-x} * \epsilon_{c,tension}$.

- $N_s = A_s * E_s * \epsilon_s$,

  where:

  $\epsilon_s = \epsilon_{c,tension} * \frac{h-x-z}{h-x}$
  z is the distance between the bottom of the slab and the reinforcement at the tension side,

$$z = h - d_s \ [mm]$$

- $N_{c,tension} = \frac{1}{2} * b * (h - x) * \epsilon_{c,tension} * E_c$

The forces listed above and the normal force N_d have to make equilibrium:

$$N_c + N_{s,compression} - N_s - N_c tension - N_d = 0.$$

The compression height x can be found by solving the equation above. A compression height of $x = 1169mm$ is found. x is bigger than t_f. N_c and $N_{c,tension}$ have to be divided in a part acting over the width b and a part acting over a width of t_w.
N_c is divided in three different parts: N_{c1}, N_{c2} and N_{c3}, Figure D.19.

- $N_{c1} = b * t_f * \epsilon_{c,tension} * \frac{x - t_f}{h - x} * E_c$

- $N_{c2} = \frac{1}{2} * b * t_f * \epsilon_{c,tension} * (\frac{x}{h-x} - \frac{x-t_f}{h-x}) * E_c$

- $N_{c3} = \frac{1}{2} * t_w * (x - t_f) * \epsilon_{c,tension} * \frac{x-t_f}{h-x} * E_c$

N_c is divided in three different parts: $N_{c1,tension}$, $N_{c2,tension}$ and $N_{c3,tension}$.

- $N_{c1,tension} = b * t_f * \epsilon_{c,tension} * \frac{h-x-t_f}{h-x} * E_c$

- $N_{c2,tension} = \frac{1}{2} * b * t_f * \epsilon_{c,tension} * (1 - \frac{h-x-t_f}{h-x}) * E_c$

- $N_{c3,tension} = \frac{1}{2} * t_w * (h - x - t_f) * \epsilon_{c,tension} * \frac{h-x-t_f}{h-x} * E_c$

By solving the equilibrium a new compression height is found, $x = 1232mm$. The strain and stress distribution are given in Figure D.20 & D.21. The rupture moment M_r can now be solved. The point of rotation is the center of the cross section.

$$M_r = N_{c1} * (\frac{h}{2} - \frac{t_f}{2}) + N_{c2} * (\frac{h}{2} - \frac{t_f}{3}) + N_{c3} * (\frac{h}{2} - \frac{x-t_f}{3} + t_f) + N_{s,compression} * (\frac{h}{2} - a) + N_s * (\frac{h}{2} - z) + N_{c1,tension} * (\frac{h}{2} - \frac{t_f}{2}) + N_{c2,tension} * (\frac{h}{2} - \frac{t_f}{3}) + N_{c3,tension} * (\frac{h}{2} - \frac{h-x-t_f}{3} + t_f) = 2457kNm.$$
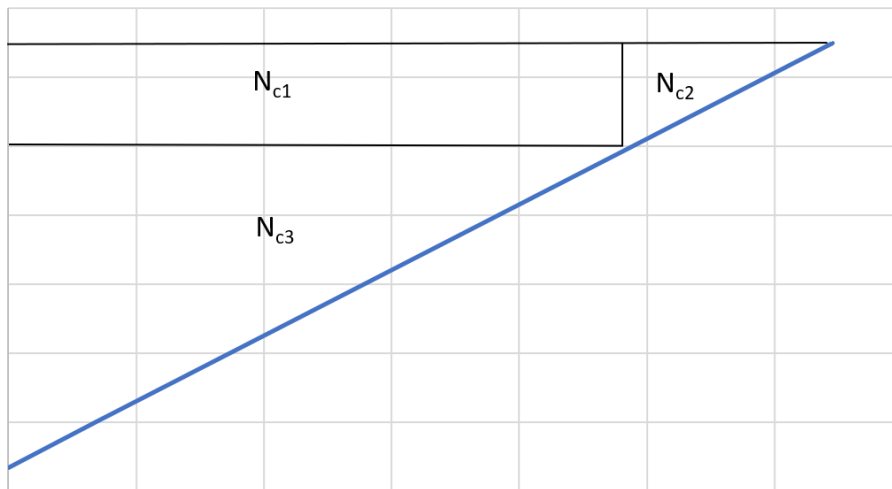
Figure D.19: Dividing the concrete force
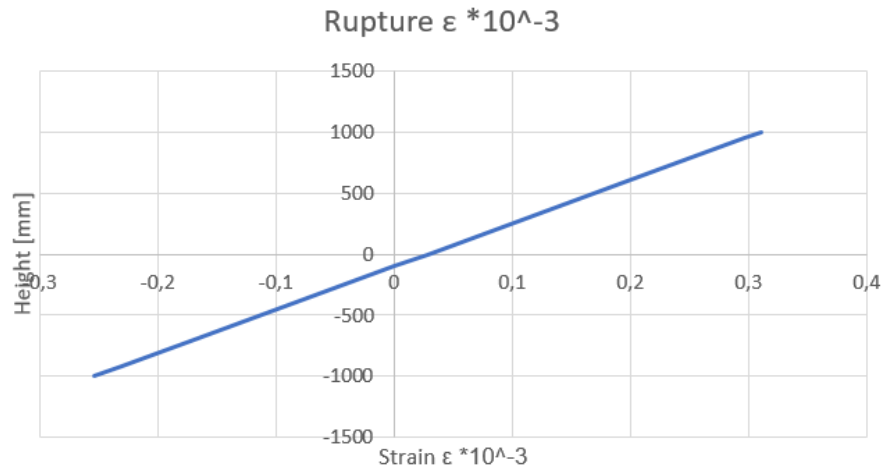
Figure D.20: Strain distribution Rupture moment
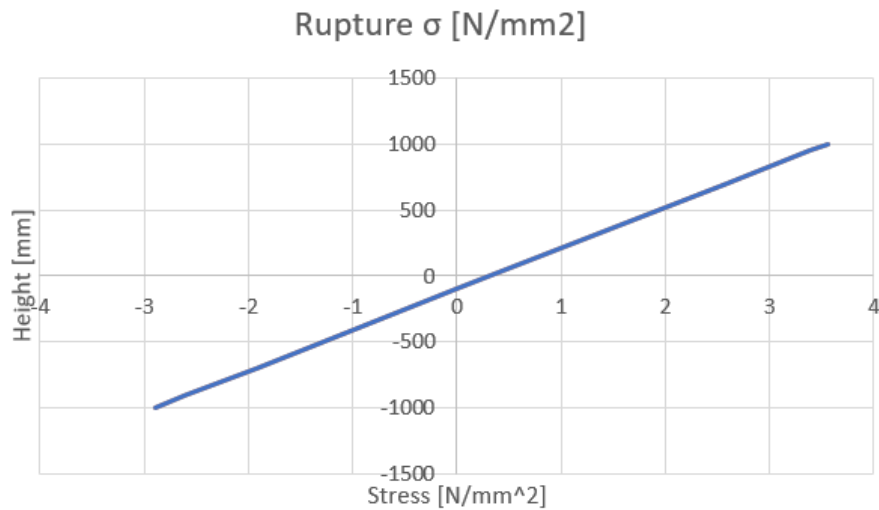
Figure D.21: Stress distribution Rupture moment

Yielding Moment

At this point the reinforcement at the tension side of the cross section has begun to yield. At this moment the strain in the reinforcement is

$$\epsilon_s = \frac{f_{yd}}{E_s} = \frac{435}{200000} = 2.175‰.$$

The forces acting on the cross section are:

- $N_c = \frac{1}{2} * b * x * \epsilon_c * E,$

  where:

  $$\epsilon_c = \frac{\epsilon_{c,tension} * x}{d_s - x}.$$

- $N_{s,compression} = A_{s,compression} * E_s * \epsilon_{s,compression},$

  where:

$$\epsilon_{s,compression} = \frac{x-a}{d_s-x} * \epsilon_{c,tension}.$$

- $N_s = A_s * E_s * \epsilon_s$.

Solving the equilibrium:

$$N_c + N_{s,compression} - N_s - N_d = 0,$$

gives a compression height of $x = 636mm$. Again the compression height x is bigger than the flange height t_f. The compression zone has to be split up in a part acting over the full width b and a part acting over the width t_w. Applying the same principle as in the previous section, a compression height of $x = 694.6mm$ is found. The resulting strain and stress distribution are shown in Figure D.22 & D.23. The resulting moment is:

$$M_y = N_{c1}*(\frac{h}{2}-\frac{t_f}{2})+N_{c2}*(\frac{h}{2}-\frac{t_f}{3})+N_{c3}*(\frac{h}{2}-\frac{x-t_f}{3}+t_f)+N_{s,compression}*(\frac{h}{2}-a)+N_s*(\frac{h}{2}-z) = 6992kNm.$$
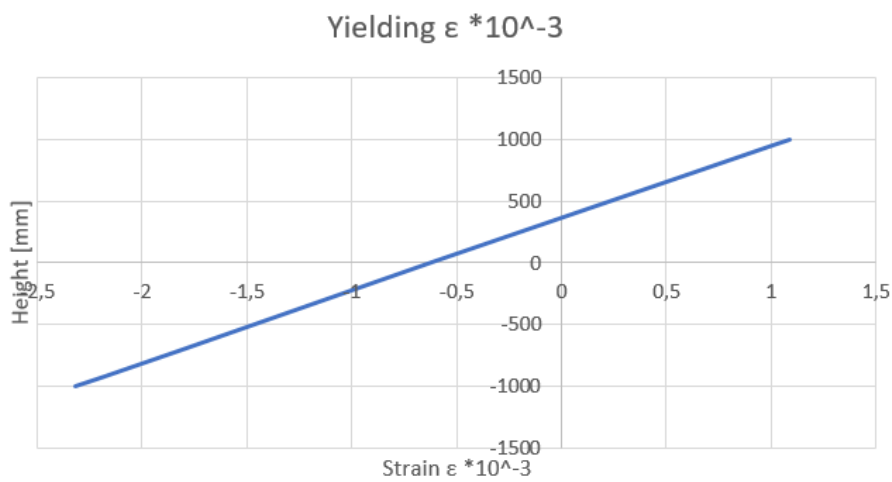
Figure D.22: Strain distribution Yielding moment
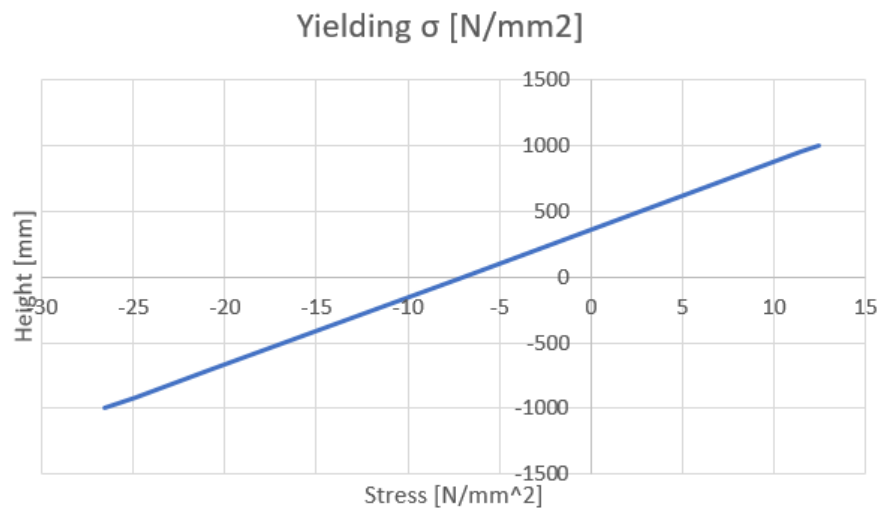
Figure D.23: Stress distribution Yielding moment

Stuik Moment

The forces acting on the cross section are:

- $N_c = \frac{1}{2} * b * x * \epsilon_{c3} * E,$

  where:

  $\epsilon_{c3} = 1.75‰.$

- $N_{s,compression} = A_{s,compression} * E_s * \epsilon_{s,compression},$

  where:

  $\epsilon_{s,compression} = \frac{x-a}{x} * \epsilon_{c3}.$

- $N_s = A_s * E_s * \epsilon_s.$

By solving the force equilibrium a compression height of $x = 300mm$ is found. This is the same height as the flange. It has to be checked if the reinforcement has started to yield. $\epsilon_s = \epsilon_{c3} * \frac{h-x-z}{z} = 10.54‰,$ so the reinforcement is yielding. The resulting moment is $M_{c,pl} = 7241kNm.$
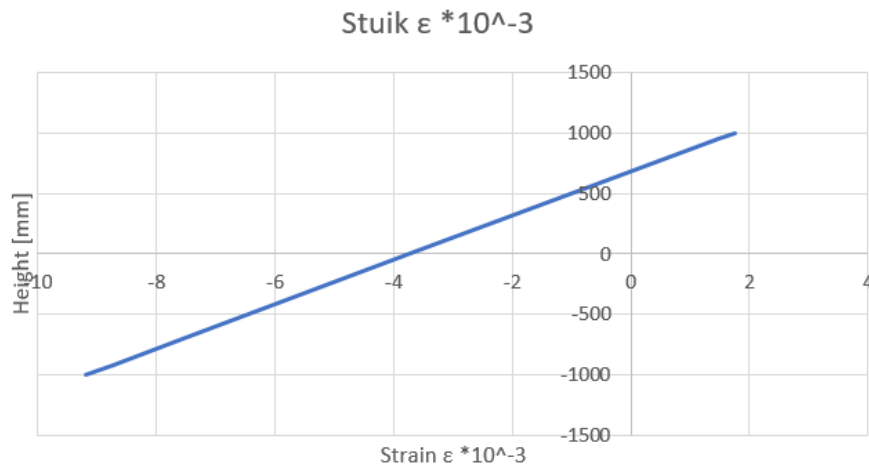
Figure D.24: Strain distribution Stuik moment

Stuik σ [N/mm2]
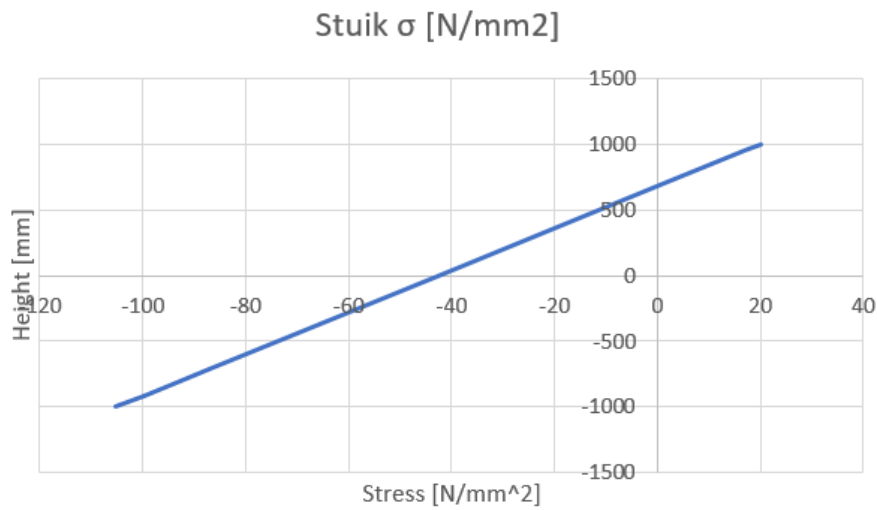
Figure D.25: Stress distribution Stuik moment

Ultimate Moment

At this moment the strain in the compression zone is $\epsilon_c = 5.5$‰ and the reinforcement at the tension side and compression side are both yielding. The forces acting on the cross section are:

- $N_c = 0.75 * x * b * f_{cd}$,

- $N_{s,compression} = A_{s,compression} * f_{yd}$.

- $N_s = A_s * f_{yd}$.

The ultimate bending moment resistance is $M_{Rd} = 7341 kNm$.

Ultimate ε *10^-3
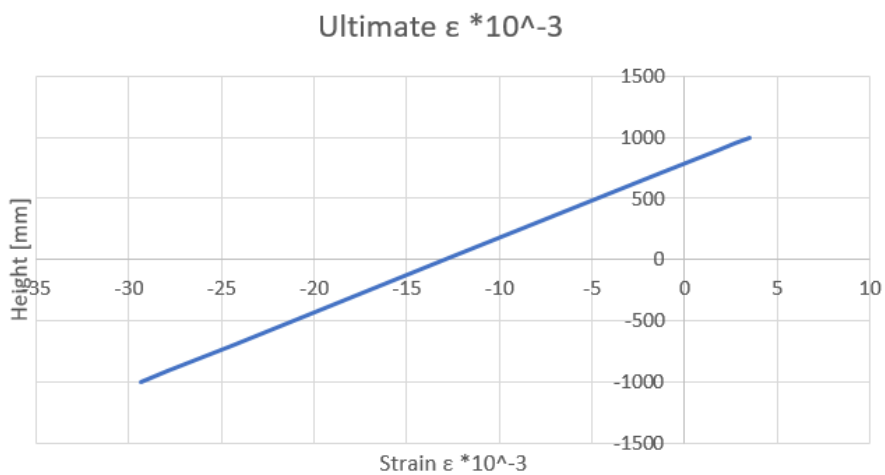
Figure D.26: Strain distribution Ultimate moment
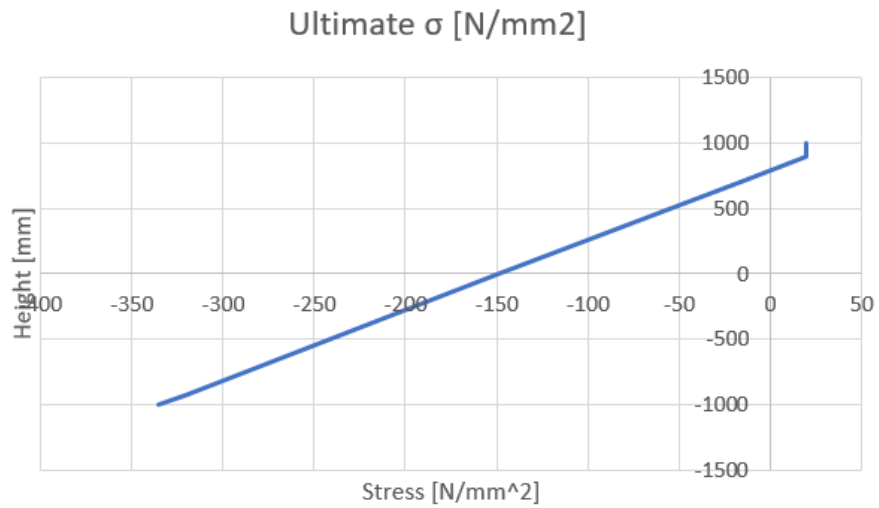
Figure D.27: Stress distribution Ultimate moment

Moment-Curvature Diagram
The moment curvature is calculated as in Appendix D.2.1.

Table D.5: Moment-Curvature diagram

	$M\ [kNm]$	$\kappa * 10^{-3}\ [m^{-1}]$
Start	0	0
Rupture moment M_r	2457	0.26
Yielding moment M_y	6992	1.54
Stuik moment $M_{c,pl}$	7241	5.83
Ultimate moment M_{Rd}	7341	20.10
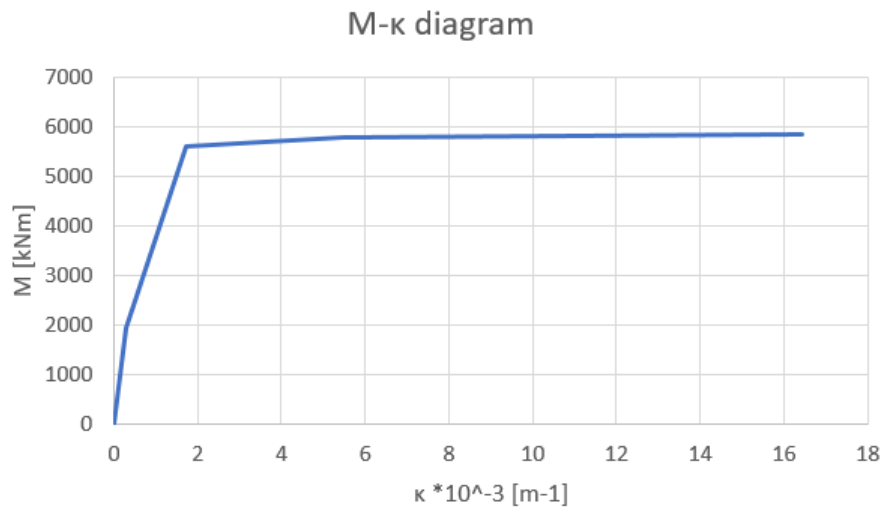
Figure D.28: Moment Curvature diagram

Shear Force Resistance

First it has to be checked if shear reinforcement is necessary, with:

$$V_{Rd,c} = [C_{Rd,c}k(100\rho_l f_{ck})^{(1/3)}]b_w d = 275kN \leq 1563kN$$

where:

$$b_w = t_w = 300mm$$

Shear reinforcement is needed. The next step is to calculate the amount of shear reinforcement, according to:

$$V_{Rd,s} = \frac{A_{sw}}{s}z f_{ywd}\cot\theta = 1585kN$$

where:

$$z = 0.9 * d \ [mm]$$
$$\theta = 16mm$$
$$s = 190mm$$
$$f_{ywd} = 435N/mm^2$$

Crack Width

The principle is the same as for the crack width calculation for prestressing, except there is no external prestressing force. This has an influence on the horizontal force equilibrium and moment equilibrium. The horizontal force equilibrium is as follows:

$$N_{c1} + N_{c2} = N_s$$

The moment equilibrium is:

$$M_{max} = N_{c1}e_{c1} + N_{c2}e_{c2} + N_s e_s$$

where:

$$e_{c1} = \frac{h}{2} - \frac{x}{3} \ [mm]$$
$$e_{c2} = \frac{h}{2} - t_f - \frac{x-t_f}{3} \ [mm]$$
$$e_s = d_s - \frac{h}{2} \ [mm]$$

The resulting crack width is $0.34mm$.

Points of Attention

Extra reinforcement is needed in the flanges of the cross section in x-direction. To get an indication of the moment distribution and shear force distribution, Maple is used (Figure D.29). Part of the floor is modelled as an beam with a lenght of $5m$. The beam is supported at the locations of the webs. The beam is loaded by the weight of the water inside the lock with a water level of MHW. The EI in the script is a random number since the results do not depend on EI.

```
[> restart;
[> ODE1 := EI·diff(w1(x), x$4) = q :
[> ODE2 := EI·diff(w2(x), x$4) = q :
[> ODE3 := EI·diff(w3(x), x$4) = q :
[> ODE4 := EI·diff(w4(x), x$4) = q :
[> ODE5 := EI·diff(w5(x), x$4) = q :
[> sol1 := dsolve({ODE1, ODE2, ODE3, ODE4, ODE5}, {w1(x), w2(x), w3(x), w4(x), w5(x)}) : assign(sol1);
[> w1 := w1(x) : w2 := w2(x) : w3 := w3(x) : w4 := w4(x) : w5 := w5(x) :
[> phi1 := -diff(w1, x) : kappa1 := diff(phi1, x) : M1 := EI·kappa1 : V1 := diff(M1, x) :
[> phi2 := -diff(w2, x) : kappa2 := diff(phi2, x) : M2 := EI·kappa2 : V2 := diff(M2, x) :
[> phi3 := -diff(w3, x) : kappa3 := diff(phi3, x) : M3 := EI·kappa3 : V3 := diff(M3, x) :
[> phi4 := -diff(w4, x) : kappa4 := diff(phi4, x) : M4 := EI·kappa4 : V4 := diff(M4, x) :
[> phi5 := -diff(w5, x) : kappa5 := diff(phi5, x) : M5 := EI·kappa5 : V5 := diff(M5, x) :
[> x := 0 : eq1 := M1 = 0 : eq2 := w1 = 0 :
[> x := L : eq3 := w1 = 0 : eq4 := M1 = M2 : eq5 := phi1 = phi2 : eq6 := w2 = 0 :
[> x := 2·L : eq7 := w2 = 0 : eq8 := M2 = M3 : eq9 := phi2 = phi3 : eq10 := w3 = 0 :
[> x := 3·L : eq11 := w3 = 0 : eq12 := M3 = M4 : eq13 := phi3 = phi4 : eq14 := w4 = 0 :
[> x := 4·L : eq15 := w4 = 0 : eq16 := M4 = M5 : eq17 := phi4 = phi5 : eq18 := w5 = 0 :
[> x := 5·L : eq19 := M5 = 0 : eq20 := w5 = 0 :
[> sol2 := solve({eq1, eq2, eq3, eq4, eq5, eq6, eq7, eq8, eq9, eq10, eq11, eq12, eq13, eq14, eq15, eq16, eq17, eq18, eq19, eq20}, {_C1, _C2, _C3, _C4, _C5, _C6, _C7, _C8, _C9, _C10, _C11,
        _C12, _C13, _C14, _C15, _C16, _C17, _C18, _C19, _C20}) : assign(sol2);
[> L := 1 : q := 200 : EI := 10 :
```

Figure D.29: Maple script for the moment and shear force distribution

Cost

The cost calculations takes the same objects into account as the MKI calculations. The calculations are the same, only the MKI factor changes to the cost of the individual objects. The value of these object are already mentioned in calculations above. The increase in cost is 952€ per meter.

MKI

The MKI calculations take into account concrete, shear reinforcement and additional reinforcement in the flanges in the x-direction.
The reduce in MKI due to concrete of the floor is:

$$(V_{new} - V_{old})27.92 = -9462€$$

The increase in MKI due to shear reinforcement is:

$$(A_{s,new} - As, old)lb\gamma_s MKI_{reinforcement} = (2116 - 1005)13.3 * 26 * 7.8 * 106 = 318€$$

Assumed is that reinforcement $\theta16 - 200$ needs to be applied in the flanges. This leads to an increase in MKI of:

$$2A_s nlb\gamma_s MKI_{reinforcement} = 575€$$

where n is the number of reinforcement bars per meter.
The total decrease in MKI is 496€ per meter.
The weighing factor is:

$$1058/11206 = 0.09$$

E
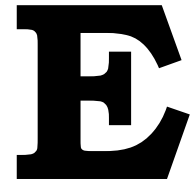
Parametric model

E.1. Unified Model Language

The unified model language (UML) is a standardized modeling language enabling developers to specify, visualize, construct and document artifacts of a software system (techopedia, 2019). A model consists out of different classes. Each class has its own bracket. Each bracket is divided in three divisions. The top division gives the name of the class. The middle division contains all the information related to the class. The last division contains all the calculations done in that class. The UML diagram for the lock head only shows the most important information and calculations for each class. The classes are connected to each other with lines. Three different lines are used in this model. The first line is a line without an arrow. Classes connected with each other with this line exchange information. A line with an arrow means that one class only gives information and the other class only receives information from that class. A line with an open arrow means that the class inherents a part of the other class.

The classes Cost, MKI, Reinforcement, Concreteclass and Vessel only contain information. Note the empty bottom division. The classes are connected to the main class Lockhead with a line with an arrow. The Lockhead class therefore only receives information from these classes.

The classes Floor, Wall, Gate, Load and Soil are connected to the lock head with a simple line. The classes need information of each other to perform the calculations.

The Gate class is connected to the Gatemitre and Gatesingleleaf to make a distinction between the two gate types. The class Soil is connected to the class Soillayer, since for every possible soil layer an instance has to be made.

The classes Floor and Wall are connected to respectively a Wallsection and a Floorsection. The Wallsection and Floorsection are both connected to the Section class. The connection are with an open arrow, since the classes inherent part of their definition from the previous class.

The main class Lockhead is located in the middle in the figure. Every class is accessible via the lockhead.

E.2. Matrix Method

The stiffness matrix and the force vector have to be adjusted to account for the effect of the elastic soil. The maple script in Figure E.1 gives the result of these calculations.

189

```
> restart:
> with(CodeGeneration) :
> ODE := diff(w(x), x$4) + 4·β^4·w(x) = q/EI :
> w := rhs(dsolve(ODE, w(x))) :
> phi := -diff(w, x) : kappa := diff(phi, x) :
> M := EI·kappa : V := diff(M, x) :
> x := 0 : eq1 := w = w1 : eq2 := phi = phi1 :
> x := L : eq3 := w = w2 : eq4 := phi = phi2 :
> sol := solve( {eq1, eq2, eq3, eq4}, {_C1, _C2, _C3, _C4} ) : assign(sol);
> x := 0 : Fz1 := -simplify(V) : Ty1 := -simplify(M) :
> x := L : Fz2 := simplify(V) : Ty2 := simplify(M) :
> k11 := coeff(collect(Fz1, w1), w1) : k12 := coeff(collect(Fz1, phi1), phi1) : k13 := coeff(collect(Fz1, w2), w2) : k14 := coeff(collect(Fz1, phi2), phi2) :
> k21 := coeff(collect(Ty1, w1), w1) : k22 := coeff(collect(Ty1, phi1), phi1) : k23 := coeff(collect(Ty1, w2), w2) : k24 := coeff(collect(Ty1, phi2), phi2) :
> k31 := coeff(collect(Fz2, w1), w1) : k32 := coeff(collect(Fz2, phi1), phi1) : k33 := coeff(collect(Fz2, w2), w2) : k34 := coeff(collect(Fz2, phi2), phi2) :
> k41 := coeff(collect(Ty2, w1), w1) : k42 := coeff(collect(Ty2, phi1), phi1) : k43 := coeff(collect(Ty2, w2), w2) : k44 := coeff(collect(Ty2, phi2), phi2) :
> Ksys := Matrix(4, 4, [ [k11, k12, k13, k14], [k21, k22, k23, k24], [k31, k32, k33, k34], [k41, k42, k43, k44] ]);
```

$$Ksys := [\ldots]$$

```
> f1 := simplify(-coeff(collect(Fz1, q), q)·q) :
> f2 := simplify(-coeff(collect(Ty1, q), q)·q) :
> f3 := simplify(-coeff(collect(Fz2, q), q)·q) :
> f4 := simplify(-coeff(collect(Ty2, q), q)·q) :
> fsys := vector( [ f1, f2, f3, f4 ]);
```

$$fsys := [\ldots]$$

Figure E.1: Stiffness matrix and load vector for a soil a beam on elastic soil

E.3. Parametric Model

E.3.1. Gate Load

The weight of the gate is based on the properties of three single leaf gates. For this purpose two gates from the Reevesluis and one gate from the navigation lock in Empel have been used. The ratio between the weight of the gate and the dimensions of the gate has been calculated, Table E.1. The formula used in the parametric model used to calculate the weight of the gate becomes:

$$F_{z,gate} = 4.5 l_{gate} b_{gate} + 50 [kN]$$

An additional $50 kN$ is added due to uncertainties.

Table E.1: Weight gate ratio

Location	Weight [ton]	height [m]	width [m]	ratio
Reeve	43	7.7	12.5	0.45
Reeve	51	9.7	12.5	0.42
Empel	80	12.7	-1778	0.45

E.4. Validation

E.4.1. Loads

The gate load and crane load calculated by the parametric model deviate from the values from Empel. The reason why the crane load deviates is due to the different calculation method. VolkerWessels Infra Competence Centre multiplies the vertical crane load with a factor of 0.5, whereas the parametric model uses the formula from B to calculate the crane load.

The horizontal force of the gate is calculated according to the following formula:

$$F_x = F_z(\frac{b}{2} + e)/(z_h - z_p)$$

where:

b = the width of the gate $[m]$
e = eccentricity, set to $0.4m$
z_h = location of the gate hinge relative to $mNAP$

z_p = location of the pivot bearing relative to $mNAP$

E.4.2. Moment per Section

For this purpose the western wall of the lock head Empel has been used, see Figure 4.3. The wall has been divided in three different sections. The dimensions of the sections are given in Table E.2.

Table E.2: Dimensions different sections

Section	$L[m]$	$b[m]$
Head	2.0	3.3
Chamber	6.0	2.2
Tail	4.0	3.3

The first step is to calculate the center of gravity of the total cross section, $z = 1.43m$. Next the moment of inertia is calculated, $I = 25.7m^4$. Now the stress distribution can be determined via the following formula:

$$\sigma = \frac{My}{I}$$

Figures E.2 & E.3 show the stress distribution in blue over each section due to the external bending moment of $M = 103781 kNm$. The stress distribution can be divided in a part due to pure bending (orange) and a part due to a normal force (grey). For each component the bending moment has to be calculated. The total bending moment per section becomes:

$$M = \sigma_m W_i + N e_i$$

where:

W_i = the moment of resistance per section $[m^3]$
e_i = the distance from the centre of gravity to the centre of gravity of the individual section $[m]$

The results of the calculations are shown in Table E.3.

Table E.3: Moment distribution due to pure bending and a normal force

$W[m^3]$	$e[m]$	$\sigma_M[kN/m^2]$	$\sigma_N[kN/m^2]$	$N[kN]$	$M_M[kNm]$	$M_N[kNm]$	$M_{total}[kNm]$
3.63	0.22	6666	-889	-5866	24198	1290	25488
4.84	-0.33	4444	1333	17598	21509	5807	27316
7.26	0.22	6666	-889	-11732	48395	2581	50976
Sum				0			103781
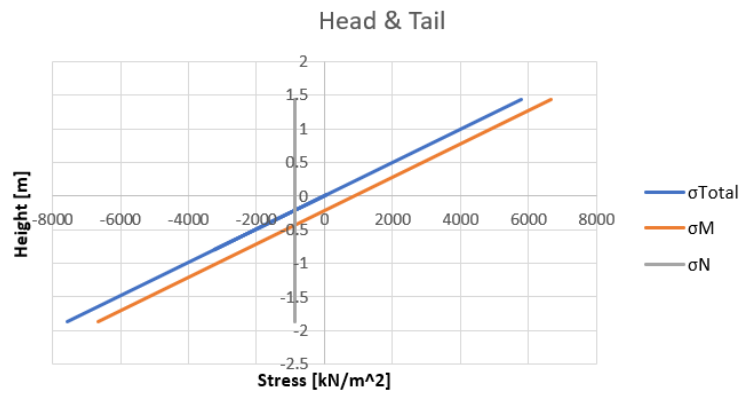
Figure E.2: Stress distribution western wall lock head Empel section head and tail
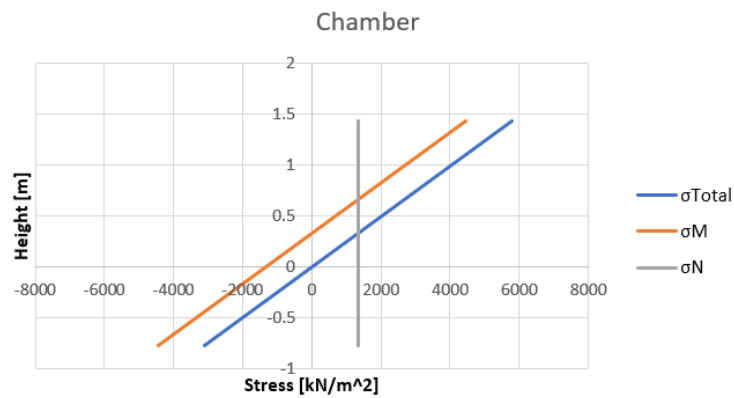
Figure E.3: Stress distribution western wall lock head Empel section chamber

E.4.3. Pile Foundation

The floor has been modelled in the parametric model with the matrix method. To validate the calculations, the beam in Figure E.4 has been calculated with the parametric model and Maple. The result of the calculations can be found in the main report. The Maple script is shown in Figure E.5.
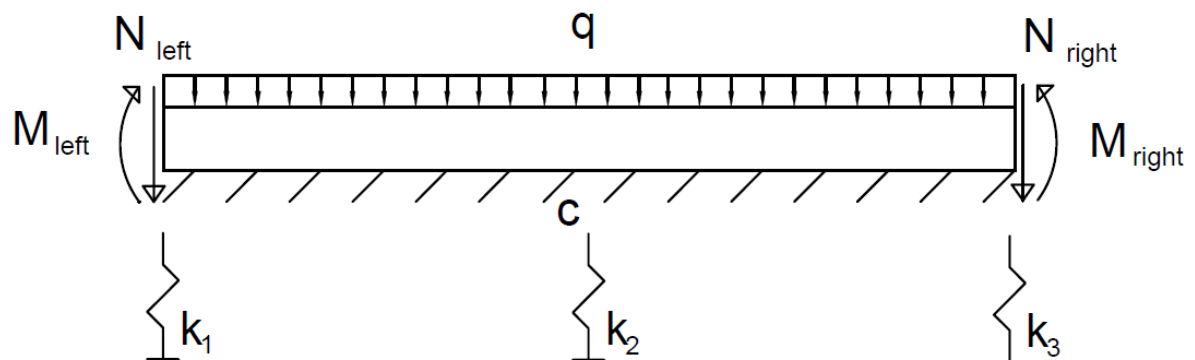
Figure E.4: Schematisation of the beam used to validate the matrix method

```
> restart;
> ODE1 := diff(w1(x), x$4) + 4·β^4·w1(x) = q/EI :
> ODE2 := diff(w2(x), x$4) + 4·β^4·w2(x) = q/EI :
> sol1 := dsolve({ODE1, ODE2}, {w1(x), w2(x)}) : assign(sol1) :
> w1 := w1(x) : w2 := w2(x) :
> phi1 := -diff(w1, x) : kappa1 := diff(phi1, x) : M1 := EI·kappa1 : V1 := diff(M1, x) :
> phi2 := -diff(w2, x) : kappa2 := diff(phi2, x) : M2 := EI·kappa2 : V2 := diff(M2, x) :
> x := 0 : eq1 := V1 + N_left = k·w1 : eq2 := M1 = M_left :
> x := L : eq3 := w1 = w2 : eq4 := M1 = M2 : eq5 := phi1 = phi2 : eq6 := V1 + k·w1 = V2 :
> x := 2·L : eq7 := V2 + k·w2 = N_right : eq8 := M2 = M_right :
> sol2 := solve({eq1, eq2, eq3, eq4, eq5, eq6, eq7, eq8}, {_C1, _C2, _C3, _C4, _C5, _C6, _C7, _C8}) : assign(sol2);
> x := 'x':
> N_left := 50 : N_right := 50 : M_left := 100 : M_right := 100 : q := 100 :
> beta := (c/(4·EI))^0.25 :
> c := 10000 : EI := 10000000 : k := 50000 :
> L := 5 :
```

Figure E.5: Maple script for a beam on an elastic soil an supported by springs

E.4.4. Moment Resistance

The moment resistance calculation in the model is modelled as an independent code. Based on the received arguments, it calculates the bending moment resistance. VWICC uses Dako to calculate the bending moment resistance. As an example the properties from Figure E.6 has been applied to the bending moment resistance calculation of the parametric model. The result of the Dako sheet is $5821 kNm$, the result of the parametric model is $5852 kNm$

Project:	WU - Sluishoofd Empel		
Projectnummer:	C 3774	Onderdeel: Vloer, boven wand oost	
Constructeur:	B. Weninger	Datum: 20-mrt-12	versie: 2.00
	Berekening wapening in betondoorsnede (plaat) volgens NEN 6720		

Betondoorsnede (brugdek volgens VBB/ROBK)

						Betonsterkteklasse	C28/35
Breedte b =	1000	mm				f_{ck} = 35 N/mm^2	
Hoogte h =	2000	mm				f_b = 21 N/mm^2	
Trekzijde	Corrosie ingeleid door carbonatatie					f_s = 1,40 N/mm^2	
Milieuklasse:	XC1 Droog of blijvend nat					f_{bm} = 2,74 N/mm^2	
Betondekking c =	50	mm	toeslag:	0	mm	**Betonstaalsoort**	FeB500
Verdeelwapening =	25	mm	c_{min} =	52,95	mm	f_s = 435 N/mm^2	
Drukzijde	Corrosie ingeleid door carbonatatie						
Milieuklasse:	XC1 Droog of blijvend nat						
Betondekking c =	50	mm	toeslag:	0	mm		
Verdeelwapening =	25	mm	c_{min} =	50	mm		

Belastingen explosie/stoot/botsing: nee

M_{rep} = 3900,0 kNm N_{rep} = 0 kN
M_d = 4500,0 kNm N_d = 0 kN
M_v = n.v.t. kNm N_v = n.v.t. kN (trek)

Toegepaste wapening

		trekzijde					*drukzijde*			
	ϕ	h.o.h.		A_s		ϕ	h.o.h.		A_s	
staven laag 1	35,3	- 200	=	4893	mm^2	25	- 200	=	2454	mm^2
staven laag 2	25	- 200	=	2454	mm^2	16	- 200	=	1005	mm^2
			$A_{s;tot}$ =	7348	mm^2			$A_{s;tot}$ =	3460	mm^2
	afstand tussen laag 1 en laag 2	x =	20	mm				x =	20	mm
		nuttige hoogte d =	1891	mm				d =	99	mm

Controle wapening art. 8.1.1

$A_{s;tot}$ = 7348 mm^2 $A_{s;ben}$ = 5641 mm^2
x_u = 161,18 mm $A_{s;min}$ = 5641 mm^2 → accoord!
   $A_{s;max}$ = 40092 mm^2
$M_u > M_d$ ==> 5820,5 kNm > 4500,0 kNm → accoord!

Figure E.6: Bending moment resistance Dako

F

Results

In Chapter 8 the results of CEMT class were discussed. In this appendix the other CEMT classes will be discussed. For CEMT class I and VI no comparison is made, since only a single leaf gate applies for CEMT class I and only a mitre gate applies for CEMT class VI.

F.1. Influence Difference in Water Head

F.1.1. Single Leaf Gate
Class I
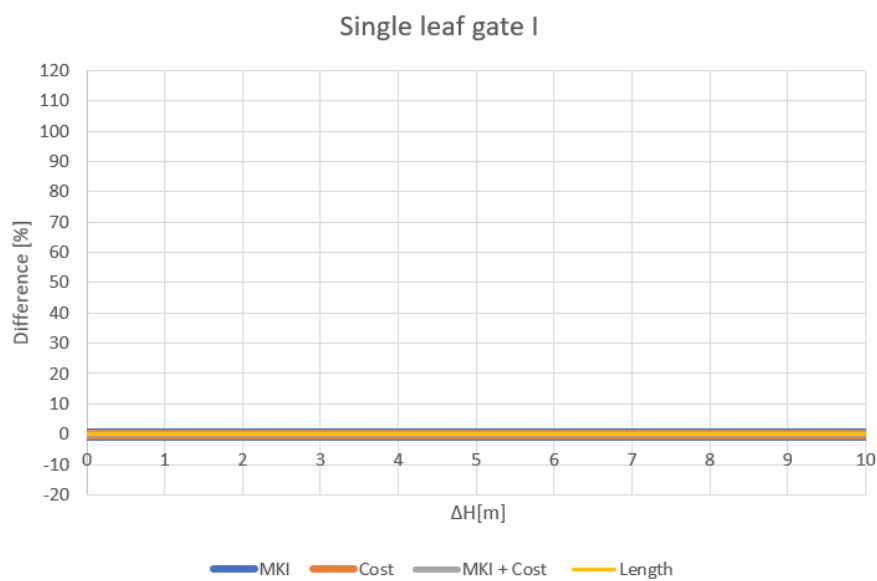
Figure F.1: Difference in Cost and MKI due to a difference in water head
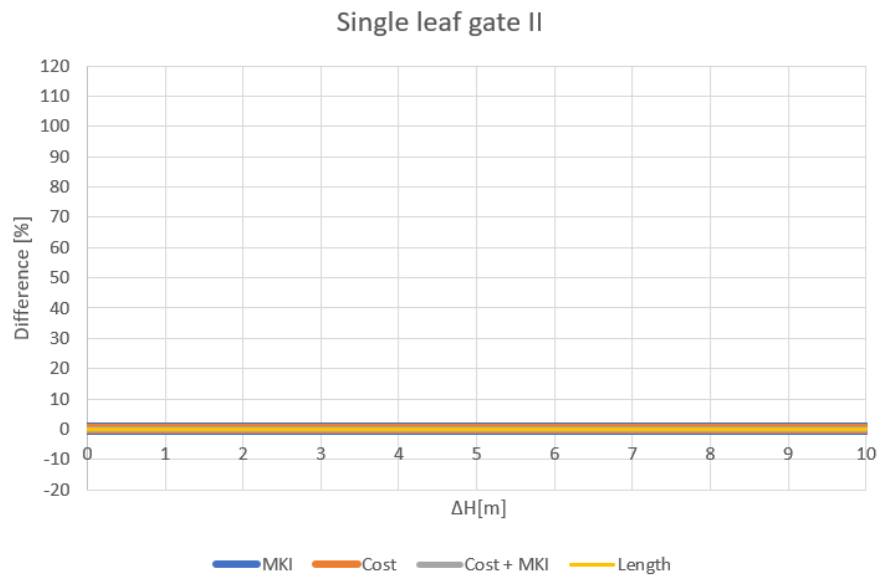
Class II

Figure F.2: Difference in Cost and MKI due to a difference in water head
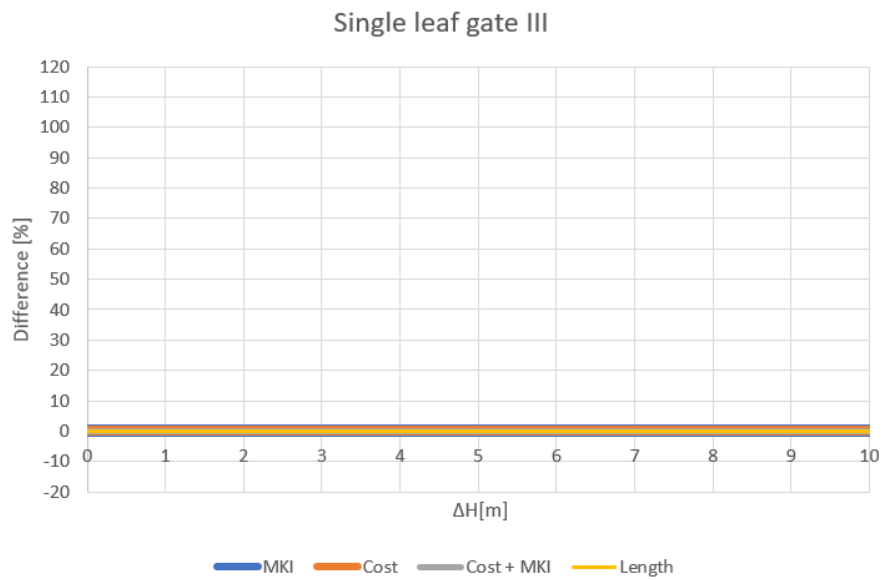
Class III

Figure F.3: Difference in Cost and MKI due to a difference in water head
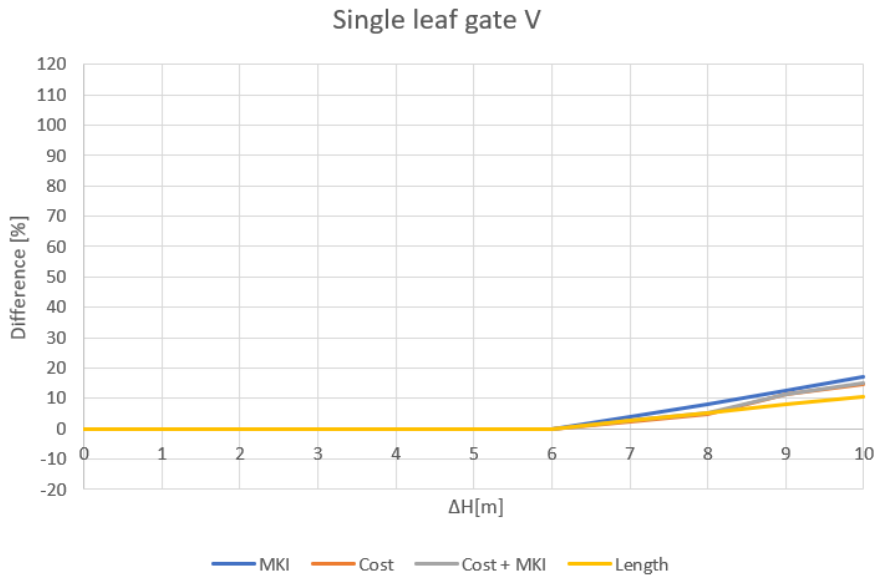
Class V

Figure F.4: Difference in Cost and MKI due to a difference in water head

Conclusion

The lock head design of a single leaf gate CEMT classes I, II and III are independent of the difference in water head. A single leaf gate for CEMT class V is dependent of the difference in water head. This is due to the bigger width of class V in comparison with class I, II, III and IV.

F.1.2. Mitre Gate

Class II
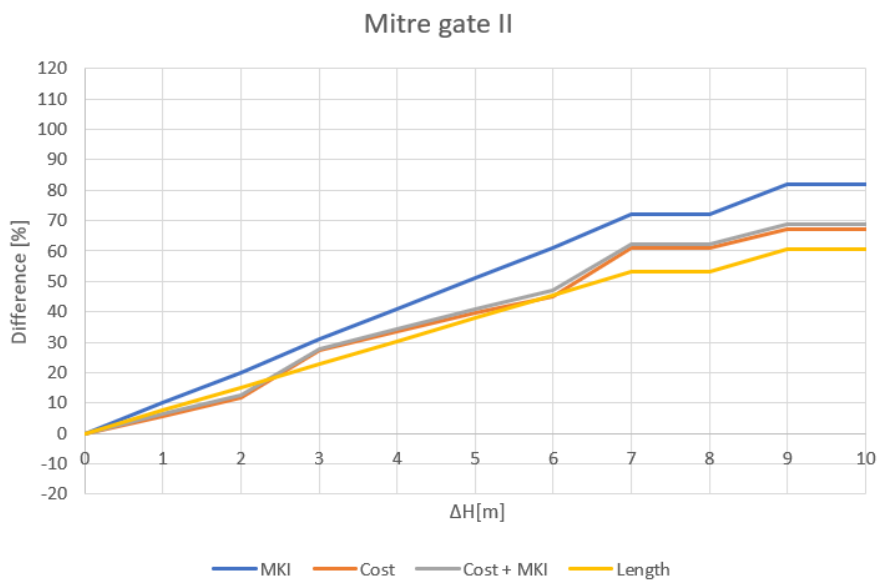
Figure F.5: Difference in Cost and MKI due to a difference in water head

Class III
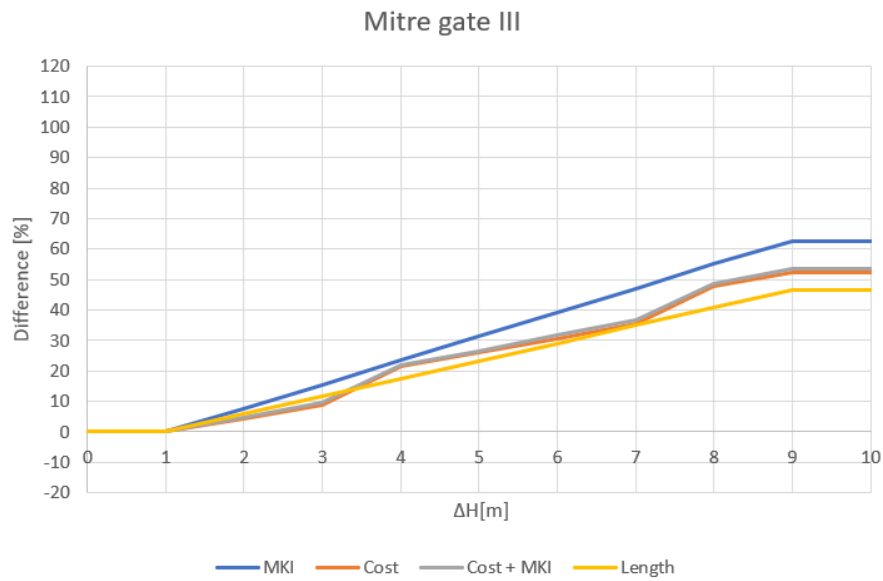
Figure F.6: Difference in Cost and MKI due to a difference in water head
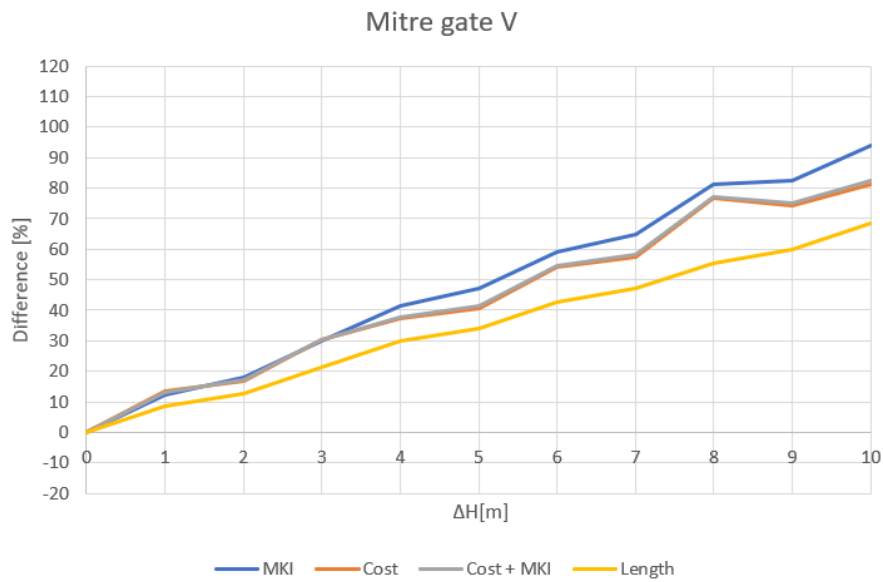
Class V

Figure F.7: Difference in Cost and MKI due to a difference in water head

Class VI
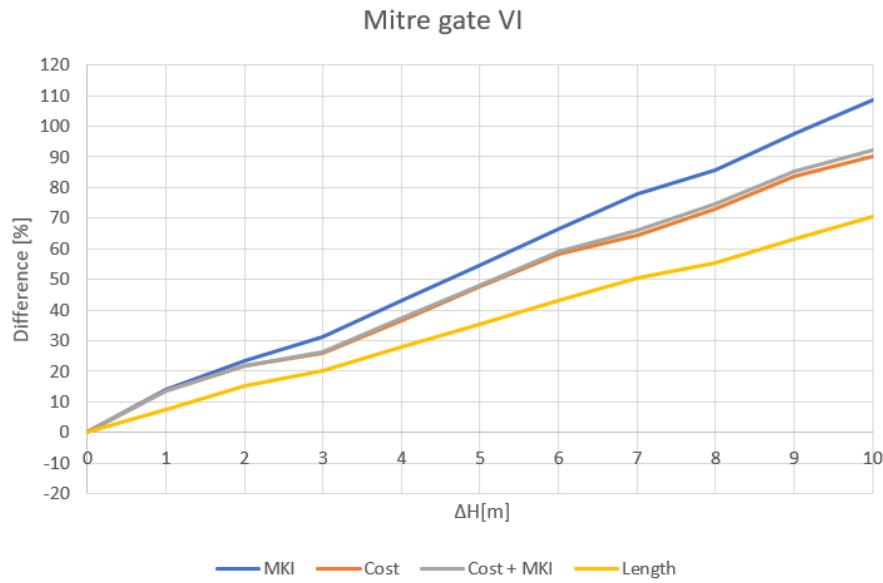
Figure F.8: Difference in Cost and MKI due to a difference in water head

Conclusion

The lock head design of a mitre gate CEMT classes II, III, IV, V and VI depends on the difference in water head.

F.1.3. Comparison

Class II
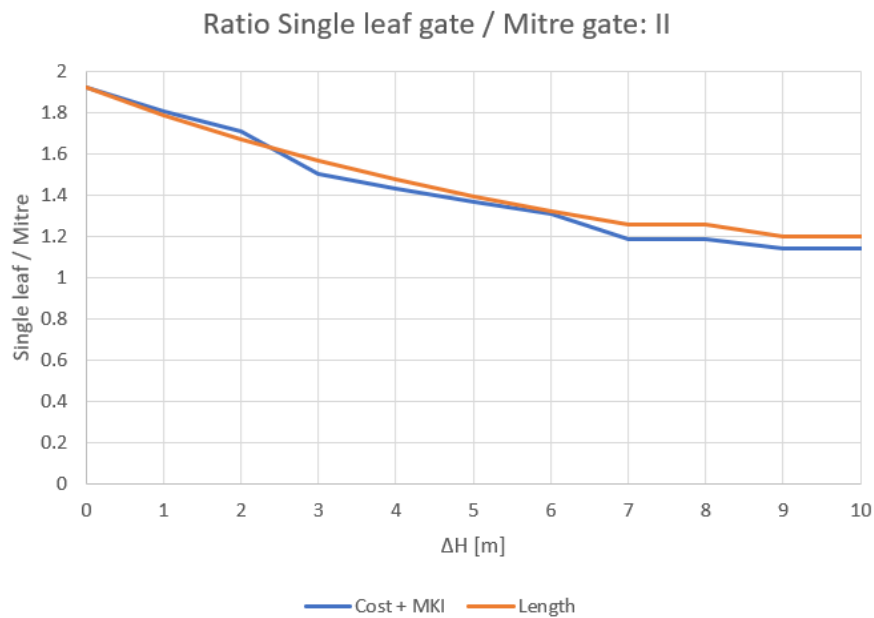
Figure F.9: Cost + MKI comparison between a mitre gate and a single leaf gate due to a difference in water head

Class III

Ratio Single leaf gate / Mitre gate: III
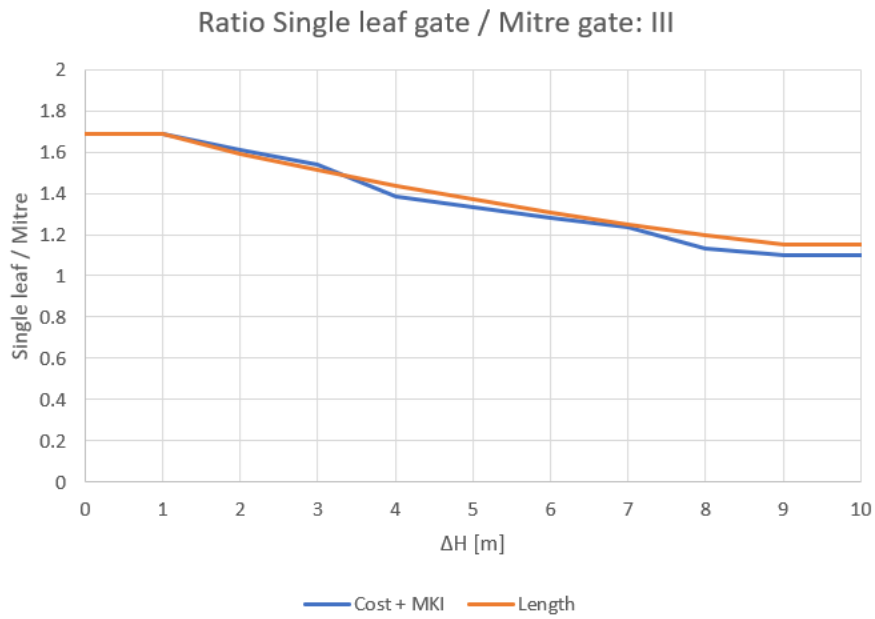
Figure F.10: Cost + MKI comparison between a mitre gate and a single leaf gate due to a difference in water head

Class V

Ratio Single leaf gate / Mitre gate: V
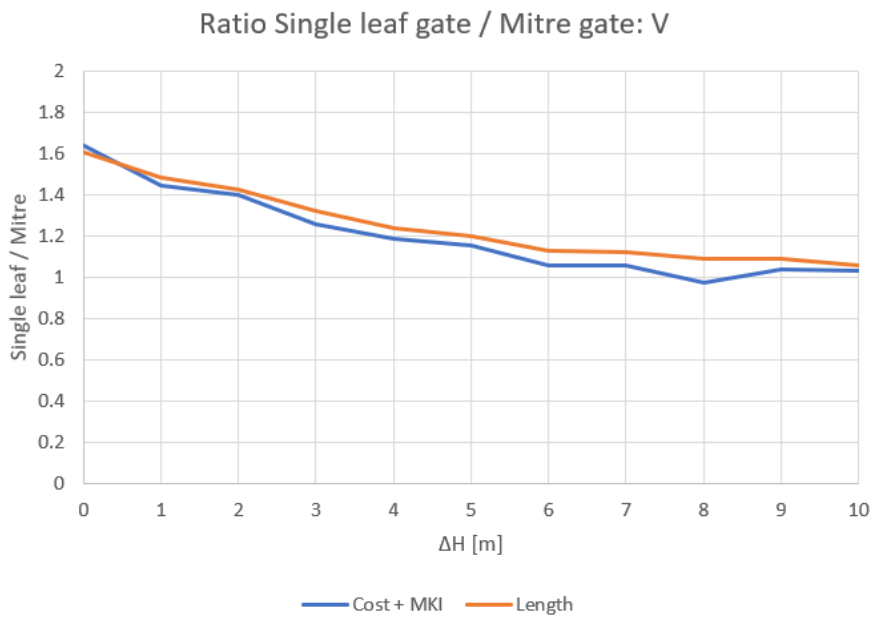
Figure F.11: Cost + MKI comparison between a mitre gate and a single leaf gate due to a difference in water head

Conclusion

The difference between the mitre gate and single leaf gate becomes smaller per CEMT class.

F.2. Influence Thickness

F.2.1. Single Leaf Gate
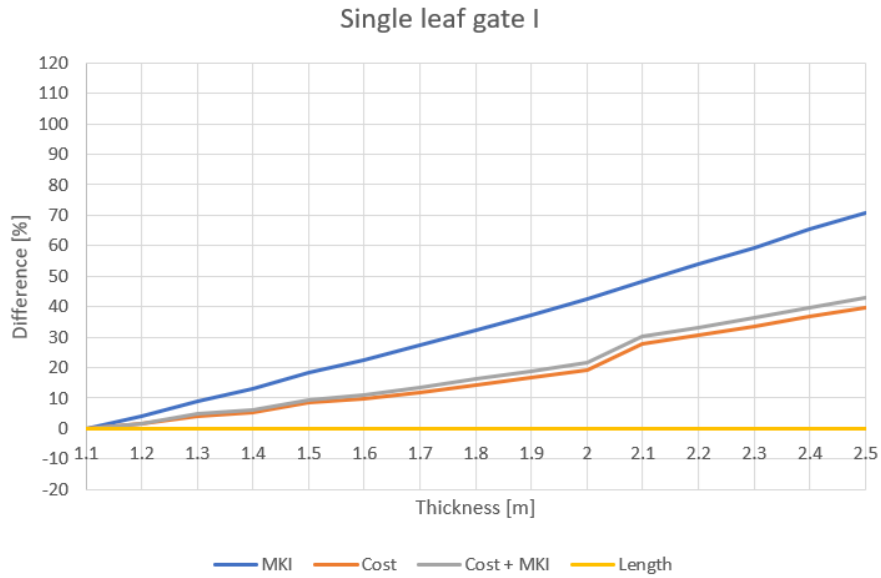
Class I

Figure F.12: Difference in Cost and MKI due to a difference in thickness
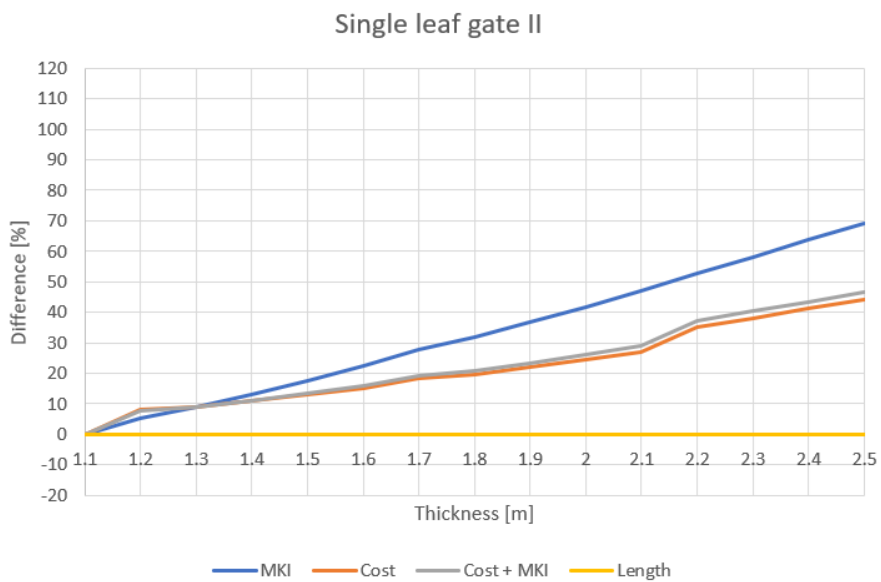
Class II

Figure F.13: Difference in Cost and MKI due to a difference in thickness
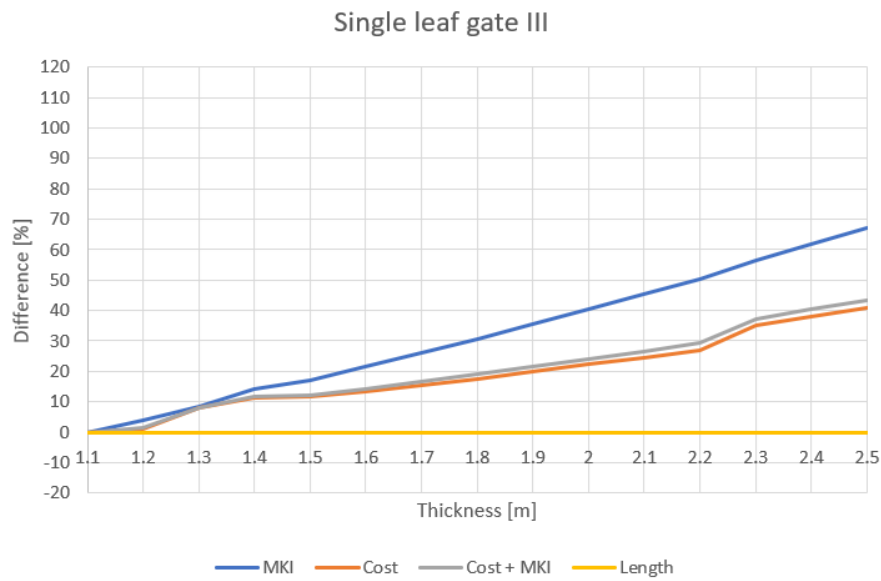
Class III

Figure F.14: Difference in Cost and MKI due to a difference in thickness
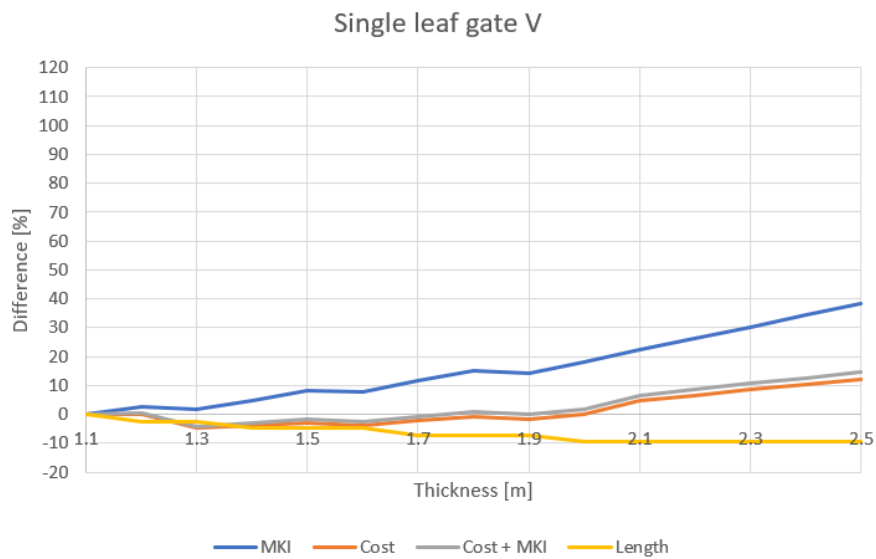
Class V

Figure F.15: Difference in Cost and MKI due to a difference in thickness

Conclusion

The lock head design of a single leaf gate CEMT class I, II, III, IV does not depend on the horizontal bearing capacity. This is because the length of the lock head does not change. The cost and the MKI only increase due to the increase in thickness.

The lock head design for a single leaf gate CEMT class V does depend on the horizontal bearing capacity. By increasing the thickness, the weight of the lock head increases, resulting in more friction between the floor and the soil. This can be seen by the decrease in length.

F.2.2. Mitre gate

Class II
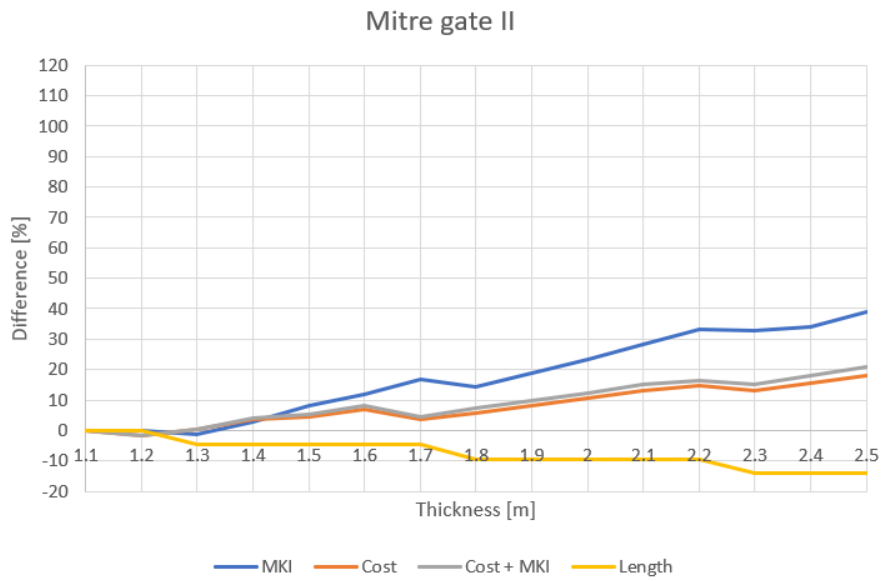
Figure F.16: Difference in Cost and MKI due to a difference in thickness

Class III
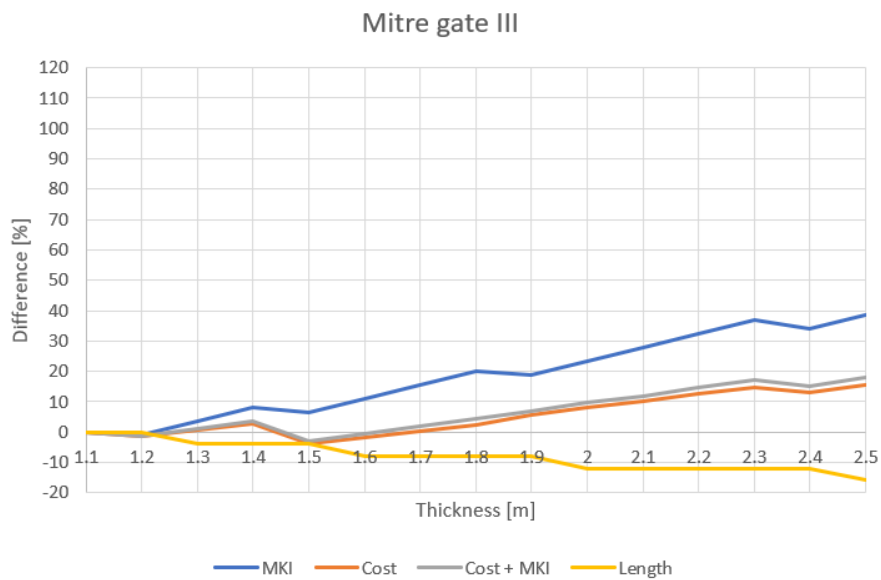
Figure F.17: Difference in Cost and MKI due to a difference in thickness
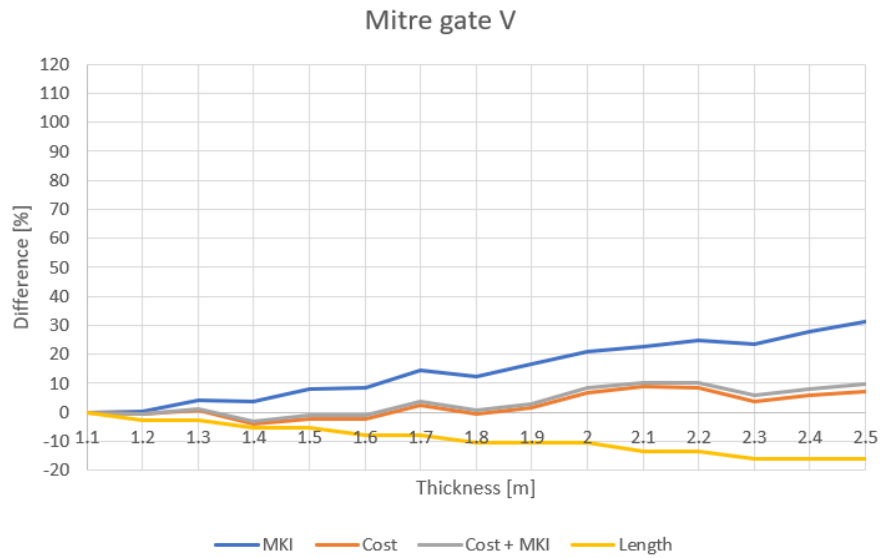
Class V

Figure F.18: Difference in Cost and MKI due to a difference in thickness

Class VI
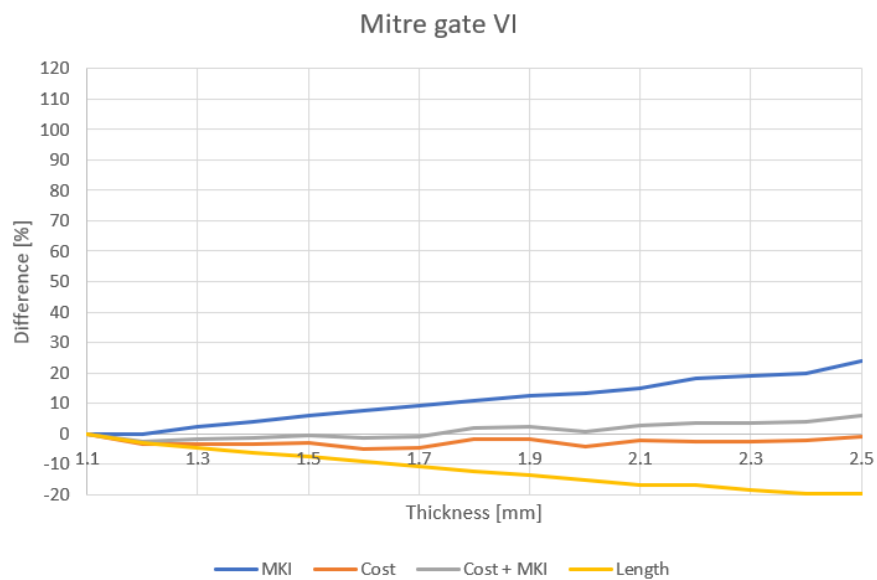
Figure F.19: Difference in Cost and MKI due to a difference in thickness

Conclusion

The lock head design of a mitre gate for CEMT classes II, III, IV, V and VI does depend on the horizontal bearing capacity. This can be seen by the decrease in length. The influence of the horizontal bearing capacity becomes bigger as the CEMT class increases. This can be seen by the smoothing of the length line over the course of the different graphs.

F.2.3. Comparison

Class II
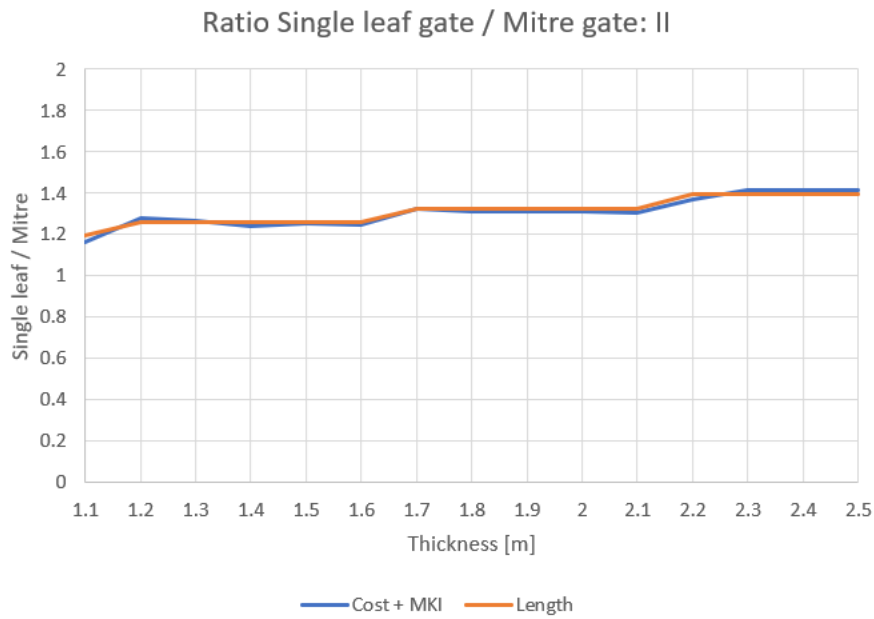
Figure F.20: Cost + MKI comparison between a mitre gate and a single leaf gate due to a difference in thickness

Class III
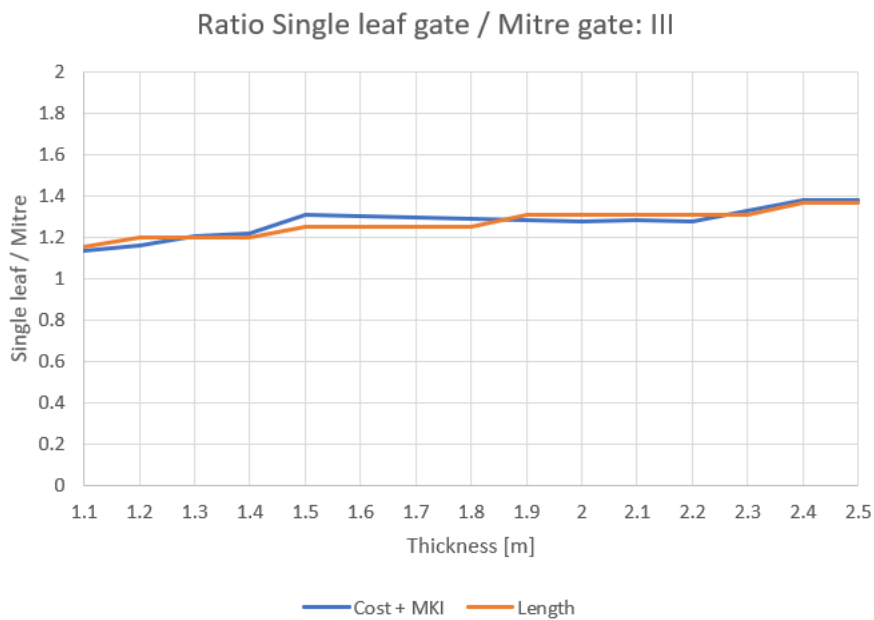
Figure F.21: Cost + MKI comparison between a mitre gate and a single leaf gate due to a difference in thickness
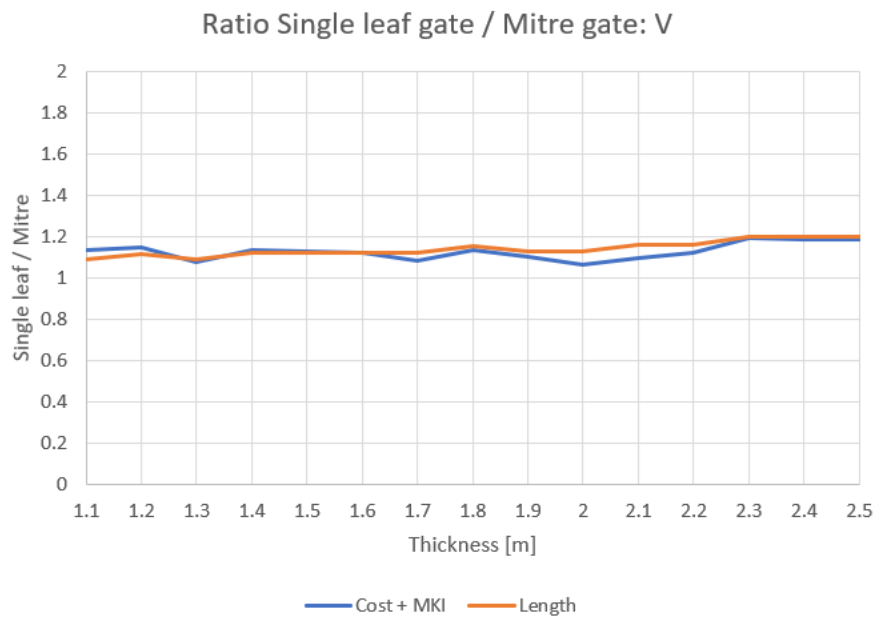
Class V

Figure F.22: Cost + MKI comparison between a mitre gate and a single leaf gate due to a difference in thickness

Conclusion

The overall difference between the mitre gate and the single leaf gate becomes smaller per CEMT classes.

The comparison graphs are less gradually than the comparison graphs due to a difference in water head. This is mainly due to an increase in width, requiring a different GEWI pile configuration. The difference between the mitre gate and the single leaf gate becomes bigger for an increase in thickness due to a decrease in length.

F.3. Influence Concrete Class

The influence of the concrete is not taken in to account for the other CEMT classes. From CEMT class IV it is already apparant that the influence of the concrete is negligible and mainly depends on the environment class.

F.4. MKI Factor

The MKI factor from literature is 0.2 (*Duurzaam GWW aanbesteden*, 2019). The MKI factor in this research is around the 0.1. In the following section the MKI factor due to a difference in water head, thickness and concrete class is investigated. The CEMT class is IV.

F.4.1. Influence Difference in Water Head
The MKI factor is around the 10%, see Figure F.23.
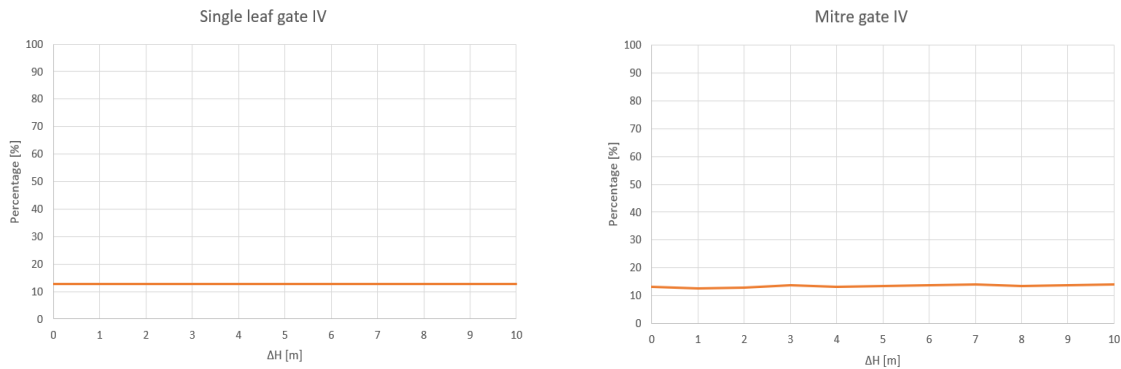
(a) Single leaf gate

(b) Mitre gate

Figure F.23: Percentage of the MKI of the total cost due to a difference in water head

F.4.2. Influence Thickness
The MKI factor is around the 10%, see Figure F.24.
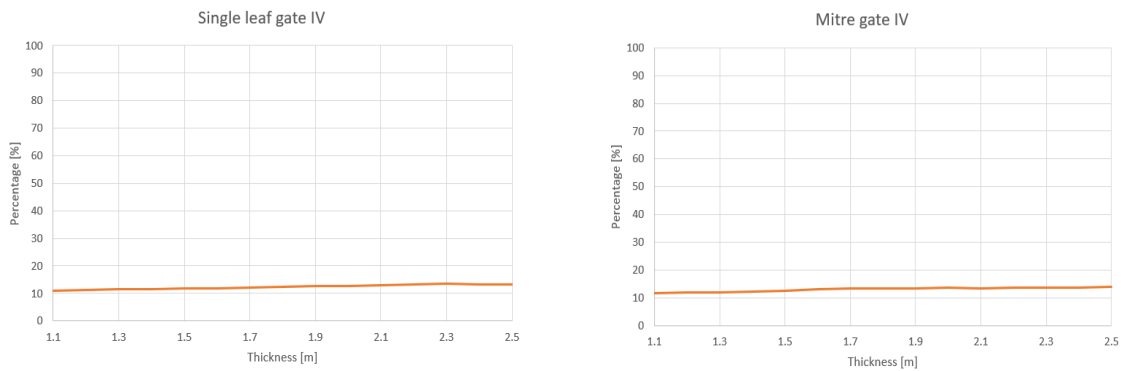
(a) Single leaf gate

(b) Mitre gate

Figure F.24: Percentage of the MKI of the total cost due to a difference in thickness

F.4.3. Influence Concrete Class
The MKI factor is around the 10%, see Figure F.25.
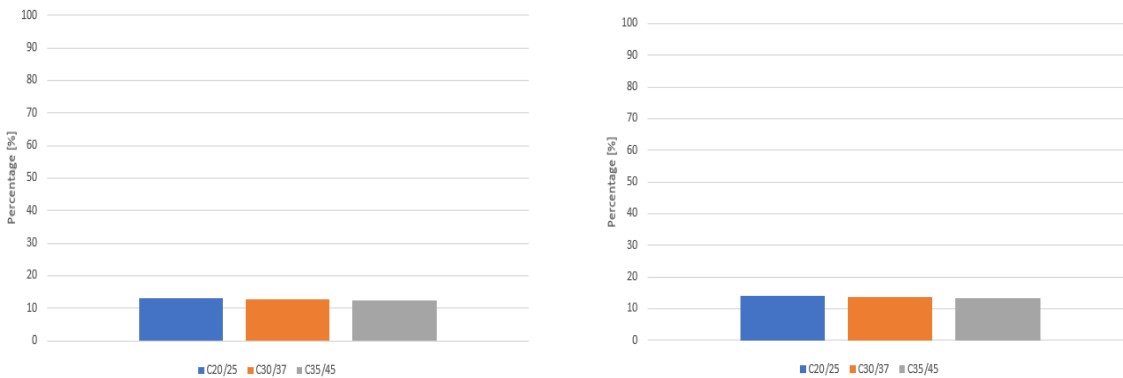
(a) Single leaf gate

(b) Mitre gate

Figure F.25: Percentage of the MKI of the total cost due to a difference in concrete class

F.4.4. Empel

The cost for Empel are $905227€$. The MKI for Empel is $67951€$. This result in a factor of $67951/905227 = 0.08$.